



Norwegian University of Life Sciences  
Faculty of Science and Technology

Philosophiae Doctor (PhD)  
Thesis 2020:68

# Innovative Surveillance and Process Control in Water Resource Recovery Facilities

Innovativ overvåking og prosesskontroll  
i avløpsrensaneanlegg

Abhilash Muralidharan Nair



# Innovative Surveillance and Process Control in Water Resource Recovery Facilities

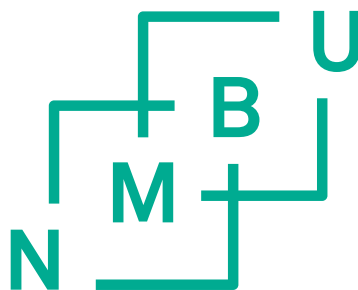
Innovativ overvåking og prosesskontroll i avløpsreanseanlegg

Philosophiae Doctor (PhD) Thesis

Abhilash Muralidharan Nair

Norwegian University of Life Sciences  
Faculty of Science and Technology

Ås (2020)



## **Supervision team**

### *Main supervisor*

Prof. Harsha Ratnaweera  
Faculty of Science and Technology (RealTek),  
Norwegian University of Life Sciences,  
Ås, Norway.

### *Co-supervisor*

Prof. Finn Aakre Haugen  
Faculty of Technology, Natural Sciences and Maritime Sciences,  
University of South-Eastern Norway,  
Porsgrunn, Norway.

### *Co-supervisor*

Prof. Lars John Hem  
Faculty of Science and Technology (RealTek),  
Norwegian University of Life Sciences,  
Ås, Norway.

## **Evaluation Committee**

### *First opponent*

Prof Emer. Gustaf Olsson  
Industrial Electrical Engineering and Automation,  
Lund University,  
Lund, Sweden.

### *Second opponent*

Prof. Rune Bakke  
Faculty of Technology, Natural Sciences and Maritime Sciences,  
University of South-Eastern Norway,  
Campus Porsgrunn, Norway.

### *Committee Coordinator*

Assoc Prof. Zakhar Maletskyi  
Faculty of Science and Technology (RealTek),  
Norwegian University of Life Sciences,  
Ås, Norway.







---

## Summary

Water Resource Recovery Facilities (WRRF), previously known as Wastewater Treatment Plants (WWTP), are getting increasingly complex, with the incorporation of sludge processing and resource recovery technologies. Along with maintaining a stringent effluent water quality standard, the focus is gradually shifting towards energy-efficient operations and recovery of resources. The new objectives of the WRRF demand an economically optimal operation of processes that are subjected to extreme variations in flowrate and composition at the influent. The application of online monitoring, process control, and automation in WRRF has already shown a steady increase in the past decade. However, the advanced model-based optimal control strategies, implemented in most process industries, are less common in WRRE. The complex nature of biological processes, the unavailability of simplified process models, and a lack of cost-effective surveillance infrastructure have often hindered the implementation of advanced control strategies in WRRE. The ambition of this research is to implement and validate cost-efficient monitoring alternatives and advanced control strategies for WRRF by fully utilizing the powerful Internet of Things (IoT) and data science tools.

The first step towards implementing an advanced control strategy is to ensure the availability of surveillance infrastructure for monitoring nutrient compositions in WRRF processes. In **Paper A**, a soft sensor, based on Extended Kalman Filter, is developed for estimating water-quality parameters in a Sequential Batch MBBR process using reliable and inexpensive online sensors. The model used in the soft sensor combines the mechanistic understanding of the nutrient removal process with a statistical correlation between nutrient composition and easy-to-measure parameters. **Paper B** demonstrates the universality of the soft sensor through validation tests conducted in a Continuous Multistage MBBR pilot plant. The drift in soft-sensor estimation caused by a mismatch between the mathematical model and process behavior is studied in **Paper B**. The robustness of the soft sensor is assessed by observing estimated nutrient composition values for a period of three months. A systematic method to calibrate the measurement model and update model parameters using data from periodic lab measurements are discussed in **Paper B**.

The term SCADA has been ubiquitous while mentioning online monitoring and control strategy deployment in WRRFs. The present digital world of affordable communication hardware, compact single board processors, and high computational power presents several options for remote monitoring and deployment of soft sensors. In **Paper C**, a cost-effective IoT strategy is developed by using an open-source programming language and inexpensive

hardware. The functionalities of the IoT infrastructure are demonstrated by using it to deploy a soft sensor script in the Continuous Multistage MBBR pilot plant. A cost-comparison between the commercially available alternatives presented in **Paper A** and the open-source IoT strategy in **Paper B** and **Paper C** highlights the benefits of the new monitoring infrastructure.

Lack of reliable control models have often been the cause for the poor performance of advanced control strategies, such as Model Predictive Controls (MPC) when implemented to complex biological nutrient removal processes. **Paper D** attempts to overcome the inadequacies of the linear prediction model by combining a recursive model parameter estimator with the linear MPC. The new MPC variant, called the adaptive MPC (AMPC), reduces the dependency of MPC on the accuracy of its prediction model. The performance of the AMPC is compared with that of a linear MPC, nonlinear MPC, and the traditional proportional-integral cascade control through simulator-based evaluations conducted on the Benchmark Simulator platform (BSM2). The advantages of AMPC compared to its counterparts, in terms of reducing the aeration energy, curtailing the number of effluent ammonia violations, and the use of computational resources, are highlighted in **Paper D**.

The complex interdependencies between different processes in a WRRF pose a significant challenge in defining constant reference points for WRRFs operations. A strategy that decides control outputs based on economic parameters rather than maintaining a fixed reference set-point is introduced in **Paper E**. The model-based control strategy presented in **Paper D** is further improved by including economic parameters in the MPC's objective function. The control strategy known as Economic MPC (EMPC) is implemented for optimal dosage of magnesium hydroxide in a struvite recovery unit installed in a WRRF. A comparative study performed on the BSM2 platform demonstrates a significant improvement in overall profitability for the EMPC when compared to a constant or a feed-forward flow proportional control strategy. The resilience of the EMPC strategy to variations in the market price of struvite is also presented in **Paper E**.

A combination of cost-effective monitoring infrastructure and advanced control strategies using advanced IoTs and data science tools have been documented to overcome some of the critical problems encountered in WRRFs. The overall improvement in process efficiency, reduction in operating costs, an increase in resource recovery, and a substantial reduction in the price of online monitoring infrastructure contribute to the overall aim of transitioning WRRFs to a self-sustaining facility capable of generating value-added products.

## Sammendrag

Water Resource Recovery Facilities (WRRF), tidligere kjent som avløpsrensaneanlegg (WWTP), blir stadig mer komplekse ettersom flere prosess steg tillegges anleggene i form av slambehandling og ressursgjenvinningsteknologi. Foruten hovedmålet om å imøtekomme strenge avløpsvannskvalitetskrav, har anleggenes fokus gradvis skiftet mot energieffektiv drift og gjenvinning av ressurser. Slike nye mål krever økonomisk optimal drift av prosesser som er utsatt for ekstreme variasjoner i volum og sammensetning av tilløp. Bruk av online overvåking, prosesskontroll og automatisering i WRRF har jevnt økt det siste tiåret. Likevel er avanserte modellbaserte kontrollstrategier for optimalisering ikke vanlig i WRRF, i motsetning til de fleste prosessindustrier. Komplekse forhold i biologiske prosesser, mangel på tilgang til pålitelige prosessmodeller og mangel på kostnadseffektiv overvåkingsinfrastruktur har ofte hindret implementeringen av avanserte kontrollstrategier i WRRF. Ambisjonen med denne avhandlingen er å implementere og validere kostnadseffektive overvåkingsalternativer og avanserte kontrollstrategier som utnytter kraftige Internet of Things (IoT) og datavitenskapelige verktøy i WRRF sammenheng.

Det første steget mot implementering av en avansert kontrollstrategi er å sørge for tilgjengelighet av overvåkingsinfrastruktur for måling av næringsstoffer i WRRF-prosesser. **Paper A** demonstrerer en virtuell sensor basert på et utvidet Kalman filter, utviklet for å estimere vannkvalitetsparametere i en sekvensiell batch MBBR-prosess ved hjelp av pålitelige og rimelige online sensorer. Modellen som brukes i den virtuelle sensoren kombinerer en mekanistisk forståelse av prosessen for fjerning av næringsstoffer fra avløpsvann med et statistisk sammenheng mellom næringsstoffsammensetning i avløpsvann og parametere som er enkle å måle. **Paper B** demonstrerer det universale bruksaspektet til den virtuelle sensoren gjennom valideringstester utført i et kontinuerlig flertrinns MBBR pilotanlegg. Feilene i sensorens estimering forårsaket av uoverensstemmelse mellom den matematiske modellen og prosesseatferden er undersøkt i **Paper B**. Robustheten til den virtuelle sensoren ble vurdert ved å observere estimerte næringsssammensetningsverdier i en periode på tre måneder. En systematisk metode for å kalibrere målemodellen og oppdatere modellparametere ved hjelp av data fra periodiske laboratoriemålinger er diskutert i **Paper B**.

Begrepet SCADA har alltid vært til stede når online overvåking og kontrollstrategi innen WRRF er nevnt. Den nåværende digitale verdenen med god tilgjengelighet av rimelig kommunikasjonsmaskinvare, kompakte enkeltkorktprosessorer og høy beregningskraft presenterer flere muligheter for fjernovervåking og implementering av virtuelle sensorer. **Paper C** viser til

utvikling av en kostnadseffektiv IoT-strategi ved hjelp av et programmeringsspråk med åpen kildekode og rimelig maskinvare. Funksjonalitetene i IoT-infrastruktur demonstreres gjennom implementering av et virtuelt sensorprogram i et kontinuerlig flertrinns MBBR pilotanlegg. En kostnadssammenligning mellom de kommersielt tilgjengelige alternativene som presenteres i **Paper A** og åpen kildekode-IoT-strategi i **Paper B** og **Paper C** fremhever fordelene med den nye overvåkingsinfrastrukturen.

Mangel på pålitelige kontrollmodeller har ofte vært årsaken til svake resultater i avanserte kontrollstrategier, som for eksempel Model Predictive Control (MPC) når de implementeres i komplekse biologiske prosesser for fjerning av næringsstoffer. **Paper D** prøver å løse manglene i MPC ved å kombinere en rekursiv modellparameterestimator med lineær MPC. Den nye MPC-varianten, kalt Adaptiv MPC (AMPC), reduserer MPCs avhengighet av nøyaktigheten i prediksjonsmodellen. Ytelsen til AMPC sammenlignes med ytelsen til en lineær MPC, ikke-lineær MPC og tradisjonell proportional-integral kaskadekontroll gjennom simulatorbaserte evalueringer utført på Benchmark Simulator plattformen (BSM2). Fordelene med AMPC sammenlignet med de andre kontrollstrategiene er fremhevet i **Paper D** og demonstreres i sammenheng med reduksjon av energibruk ved lufting i luftebasseng, samt reduksjon i antall brudd på utslippskrav for ammoniakk og bruk av beregningsressurser.

De komplekse avhengighetene mellom forskjellige prosesser i en WRRF utgjør en betydelig utfordring når man skal definere konstante referansepunkter for WRRF under drift. En strategi som bestemmer kontrollsignaler basert på økonomiske parametere i stedet for å opprettholde et fast referansesettpunkt introduseres i Paper E. Den modellbaserte kontrollstrategien fra **Paper D** forbedres ytterligere ved å inkludere økonomiske parametere i MPCs objektive funksjon. Denne kontrollstrategien kalles Economic MPC (EMPC) og er implementert for optimal dosering av magnesiumhydroksid i en struvit utvinningsenhet installert i en WRRF. En sammenligningsstudie utført på BSM2-plattformen viste en betydelig forbedring i den totale lønnsomheten ved bruk av EMPC sammenlignet med en konstant eller en flow proportional kontrollstrategi. Robustheten til EMPC-strategien for variasjoner i markedsprisen på struvit er også demonstrert i **Paper E**.

En kombinasjon av kostnadseffektiv overvåkingsinfrastruktur og avanserte kontrollstrategier ved hjelp av avansert IoT og datavitenskapelige verktøy er brukt for å løse flere kritiske utfordringer i WRRF. Den samlede forbedringen i prosesseffektivitet, reduksjon i operasjonskostnader, økt ressurgjenvinning og en betydelig reduksjon i pris for online overvåkingsinfrastruktur bidrar til det overordnede målet om å gå over til bærekraftige WRRF som er i stand til å generere verdiskapende produkter.

**Thinking is more interesting than knowing,  
but less interesting than looking.**

*- Johann Wolfgang von Goethe*





---

## Acknowledgments

Every journey that begins has an end and every journey that end marks the beginning of something new. This would be the closing remark for a rather arduous and long journey of my doctoral studies that took me through the highest and lowest points of my personal as well as professional life.

First, I would like to thank my parents (Lathika and Muralidharan) for bringing me to this world and despite a rather conventional outlook, always gave me the freedom to choose my path. Nothing would have been possible without the constant encouragement and advice from my supervisor Prof. Harsha Ratnaweera. His vision, vast knowledge, and impeccable judgment have helped steer the research activities during my Ph.D. Thank you for all the help, support, and guidance you offered me through the journey.

I am deeply obliged to my co-supervisor Prof. Finn Aakre Haugen. Having Finn as my co-supervisor has helped me understand the practical applicability of dynamic state estimations and advanced control strategies that form the core of my thesis. I would also like to thank my co-supervisor Prof. Lars John Hem for the guidance in structuring my tasks and thesis work.

Special thanks to my wife, Dr. Aathira Menon, who despite my absent-minded demeanor and workaholic routine had my back with great patience and love. I owe a lot for the support and morale boost, especially in times when I felt low.

My gratitude to the little Indian family (Mangu, Anu, Ranjhu, and Nive) in Norway that always kept me connected to the traditions, music, culture, and cuisines from my home country. A special thanks to Sandeep who has been more than a brother to me, a person I trusted with pulling me out of the deepest and darkest of pits, which I have often found myself slipping into. I would not imagine getting back on my feet without his help.

In this ever-changing world, where people around us are in a state of constant flux, I had the utmost privilege to call some of them as true friends. To mention a few, Dr. Xiaodong Wang for all the late-night discussions and fiery debates (which i shall always miss) and Dr. Nataly who would occasionally be the moderator between us. I would like to thank Sergii, Dino, Olga, and Duo for making my stay at the office enjoyable and pleasant.

The never-ending energy and laughter of Martina and the strong-witted rhetorics of Sara always assured me that laughter was just around the corner. Special gratitude to the celebrated genius of the group, Aleksander Hykkerud, who helped me sustain my interest in math through our debates, discussions, and war of words. I would always hold him responsible for decimating

my ten-year long fidelity with MATLAB and enticing me to flirt with my new found love of Python.

My Ph.D. fellowship was a part of project RECOVER, which was approved and supported by The Research Council of Norway. My special thanks to the technical and financial support from DOSCON AS. I would also like to acknowledge the help and guidance from the water group at NTNU, specially Dr. Blanca and Abaynesh with whom I had the privilege to work closely during my research.

*Ås, September 15, 2020*

*Abhilash M Nair*

# Contents

<b>1</b>	<b>Introduction and Research Motivation</b>	<b>1</b>
1.1	A historical prologue . . . . .	1
1.2	Need for resource recovery . . . . .	3
1.3	From WWTP to WRRF . . . . .	5
1.4	Challenges in WRRF . . . . .	8
1.4.1	Need for optimizing WRRF processes . . . . .	8
1.4.2	Inadequacies of current control strategies . . . . .	9
1.4.3	Shortcomings of monitoring infrastructure . . . . .	9
<b>2</b>	<b>Research Objective and Thesis Overview</b>	<b>11</b>
2.1	Objectives . . . . .	11
2.2	Synopsis of the appended papers . . . . .	13
<b>3</b>	<b>Theoretical Framework and Literature Review</b>	<b>15</b>
3.1	Principles of soft sensing . . . . .	15
3.1.1	Data-driven models for soft sensing . . . . .	16
3.1.2	Mechanistic models for soft sensing . . . . .	17
3.2	Hybrid models for soft sensing . . . . .	18
3.3	Soft sensor algorithm . . . . .	19
3.4	Standard simulator platform for WRRF . . . . .	21
3.5	Process optimization in WRRF . . . . .	22
3.5.1	Biological nutrient removal . . . . .	22
3.5.2	Nutrient recovery . . . . .	25
3.6	Model-based optimal control in WRRF . . . . .	26
3.6.1	Conventional optimal control strategies . . . . .	26
3.6.2	Advanced variants of MPC . . . . .	28
<b>4</b>	<b>Research Methodology</b>	<b>31</b>
4.1	Model development . . . . .	32
4.1.1	Selecting state-variables and state-space equations . . . . .	32
4.1.2	Selecting measurement equations . . . . .	32
4.2	Offline estimation of model parameters . . . . .	33
4.2.1	Experimental study . . . . .	33

---

4.2.2	Model calibration . . . . .	33
4.3	Simulator based evaluation and tuning of EKF parameters . . . .	34
4.4	Pilot-scale implementation . . . . .	35
4.4.1	Processes for soft sensor evaluation . . . . .	35
4.4.2	Surveillance infrastructure and deployment strategy . . . .	38
4.5	Evaluating soft sensor performance . . . . .	39
4.5.1	Short-term performance evaluation . . . . .	39
4.5.2	Long-term performance evaluation and recalibration . . . .	39
4.5.3	Lab measurements . . . . .	39
4.6	Control strategy for nutrient removal . . . . .	40
4.6.1	Basic control strategies . . . . .	40
4.6.2	Advanced MPC strategy . . . . .	41
4.7	Control strategy for nutrient recovery . . . . .	43
4.7.1	Feed forward flow proportional control strategy . . . . .	43
4.7.2	Advanced EMPC strategy . . . . .	43
4.8	Simulation procedure . . . . .	45
<b>5</b>	<b>Results and Discussion</b>	<b>47</b>
5.1	Validating hybrid models . . . . .	48
5.2	Estimating water-quality parameters . . . . .	50
5.2.1	Real-time estimations in SB-MBBR . . . . .	50
5.2.2	Real-time estimations in CM-MBBR . . . . .	51
5.3	Long-term performance evaluation and recalibration . . . . .	54
5.4	Economic evaluation of new IoT infrastructure . . . . .	56
5.5	Impact of control strategy on nutrient removal process . . . . .	58
5.6	Impact of control strategy on struvite recovery process . . . . .	61
<b>6</b>	<b>Thesis Contributions</b>	<b>65</b>
<b>7</b>	<b>Conclusions and Outlook</b>	<b>67</b>
<b>8</b>	<b>Recommendations for Future Work</b>	<b>69</b>
	<b>References</b>	<b>71</b>
	<b>List of Appended Papers</b>	<b>83</b>

# Chapter 1

## Introduction and Research Motivation

### 1.1 A historical prologue

Since the beginning of the 20<sup>th</sup> century, engineers and scientists have realized that natural processes are not capable of coping with the rapid increase of pollution in water bodies. Human intervention was deemed necessary to treat the amount of waste produced by the ever-increasing urban population and to protect rivers, lakes, and other vital sources of drinking water. These demands led to the foundation of the centralized urban 'wastewater management system' in which the Wastewater Treatment Plants (WWTPs) played a vital role. Initially, sewage was handled either by diverting them to sewage farms or by chemical precipitation and subsequent sedimentation (Metcalf and Eddy, 1914). A great leap in the wastewater treatment industry came in 1914 with the discovery of microorganisms that were capable of removing organics and also oxidize ammonia (Jenkins and Wanner, 1999). Since then, the activated sludge process became the core of most WWTPs in the world. Some WWTPs continued using chemical coagulation and flocculation as their main unit process (Bratby, 2006), considering local conditions. Several technological, environmental, economic, and ecological factors played a role in the selection of the core process in WWTP (El-Bestawy et al., 2005). However, quite a few WWTPs also use a combination of both biological and chemical processes to achieve better treatment efficiencies.

WWTPs have undergone several stages of evolution in terms of new designs, processes, and operational objectives. A modern WWTP uses a combination of mechanical, biological, and chemical treatment processes to remove Total Phosphorus (TP), Total Nitrogen (TN), organic matter (determined as Bio-

chemical Oxygen Demand (BOD), Chemical Oxygen Demand (COD) or Total Organic Carbon (TOC)), and Suspended Solids (SS) present in raw wastewater. Over time, the stringent effluent standards motivated engineers to upgrade their processes and introduce more compact and energy-intensive designs. Technologies such as Moving Bed Biofilm Reactors (MBBR) (Ødegaard et al., 1994) and Integrated Fixed Film Activated Sludge System (IFAS) (Sriwiyarat et al., 2005), significantly reduced the overall footprint of the conventional suspended growth activated sludge processes. The gravity separation concepts used in primary and secondary clarifiers were receiving design upgrades in the form of Chemical Enhanced Primary Tanks (CEPT), Lamella separators, or ballasted flocculation (Gasperi et al., 2012). A few WWTPs entirely replaced their conventional separation equipments with Membrane Bio-Reactors (MBRs) or fine sieves.

As the wastewater treatment industry evolved with time, WWTPs also assimilated various other technologies that were developing in parallel. The 1960's witnessed the beginning of online sensors and computers in process industries, and the wastewater treatment sector began to explore their applicability in WWTPs. By the early 1970s, IAWPR, the predecessor of the International Water Association (IWA), recognized the potential of Instrumentation Control and Automation (ICA) in producing significant improvements in the operations of both water and wastewater treatment processes (Olsson et al., 2012). However, the nascent years of ICA were clouded with uncertainties and a definitive lack of motivation among operators to adopt process automation in treatment plants. The implementation of ICA in wastewater treatment plants dwarfed in comparison to similar biochemical processes such as beer or pharmaceutical industry. The knowledge of reaction kinetics necessary to implement automation systems was still developing. The inherent complexity of biological processes, lack of a standardized kinetic model, and limited availability of online sensors posed a significant challenge in their initial days (Olsson et al., 2005).

With time, the benefits of ICA in WWTP became more discernible. The treatment plant operators were aware of the suboptimal performance of WWTP caused by the variations in influent wastewater flowrate and composition. The advantages of process control and the relevance of ICA in the stable operation of WWTPs were becoming self-evident. The development of process computers and the availability of several online water-quality sensors further incentivized the use of ICA in WWTPs. The introduction of control equipment such as Variable Frequency Drives (VFD) allowed the adjustment of control handles in a continuous way to obtain smooth and varied control (Olsson et al., 2012). The simple error-driven on/off control strategies can now be replaced with better performing proportional-integral-derivative (PID) con-

trollers. The most significant impact of ICA on WWTPs was felt with the implementation of aeration control. Aeration accounted for up to 70% of the overall operating costs, and the ability to control the air-pumps based on the feedback signals from the dissolved oxygen sensors resulted in reduced power consumption during low influent loads. Improving efficiency using aeration control was the demonstrative example of significant energy saving produced by automation in WWTP (Olsson and Jeppsson, 2006; Åmand et al., 2013). Some of the commonly used control strategies in a conventional WWTP are presented in Table 1.1.

When the processes related to WWTPs evolve, so does the instrumentation and control objectives associated with it. ICA has been continuously adapting to the trends, changes, and requirements of treatment plant operators and managers. The present decade is witnessing a gradual shift from a linear to a circular economy, and WWTPs will be expected to play a vital role in this transformation (Udugama et al., 2020). The advent of innovative processes and the adoption of new operational strategies are expected to introduce several changes for ICA in WWTPs.

## 1.2 Need for resource recovery

The agricultural industry is heavily dependent on elements such as Nitrogen, Phosphorus, and Potassium that are essential to plant growth. Implementation of intensive farming methods, an increase in population, a rise in meat consumption, and cultivation of cash crops further increased their dependency on these mineral sources (Godfray et al., 2010). Various studies indicate that current mineral reserves will deplete within 93 to 291 years for Phosphorus, 235 to 510 years for Potassium, and 20 years for Zinc (Elser and Bennett, 2011). The expected timeline can further shorten due to unfavorable government policies, a negligent attitude towards dwindling resources, and a lack of consensus among the research community over the imminence of the threat (Neset and Cordell, 2012). Given the current limitation in technology, no substitute exists for the production and supply of these essential minerals. Nitrogen, on the other hand, can be manufactured in the form of ammonia using the Haber-Bosch process (Erisman et al., 2008). However, industrial ammonia manufacturing requires hydrogen, which is sourced from natural gas. The high energy requirement of the process and their dependency on natural gas make their production and supply line highly dependent on fossil fuels. A significant amount of fossil fuel is also necessary for the production, processing, and transportation of mineral fertilizers which make the cost of mineral fertilizers intertwined with fossil fuel prices (Gellings and Parmenter, 2004). The increase in demand for mineral fertilizers, unstable energy costs,

and the reduction in both quality and quantity of mineral reserves could result in a sharp increase in their price and pose a threat to future human food security (Sutton et al., 2013). The expected trends in phosphorus resources, presented in Figure 1.1, show that immediate intervention, in terms of better resource management as well as exploring alternative sources, is necessary to prevent a crisis in the future. (Cordell and White, 2011).

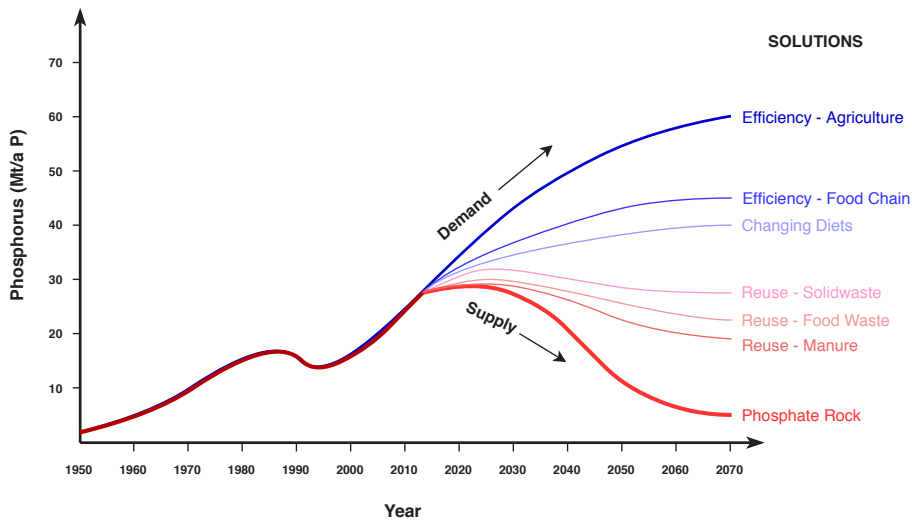


**Figure 1.1.** Global trends in the phosphorus demand and available reserves (redrawn from (Cordell and White, 2011)).

Increased urbanization, rapid industrialization, and the associated rise in waste-generation have imposed a significant burden on waste management and waste disposal infrastructure. Practices such as overuse of chemical mineral fertilizers and unguarded landfills have resulted in mineral-rich runoffs, often ending up in water sources. The mineral-rich runoffs cause serious problems such as eutrophication and the subsequent decimation of aquatic life (Chislock et al., 2013). Although the consistent degradation of water bodies has stimulated a few government authorities to introduce stringent regulations for the quality of discharge/emission from WWTPs, these efforts might not be adequate. It can be noted that most solid waste discharged in the environment, such as household waste, sewage sludge, industrial effluents, manure, incineration ashes, etc. are mostly the non-bio-available form of the Nitrogen, Phosphorus, and Potassium sources that we often scour the planet in search of (Hou et al., 2012). In the present scenario, where a shortage of mineral resources seems imminent, we also observe phenomena such as surplus fertilization and inefficient waste disposal systems.



## 1.3 From WWTP to WRRF

In a conventional framework, wastewater is seen as a waste to be treated before discharging it to the environment. WWTPs strictly adhered to the stringent effluent norms to avoid the penalties levied by the environment regulatory authority. WWTPs are considered an indispensable part of urban civic infrastructure dedicated to removing harmful constituents (COD, TN, and TP) detrimental to the environment. However, the potential of WWTPs in recovering resources is often ignored.

The depletion of mineral resources, shortage of potable water, a rise in energy demands, and a rampant increase in household and industrial waste generation have motivated industries to close nutrient cycles and migrate towards sustainable management of resources (Sutton et al., 2013). WWTPs receive a majority of the waste generated from urban household and small-scale industries, making them receiving stations for nutrients and placing them at the nexus for the concept of cradle-to-cradle (Udugama et al., 2020). The significance of WWTPs in the vision of a circular economy has transformed the way we look at wastewater. The official re-christening of Waste Water Treatment Plants (WWTs) as Water Resource Recovery Facilities (WRRFs) by the Water Environment Federation (Sweeney et al., 2015) reflects the changing paradigm. In this context, wastewater is now considered to be a diluted form of 'resource', that should be concentrated and eventually recovered rather than a 'waste' that should be treated.

The new perspective of looking at wastewater as a resource led to the introduction of several new processes in WRRFs. The traditional method of categorizing WWTPs as primary, secondary, and tertiary processes is gradually changing. The new resource-oriented approach categorizes WRRF processes as **a.** Concentration - processes that capture nutrients from wastewater in the form of sludge, **b.** Release - processes that release nutrients and energy from sludge, and **c.** Extraction - processes that transform resources to marketable value-added products (Vanrolleghem and Vaneckhaute, 2014). The differences between the layout of a modern WRRF and a conventional WWTP is presented in Figure 1.2. The new outlook has also introduced various incentives to improvise the operational strategies of a WRRF. Several energy-intensive processes are now re-visited to explore the possibility of process optimization and reduce their operational cost. New processes are introduced with a goal of enabling water reclamation and reuse (Leverenz and Asano, 2011). Although compliance with stringent effluent standards is still the primary goal of WRRFs, the focus is gradually shifting towards maximizing nutrient recovery at the lowest possible energy and resource consumption.

**Table 1.1.** A selected list of commonly used control strategies in conventional WWTP.

Control Strategy	Control Variable	Measured Variable	Control Handle	Algorithm	References
Aeration Control	DO (Aerobic)	DO	Air Flow	PI	(Åmand et al., 2013)
Nitrate Control (Pre-Den.)	NO <sub>3</sub> -N (Anoxic)	NO <sub>3</sub> -N	MLSS Recycle	PI	(Yuan et al., 2002)
Nitrate Control (Post-Den.)	NO <sub>3</sub> -N (Anoxic)	NO <sub>3</sub> -N, ORP	Carbon dosing	PI Cascade	(Lindberg and Carlsson, 1996) (Puznava et al., 1998)
Ammonia Control	NH <sub>4</sub> -N (Aerobic)	NH <sub>4</sub> -N, DO	Air Flow	Cascade	(Ingildsen et al., 2002) (Vrečko et al., 2006)
SRT Control	TSS (Aerobic)	TSS	Sludge Recycle Sludge Wastage	PI	(Cakici and Bayramoglu, 1996)
Sludge Blanket Level Control	Level (Clarifier)	Level	Sludge Recycle	PI	(Yuan et al., 2001)
Phosphate Control (Biological)	PO <sub>4</sub> -P (Effluent)	VFA	Acetate Dosage	PI	(Olsson et al., 2005)
Phosphate Control (Chemical)	PO <sub>4</sub> -P (Effluent)	PO <sub>4</sub> -P, TSS	Coagulant Dose	statistical	(Devisscher et al., 2002) (Manampertuma et al., 2017)
SBR Cycle time	NH <sub>4</sub> -H, NO <sub>3</sub> -N	pH, ORP	Cycle Time	ON-OFF	(Yu et al., 1997)

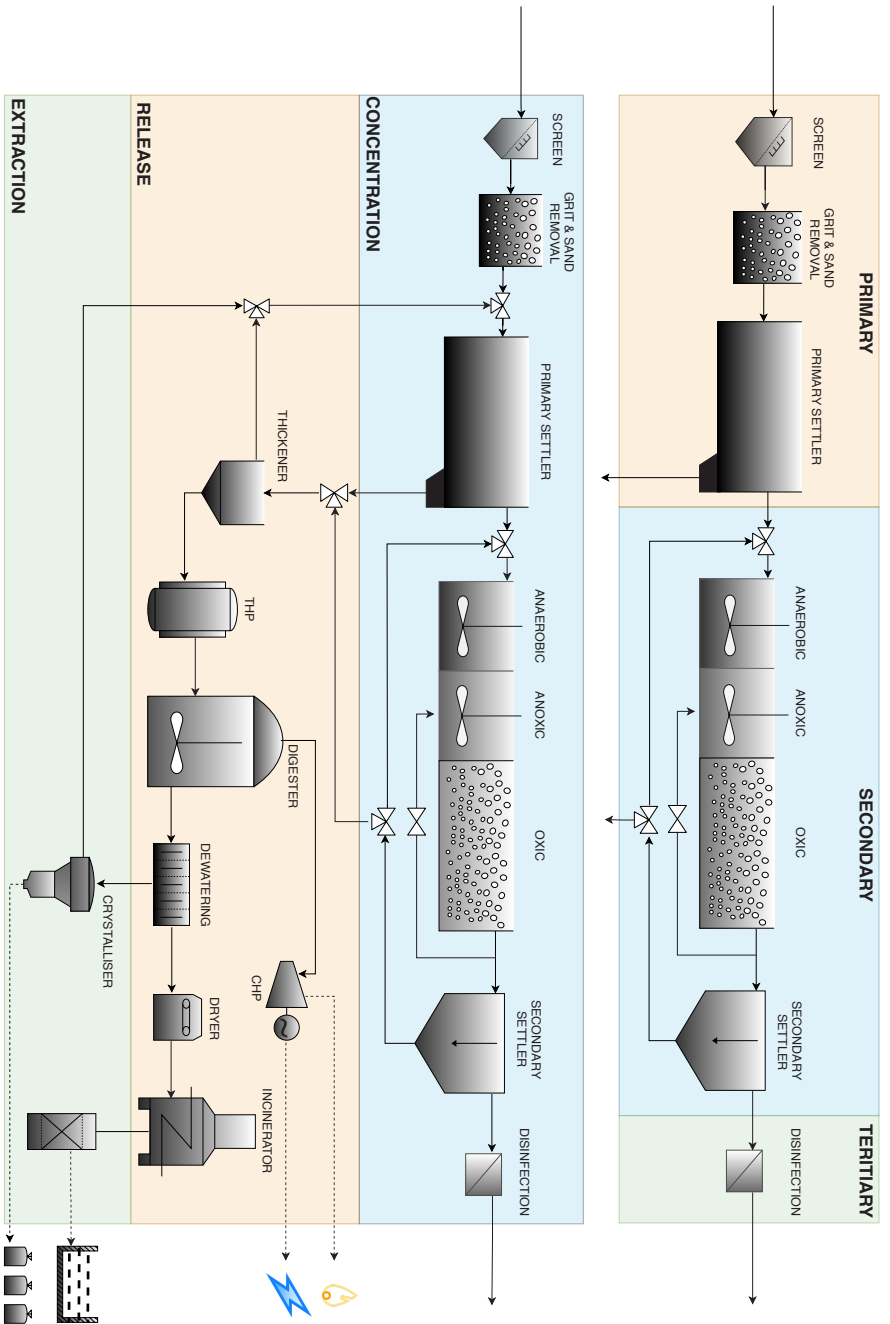


**Figure 1.2.** Plant layout and selected unit processes, typically used in (Top) a conventional WWTP and (Bottom) a modern WRRF

## 1.4 Challenges in WRRF

Maintaining the economical operation of WRRFs is a challenging task. The technical, operational, and economical challenges encountered in the operations of WRRF are presented in the subsequent section.

### 1.4.1 Need for optimizing WRRF processes

WRRFs consume large quantities of energy and material to remove and recover nutrients from wastewater (Xu *et al.*, 2017). Biological aerobic process, which forms the core of most nutrient removal facilities, is the highest energy-consuming process in a WRRF. Since the primary focus was on maintaining good effluent quality, optimizing the energy consumption in the biological aeration stage have sometimes been considered secondary. Attempts to improve aeration through redesign of aerators (Rosso *et al.*, 2008) or introducing aeration control (Sahlmann *et al.*, 2004) have been reported in literature. However, an increasing number of studies on nutrient-based aeration control indicate the potential to improve the process even further. Processes such as anaerobic digestion produce biogas that can generate energy and partially offset the energy requirements of the WRRF. However, generating a surplus is a challenging endeavor. In addition to the excessive energy consumption, WRRFs also require coagulants, polymers, external carbon-source, and other associated chemicals, that further increase the overall operating costs.

Several WRRFs processes, such as precipitation, leaching, and stripping, have the potential to produce marketable products (struvite, brushite, k-phosphate, ammonium nitrate, etc.). However, these products generated from the nutrient recovery stage face tremendous challenges in matching the quality of similar products currently available in the market today (Vanrolleghem and Vaneeckhaute, 2014). Processes such as struvite precipitation, intended to recover phosphorus, are often used as a strategy to reduce the maintenance costs of WRRF (Solon *et al.*, 2019). Several experiments have been conducted to maximize phosphorus recovery, improve crystal properties, and reduce material consumption in a struvite recovery unit (Shaddel *et al.*, 2019). However, high influent fluctuations often disrupt optimal operation of recovery processes. Given the current limitations, it is a challenge to imagine a situation where WRRFs can operate as an energy-surplus entity capable of generating commercially marketable products (Solon *et al.*, 2019). Finding energy-efficient pathways, improving processes efficiencies, and introducing operational strategies less susceptible to influent fluctuations, could improve the economics of a WRRF without compromising the effluent quality.

### 1.4.2 Inadequacies of current control strategies

Deploying a reliable control strategy is the most commonly adopted solution to counter process disturbances and ensure stable operating conditions. In a present scenario, most WRRFs still rely on basic control philosophies to operate most of their processes. Due to the complex nature of WRRF processes, simple control strategies cannot guarantee good performance (Brdys et al., 2008). Simple single-input-single-output (SISO) controllers are not sufficiently robust since most control parameters in WRRFs are influenced by more than one manipulated variable. Therefore, a predictive optimization-based control strategy using a mechanistic or a data-driven model would be necessary to tackle the inherent complexities of various processes constituting a WRRF (Zhang et al., 2019; Steffens and Lant, 1999).

Several advanced model-based control strategies, such as Model Predictive Control (MPC), are available in literature (O'Brien et al., 2011). In the past decade, a few advanced control strategies, have been evaluated for several processes such as carbon source dosing (Stare et al., 2007), coagulant dosing (Wei and Ratnaweera, 2016), and anaerobic digestion (Haugen et al., 2014). However, the lack of simplified control models often affect their performance (Stentoft et al., 2019). A detailed review of the problems faced by control systems in WRRFs is presented in (Rieger and Olsson, 2012). Linearized models that form the core of most MPCs fail to explain the complex biological processes occurring in WRRFs. A severe mismatch between the actual process and the mathematical models is one of the underlying causes for the poor performance of MPC compared to the basic proportional-integral (PI) controllers in WRRFs (Vrečko et al., 2011).

### 1.4.3 Shortcomings of monitoring infrastructure

Real-time measurement of nutrient composition is necessary for implementing control strategies in WRRFs (Olsson et al., 2014). Most conventional small to medium treatment facilities rely on standardized lab tests to measure water quality parameters such as COD, BOD, TN, TP,  $\text{NH}_4\text{-N}$ ,  $\text{NO}_3\text{-N}$ , and VFA. Although the data received from standardized lab tests (of grab or composite samples) provide an insight into the performance and removal efficiencies of the treatment process, they cannot be used directly to implement control strategies or in automation systems (Thomas and Pouet, 2005). It is also possible to measure some of these parameters online using automated wet-analyzers (Wacheux *et al.*, 1996), ion-selective electrodes (ISE) (Thomson and Kisbye, 1996), or in-situ probes based on Ultraviolet-Visible (UV-Vis) absorbance (Thomas et al., 2005). However, the high prices of automated wet-analyzers, measurement uncertainties in ISE electrodes, and a need for

regular maintenance and recalibration limit their presence in most WRRFs (Barnard and Crowther, 1993). A review of the online monitoring system in WWTP (Jeppsson et al., 2002; Vanrolleghem and Lee, 2003; Al-Dasoqi et al., 2011; Ratnaweera and Fettig, 2015), shows that parameters such as pH, ORP, electrical conductivity (EC), flow-rate, temperatures, and dissolved oxygen (DO) are monitored online in most WRRFs (even small and medium treatment facilities) since they can be measured easily using reliable and inexpensive online sensors. One of the challenges for the deployment of advanced control strategies in WRRF is the inaccessibility of reliable and inexpensive online monitoring systems for obtaining real-time water quality parameters from a WRRF (Haimi et al., 2009).

In addition to the inadequacies of online sensors, the communication, and data-acquisition infrastructure also require a considerable upgrade. Commercial suppliers of Supervisory Control and Data Acquisition system (SCADA) provide a variety of options to access, log, and visualize data from online sensors. Standardized communication protocols such as Modbus TCP, ProfiNET, OPC-UA, etc., are provided to allow cross-platform communication between hardware manufactured by different suppliers. However, the price of most communication hardware and services provided by commercial SCADA suppliers is very high. Implementing control strategies, soft sensors, or fault detection algorithms, require the knowledge of writing scripts in the SCADA's proprietary programming suite (which also comes at exorbitant prices). The growing popularity of single board computers (Basford et al., 2020) has resulted in a considerable drop in the price of computational hardware and internet-enabled devices. However, this drop in price is not proportionally reflected in the price of the hardware or the services provided by SCADA suppliers. Moreover, the necessity to write the scripts in the software's proprietary program suite limits the integration of most optimization packages, simulation software, digital twins (written in scientific programming languages such as MATLAB and Python) to the commercially available SCADA systems.

# Chapter 2

## Research Objective and Thesis Overview

### 2.1 Objectives

As emphasized in the previous section, the integration of resource recovery technologies and the resulting increase in operational complexity demands a considerable upgrade in the monitoring infrastructure and control strategies of the WRRF. The overall objective of this thesis is to develop a reliable, cost-effective monitoring system and devise an optimal control strategy to improve process efficiency, reduce operating costs, and increase resource recovery in WRRF. In this respect, few critical processes exhibiting a potential for optimization through control are selected from the wide variety of operations constituting the WRRF. A combination of pilot-scale testing and simulator-based evaluations are performed on these selected processes to assess and validate the monitoring techniques and optimal control methods developed in this work. The following research directions have been chosen to address the main objectives of the thesis.

1. Develop and validate soft sensors for nutrient removal processes. **Paper A** and **Paper B**
2. Introduce an open-source IoT infrastructure and conduct an economic assessment of available monitoring options. **Paper C**
3. Evaluate the performance of model-based aeration control strategies and identify their benefits in nutrient removal process. **Paper D**
4. Verify the advantages of implementing an economic oriented dosing control strategy for resource recovery process in WRRF. **Paper E**

The interaction between the overall objectives, research direction, WRRF processes used in verification, and resulting papers are presented in Figure 2.1.

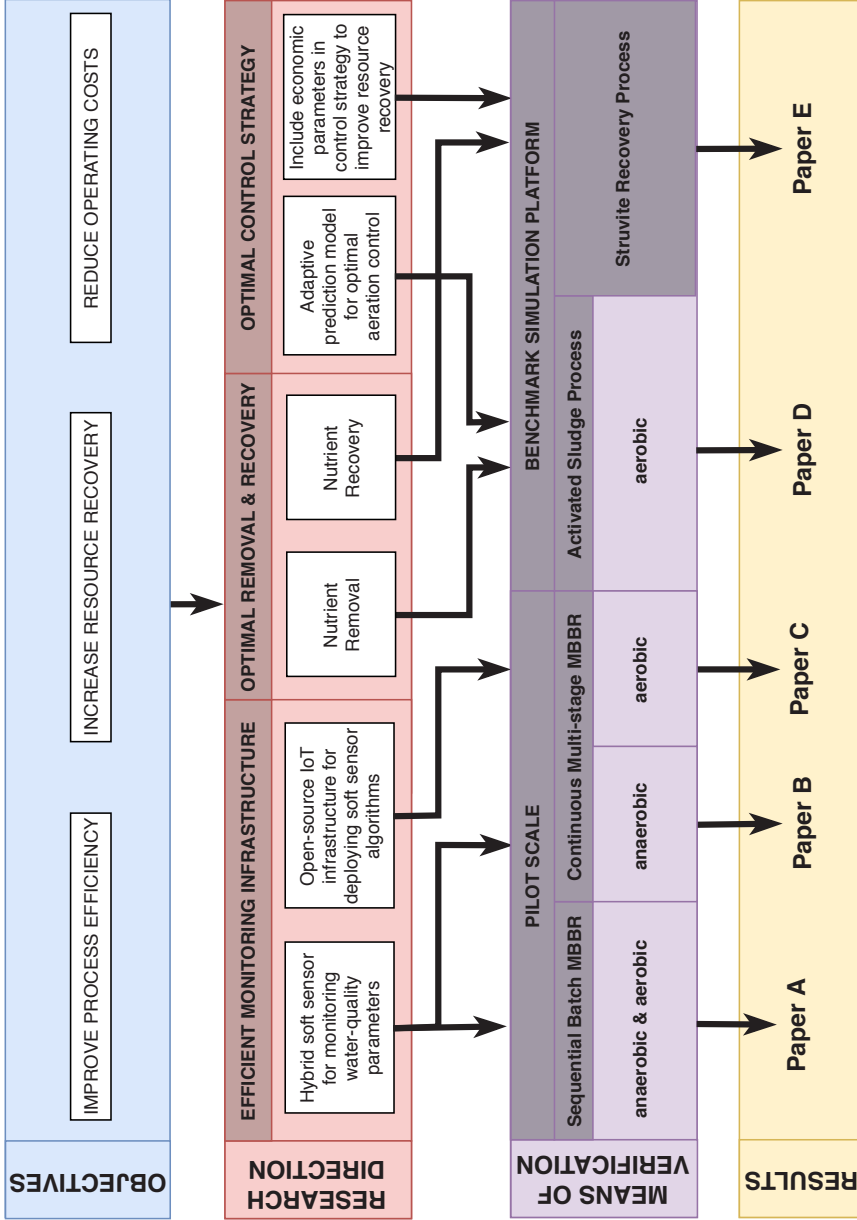


Figure 2.1. Interaction between research objectives, research directions, means of verification, and the papers.



## 2.2 Synopsis of the appended papers

### **Paper A** - *Introducing a proof-of-concept for hybrid soft sensor*

Real-time monitoring of water-quality parameters is essential for deploying advanced optimal control strategies in WRRF. A hybrid model is developed by combining mechanistic elements explained in the Activated Sludge Model 2d with a statistical correlation between nutrient compositions and easy-to-measure physical parameters. The hybrid model is used in conjunction with the Extended Kalman Filter (EKF) to provide real-time estimations of ammonia ( $\text{NH}_4\text{-N}$ ), nitrate ( $\text{NO}_3\text{-N}$ ), and phosphates ( $\text{PO}_4\text{-P}$ ) in a Sequential Batch Moving Bed Biofilm Reactor (SB-MBBR) using pH and Dissolved Oxygen (DO) sensors. The paper introduces a proof-of-concept through validation tests conducted in a pilot-scale unit, for using a well-calibrated hybrid model to estimate the water-quality parameters in a nutrient removal process.

### **Paper B** - *Universality and robustness assessment of the hybrid soft sensor*

The adaptability of hybrid soft-sensing method (discussed in **Paper A**) to a new process is demonstrated by implementing it in a more complex Continuous Multi-stage MBBR (CM-MBBR) pilot plant. In this paper, the soft sensor is used for real-time estimations of  $\text{PO}_4\text{-P}$  and soluble COD (sCOD) concentrations in the anaerobic stages using conductivity and flow measurements. The drift in soft sensor estimation caused by a mismatch between the mathematical model and the process behavior is studied. The stability of the soft sensor is assessed by monitoring its performance for a period of three months. A systematic method to update model parameters using data from periodic lab measurements are discussed in this paper.

### **Paper C** - *Developing a cost-effective IoT infrastructure*

The commercial SCADA providers offer a multitude of options to execute soft sensor codes and deploy control algorithms in a full-scale WRRF. However, it is imperative to have a quantitative assessment of the available alternatives and choose the option which best suits the current requirements. The paper describes a cost-effective Internet of Things (IoT) infrastructure for online visualization of sensor data and remote deployment of soft sensor script. A cost-comparison between the commercial remote deployment strategy used in **Paper A** and the open-source IoT infrastructure used in **Paper B** and **Paper C** are provided. The paper also substantiates the universality of the hybrid soft-sensing method explained in **Paper A** by presenting a case study on estimating the  $\text{NH}_4\text{-N}$  concentration and nitrification rate in the aerobic zones and the influent of the CM-MBBR pilot plant.

**Paper D** - *Improving nutrient removal process through adaptive MPC*

Aeration accounts for up to 70% of the overall operational costs in a WRRF. Therefore, optimal aeration control is essential to maintain low operating costs in a WRRF without compromising the effluent quality. An advanced variant of the optimization-based Model Predictive Control (MPC), called the Adaptive Model Predictive Control (AMPC), is constructed for ammonia-based aeration control in the biological stages of a WRRF. The paper demonstrates the advantages of updating the linear prediction model using a recursive model parameter estimator. A systematic procedure for developing the linear prediction model, configuring the recursive model parameter estimator, and tuning the MPC parameters is also explained. The advantages of implementing AMPC in terms of curtailing the number of effluent violations at reduced aeration energy are also presented in this work.

**Paper E** - *Enhancing nutrient recovery through economic MPC*

Struvite precipitation is a popularly used process for recovering resources (phosphorus and nitrogen) in a WRRF. Optimal dosing of magnesium hydroxide is necessary to improve the recovery of phosphorus in the form of struvite. A similar version of the advanced MPC variant discussed in **Paper D**, called the Economic Model Predictive Control (EMPC), is used in this work. The EMPC's objective function is structured to not only include real-time information from online sensors but also include market prices of struvite and magnesium hydroxide. Therefore, EMPC presents a possibility to decide the optimal magnesium hydroxide dose based on the overall profitability of the struvite recovery unit. The advantage of the EMPC strategy is demonstrated through validation studies conducted on the standard Benchmark Simulation Model No.2 (BSM2). The improvement in phosphorus recovery, reduction in the consumption of magnesium hydroxide, and the robustness of the controller, when faced with a time-varying market price, are presented in **Paper E**.

# Chapter 3

## Theoretical Framework and Literature Review

### 3.1 Principles of soft sensing

Software sensors, also known as soft sensors or virtual sensors are computer programs that provide real-time information of system parameters that are otherwise difficult to measure using physical sensors. These soft sensors are constructed by combining a mathematical model with data from a physical sensor (or a series of physical sensors), to obtain additional process information. Soft sensors present an economical alternative to physical sensors that are expensive, unreliable and require frequent maintenance (Haimi et al., 2015), or for parameters which are simply impossible to measure online.

The mathematical model forms a vital part of soft sensor. Although the concept is not limited by the model-type, the fundamental structure of the model can have a significant impact on the accuracy and performance of the soft sensors. In a conventional outlook, based on the underlying mathematical model, soft sensors have been classified as mechanistic (white-box) or data-driven (black-box). A mechanistic or phenomenological model is based on a systematic understanding of the process kinetics. On the other hand, data-driven models are purely constructed on historical data obtained from the process. Although no clear consensus exists over the superiority of one model form over the other, researchers agree that the choice of soft sensor model should be based on the final objective, the availability of a reliable mechanistic model, accessibility to process data, and ease of implementation. The model forms for most commonly used soft sensors in WRRFs are presented in the following subsections.

### 3.1.1 Data-driven models for soft sensing

An increase in the number of online sensors and the emergence of affordable data acquisition infrastructure has resulted in an abundance of data. A data-rich environment, availability of various system-identification algorithms, and a plethora of machine-learning based systems make data-driven models an obvious choice (Pisa et al., 2019). A literature review on different types of data-driven models used for soft sensing in WWTPs is presented in (Haimi et al., 2013). Data-driven models are based on statistical correlations between easy to measure secondary variables and primary variables that are often measured using unreliable, expensive, high maintenance sensors or wet-analyzers (Abonyi et al., 2014). A systematic procedure for data acquisition, data pre-processing, model development, and deployment is presented in Figure 3.1. (Haimi et al., 2013; Budka et al., 2014). The complex structure of most black-box models such as Artificial Neural Network (ANN), Support Vector Machines (SVM), or Ensemble Tree (ET) can establish a statistically significant correlation between a wide variety of the input-output data sets.

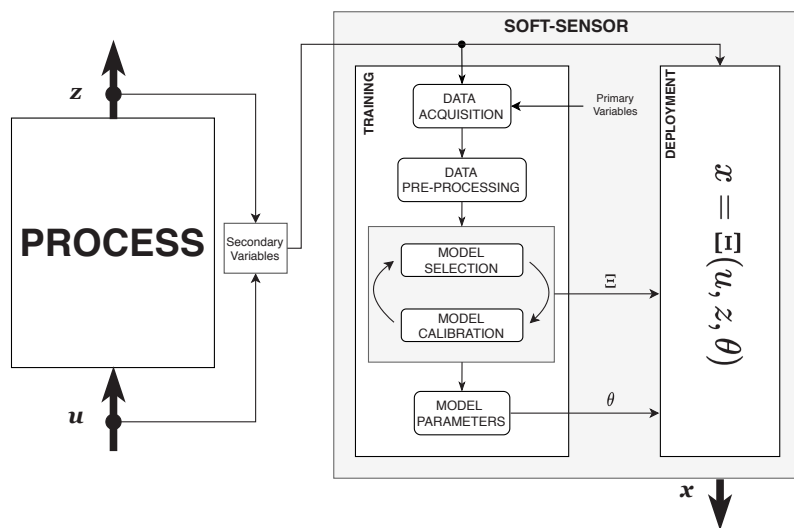


**Figure 3.1.** Soft sensor using data-driven models (redrawn from (Haimi et al., 2013)).

Black-box models also have their disadvantages. Correlations between input and output variables do not necessarily follow the principle of mass balances or maintain the stoichiometric ratios between various species in a process. Data-driven models could potentially identify correlations between variables that might not be phenomenologically connected. Black-box models also have a risk of identifying correlation that would only be pertinent to the dataset used to generate the model. Although black-box models exhibit excellent

interpolative ability, they often fail when there is a need to extrapolate beyond the data used for calibration (Glassey et al., 1994). A dependency of data-driven models on data itself without any mechanistic basis makes it vulnerable to outliers and faulty sensor data. Therefore, pre-processing and data-cleaning become a very important and time-consuming step. Data-driven models could also be rendered ineffective when faced with time-evolving process conditions (Haimi et al., 2013). The model loses its predictive capability when the plant enters a process condition which is not previously used while training the model.

### 3.1.2 Mechanistic models for soft sensing

Mechanistic models, also known as phenomenological or white-box models can be used in conjunction with dynamic state-estimation techniques to estimate difficult-to-measure parameters in WRRFs (Busch et al., 2013). Figure 3.2 presents the schematic of soft sensors based on mechanistic models (in the state-space form). Mechanistic models used in wastewater treatment were developed as a result of a substantial number of studies aimed at explaining the mechanisms of various microbial processes involved in biological nutrient removal systems. The preliminary works on modeling biological wastewater treatment began as early as the 1950s (Orhon, 1997; Brdjanovic, 2015). Since then, several experiments were conducted to acquire a deeper conceptual understanding of the processes and develop mathematical models.

The first attempt to standardize the biological nutrient removal process resulted in the Activated Sludge Model No. 1 (ASM1) (Henze et al., 1987). The ASM1 explains substrate and biomass kinetics involved in the removal of carbon and nitrogen from wastewater. Ten years later, the ASM2 (Gujer et al., 1995) and its extension ASM2d (Henze et al., 1999) were developed to describe biological phosphorus removal process. Over the last decade, the ASM models have been widely used in the design of WRRFs, assessment of operational sequences, and development of simulators. However, it is rarely used as a tool for model-based predictive control or state-estimation. A high number of state-variables (13 in ASM1 and 19 in ASM2d), necessary to describe an increasingly complex process and a comparatively lower number of available measurements can cause problems in their use for state-estimation. Although a significant increase in sensor technology and a steady drop in the price of online sensors have occurred in recent times, the observability issues in the complex ASM models still pose a challenge.

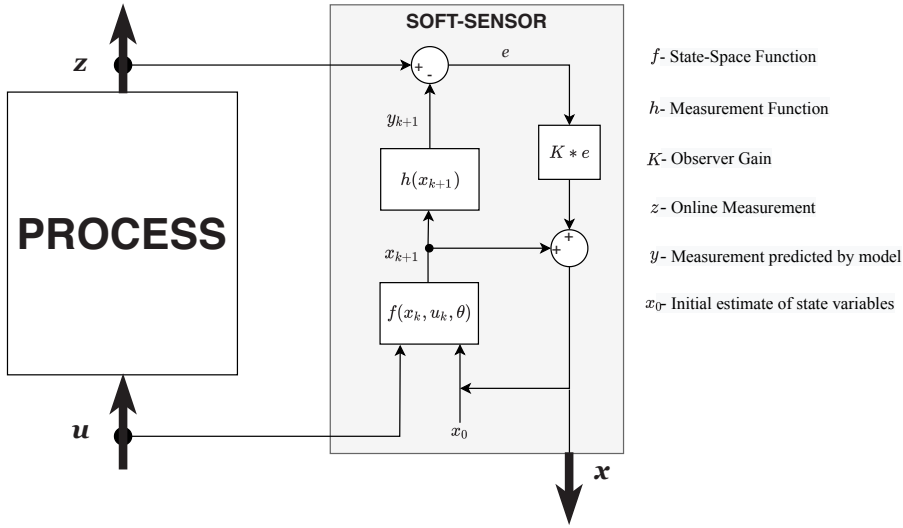


**Figure 3.2.** Soft sensor using a mechanistic models in state-space form.

### 3.2 Hybrid models for soft sensing

In reality, it is unlikely that purely, white-box or black-box would be the ultimate choice of model to be used for state-estimation. Although the ASM family of models are considered as mechanistic, they are not universal in nature (Regmi et al., 2019). In most cases, the ASMs have to be recalibrated before they can be used to represent a real treatment plant (Machado et al., 2014). On the other hand, the drawbacks of data-driven models (discussed in Section 3.1.1) have added a certain level of skepticism in their potential use as a substitute for physical sensors. As the shortcomings in black or white box models become evident, attempts have been made to use a combination of mechanistic and data-driven principles to curtail their individual disadvantages. Hybrid models, also known as grey-box models, combine the mechanistic elements of phenomenological models with data-driven techniques to obtain mathematical expressions that can be used for state-estimation (Carstensen et al., 1996; Bohlin, 2006; Sohlberg and Jacobsen, 2008). Several theoretical formulations and simulator-based studies for combining black and white box models in series and parallel are available in literature (Ahmad et al., 2020). A considerable improvement in robustness and accuracy can be expected from a model form that combines statistical regression techniques with the mechanistic understanding of the processes (Zhao et al., 2006).

### 3.3 Soft sensor algorithm

Several dynamic state estimation algorithms are available for use as soft sensors. These algorithms range from simple recursive estimators such as Kalman Filter (KF) to optimization-based approaches such as Moving Horizon Estimator (MHE). KF uses the most recent set of measurements to estimate the current state while MHE uses a moving window approach covering a fixed number of past measurements. The successful implementation of both EKF and MHE based soft sensors on several biochemical processes has been reported in literature (Robertson et al., 1996). A comparison between KF and MHE algorithms for estimating the water quality parameters in a large-scale WWTP, presented in (Busch et al., 2013), concludes that KF shows marginally better performance for some cases. Similar results are presented in (Zeng et al., 2016) demonstrating the versatility of KF in estimating the states of biological nutrient removal processes.

The KF algorithm consists of two stages: a prediction stage, where the value of the state-variable for the next time-step is predicted with the help of a mathematical model, and a measurement update stage, where the predicted state variable is corrected by considering the error between the predicted and the measured output (Chai et al., 2007). Although KF was originally designed for linear systems, several variations such as the Extended Kalman filter (EKF), Unscented Kalman Filter (UKF), and Particle Filter (PF), were introduced to expand their applicability to nonlinear systems. EKF adapts to the nonlinear systems by linearizing the model around the current estimate to obtain the linearized state (F) and output (H) matrices. The equations explaining the implementation of the EKF algorithm to estimate the states of a nonlinear model are presented in the following subsections.

#### ***Nonlinear state-space model***

The nonlinear process model (in a continuous state-space form) required to implement the EKF, is presented in Equations 3.1 and 3.2.

$$\frac{dx}{dt} = f(x, u, \theta) \quad (3.1)$$

$$y = h(x) \quad (3.2)$$

$x$  is the state vector,  $u$  is the process input,  $f$  is the nonlinear state transition function,  $h$  is the nonlinear measurement function and  $\theta$  is the model parameter vector.

### Initialization

$$\text{at } t = 0: \quad x^+ = x_0^+; \quad P^+ = P_0^+ \quad (3.3)$$

where  $x_0^+$  is the initial estimation of state variables and  $P_0^+$  is the initial estimation of auto-covariance matrix.

### Model-based prediction

The continuous state-space model (Equation 3.1) is converted to a discrete form (Equation 3.4) using explicit Euler forward method with a constant sampling time of  $T_s$ .

$$x_{k+1}^- = x_k^+ + T_s f(x_k^+, u_k, \theta) \quad (3.4)$$

$$F_k = I + T_s \left. \frac{\partial f}{\partial x} \right|_{x_k^+, u_k} \quad (3.5)$$

$$P_{k+1}^- = F_k P_k F_k^T + Q_k \quad (3.6)$$

$T_s$  is the time step and  $k$  is the discrete time-index.  $F_k$  is the linearized form of the nonlinear state space function  $f$ . The  $x_{k+1}^-$  and  $P_{k+1}^-$  are the *a priori* estimates of the state variable and the auto-covariance matrices respectively.  $Q_k$  is the covariance matrix of the process model error.

### Measurement update

$$H_k = \left. \frac{\partial h}{\partial x} \right|_{x_{k+1}^-} \quad (3.7)$$

$$K_k = P_{k+1}^- H_k^T (H_k P_{k+1}^- H_k^T + R_k)^{-1} \quad (3.8)$$

$$x_{k+1}^+ = x_{k+1}^- + K_k [z_k - h(x_{k+1}^-)] \quad (3.9)$$

$$P_{k+1}^+ = (I - K_k H_k) P_{k+1}^- \quad (3.10)$$

$H_k$  is the linearized form of the nonlinear measurement function  $h$ ,  $z_{k+1}$  is the measured variable and  $R$  is the covariance matrix of measurement noise.  $x_{k+1}^+$  and  $P_{k+1}^+$  are the *posteriori* estimates of the state variable and auto-convenience matrix respectively.  $I$  is the identity matrix and  $K_k$  is the Kalman Gain used for correcting the *a priori* estimate of state variable.



### 3.4 Standard simulator platform for WRRF

The concept of using a benchmark to objectively assess process performances and evaluate control strategies is well established within process industries (Yin *et al.*, 2012). The idea of creating a similar benchmark for WRRFs was initiated within the Scientific and Technical Research (COST) Action 682 and Action 624 and later continued as IWA Task Group on Benchmarking of Control Strategies for Wastewater Treatment Plants (Copp, 2002). The collaboration between various research groups resulted in a protocol known as the Benchmark Simulation Model No.1 (BSM1). The BSM1 provided detailed descriptions of the process model, influent wastewater characteristics and disturbances, evaluation period, and performance parameters to assess control strategies. The processes in BSM1 included a biological stage for carbon and nitrogen removal followed by a secondary clarifier for separating sludge from mixed-liquor. The biological process has an anoxic-oxic (AO) configuration described using the ASM1 (Henze *et al.*, 1987). The secondary clarifier was modeled as a 10-layer non-reactive unit and the sludge settling was described using a double-exponential settling velocity function (Takács *et al.*, 1991). The schematics of treatment process, dimensions of process equipment, and model parameters are described in the simulator manual (Copp, 2002).

The growing interest in BSM1 as an evaluation tool encouraged the research community to upgrade the BSM1 to a plant-wide level (Jeppsson and Pons, 2004). The new version intended to provide a benchmark that would represent treatment facilities not only at an individual process level but also on a plant-wide basis (Jeppsson *et al.*, 2006). The Benchmark Simulation Model No. 2 (BSM2) was created, which introduced additional nutrient removal and sludge treatment processes. The BSM2 now consisted of a primary clarifier, biological stage, secondary clarifier, sludge thickener, anaerobic digester, and sludge dewatering unit. The performance evaluation period in BSM2 was also increased to one year compared to the two weeks (dry, wet, and stormy weather) evaluation period mentioned in BSM1 (Rosen *et al.*, 2004). The dynamic influent file was also updated by using a phenomenological influent model to include more realistic diurnal and seasonal variations.

Although several new features were already available in BSM2, improvements, and updates in terms of the process models (Nopens *et al.*, 2010), evaluation criteria, and standardization of influent data (Gernaey *et al.*, 2011) file were continuously introduced. An increasing interest in phosphorus removal and recovery (both biological and chemical) in WRRF led to the use of ASM2d and the integration of physico-chemical models, to incorporate phosphorus, sulphur, and iron transformations in the BSM2 (Flores-Alsina

et al., 2016). The treatment configuration for the biological stage was changed to anaerobic-anoxic-oxic ( $A^2O$ ) process as compared to the AO process described in the preliminary versions of BSM2. The updated models in BSM2 allowed the introduction of several new processes such as phosphorus removal process through ferric dosing (Mbamba et al., 2019) and recovery of phosphorus through struvite precipitation. Extensions to the already existing models, such as pH and ion speciation (Solon et al., 2015), multiple mineral precipitation (Mbamba et al., 2016), and gas-liquid transfer (Lizarralde et al., 2015), provided by several researchers, were finally consolidated into a plant-wide model and provided in the latest version of BSM2 (Solon et al., 2017). The implementation of BSM2d is available in most commercial WRRF simulator packages such as BioWin, GPS-X, Matlab/Simulink, Simba, STOAT, WEST, etc. (Gernaey et al., 2014). The Simulink implementation of the latest BSM2 version presents a comprehensive platform to evaluate control strategies pertaining not only to removal but also recovery processes. The layout of the WRRF processes presented in the latest version of the BSM2 is presented in Figure 3.3.

## 3.5 Process optimization in WRRF

### 3.5.1 Biological nutrient removal

Biological processes form the core of most nutrient removal systems. The location of the biological stage in the latest version of BSM2 simulator is presented in Figure 3.3. The  $A^2O$  process consists of two anaerobic stages of  $1000\text{ m}^3$  each followed by two anoxic chambers of  $1500\text{ m}^3$ , and three aerobic chambers in series, each with a volume of  $3000\text{ m}^3$ . The secondary clarifier provided after the biological stage separates the sludge from mixed-liquor and recycles it back to the first anaerobic chamber. The steady-state operating values of influent flowrate  $Q_{IN}$ , internal recycle  $Q_{IR}$ , return activated sludge  $Q_R$ , and sludge wastage  $Q_W$  are mentioned in (Solon et al., 2017).

$A^2O$  is the most commonly used configuration for removing phosphorus, nitrogen, and carbon from wastewater (Ma et al., 2009). The anaerobic chambers operate without DO or  $NO_3\text{-N}$  to promote the release of phosphorus and provide a competitive advantage to the growth of phosphorus accumulating organisms (PAOs) over other microorganisms. The mixed-liquor recycle from the aerobic to anoxic chambers maintains a sufficient concentration of  $NO_3\text{-N}$  (in the anoxic chambers) necessary to achieve denitrification. The aeration is also turned off in the anoxic zones to enrich denitrifying microorganisms that use  $NO_3\text{-N}$  as electron acceptor instead of DO. During this process, the heterotrophic denitrifying biomass converts  $NO_3\text{-N}$  to  $N_2$  gas. The three aer-

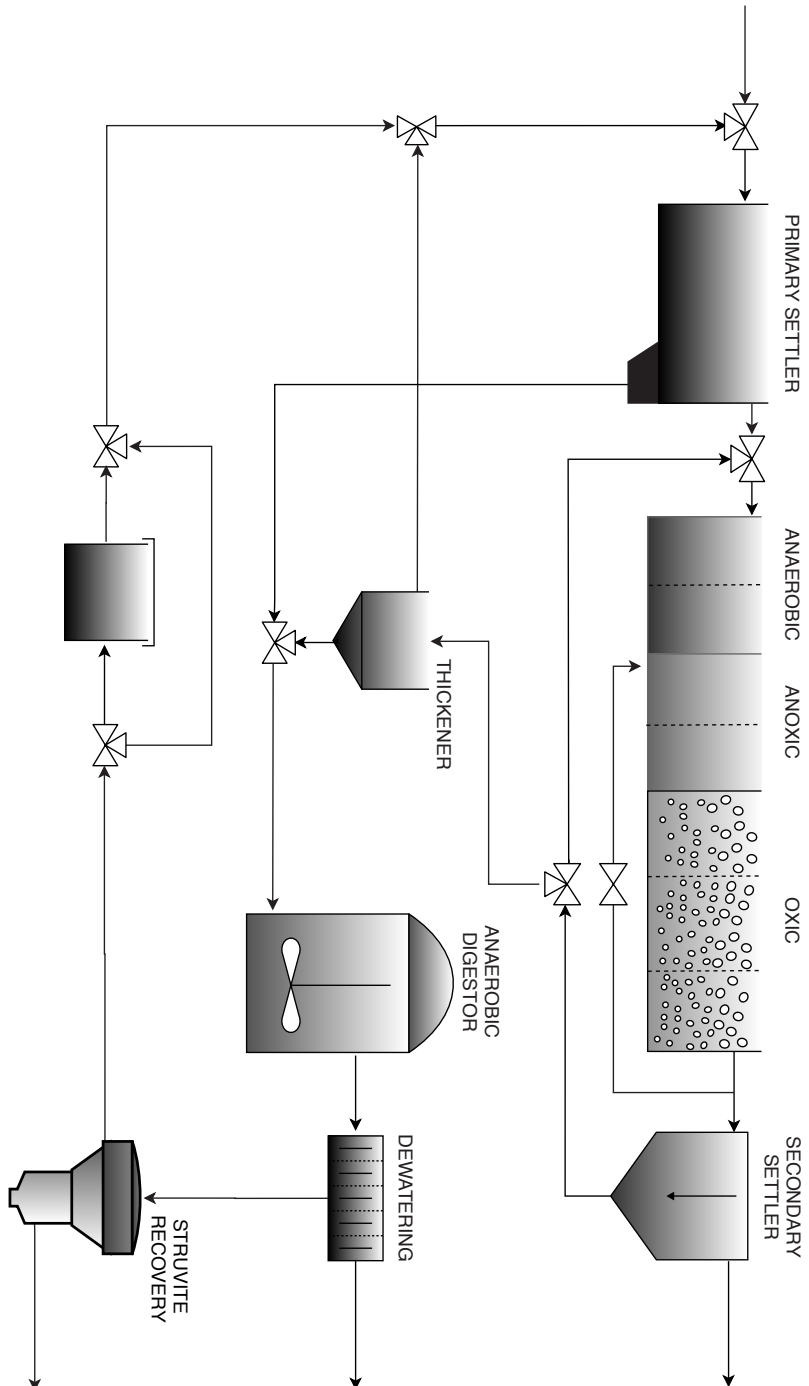


**Figure 3.3.** WRRF layout in BSM2 simulator with struvite recovery unit (redrawn from (Solon et al., 2017)).

obic chambers are aerated to ensure sufficient DO concentration for biomass growth. In this section, the autotrophic nitrifiers convert  $\text{NH}_3\text{-N}$  to  $\text{NO}_3\text{-N}$ . The rate of aeration in the aerobic chambers is controlled by changing the aeration intensity (or mass transfer coefficient)  $K_L a$  in each biological chamber. In the open-loop configuration, the aeration intensity of the first and second aerobic chambers are maintained at  $120 \text{ d}^{-1}$ , and chamber 3 has an aeration intensity of  $60 \text{ d}^{-1}$  (Nopens et al., 2010).

WRRFs have strict limits on several nutrient compositions at the effluent. The effluent ammonia nitrogen ( $S_{\text{NH},e}$ ) is one such critical parameter monitored in most WRRFs. The performance criteria in BSM2 protocol stipulates the effluent limit for ammonia to be  $4 \text{ mgN/L}$ . The  $S_{\text{NH},e}$  for the open-loop constant aeration strategy indicates that the upper limit of the effluent is violated on numerous occasions. A marginal improvement occurred by adopting DO control, which demonstrated lower violations of  $S_{\text{NH},e}$  compared to constant aeration. However, there were situations where the  $S_{\text{NH},e}$  was much lower than the effluent limit, which is a clear indication of excessive aeration.

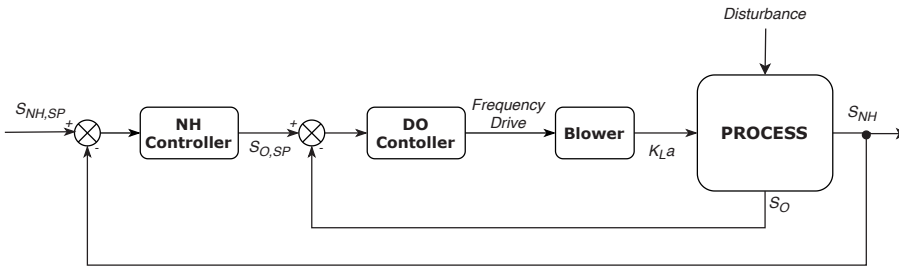
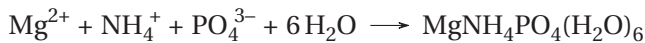


**Figure 3.4.** Schematic for feedback ammonia-based aeration control.

The ammonia-based aeration control was introduced to have better control over  $S_{\text{NH},e}$ . Real-time data from  $\text{NH}_4\text{-N}$  sensors can be used as a feedback to steer the aeration intensity in aerobic stages. The conventional strategy used for ammonia-based aeration control is based on a cascade PI algorithm (Stare et al., 2007). The cascade PI strategy uses an ammonia control in the outer loop providing set-point variations to a DO control working in the inner loop. The control loop for a cascade PI ammonia-based aeration control strategy is presented in Figure 3.4. A multiple-input-multiple-output (MIMO) control strategy (such as MPC) has the potential to further improve the aeration control (Åmand et al., 2013). However, preliminary studies have indicated a marginally lower performance of MPC when compared to feed-forward feedback PI control. The inadequacy of a linear prediction model in explaining the complex behavior of biological ammonia nitrification process could be a possible reason for the poor performance of MPC (Vrečko et al., 2011).

### 3.5.2 Nutrient recovery

Among all the resources that can be recovered from WRRF, struvite (magnesium ammonium phosphate hexahydrate) has been of special interest due to its potential applicability as a slow-release fertilizer. Struvite can be precipitated by adding magnesium hydroxide ( $\text{Mg}^{2+}$ ) to a stream rich in ammonium ( $\text{NH}_4^+$ ) and phosphate ( $\text{PO}_4^{3-}$ ) ions. Struvite is naturally precipitated in the pipelines recycling digestate from the post-digestion dewatering unit to the anaerobic stages of the biological process. A struvite recovery unit helps remove excessive ions that would otherwise precipitate in the pipeline and cause scaling. Therefore, installing a struvite recovery unit in a WRRF not only helps recover phosphorus as a commercially marketable product but also reduces the maintenance costs associated with scale removal from the pipeline. Several secondary benefits of struvite recovery, in terms of lowering the phosphorus load to the biological stages and reducing effluent phosphorus concentrations, are also reported in literature (Mbamba et al., 2016). The reaction involved in struvite precipitation is presented below.



The location of the struvite recovery unit in the latest version of the BSM2 simulator is shown in Figure 3.3. The recovery unit operates at an approximate residence time of 2h. Magnesium hydroxide is added continuously at a constant flowrate ( $Q_{\text{Mg}}$ ) of  $0.13 \text{ m}^3/\text{day}$ . A comparison between the Operational Cost Index (OCI), Effluent Quality Index (EQI), and the quantity of recovered struvite for different values of  $Q_{\text{Mg}}$  is presented in (Solon et al., 2017). The study shows a correlation between  $Q_{\text{Mg}}$  and the quantity of phosphorus recovered in the form of struvite and concludes that increasing  $Q_{\text{Mg}}$  above the limit would result in an increase in material costs without any further phosphorus recovery. Several parallel studies on identifying the optimal dosing conditions for struvite recovery process are reported in literature (Jeong and Hwang, 2005). However, most of these studies have been performed at steady-state conditions and do not account for fluctuations in the influent of the struvite recovery unit installed in a WRRF.

Dynamic variations in  $\text{NH}_4^+$  and  $\text{PO}_4^{3-}$  concentrations is a usual characteristic of the flow entering the struvite recovery unit in a WRRF. These variations could disturb the P:N:Mg ratio in the recovery unit, which plays an important role in determining the recovery percentage and the crystal properties of struvite (Marti et al., 2008). Therefore, maintaining a constant  $Q_{\text{Mg}}$  would not be the ideal operational strategy. Adopting a control strategy that would adjust the  $Q_{\text{Mg}}$  based on the influent flowrate,  $\text{PO}_4^{3-}$  concentrations, or both could potentially stabilize the process and improve phosphorus recovery.

## 3.6 Model-based optimal control in WRRF

The inherent complexities of WRRF processes and the interdependencies of various operational parameters have revealed the limitations of adopting single-input-single-output (SISO) control algorithms based on error minimization approaches (Brdys et al., 2008). The availability of better control philosophies and an increasing acceptance of advanced optimal control strategies in other process industries have encouraged water engineers to think beyond PI algorithms. Optimal control refers to control strategies that are designed to minimize a given optimization criterion or performance index. Attempts to move away from error-minimization towards optimal control resulted in the introduction of Linear Quadratic Control (LQC) (Kabouris, 1990). The use of LQC for controlling aeration and return activated sludge was demonstrated in (Marsili-Libelli et al., 1984). A comparison between decentralized PI control and an LQC for activated sludge process was reported in (Zarrad et al., 2004). LQC was also used for optimizing nitrogen removal in the denitrification process (Steffens and Lant, 1999).

Most preliminary studies on LQC did not demonstrate a significant improvement in performance. However, it presented a more straightforward possibility for tuning the final objective of the control strategy (Weijers, 2000). One of the major drawbacks of LQC is its dependency on the model, as a small deviation of the model from actual process behavior can result in a severe under-performance (Lukaskase, 1999). The problem was later solved by the introduction of receding horizon control, also known as Model Predictive Control (MPC). MPC adapts for model uncertainties by sampling the output variable at every sampling instance and updating the model states using an observer. The only drawback of an MPC compared to an LQC is the use of more computational resources. As the processing power is no longer the biggest concern, the choice of receding horizon control (MPC) as an optimal control strategy is getting more ubiquitous.

### 3.6.1 Conventional optimal control strategies

MPC has become the most preferred choice for optimal control in most process industries. A list of commercially available MPC softwares is presented in (Qin and Badgwell, 2003). The mathematical formulation of MPC is described in Equations 3.11 - 3.12. The MPC uses the state variables  $x_k$  at each sampling instance  $k$ , to estimate the outputs  $y_{k+i}$  (where  $i = 0, 1, 2 \dots N_p$ ) over a prediction horizon  $N_p$ . A series of control moves  $u_{k+i}$  along a control horizon  $N_c$  are used to calculate the optimal trajectory by minimizing an objective function  $J$ . The first control move of the optimal sequence is then applied to the

plant and the state variables are updated using the information on the new measured and disturbance variables. One of the strongest feature of MPC is the possibility to implement constraints on  $u$  and  $\Delta u$  as shown in Equations 3.11b and 3.11c.

$$\min_{u_{k+i}; i=1, \dots, N_c} J \quad (3.11a)$$

$$\text{subject to,} \quad u_{\min} \leq u \leq u_{\max}, \quad (3.11b)$$

$$\Delta u_{\min} \leq \Delta u \leq \Delta u_{\max}. \quad (3.11c)$$

where,

$$J = \sum_{i=0}^{N_p-1} \|r_{k+i} - y_{k+i}\|_{w_{sp}}^2 + \sum_{i=1}^{N_c} \|\Delta u_{k+i-1}\|_{w_{\Delta u}}^2 + \sum_{i=1}^{N_c} \|u_{k+i-1}\|_{w_u}^2 \quad (3.12)$$

The standard objective function  $J$ , used in MPC, is defined as a weighted sum of set-point error ( $r_{k+i} - y_{k+i}$ ), manipulated variable  $u_{k+i}$ , and change in control moves  $\Delta u_{k+i}$ . The terms  $w_{sp}$ ,  $w_u$ , and  $w_{\Delta u}$  are the weights associated with the control error, manipulated variable, and change in control moves respectively. Equations 3.13 and 3.14 presents the state-space form of the linear prediction model used to describe the process, where  $u_{k+i}$  is the manipulated variable,  $d_{k+i}$  is the measured disturbance.

$$x_{k+1} = A x_k + B \begin{bmatrix} u_k \\ d_k \end{bmatrix} \quad (3.13)$$

$$y_k = C x_k + D \begin{bmatrix} u_k \\ d_k \end{bmatrix} \quad (3.14)$$

Although MPC is widely used in most process industries, their implementation in WRRFs are often limited (Newhart et al., 2019). The inadequacy of linear state-space models in explaining the complex biological nutrient removal processes could be one of the reasons (Patton et al., 2000; Vrečko et al., 2011). Simplified nonlinear expressions derived from nutrient removal kinetics were also occasionally used as a prediction model for MPC (Stare et al., 2006). However, a considerable increase in computational resources for using nonlinear models compared to their linear counterparts often discourages their implementation in WRRFs.

### 3.6.2 Advanced variants of MPC

Several upgrades to the conventional MPC strategy regarding the prediction model, optimization algorithms, and improvised objective functions have been introduced over time. A detailed review of the present status and future direction of MPC has been presented in (Mayne, 2014). The advantages of two new versions of the conventional MPC are discussed in the following subsections.

#### ***Adaptive Model Predictive Control - AMPC***

One of the most widely-used methods for improving the performance of linear MPC when implemented to a time-varying system is known as the Adaptive MPC (AMPC). The AMPC uses a linear plant model form (Equations 3.13 - 3.14) as a prediction model. However, unlike the linear MPC, the AMPC uses time-varying values of A, B, C, and D matrices. A system-identification is run in parallel to the controller that provides the values of linear prediction model parameters (A, B, C, and D) to the MPC at every time step. The on-line system identifier estimates the model parameters based on the process inputs ( $u_k$  and  $d_k$ ) and outputs ( $y_k$ ) and applies them to the controller in real-time. For every change in operating condition, an approximate linear model is updated with new parameters. The real-time model update helps the MPC adjust its prediction model at run-time to compensate for nonlinear or time-varying characteristics of the system. AMPC works best for processes that do not have a reliable mathematical model.

The structure of the auto-regressive (ARX) model used to fit the input and output measurements is presented in Equation 3.15, where  $q$  is the time-shift operator,  $n_k$  is the input delay,  $na$  and  $nb$  represent the order of the polynomial vectors  $\xi(q)$  and  $\phi(q)$  respectively.

$$\xi(q)y(t) = \phi(q) u(t - n_k) + e(t) \quad (3.15)$$

where,

$$\xi(q) = 1 + a_1 q^{-1} + \dots + a_{na} q^{-na} \quad (3.16)$$

$$\phi(q) = b_1 + b_2 q^{-1} + \dots + b_{nb} q^{-(nb-1)} \quad (3.17)$$

The recursive estimation algorithm using a KF interpretation (Zhang et al., 2000) is used to estimate the model parameters. This is accomplished by expressing the ARX model as Equations 3.18 - 3.19, where  $w_k$  and  $v_k$  are white noise with covariances  $R_1$  and  $R_2$  respectively.

$$\theta_k = \theta_{k-1} + w_k \quad (3.18)$$



$$y_k = \Psi_k^T \theta_{k-1} + v_k \quad (3.19)$$

where,

$$\theta = [a_1 \ a_2 \ \dots \ a_{na} \ b_1 \ b_2 \ \dots \ b_{nb}] \quad (3.20)$$

$$\Psi_k^T = [y_{k-1} \ y_{k-2} \ \dots \ y_{k-na} \ u_{t-n_k} \ u_{t-n_k-1} \ \dots \ u_{t-n_k-nb}] \quad (3.21)$$

The KF adaptation method is described in Equations 3.22 - 3.24, where  $\hat{\theta}_k$  is the estimated parameter and  $P_k$  is the auto-covariance matrix.

$$\hat{\theta}_k = \hat{\theta}_{k-1} + K_k (y_k - \Psi_k^T \hat{\theta}_{k-1}) \quad (3.22)$$

$$K_k = P_k \Psi_k = \frac{P_{k-1} \Psi_k}{R_2 + \Psi_k^T P_{k-1} \Psi_k} \quad (3.23)$$

$$P_k = P_{k-1} + R_1 - \frac{P_{k-1} \Psi_k \Psi_k^T P_{k-1}}{R_2 + \Psi_k^T P_{k-1} \Psi_k} \quad (3.24)$$

The parameters estimated by the recursive estimator is converted to a standard state-space form using the procedure mentioned in (Ljung, 1999). The linear state-space model, thus identified, is used as the prediction model for a linear MPC. According to (Forbes et al., 2015), AMPC has been one of the most promising developments in MPC technology. Several implementations of AMPC in semiconductor manufacturing (Koo et al., 2019), heating control in building (Lindelöf et al., 2015), and temperature regulation of high-speed machine tools (Tsai et al., 2003) are mentioned in literature. Due to its ability to adapt to changing process conditions, AMPC has the potential to be used in complex biological processes constituting a WRRF.

### ***Economic Model Predictive Control - EMPC***

A variant of MPC that has recently gained popularity is the Economic Model Predictive Control (EMPC) (Forbes et al., 2015). The increasing pressure to achieve an efficient, cost-effective, and energy-positive operation has encouraged researchers to integrate economic parameters into the control strategies. A hierarchical approach is usually adopted for economic optimization of processes. In the conventional framework, a static optimization problem is solved in an upper (economics)-layer to decide the optimal operating set-points. The steady operating set-points are then maintained by a lower (control)-layer using either a conventional PI algorithm or an advanced control strategy such as MPC. EMPC combines both these layers by incorporating economic parameters in the objective function of the MPC. A systematic method for the formulation of EMPC, selecting an algorithm, and assessing the stability criteria are available in literature (Ellis et al., 2014, 2017). The standard objective function of an EMPC is presented in Equation 3.25.

$$J = \sum_{i=0}^{N_p-1} J_{\text{ECO1}} + J_{\text{ECO2}} + J_{\text{ECO3}} + \dots \quad (3.25)$$

Unlike the objective function presented in Equation 3.12 which aims at maintaining the process close to a reference point, EMPC's objective function (Equation 3.25) attempts to simultaneously minimize several economic parameters described as  $J_{\text{ECO}}$ . The objective functions can include parameters such as total production quantity, energy consumed, product quality, etc. For processes in WRRF, EMPC offers a straightforward possibility of optimizing performance parameters such as OCI, EQI, aeration energy, and percentage of effluent violations. Case studies on successful implementation of EMPC for economically optimal control of a wide variety of processes can be found in literature. (Ma et al., 2014) describes the use of an EMPC for energy and demand-minimization in a commercial building. Implementation of EMPCs in industrial processes, such as chlor-alkali process (Wang *et al.*, 2014), diesel hydro-processing (Aydn et al., 2016), ethylbenzene production (Chen et al., 2012), etc., have also been reported. EMPC have also been used to improve the operational safety of a chemical process by including a mathematical formulation of safety-criteria and operational limits in the objective function (Albalawi et al., 2017). In the wastewater treatment process, a few simulator-based evaluations of EMPC on the BSM1 has been reported (Zhang et al., 2019). However, EMPC implementations for the recovery processes described in updated BSM2 are rarely reported in literature.

# Chapter 4

## Research Methodology

An overview of the research methodology used to develop and validate the hybrid soft sensors and the advanced control strategies are presented in this chapter. Sections 4.1 to 4.5 sequentially enumerate the steps followed in order to construct, calibrate, deploy, and evaluate the hybrid soft sensors explained previously in Sections 3.2 and 3.3. The mathematical expressions defining the state-space and measurement models are presented in Section 4.1. The experimental set-up and the model calibration method used to obtain the parameters of the hybrid model are discussed in Section 4.2. Section 4.3 explains the importance of simulator-based evaluation and an overview of the procedure followed to tune the EKF parameters. A description of the pilot-scale processes used to evaluate the soft sensors is presented in Section 4.4. This section also presents the online monitoring and data acquisition systems and explains the two different deployment strategies used to implement the hybrid soft sensors in the pilot-scale treatment facilities. The methods used to evaluate the accuracy and robustness of the soft sensors and the lab-equipment used to measure water quality parameters are explained in Section 4.5.

A description of the basic and advanced control strategies used to optimize biological nutrient removal is presented in Section 4.6. The section also presents the modified objective function and explains the different prediction models used in the advanced MPC strategy. Section 4.7 explains the control strategies used to optimize the struvite precipitation process. The schematics of EMPC strategy, formulation of an economic objective function, and the procedure used to evaluate the influence of time-varying economic parameters are presented in this section. Details regarding the standard simulator platform, the toolboxes used to configure different MPCs, and the systematic procedure to evaluate control strategies are explained in Section 4.8.

## 4.1 Model development

### 4.1.1 Selecting state-variables and state-space equations

The number of state-variables in the soft sensor model is an important factor. Overly simplified models could fail to explain the inherent complexities of biological processes. On the other hand, extremely complex models can render it unusable for state estimation. Model order-reduction is a well-known approach to simplify the existing mechanistic models to render it observable (Jeppsson and Olsson, 1993; Julien et al., 1998). The state-variables are selected such that it adequately explains the dynamics of the process without compromising model observability. Simplified models are constructed using mass balances of various species in the reaction chambers. The Monod's substrate degradation kinetics, simplified with a few practical assumptions, are adopted in these models (Zhang et al., 2010; Cadet, 2014; Li et al., 2018). Details regarding the model simplification strategies for two different processes are described in **Paper A** and **Paper B** respectively.

### 4.1.2 Selecting measurement equations

The mechanistic ASM models explain the kinetics of substrate degradation, biomass kinetics, and particulate hydrolysis. However, they do not include correlations between nutrient composition and easy-to-measure parameters such as pH, electrical conductivity (EC), or ORP. Extensions of the original ASM models were created to incorporate EC and pH measurements (Aguado et al., 2006; Serralta et al., 2004). However, in both these cases, the correlation was achieved by incorporating additional chemical species that further increase the number of state variables in the extended mechanistic model. Therefore, a simpler data-driven approach is chosen to regress the state-variables selected in section 4.1.1 and the measurements from the online sensors. The following generic equation form is used to describe the correlation.

$$y = \alpha_0 + \sum_{i=1}^N \alpha_i x_i + \sum_{i=1}^N \beta_i x_i^2 + \sum_{i=0}^{N-1} \sum_{j=i+1}^N \gamma_{i,j} x_i x_j \quad (4.1)$$

In equation 4.1,  $x_i$  is a state variable that influences the physical measurements.  $\alpha_0$  is the constant parameter,  $\alpha_i$  is the linear parameters,  $\beta_i$  is the squared parameters, and  $\gamma_i$  is the binary interaction parameters of the regression model. Similar model structures have been previously used in several processes to identify a statistically significant correlation between various parameters (Wei and Ratnaweera, 2016). Correlation between several ionic species and pH is described in **Paper A**, whereas **Paper B** uses a similar model structure to explain a correlation between  $\text{PO}_4\text{-P}$ , sCOD, and EC.

## 4.2 Offline estimation of model parameters

A simplified reduced-order model entails several approximations imposed on the original biochemical kinetics mentioned in (Henze et al., 1999). Therefore, the stoichiometric and kinetic parameters mentioned in the original ASM models cannot be used directly in the simplified version. Model calibration is necessary to obtain the updated parameters of the simplified model.

### 4.2.1 Experimental study

A batch kinetic experiment is designed where the biomass and raw wastewater are mixed in the same condition as found in the continuous treatment process. Samples are collected at regular intervals and water quality parameters are measured using standardized lab tests. Simultaneously, online sensors are used to monitor the changes in physical parameters such as pH, DO, or EC. A detailed description of the experimental set-up and procedures used to obtain data for model-calibration are presented in **Paper B**. For the SBR process, presented in **Paper A**, the data required for model calibration are collected during a regular operational cycle.

### 4.2.2 Model calibration

The batch-optimization procedure using the minimization of quadratic-error function (Marsili-Libelli et al., 2001; Nair et al., 2017), is used to fit the model and obtain the stoichiometric and kinetic parameters. The mathematical formulation of the optimization problem is presented in Equations 4.2.

$$\min_{\theta} \sum_{i=1}^N \|\varphi_{\text{Model}}(\theta) - \varphi_{\text{Experiment}}\|^2 \quad (4.2a)$$

$$\text{subject to,} \quad lb \leq \theta \leq ub \quad (4.2b)$$

In Equations 4.2,  $\theta$  is a vector consisting of model parameters to be estimated,  $ub$  and  $lb$  are the upper and lower bounds of the parameter vector, and  $N$  is the number of data-points obtained from the batch kinetic experiments. The objective function is defined as the least-square error between the experimental data  $\varphi_{\text{Experimental}}$ , and their corresponding values predicted by the model  $\varphi_{\text{Model}}$ . The optimization problem is solved using 'fmincon' function, provided as a part of MATLAB's Optimization Toolbox. Details regarding the choice of  $ub$  and  $lb$ , and the initial estimates of the parameter vector ( $\theta_0$ ) are presented in **Paper A** and **Paper B**. MATLAB's Regression Learner App is used to identify the correlation between the state-variables and the online sensor data, and obtain the parameters mentioned in Equation 4.1.

### 4.3 Simulator based evaluation and tuning of EKF parameters

A simulator-based evaluation is essential before real-time deployment of the EKF based soft sensor (Haugen et al., 2014). The evaluation helps identify the appropriate tuning parameters that would result in a reasonably good correction of the model states. The mathematical model and the EKF are implemented in a simulation platform (MATLAB in **Paper A** and Python in **Paper B**). The implementation schematic is presented in Figure 4.1.

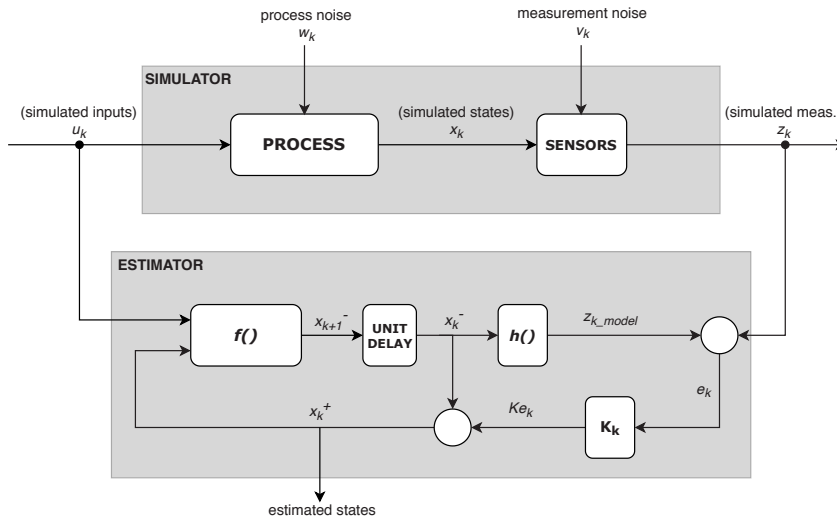


**Figure 4.1.** Schematic for simulator-based evaluation of soft sensor.

The block mentioned as 'simulator' is the mathematical model, and the algorithm for state-estimation (EKF) is shown as 'estimator' in Figure 4.1. Random noises  $w_k$  and  $v_k$  were added to the process and measurement models respectively, to introduce the phenomenon of sensor-noise and plant-model-mismatch. At  $t = 0$  the simulation is initialized with different values of estimated ( $x_0^+$ ) and simulated ( $x_0$ ) state variables. The values of simulated state-variables were compared to the estimated values in real-time to study the ability of EKF to track the actual values. The tuning parameters  $x_0^+$ ,  $P_0^+$ ,  $Q$ , and  $R$  play an important role in the performance of the EKF. Although some guidelines for tuning EKF parameters are suggested in (Simon, 2006), in practical applications, some trial-and-error combined with operational knowledge of the process would be necessary. A practical approach is adopted, following the guidelines mentioned in (Haugen et al., 2014), to tune the EKF parameters in **Paper A**, **Paper B**, and **Paper C**.

## 4.4 Pilot-scale implementation

After tuning the EKF parameters to achieve satisfactory performance during the simulator-based evaluation, the soft sensor is implemented in the pilot plant. Details regarding the pilot plant operations and the surveillance rig used to deploy the soft sensors are presented in the following sections.

### 4.4.1 Processes for soft sensor evaluation

Two different pilot-scale treatment units are chosen to test and evaluate the hybrid soft-sensing methods explained in Section 3.3. The pilot plants are located at the wastewater lab of the Norwegian University of Science and Technology (NTNU) in Trondheim, Norway. The wastewater necessary for operating the pilot plant is received from a nearby sewer. The wastewater undergoes a preliminary mechanical treatment using a fine sieve before the biological nutrient removal stages.

#### *Sequential batch MBBR pilot plant - Paper A*

The pilot plant described in **Paper A** is a Sequential Batch MBBR (SB-MBBR) process designed to remove COD,  $\text{PO}_4\text{-P}$ , and  $\text{NH}_4\text{-N}$  from municipal wastewater. Figure 4.2 presents the plant layout and data-acquisition system.

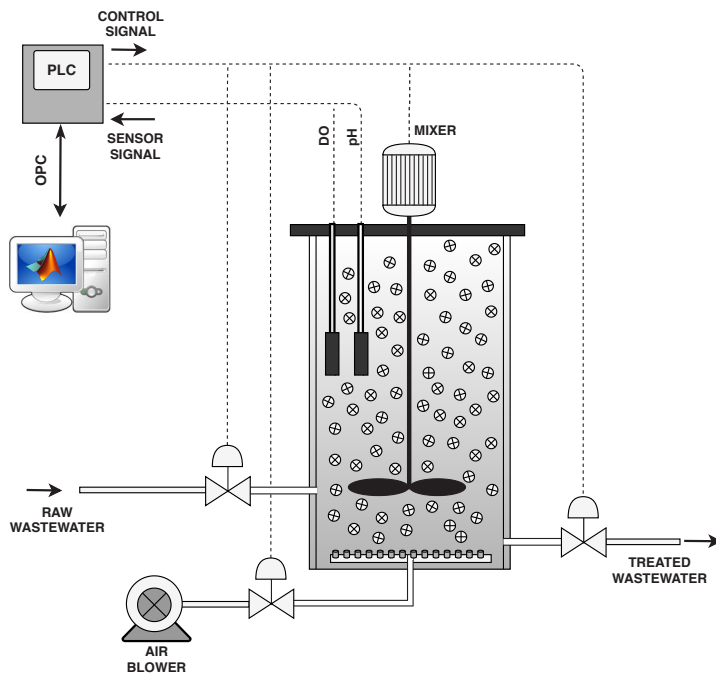


**Figure 4.2.** Plant layout and data acquisition system of SB-MBBR pilot plant.

The SB-MBBR has a working volume of 13 liters and contains polyurethane carriers (Kaldness K1) at 60% filling volume. A mechanical agitator ensures sufficient mixing of the carriers and wastewater in the reactor. The SB-MBBR operates with a fixed cycle time of 485 minutes, distributed as 3 minutes filling, 180 minutes anaerobic stage, 300 minutes aeration, and 2 minutes emptying. The carrier media with the active biomass is retained in the SB-MBBR using a sieve, installed in the effluent line. Since all the active biomass is retained in the reactor, the SB-MBBR can be operated with a 100% volume exchange ratio, resulting in a cycle time equal to the hydraulic retention time. The SB-MBBR is equipped with online sensors to monitor pH and DO concentrations. A description of the biological processes occurring at different stages of the SB-MBBR is presented in **Paper A**.

### ***Continuous Multi-stage MBBR pilot plant - Paper B***

The pilot plant described in **Paper B** is a Continuous Multi-stage MBBR (CM-MBBR) designed to achieve biological phosphorus removal in a biofilm process (Saltnes et al., 2017). The reactor has 10 chambers, each with a working volume of 0.1 m<sup>3</sup>. The CM-MBBR contains the standard biofilm carriers (Kaldnes K1) with 60% filling in each of the chambers. The walls separating each chamber have an opening that allows wastewater and carriers to flow between them. The rate of flow of carriers along the chambers can be controlled by adjusting the size of the opening on separator walls. The anaerobic chambers are equipped with mechanical agitators to ensure sufficient mixing of the carriers and wastewater. A conveyor belt is installed in the CM-MBBR to transport carriers from the last aerobic zone to the first anaerobic zone. The pilot plant layout and online monitoring system are presented in Figure 4.3.

The CM-MBBR is equipped with EC sensors at the influent, Chamber 1, and Chamber 3. The pilot plant also has DO sensors in all seven aerated chambers and an ISE NH<sub>4</sub>-N sensor at chamber 10. Control valves are installed in the air inlet of each chamber to adjust the rate of aeration. The aeration control valves provide operational flexibility to create anoxic or anaerobic conditions by shutting off the air supply to that particular chamber. During normal operating conditions, aeration is shut-off in the first three chambers, whereas chambers 5 to 10 are aerated. The aeration in Chamber 4 is used as a manipulated variable to manually control the anaerobic/aerobic residence time in the pilot plant. In situations with low influent phosphorus load, aeration is shut-down to have higher anaerobic cycle time. The average values of raw and treated wastewater in the pilot plant and the biological processes occurring in different chambers of the CM-MBBR are presented in **Paper B**.





Figure 4.3. Plant layout and online monitoring system in the continuous multi-stage MBBR pilot plant.

## 4.4.2 Surveillance infrastructure and deployment strategy

The online sensors, flow control valves, and variable-frequency drives installed in the pilot plant are connected to a SCADA system provided by a Norwegian supplier DOSCON ([www.doscon.no](http://www.doscon.no)). DOSCON's remote surveillance capabilities allow plant operators to access sensor data from a remote location. Possibilities are explored, to deploy soft sensor scripts written in popularly used programming languages such as MATLAB or Python, without having to write them in the SCADA provider's proprietary programming suite. The details of two possible deployment options are enumerated in the following subsections.

### ***OPC and MATLAB***

The pilot plant's SCADA provides an Open Platform Communication - Data Access (OPC-DA) server, which enables connection with other devices through the OPC protocol. The OPC-DA server can be accessed remotely with a secure Virtual Private Network (VPN) tunnel provided by Insys ([www.insysicom.com](http://www.insysicom.com)). MATLAB's OPC Toolbox provides functions to access live and historical data from an active OPC-DA server. A communication layer is developed to read data from the server to the MATLAB workspace. The communication layer is then integrated with the soft sensor script (also written in MATLAB) and deployed in a remote machine. The script reads the latest values of measurement variables ( $z_k$ ), input variables ( $d_k$  and  $u_k$ ), and the estimated states of previous time-step  $x_k$  from the server. The soft sensor then calculates the updated estimate of state variable  $x_{k+1}$  and the auto-covariance matrix  $P_{k+1}$  following the sequence described in Section 3.3.

### ***SQL and Python***

The second option uses an IoT gateway, which forms an interface between the SCADA and a remote MySQL server. The MySQL server is made accessible over the internet using a Dynamic DNS (DDNS) service. The soft sensor algorithm is written as a Python script, which is then deployed on a single board computer – Raspberry Pi (RPI). The IoT gateway at the pilot plant collects data from online sensors and inserts them as a new row in a table created in the remote MySQL server. The client running the EKF code (in the RPi) begins the cycle by reading the last row of the table. This table consists of the estimated states  $x_k$ , the covariance matrix of estimation error  $P_{k+1}$ , measurements from online sensor  $z_k$ , and input variable  $u_k$  and  $d_k$ . The soft sensor then calculates new values of the estimated state  $x_{k+1}$  and covariance matrix of estimation error  $P_{k+1}$ . The updated values are inserted as a new row in the MySQL table.

## 4.5 Evaluating soft sensor performance

The performance of the soft sensor is assessed by comparing the estimated values with the corresponding water-quality measurements obtained from standardized lab tests. In addition to the accuracy of the estimated values, the robustness of soft sensor has also been evaluated.

### 4.5.1 Short-term performance evaluation

In a short-term evaluation, grab samples are collected more frequently for a shorter evaluation period and compared to the values estimated by the soft sensor. In the SB-MBBR process in **Paper A**, samples were collected once every 30 minutes for a period of eight hours (one complete SBR cycle). For the CM-MBBR process described in **Paper B**, samples were collected once every day for an evaluation period of ten days. The values estimated by the soft sensor were logged in the plant's SCADA system and can be retrieved using a web-based interface.

### 4.5.2 Long-term performance evaluation and recalibration

The phenomenon of sensor drift and the importance of sensor calibration is well-known (Tscheikner et al., 2016). To assess the stability of the hybrid soft sensors, the estimated values are regularly observed for a longer duration of 2-3 months. During this period, the biweekly measurements of water quality parameters in the influent of the CM-MBBR pilot plant are compared with the water-quality parameters estimated by the soft sensor. The long-term evaluation provides information on the frequency at which the soft sensors should be calibrated. Specific details regarding the calibration frequency, possible reasons for the drift, the model parameters causing the plant-model mismatch are provided in **Paper B**. An alarm is created in the plant's SCADA, which prompts the operator to calibrate the soft sensor model when the difference between the estimated and the measured value is more than 50%. **Paper B** also describes the procedure for recalibrating the hybrid soft sensor and updating the measurement model. The estimated values of both calibrated and uncalibrated soft sensors are logged in the plants SCADA for comparison.

### 4.5.3 Lab measurements

The measurement of sCOD,  $\text{NH}_4\text{-N}$ ,  $\text{NO}_3\text{-N}$ , and  $\text{PO}_4\text{-P}$  are performed according to the procedures outlined in the Standard Methods (APHA, 2012). The water-quality parameters are measured using the Hach-Lange kits LCI400/LCK314 for sCOD, LCK 350/348 for  $\text{PO}_4\text{-P}$  LCK303/304  $\text{NH}_4\text{-N}$ , LCK339/340 for  $\text{NO}_3\text{-N}$ , and Hach Lange DR 1900 spectrophotometer.

## 4.6 Control strategy for nutrient removal

The potential of aeration control in improving the WRRF's nutrient removal process is already discussed in Section 3.5.1. The following section presents the basic and advanced control strategies evaluated in this thesis.

### 4.6.1 Basic control strategies

Understanding the performance of conventional control strategies based on PI algorithm is essential before comparing them to advanced control strategies. Figure 4.4 presents the two different conventional aeration control strategies implemented in WRRF.

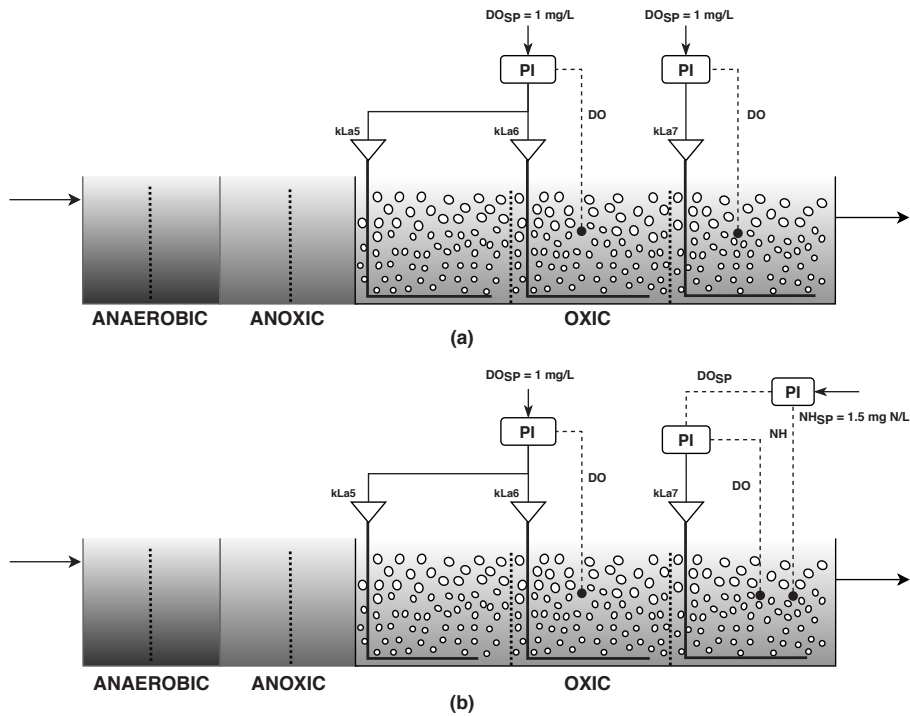


**Figure 4.4.** Conventional aeration control **a.** DO control **b.** PI-NH cascade control.

The DO control (Figure 4.4a) consists of two PI controllers maintaining DO set-point of 1 mg/L in chamber 4 (by manipulating  $K_{La5}$  and  $K_{La6}$ ) and chamber 7 (by manipulating  $K_{La7}$ ). The strategy presented in (Figure 4.4b) is an ammonia-based aeration control, consisting of a PI-NH cascade control strategy (Figure 3.4) to maintain  $NH_4\text{-N}$  concentration of 1.5 mg N/L in chamber 7 and a PI controller to maintain DO concentration of 1 mg/L in chamber 6.

## 4.6.2 Advanced MPC strategy

The control structure for ammonia-based aeration control in the aerobic chambers of the biological nitrification system using an MPC is presented in Figure 4.5. The advanced control strategy consists of a cascade ammonia MPC in the outer loop, providing DO set-points to two slave DO controllers in the inner loop. The DO controllers (using a PI algorithm) in the inner loop maintain the DO set-point by manipulating the aeration intensity  $K_L a_5$  and  $K_L a_6$  for chamber 6 and  $k_L a_7$  for chamber 7. The MPC decides on the optimal DO set-points by utilizing the real-time data from DO sensors in chambers 6 and 7, ammonia sensor in the chamber 7, and the flow sensor in the influent of the biological units.

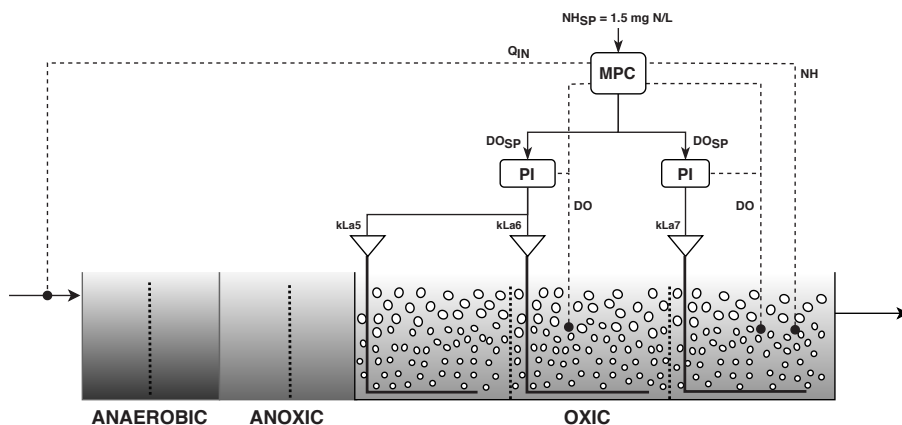


Figure 4.5. Advanced aeration control based on MPC.

### Objective function

The standard MPC objective function presented in Equation 3.12 is modified to include a term that exponentially increases when the ammonia concentration in chamber 7 approaches an upper limit ( $UL$ ). The modified objective function for the MPC strategy is presented in Equation 4.3.

$$J = \sum_{i=0}^{N_p-1} \|r_{k+i} - y_{k+i}\|_{w_{SP}}^2 + \left\| \frac{1}{UL - y_{k+i}} \right\|_{w_L}^2 + \sum_{i=1}^{N_c} \|\Delta u_{k+i-1}\|_{w_{\Delta u}}^2 + \sum_{i=1}^{N_c} \|u_{k+i-1}\|_{w_u}^2 \quad (4.3)$$

The significance of each term in the objective function is decided by adjusting the values of weight factors  $w_{SP}$ ,  $w_L$ ,  $w_{\Delta u}$ , and  $w_u$ . In MPC, the reference set-point of ammonia  $r_{k+i}$  is 1.5 mgN/L and the  $UL$  is chosen as the ammonia effluent violation limit  $C_{NH_e,lim} = 4$  mgN/L provided in (Nopens et al., 2010).

### **Prediction models**

The relevance of prediction models and the different model types used in MPCs are explained in Section 3.6.2. In this regard, three types of MPCs based on different prediction model types, called Linear MPC (LMPC), Adaptive MPC (AMPC), and Nonlinear MPC (NLMPC), are selected for comparison.

The **LMPC** consists of a time-invariant linear prediction model, where the linear model parameters stay constant during the entire evaluation period. The parameters of the linear prediction model are obtained by regressing the data from the open-loop BSM2 simulations with the dynamically changing influent file provided in (Gernaey et al., 2011). The `n4sid` function provided as a part of MATLAB's System Identification Toolbox is used to fit the simulation data and obtain the model parameters. The `n4sid` function can also be used to provide the ideal number of state variables by comparing the Hankel singular values for each state in the linear model (Boyd et al., 1994).

The **AMPC** uses the same model form as the LMPC. A recursive model parameter estimator is combined with the LMPC, which updates its prediction model in real-time. The algorithm used to recursively obtain the linear model parameters at every time-step is described in Section 3.6.2.

The **NLMPC** employs a nonlinear prediction model, derived from the biological ammonia nitrification kinetics described in the ASM2d model (Henze et al., 1999). The mathematical expression for the nonlinear prediction model is derived by performing a mass balance of  $\text{NH}_4\text{-N}$  transformations in the aerobic stages of the biological nutrient removal process.

$$S_{\text{NH}6,k+1} = S_{\text{NH}6,k} + T_s \left[ \frac{Q}{V} (S_{\text{NH}5,k} - S_{\text{NH}6,k}) - \mu \frac{S_{\text{O}6,k}}{K_{\text{O}} + S_{\text{O}6,k}} \frac{S_{\text{NH}6,k}}{K_{\text{NH}} + S_{\text{NH}6,k}} \right] \quad (4.4a)$$

$$S_{\text{NH}7,k+1} = S_{\text{NH}7,k} + T_s \left[ \frac{Q}{V} (S_{\text{NH}6,k} - S_{\text{NH}7,k}) - \mu \frac{S_{\text{O}7,k}}{K_{\text{O}} + S_{\text{O}7,k}} \frac{S_{\text{NH}7,k}}{K_{\text{NH}} + S_{\text{NH}7,k}} \right] \quad (4.4b)$$

In the Equations 4.4a and 4.4b,  $S_{\text{NH}i,k}$  ( $i = 5, 6, 7$ ) is the ammonia concentration in the aerobic chamber  $i$  at time instance  $k$ ,  $Q = Q_{\text{IN}} + Q_{\text{R}} + Q_{\text{IR}}$  is the volumetric flow-rate entering the aerobic unit,  $V$  is the volume of each aerobic reactor,  $\mu$  is the nitrification rate constant,  $K_{\text{O}}$  and  $K_{\text{NH}}$  are the Monod's half-saturation coefficients. The data that were previously used to calibrate the linear prediction model were also used to obtain the Monod's kinetic terms  $K_{\text{NH}}$  and  $K_{\text{O}}$  of the nonlinear prediction model. The time-varying reaction rate parameter  $\mu$  and the ammonia concentration in chamber 5 are modeled as random-walk and included as state variables in the model. An EKF is used to estimate the state variables, including the augmented states ( $x = [S_{\text{NH}5} \quad S_{\text{NH}6} \quad S_{\text{NH}7} \quad \mu]$ ) of the nonlinear nitrification model.

## 4.7 Control strategy for nutrient recovery

The struvite precipitation process described in Section 3.5.2 employs a constant magnesium hydroxide dosing strategy ( $Q_{Mg} = 0.13 \text{ m}^3/\text{day}$ ). The constant  $Q_{Mg}$  dosing scenario is used as a reference to compare basic and advanced control strategies presented in the following sections.

### 4.7.1 Feed forward flow proportional control strategy

The basic form of dosing control strategy adopted in most WRRFs is a feed-forward flow proportional control (Ratnaweera and Fettig, 2015). The control schematic of the basic strategy is presented in Figure 4.6a. In a flow proportional control,  $Q_{Mg}$  is proportional to the flowrate of supernatant ( $Q_{IN}$ ) entering the struvite recovery unit. A feed-forward proportionality constant  $K_P = 0.000675$  is provided to the controller.

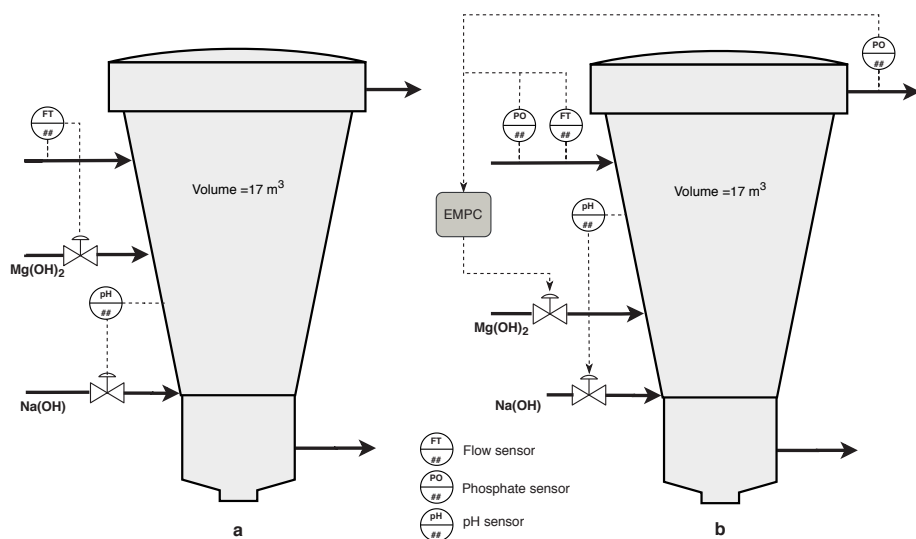


**Figure 4.6.** Control schematic for struvite recovery unit **a.** feed forward flow proportional control **b.** EMPC.

### 4.7.2 Advanced EMPC strategy

The control schematic of an advanced control strategy for struvite recovery unit is presented in Figure 4.6b. The  $Q_{Mg}$  values are calculated by an EMPC, using real-time information from the influent phosphate sensor ( $PO_{4,IN}$ ), effluent phosphate sensor ( $PO_{4,OUT}$ ), and an influent flow-sensor ( $Q_{IN}$ ). The

objective function for the EMPC strategy, presented in Equation 4.5a, includes economic parameters associated with struvite recovery unit.

$$\min_{u_{k+i}; i=1, \dots, N_c} \sum_{i=0}^{N_p-1} J_{\text{production}} + J_{\text{Material}} \quad (4.5a)$$

$$\text{where, } J_{\text{production}} = (PO_{4,\text{IN}} - PO_{4,\text{OUT}}) Q_{\text{IN}} \Phi_{\text{STR}} \quad (4.5b)$$

$$J_{\text{Material}} = Q_{\text{Mg}} M.W_{\text{Mg}} \rho_{\text{Mg}} \Phi_{\text{Mg}} \quad (4.5c)$$

In Equations 4.5a, 4.5b, and 4.5c,  $PO_{4,\text{OUT}}$  is the phosphate concentration in the overflow from the crystallizer,  $PO_{4,\text{IN}}$  is the phosphate concentration in the influent,  $Q_{\text{IN}}$  is the flowrate of supernatant to the crystallizer,  $M.W_{\text{Mg}} = 24.3 \text{ kg/kmol}$  is the molecular weight of magnesium and  $\rho_{\text{Mg}} = 25 \text{ kmol/m}^3$  is the molar density of the magnesium hydroxide solution dosed in the recovery unit.  $\Phi_{\text{STR}}$  is the market price of recovered phosphorus in the form of struvite and  $\Phi_{\text{Mg}}$  is the market price of magnesium hydroxide used in struvite production.

### Variations in price of struvite

To study the influence of introducing price factors ( $\Phi_{\text{STR}}$  and  $\Phi_{\text{Mg}}$ ) in the EMPCs objective function, a hypothetical scenario is considered, where the cost of struvite ( $\Phi_{\text{STR}}$ ) is changed once every 30 days. The values of ( $\Phi_{\text{STR}}$ ) is randomly selected between the range  $\Phi_{\text{STR}, \text{MIN}} = 7.5$  and  $\Phi_{\text{STR}, \text{MAX}} = 9.5$  in the first day of every month. It should be noted that these prices are mere representative values taken from literature (Solon et al., 2017) and do not reflect the exact price of struvite or magnesium hydroxide in the market. The price variations are presented in Figure 4.7.

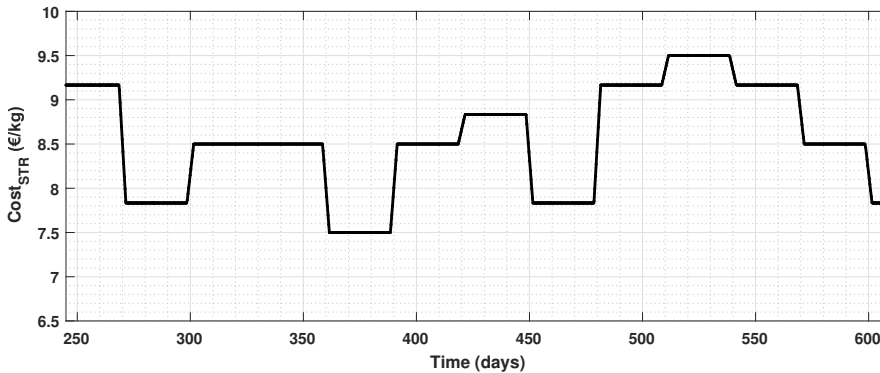


Figure 4.7. Monthly variations in the price of struvite.



## 4.8 Simulation procedure

Simulink is a graphical programming environment provided as a part of the MATLAB package. Simulink is widely used in designing automatic control and digital signal processing for dynamic systems. The implementation of BSM2 in a Simulink environment is available in literature (Solon et al., 2017). The control strategies for biological nutrient removal and nutrient recovery, described in Sections 4.6 and 4.7 are built on the base open-loop Simulink file. Simulink provides several inbuilt toolboxes to implement advanced control strategies described in Section 3.6.2. The linear, nonlinear, and adaptive MPC blocks, presented as a part of Simulink's Model Predictive Control Toolbox, are used in the control strategies explained in Sections 4.6.2 and 4.7.2. The MPC blocks also provide the possibility of implementing customized objective functions for the EMPC strategy, as explained in Equation 4.5. The System Identification Toolbox in Simulink is also used extensively in the simulations. The recursive polynomial model estimator block is combined with the ARX to SS model converter block to provide real-time estimates of the linear state-space model parameter for the AMPC. The EKF block in Simulink is used to estimate the states of NLMPC's nonlinear prediction model. The standard procedure for executing the simulations is provided in the BSM2 simulator manual (Jeppsson et al., 2007). The following steps are followed while executing the BSM2 simulations and subsequently evaluating the control strategies.

1. Initialize the process models and control states in the simulator with the default values provided in the simulator.
2. Simulate 300 days forward using the constant influent data.
3. Initialize the simulator and controller states with the final values of the steady-state simulation. This allows the next simulation (with dynamic influent data) to begin at the exact position where the steady-state simulation previously ended.
4. Simulate the model with the dynamic influent file for 609 days.
5. The data from the dynamic simulation is stored in MATLAB workspace.
6. Utilize the data recorded from T=245 day to T=609 days to assess the performance parameters.

Several performance indices for evaluating the control strategies are provided in (Jeppsson et al., 2007; Nopens et al., 2010). A description of the evaluation criteria used to compare the control performances are provided in **Paper C** and **Paper D**, respectively.



# Chapter 5

## Results and Discussion

The following chapter gathers the results presented in **Paper A**, **Paper B**, **Paper C**, **Paper D**, and **Paper E**. The results of the experiments conducted for the purpose of calibrating the simplified hybrid model of a sequential batch and a continuous multi-stage configuration is presented in Section 5.1. The performance evaluation of soft sensors used to estimate water-quality parameters in SB-MBBR and CM-MBBR pilot plants are presented in Sections 5.2.1 and 5.2.2, respectively. Section 5.3 shows the robustness assessment of the hybrid soft sensors. The reason for drift in soft sensor estimations, the factors influencing plant model mismatch, a strategy to update the model parameters using lab measurements, and the effect of recalibration strategy on soft sensor performance are presented in this section. A comparison between different deployment options based on the installation cost is presented in Section 5.4. The economic benefits of using soft sensors and the open-source IoT strategy are also discussed.

The advantages of adopting advanced optimal control strategies are presented in the subsequent sections. Section 5.5 presents a quantitative assessment of the MPC strategy as compared to the conventional DO control or PI-NH cascade control strategy used for ammonia-based-aeration control in a biological nutrient removal process. The performance evaluation of different MPC strategies based on different prediction models is also presented in this section. The effect of implementing an EMPC strategy in a struvite recovery process, when compared to constant dosing or a feed-forward flow proportional control is explained in Section 5.6. The section also presents the influence of the time-varying market price of struvite on the performance of the EMPC control strategy.

## 5.1 Validating hybrid models

Following the guidelines presented in Sections 4.1 and 4.2, two different hybrid models are developed. The mathematical model for the SB-MBBR process in **Paper A** explains the kinetics of phosphorus release in anaerobic stages, phosphorus uptake in the aerobic stage, and the aerobic nitrification of  $\text{NH}_4\text{-N}$  to produce  $\text{NO}_3\text{-N}$ . The CM-MBBR model is constructed using the mass balances of sCOD and  $\text{PO}_4\text{-P}$  in the anaerobic stages of the pilot plant. A simplified Monod's kinetic expression is used to describe the uptake of carbon source and release of phosphorus in the CM-MBBR process described in **Paper B**. A separate model is developed in **Paper C** to explain the biological nitrification process in the aerobic chambers of CM-MBBR. A detailed explanation regarding the choice of state variables, kinetic and stoichiometric parameters of the state-space model, measurement model parameters, and the strategies used for simplifying the Monod's kinetic terms are explained in their corresponding papers.

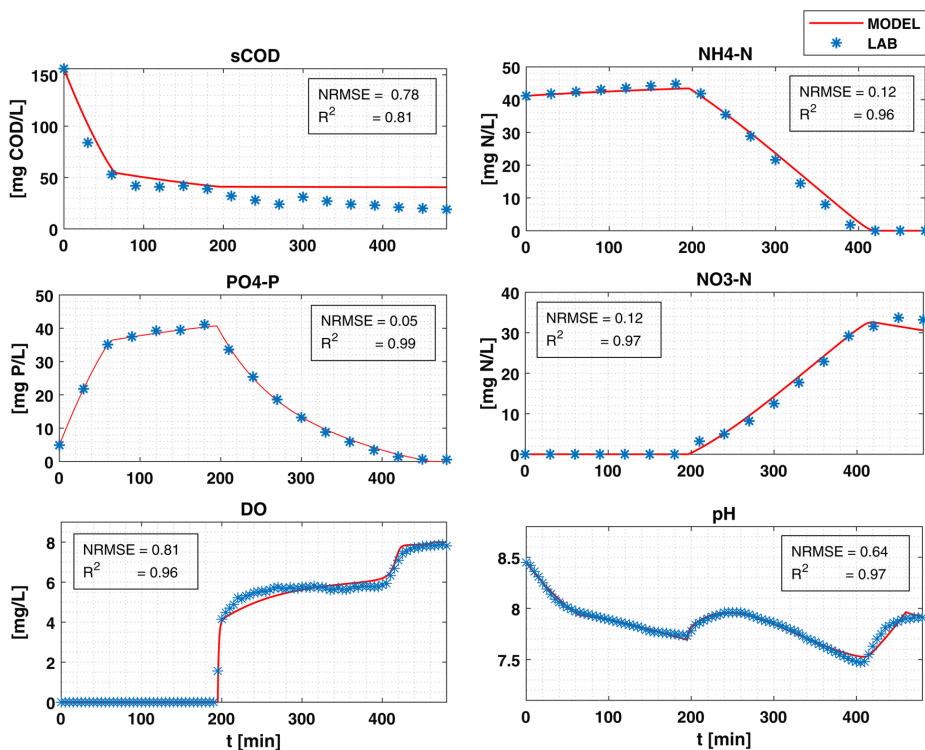


**Figure 5.1.** Experimental data versus model predicted values in SB-MBBR.

The model calibration methods explained in Section 4.2 are followed to obtain **a.** the kinetic and stoichiometric parameters of state-space model and **b.**

parameters of the measurement model presented in Equation 4.1. A comparison between the data obtained from the kinetic experiments (explained in Section 4.2.1) and the value predicted by the calibrated hybrid mathematical model for the SB-MBBR and CM-MBBR is presented in Figure 5.1 and Figure 5.2, respectively.

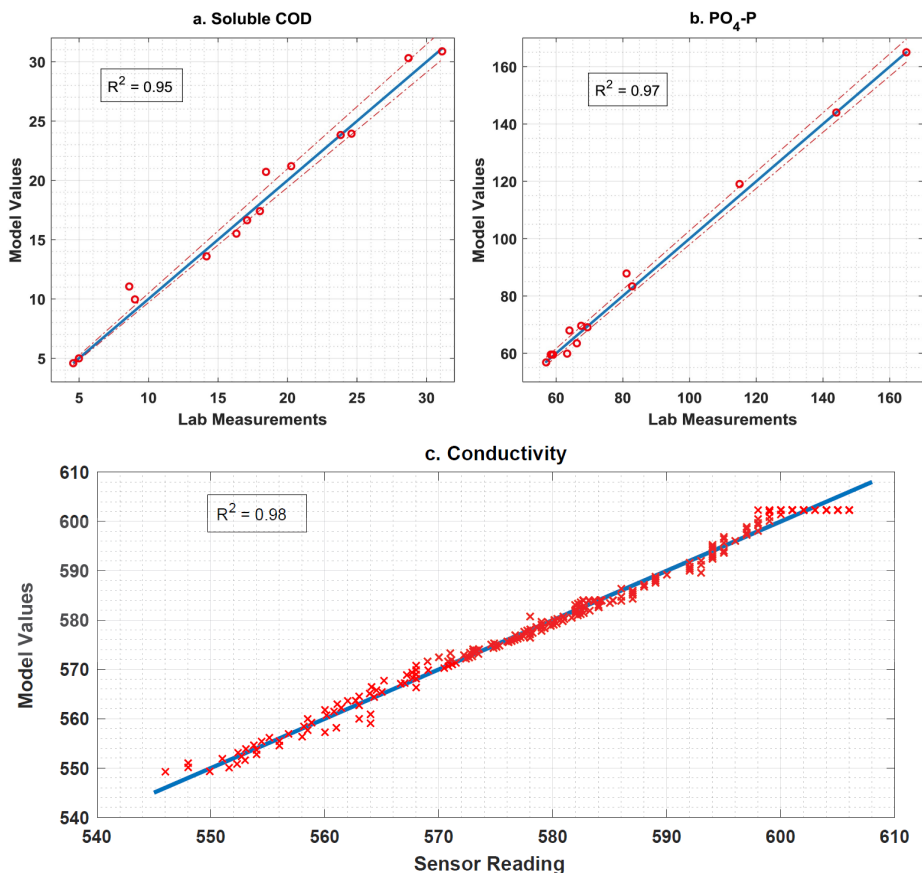


**Figure 5.2.** Experimental versus model predicted values in CM-MBBR.

The comparison plots (Figures 5.1 and 5.2) also mentions the root-mean-square-error (RSME) as well as the coefficient of determination ( $R^2$ ) for measured versus model-predicted values. The  $R^2$  value above 0.95 for most of the water-quality parameters (except for sCOD values in SBR) indicates the ability of the simplified hybrid model in explaining the biological nutrient removal processes in a sequential batch as well as a continuous process configuration. The kinetic and stoichiometric parameters used in the hybrid model for both SB-MBBR and CM-MBBR pilot plant are presented in **Paper A** and **Paper B**, respectively. In addition, the significance intervals of the measurement function parameters are also mentioned in **Paper B**.

## 5.2 Estimating water-quality parameters

The EKF described in Section 3.3 is used to estimate the state variables of the hybrid model. The values of EKF parameters ( $x_0^+$ ,  $P_0^+$ ,  $Q$ , and  $R$ ) obtained from the simulator-based evaluation of the soft sensor algorithm (Section 4.3) are presented in **Paper A** and **Paper B**. After deploying the soft sensors in the pilot plant using the strategies presented in Section 4.4.2, the accuracy of soft sensor estimations is evaluated. The evaluation results for SB-MBBR and CM-MBBR are presented in the following subsections.

### 5.2.1 Real-time estimations in SB-MBBR

The short-term performance evaluation (Section 4.5.1) for SB-MBBR was conducted on 01.11.2018. Samples were collected once every half an hour, for a complete SBR cycle (8 hours) and analyzed using standardized lab measurements. The comparison between the lab measured values of  $\text{NH}_4\text{-N}$ ,  $\text{NO}_3\text{-N}$ ,  $\text{PO}_4\text{-P}$  and their corresponding values estimated by the soft sensor are presented in Figure 5.3.

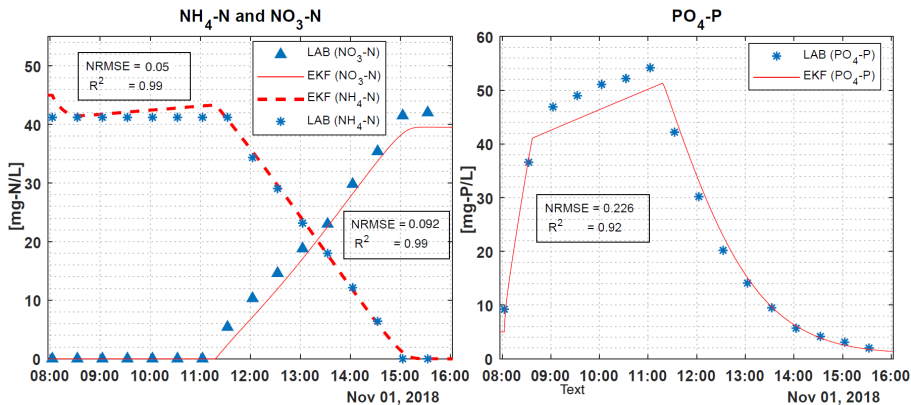


**Figure 5.3.** Estimation of  $\text{NH}_4\text{-N}$ ,  $\text{NO}_3\text{-N}$ , and  $\text{PO}_4\text{-P}$  in SB-MBBR.

The EKF is initialized at the beginning of the SBR cycle with an initial estimate of  $S_{\text{PO}0} = 5$  mg P/L for phosphates,  $S_{\text{NH}0} = 45$  mg N/L for ammonia, and  $S_{\text{NH}0} = 0$  mg N/L for nitrates. Looking at the estimated values of  $\text{NH}_4\text{-N}$  and  $\text{PO}_4\text{-P}$  from 8:00 AM to 9:00 AM in Figure 5.3, it can be observed that the estimated values reach the lab measured values in less than 30 minutes. Figure 5.3 also shows that during the entire SBR cycle, the values estimated by soft sensors are comparable to their corresponding values measured by standardized lab tests. An RSME less than 0.25 and an  $R^2$  value higher than 0.9 demonstrate the accuracy of soft sensor estimations.

## 5.2.2 Real-time estimations in CM-MBBR

### *PO<sub>4</sub>-P and sCOD in anaerobic chambers*

The hybrid soft sensor deployed in the CM-MBBR provides real-time estimations of PO<sub>4</sub>-P and sCOD concentration in the anaerobic chambers (chamber 1, 2, and 3) and the influent. Figure 5.4 presents a comparison between the estimated values of PO<sub>4</sub>-P and the corresponding values obtained from the analyses of grab samples collected every day from the anaerobic chambers and influent for ten days.

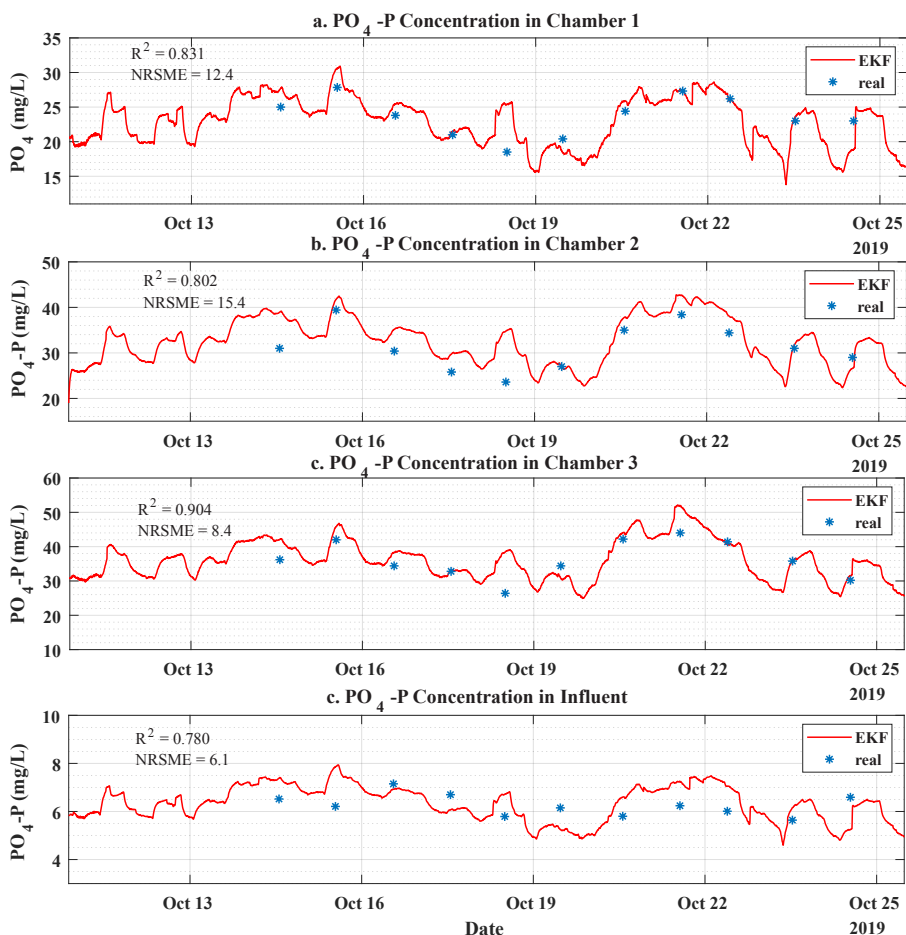


**Figure 5.4.** Validation results for PO<sub>4</sub>-P in anaerobic chambers and the influent.

The time series plot in Figure 5.4 shows that the estimated PO<sub>4</sub>-P and the values measured by standardized lab test exhibits similar variations during the short-term performance evaluation period, from 15.10.2019 to 24.10.2019. A

scatter plot showing the measured versus estimated values of all data points obtained during the short-term evaluation (along with the  $R^2$  values) and a residual plot are presented in Figure 5.5.

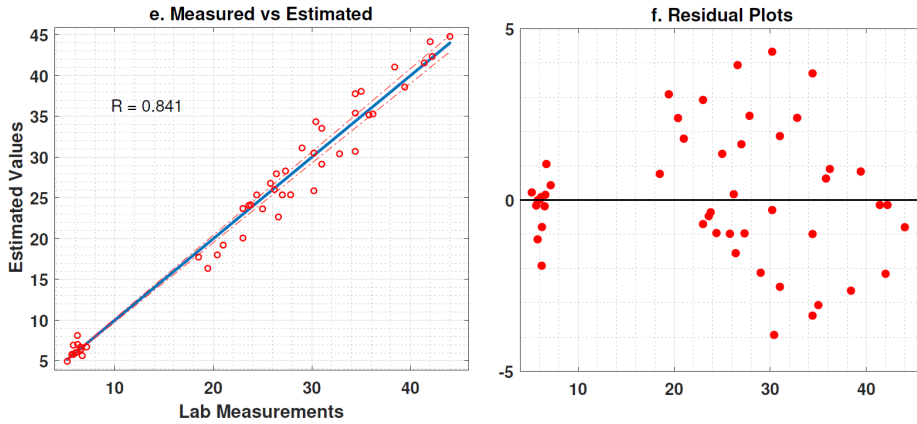


**Figure 5.5.** Measured versus estimated  $\text{PO}_4\text{-P}$  **e.** Scatter plot **f.** Residual plots.

A close match between the estimated data and the lab measured values, an  $R^2$  value above 0.8 and a random distribution of the errors along the zero-error line (presented in the Figure 5.5f), demonstrate the ability of the soft sensor in providing reliable estimations of  $\text{PO}_4\text{-P}$  in the influent and the anaerobic chambers. The soft sensor can also estimate sCOD concentrations in the CM-MBBR process. Although no rigorous short-term validation of sCOD was conducted, a comparison between the estimated and measured values of influent sCOD is presented in Figure 5.7b as well as in the appendices of **Paper B**. The comparison plots presented in these figures indicate that the sCOD values estimated by the soft sensors are sufficiently reliable.

### ***NH<sub>4</sub>-N and nitrification rate (r)***

The EKF based hybrid soft sensor can also estimate the  $\text{NH}_4\text{-N}$  concentrations in the influent as well as in each chamber of the CM-MBBR pilot plant. Real-time information from the influent flow sensor, DO sensors at the aerobic chambers (chamber 5 to 10), and an effluent ammonia ISE sensor are used as measurements for the soft sensor. The mathematical expression explaining the ammonia nitrification in the aerobic chambers of the CM-MBBR is presented in **Paper C**. The soft sensor was operational for almost six weeks (from 29.01.2019 to 12.03.2019) where the estimated  $\text{NH}_4\text{-N}$  values were stored in the plants SCADA. The comparison between estimated values obtained from SCADA and the biweekly measurement of the  $\text{NH}_4\text{-N}$  concentration in raw wastewater is presented in Figure 5.6.



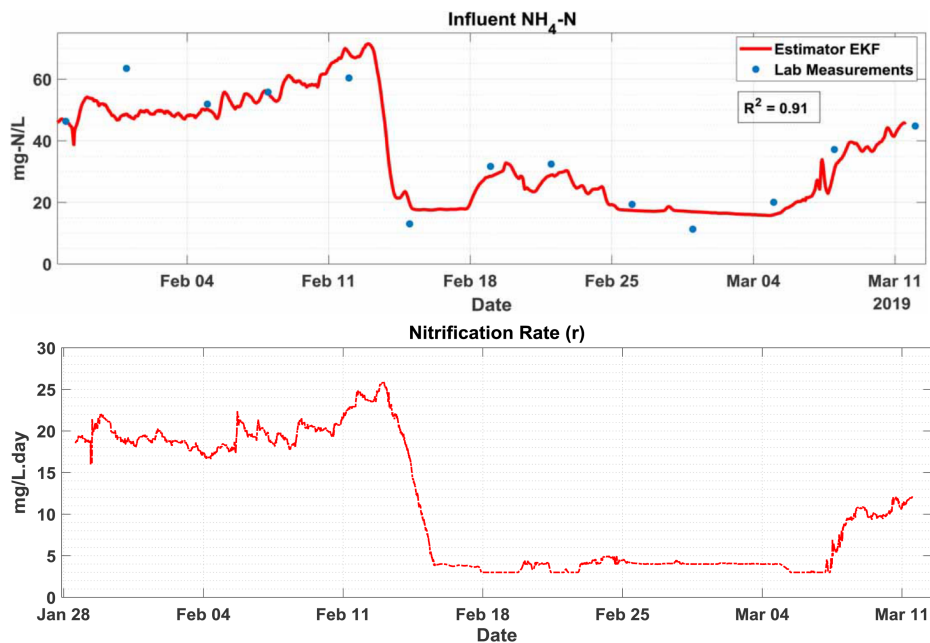


**Figure 5.6.** (Top) Measured versus estimated  $\text{NH}_4\text{-N}$  in the influent. (Bottom) Estimated values for nitrification rate ( $r$ ).

A close match between the measured and estimated values and the  $R^2$  value 0.91 demonstrate the ability of the soft sensor in estimating  $\text{NH}_4\text{-N}$  values in the CM-MBBR pilot plant.

The simplified nitrification model used in soft sensor was obtained by ignoring the growth and death kinetics of the nitrifying biomass and lumping them as a parameter  $r$  in the model. The changing concentration of biomass during the pilot plant operation is accounted for by considering  $r$  as a time-varying parameter and including it as a state variable. Similar strategies for including time-varying model parameters are reported in literature (Haugen et al., 2014). Therefore, the real-time estimation of the parameter  $r$  by the soft sensor could provide significant insight on variations in the concentration of active nitrifiers in the pilot plant. Figure 5.6 presents the value of the nitrification rates  $r$  estimated by the soft sensor during the evaluation period. A qualitative assessment of the trends in Figure 5.6 indicates that  $r$  showed a steady decline on 13.02.2019, a few hours after the influent ammonia concentration dropped. The pilot plant showed lower nitrification rates from 15.02.2019 till 06.02.2019 when the influent ammonia concentration was low. The nitrification rate started to increase after 06.03.2019 when the influent ammonia concentration started to increase. This observation corresponds to the usual behavior of nitrifiers present in a biological wastewater treatment plant.

## 5.3 Long-term performance evaluation and recalibration

The deviation of the mathematical model from the actual process behavior is an unavoidable phenomenon. The measurement model for CM-MBBR (explained in **Paper B**) correlates EC with sCOD and PO<sub>4</sub>-P. However, in reality, a multitude of ionic species (NH<sub>4</sub><sup>+</sup>, NO<sub>3</sub><sup>-</sup>, PO<sub>4</sub><sup>3-</sup>, K<sup>+</sup>, etc.) affect the conductivity measurements in a biological phosphorus removal process. The interdependencies between most ionic species in wastewater allow the correlation to be explained using the mathematical expression presented in Equation 4.1. However, a gradual change in the ionic interdependencies over time could eventually cause a drift in the measurement model. Therefore, the soft sensor estimations are susceptible to drift and would require frequent calibration. The algorithm that was used initially to obtain the measurement model parameters during the batch experiment (Section 4.2.2) is used to update the model parameters during recalibration.

Following the long-term assessment procedures explained in Section 4.5.2, the values estimated by the calibrated and uncalibrated soft sensors are compared with the biweekly lab measurement of influent sCOD and PO<sub>4</sub>-P and presented in Figure 5.7. Figure 5.7 shows that from the date of deployment 14.10.2019 till 04.11.2019 the estimated PO<sub>4</sub>-P values were close to the values measured by standardized lab tests. The first sign of drift was observed at the beginning of the fourth week when the estimated values started deviating from the measured value. The first calibration of the soft sensor was carried out on 08.11.2019 when the difference between the measured and estimated value was more than 50%. After recalibration and the subsequent update of measurement model parameters, the estimated values moved close to the measured values. The same process was repeated two more times, on 05.12.2019 and 07.01.2020, subsequently. The updated values of the measurement model parameters, along with their 95% confidence intervals obtained after each calibration instance, are presented in **Paper B**.

Although the difference between the calibrated and uncalibrated soft sensors is not significant after the first calibration instance, the difference increased considerably over time, especially after the second and third calibration instances. A scatter plot comparing the estimated and measured data, along with the corresponding R<sup>2</sup> values, presented in **Paper B**, shows that the estimations of sCOD and PO<sub>4</sub>-P with a regularly calibrated model was closer to the actual values as compared to the uncalibrated model. The plots indicate that periodic calibration of the soft sensor model by updating the model parameters could solve the estimation error caused by the drift in the measurement model.

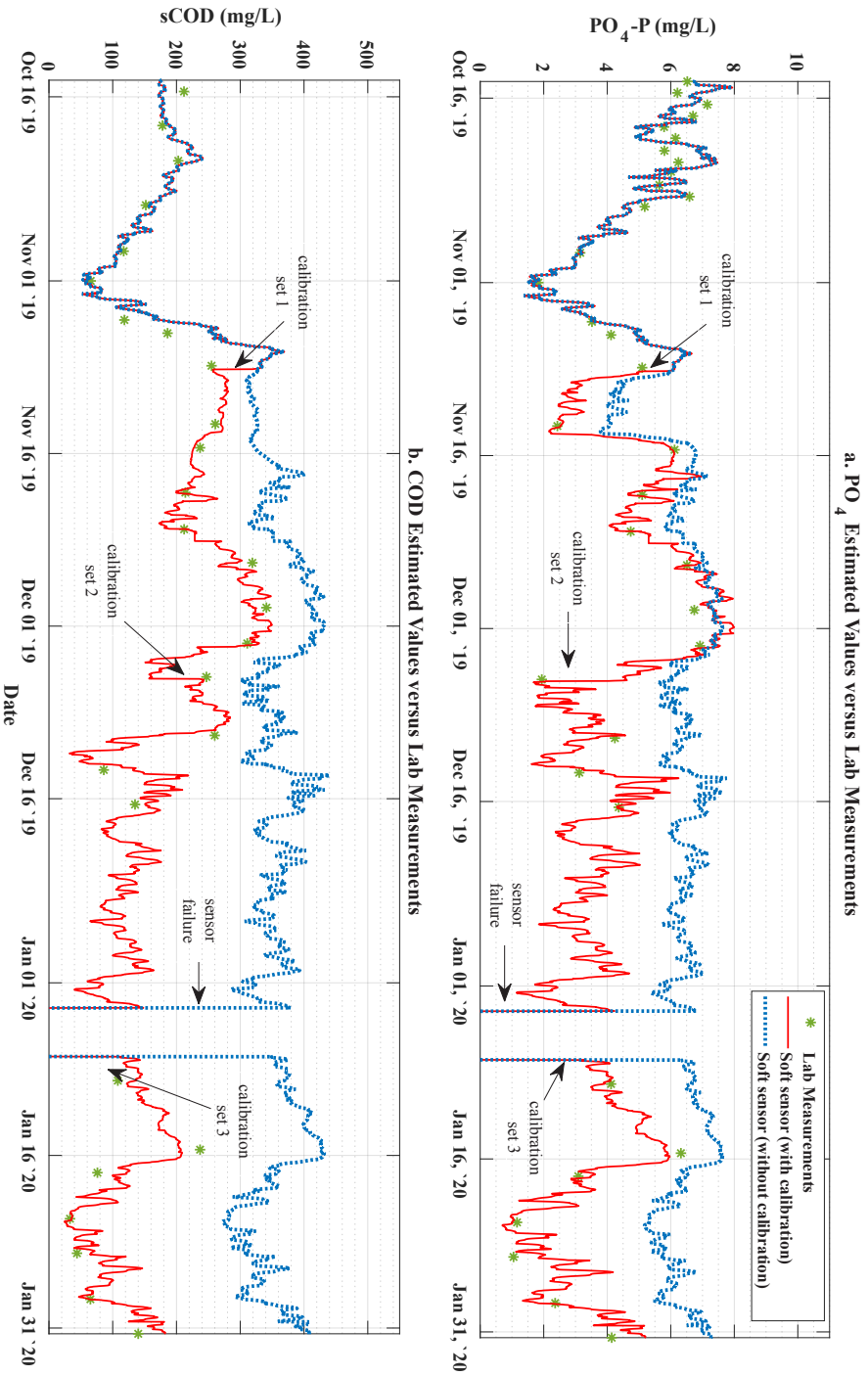


Figure 5.7. Long-term evaluation of soft-sensor performance and influence of recalibration on **a.** influent  $PO_4$ -P **b.** influent sCOD.

## 5.4 Economic evaluation of new IoT infrastructure

An economic assessment of costs associated with setting up a surveillance infrastructure for monitoring  $\text{NH}_4\text{-N}$  in the CM-MBBR is discussed in **Paper C**. The four different surveillance options used for this purpose are presented in Table 5.1. The first option includes installing physical  $\text{NH}_4\text{-N}$  ISE sensors in all six aerobic chambers of the CM-MBBR. The second, third, and fourth options include monitoring  $\text{NH}_4\text{-N}$  concentration using the soft sensors based on different deployment strategies explained in Section 4.4.2. Option 2 uses the default commercial services provided by the SCADA vendor whereas, options 3 and 4 are based on the cost-effective open-source strategy described in **Paper C**.

Option 1, using six physical  $\text{NH}_4\text{-N}$  ISE sensors, incur a total cost of 9000 euros. The possibility of monitoring of  $\text{NH}_4\text{-N}$  in the aerobic chamber using an EKF based soft sensor is already demonstrated in Section 5.2.2. The cost components for the soft sensor based monitoring system, presented as option 2, includes the price of an  $\text{NH}_4\text{-N}$  ISE sensor installed in the effluent, licenses of MATLAB software, the one-time purchase cost of OPC-DA server (Codesys OPC-DA), and the price of VPN (Insys) licenses to establish a secure connection to the OPC-DA server. The total cost for option 2 ranges from 2480 - 3440 euros, which is one-third the price of the surveillance infrastructure used in option 1.

Options 3 and 4 attempt to substitute the expensive components of option 2 with cost-effective alternatives. The cost incurred by using commercial software such as MATLAB was eliminated by writing the EKF script in an open-source programming language such as Python. The remote monitoring infrastructure based on an OPC-DA server was replaced with a MySQL database that was made accessible over the internet by using a Dynamic DNS (DDNS) service. A single-board computer (RPi) was used as a gateway for data-exchange and to execute the soft sensor scripts. Details regarding the setup of the remote infrastructure, the hardware components used, and the soft sensor deployment sequence are explained in **Paper C**. The only main cost associated with monitoring option 3 is the use of an SSL key for encrypting the data exchange between the MySQL server and the client executing the soft sensor script. The overall costs incurred are 1655 euros in option 3 and 1535 euros in option 4. The cost components of options 3 and 4 in Table 5.1 show a considerable reduction from the commercial variant presented in option 2.

**Table 5.1.** Cost comparison between different strategies for monitoring NH<sub>4</sub>-N in different stages of CM-MBBR.

	Option 1		Option 2		Option 3		Option 4	
	Service	Cost(€)	Service	Cost(€)	Service	Cost(€)	Service	Cost(€)
<b>Server</b>	-	-	OPC (Codesys)	160	MySQL	-	MySQL	-
<b>Remote access</b>	-	-	VPN (Insys)	560	DDNS	-	DDNS	-
<b>Security/encryption</b>	-	-	Inbuilt	-	SSL key	120	-	-
<b>Client hardware</b>	-	-	PC	200-1000	Raspberry Pi	35	Raspberry Pi	35
<b>Client software</b>	-	-	Matlab	220	Python	-	Python	-
<b>NH<sub>4</sub>-N sensor (ISE)</b>	6 Units	1500	1 Unit	1500	1 Unit	1500	1 Unit	1500
<b>IoT cost (€)</b>	-	-	-	980-1940	-	155	-	35
<b>Overall cost (€)</b>	-	9000	-	2480-3440	-	1655	-	1535

## 5.5 Impact of control strategy on nutrient removal process

The performance of advanced and basic control strategies for ammonia-based aeration control is evaluated by comparing the concentration of effluent ammonia ( $S_{NH,e}$ ) obtained from simulating BSM2 with the dynamic influent conditions. The performance indices presented in Table 5.2 along with their percentage change compared to the basic (DO control and PI-NH cascade control) strategies are used for the quantitative assessment of the strategies mentioned in Section 4.6. The  $S_{NH,e}$  obtained from executing the BSM2 with the PI-NH cascade control and the advanced MPC controls with different prediction models are presented in Figure 5.8. The parameters of linear and non-linear prediction models, weights of MPC objective function, and the mathematical expressions used to calculate the performance indices mentioned in Table 5.2 are explained in **Paper D**.

The difference between the AMPC strategy and PI-NH cascade control can be observed in Figures 5.8a and 5.8c. The comparison plots and the integral-absolute-error (IAE) values (184 for PI-NH cascade control and 229 for AMPC) suggest that the PI-NH cascade control has better set-point tracking compared to the AMPC. The poor set-point tracking of AMPC could be due to the weight parameter  $w_u$  which penalizes the higher values of manipulated variable (aeration intensity). Penalizing high aeration-intensity would allow deviations from the NH set-point in favor of maintaining a low aeration energy (AE) consumption (4110 for PI-NH cascade control and 3686 for AMPC). A higher percentage of effluent ammonia violation (%T  $S_{NH,e}$ ) is also observed in PI-NH cascade controller (0.210%) compared to the AMPC (0.144%). The lower %T  $S_{NH,e}$  in AMPC is primarily due to the weight parameter  $w_L$  associated with effluent violation penalty in Equation 4.3. The non-zero value of  $w_L$  results in an exponential increase of objective (or cost) function when ammonia concentration in the chamber 7 reaches close to the effluent ammonia limit ( $C_{NH,lim}$ ) of 4 mgN/L. The effect of introducing a limit penalty function can be clearly observed in Figure 5.8c, where although NH set-point is not strictly maintained, the overall number of times the  $S_{NH,e}$  exceeded  $C_{NH,lim}$  is comparatively lower. The AMPC strategy also shows a 31.4% reduction in AE and a 17.9% increase in the average effluent  $NH_4$ -N concentration (Avg  $S_{NH,e}$ ) compared to the PI-NH cascade control strategy.

The  $S_{NH,e}$  for MPC control strategies based on different prediction models (LMPC, AMPC, and NLMPC) are presented in Figures 5.8b, 5.8c, and 5.8d. respectively. The performance indices provided in Table 5.2 indicate a better performing NLMPC compared to the LMPC in terms of both AE as well as

%T  $S_{NH,e}$ . The LMPC even demonstrated higher %T  $S_{NH,e}$  when compared to PI-NH cascade control. The poor performance of LMPC could be due to the inadequacy of linear models in explaining the high nonlinearities in the biological nitrification process. The performance of AMPC is very similar to the NLMPC, which suggests that a frequent update of the linear model will result in a linear MPC performing as good as an NLMPC. The NLMPC and AMPC demonstrate a clear improvement in terms of reducing %T  $S_{NH,e}$  (31.4% for AMPC and 30.0% for NLMPC) as well as decreasing the AE (10.31% for AMPC and 12.09% for NLMPC). The Avg  $S_{NH,e}$  is also higher for AMPC (2.23 mg N/L) and NLMPC (2.28 mg N/L) compared to the LMPC (2.09 mg N/L). Although the performance indices of AMPC is similar to the NLMPC, a significant reduction in the use of computational resources has been observed in AMPC. The simulation time and the simulation speed factor (showing the ratio of the simulation time with respect to NLMPC), presented in Table 5.2, suggest that the AMPC is almost twice as fast as NLMPC. This confirms that AMPC can be used as a suitable replacement for NLMPC. Since the AMPC contains a system identifier, it is an efficient strategy to avoid prediction errors caused by model–plant mismatch and considerably reduce the dependency of the MPC on the accuracy of its prediction model.

**Table 5.2.** Performance indices of different ammonia based aeration control strategies.

Performance Criteria	DO Control	Cascade Control	LMPC	AMPC	NLMPC
<b>IAE</b>	516	184	210	229	240
<b>AE</b>	4350	4110 (-5.51%)	3990 (-2.91%)	3686 (-10.31%)	3616 (-12.09%)
<b>%T <math>S_{NH,e}</math></b>	0.314	0.210 (-33.1%)	0.221 (5.23%)	0.144 (-31.4%)	0.147 (-30.0%)
<b>Avg <math>S_{NH,e}</math> (mg N/L)</b>	0.65	1.89 (190.7%)	2.09 (10.6%)	2.23 (17.9%)	2.28 (20.6%)
<b>Simulation time (h)</b>	7.38	8.04	8.15	8.46	16.31
<b>Simulation Factor</b>	2.21	2.02	2.00	1.91	1.0

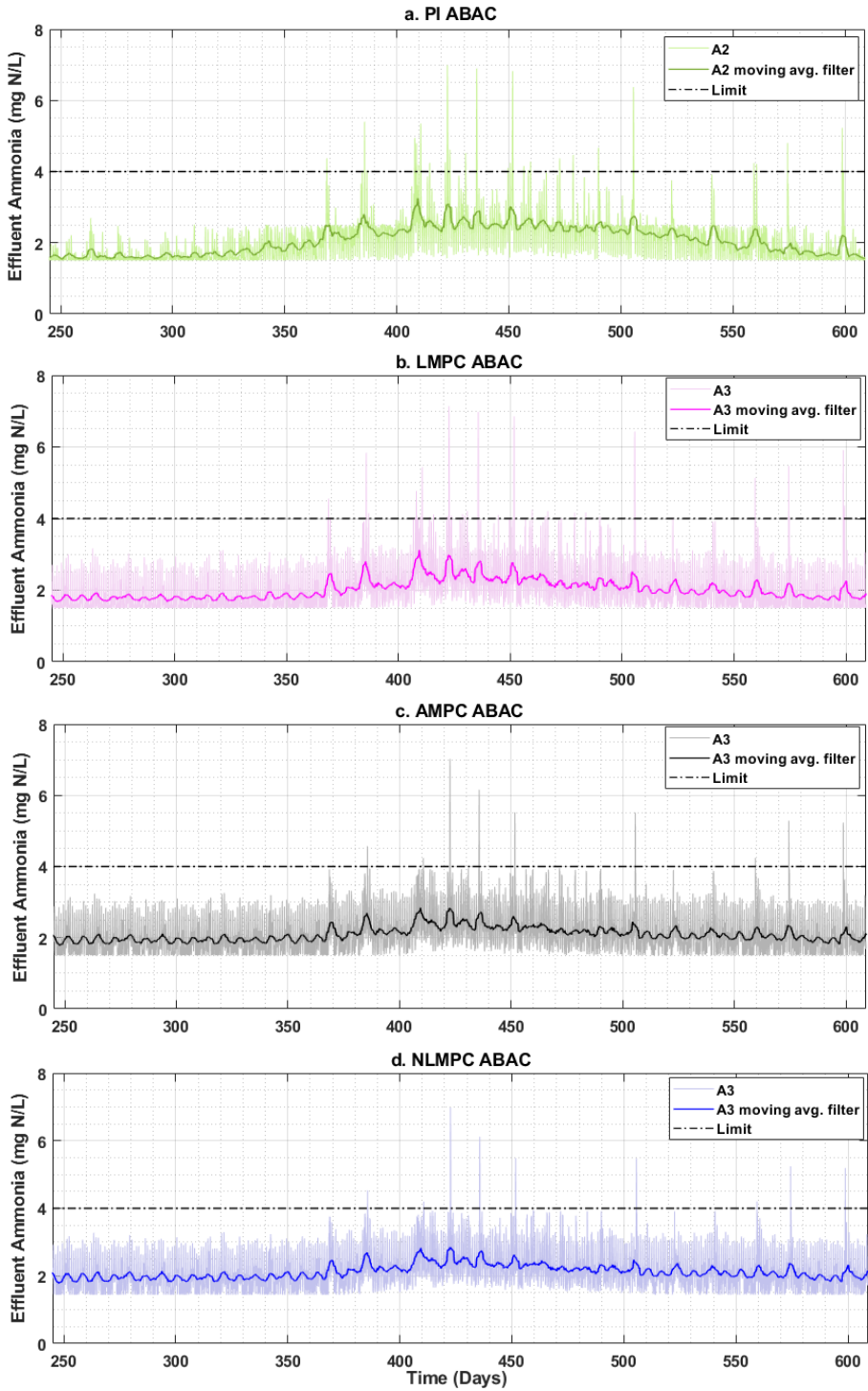


Figure 5.8.  $S_{NH,e}$  for basic and advanced control strategies.



## 5.6 Impact of control strategy on struvite recovery process

The mass flowrate of phosphates in the effluent overhead stream represents the amount of unrecovered phosphorus exiting the struvite recovery unit. Therefore, the dynamic values of phosphates in the effluent overhead stream during the evaluation period, have been used to compare the performance of different control strategies (presented in Section 4.7) implemented for optimizing struvite recovery process. The performance indices presented in Table 5.3 are also used for the quantitative assessment of the control strategies. The linear model parameters, the MPC settings, and equations for calculating the performance indices are explained in **Paper E**.

### *EMPC versus feed-forward flow proportional dosing strategy*

Figure 5.9 shows the mass flowrate of phosphates in the effluent overhead stream, during the evaluation period, for a constant  $Q_{Mg}$  scenario. As a result of high fluctuations in effluent phosphates, several under-dosing scenario (marked in blue circles in Figure 5.9) can occur where, increasing the dosage could have improved the phosphorus recovery. Figure 5.9 also indicates overdosing points (marked in green squares) where  $Q_{Mg}$  is higher than what is required.

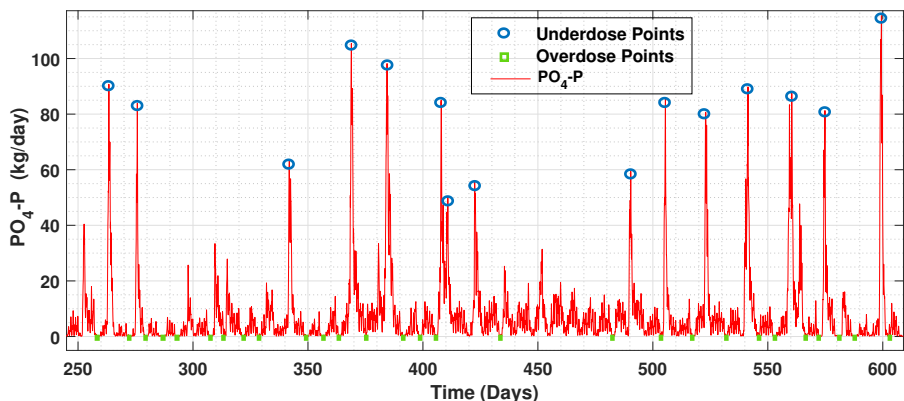


**Figure 5.9.** Mass flowrate of effluent phosphates for constant dosing scenario.

The fluctuations in the mass flowrate of effluent phosphates can be attributed to the variations in flowrate ( $Q_{IN}$ ) and the phosphate concentrations ( $PO_{4,IN}$ ) of the influent stream entering the struvite recovery unit (Figure 5.10a). The feed-forward flow proportional dosing control strategy (C1) presented in Figure 4.6a can offset the influent fluctuations by changing  $Q_{Mg}$  proportional to

$Q_{IN}$ . The performance indices in Table 5.3 show an 8.01% increase in average phosphorus recovery and an 8.62% reduction in Magnesium consumption when compared to the constant  $Q_{Mg}$  strategy. However, the dose prediction for C1 is entirely based on the flowrate and does not consider the fluctuations in  $PO_{4,IN}$ . The disadvantages of C1 can be observed in Figure 5.10b, which shows higher values of phosphates from  $T = 245$  to  $T=390$ . This is primarily due to the increase in  $Q_{IN}$  and a gradual drop in  $PO_{4,IN}$  from  $T=350$  to  $T=400$ . As a result, C1 proportionally increases  $Q_{Mg}$  without considering the drop in  $PO_{4,IN}$ . The higher quantities of phosphates in the effluent overhead stream, from  $T=245$  to  $T=390$  can be reduced by increasing  $K_P$  to a higher value. However, this would imply that for the rest of the evaluation period ( $T=390$  to  $T=609$ ) the  $Q_{Mg}$  is higher than what would be necessary.

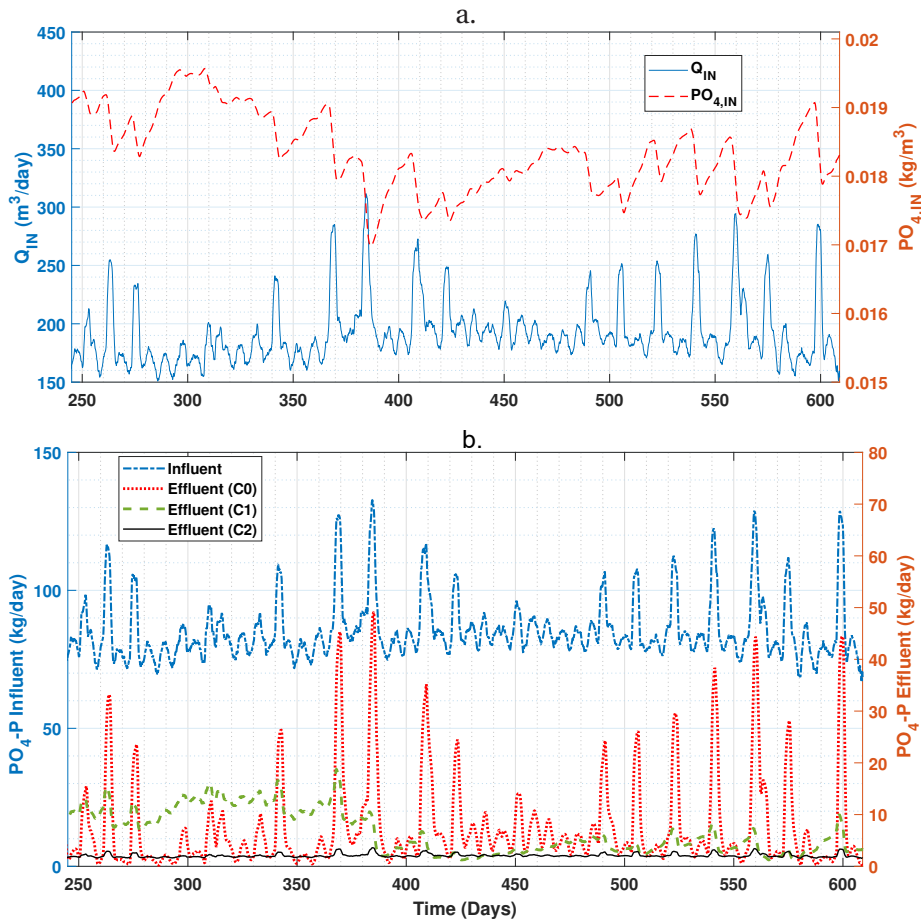


**Figure 5.10.** a. Volumetric flowrate and phosphate concentration of influent. b. Mass flowrate of phosphates in the influent and effluent streams for scenarios C0, C1, and C2.

The EMPC (C2) predicts  $Q_{Mg}$  based on the optimal value of the economic objective function as in Equation 4.5. The economic oriented objective function, considering  $Q_{IN}$ ,  $PO_{4,IN}$ , and  $PO_{4,OUT}$  is expected to have better control over the recovery of phosphorus. The comparison plots presented in Figure 5.10b show that C2 has more stable values of phosphates in the effluent compared to C0 and C1. The dynamic plots for  $Q_{Mg}$ , percentage recovery of phosphates, and mass of struvite produced are presented as supplementary material in **Paper E**. The performance indices presented in Table 5.3 indicate a 12.5% increase in the average daily struvite production and an 8.49% drop in total magnesium consumption compared to C0. The overall profits for struvite production also show an increase of 33% for C1 and 44% for C2 when compared to C0. In addition to increased profits, the EMPC also shows fewer  $PO_4$ -P violations ( $EV_{TP}$ ) in the treated effluent from WRRE, as shown in Table 5.3.

**Table 5.3.** Performance indices of different control strategies for struvite recovery unit.

Performance Criteria	Constant Dosing	Proportional Dosing	EMPC
Struvite Production (kgP/day)	91.1	98.4 (8.01%)	102.49 (12.50%)
Mg Consumed (kg/day)	78.9	72.1 (-8.62%)	72.2 (-8.49%)
OCI	9105.1	9073.4 (-0.348%)	9002.1 (-1.131%)
Profit (£/day)	314.73	418.56 (33.0%)	453.33 (44.0%)
$EV_{TP}$	21	18 (14.2%)	9 (57.1%)

### ***Resilience to changes in struvite prices***

The influence of introducing monthly changes to the cost of struvite ( $\Phi_{STR}$ ) on effluent phosphate and the  $Q_{Mg}$  values predicted by EMPC (C3) are presented in Figure 5.11. The monthly variations in  $\Phi_{STR}$  during the evaluation period are presented in Figure 4.7. It can be observed that in situations with lower  $\Phi_{STR}$ , the C3 strategy predicts a lower  $Q_{Mg}$  and a subsequent reduction in phosphorus recovery compared to C2. This is primarily because of the economic oriented objective function of the EMPC, which attempts to save up on the magnesium consumption costs when the  $\Phi_{STR}$  is low. A higher  $Q_{Mg}$  and a subsequent increase in phosphorus recovery are observed when

the  $\Phi_{STR}$  is higher than the average value of  $\Phi_{STR}$ . The comparison between all four control strategies based on the average (kgP/day) values of struvite produced, magnesium consumed, and overall profits (recalculated for time-varying  $\Phi_{STR}$  values) are presented in Table 5.4. The comparison presented in Table 5.4 indicates that using costs as inputs to the EMPC controller as opposed to a constant  $\Phi_{STR}$  in the objective function results in an additional 8.1% increase in the overall profits generated by the struvite recovery unit.

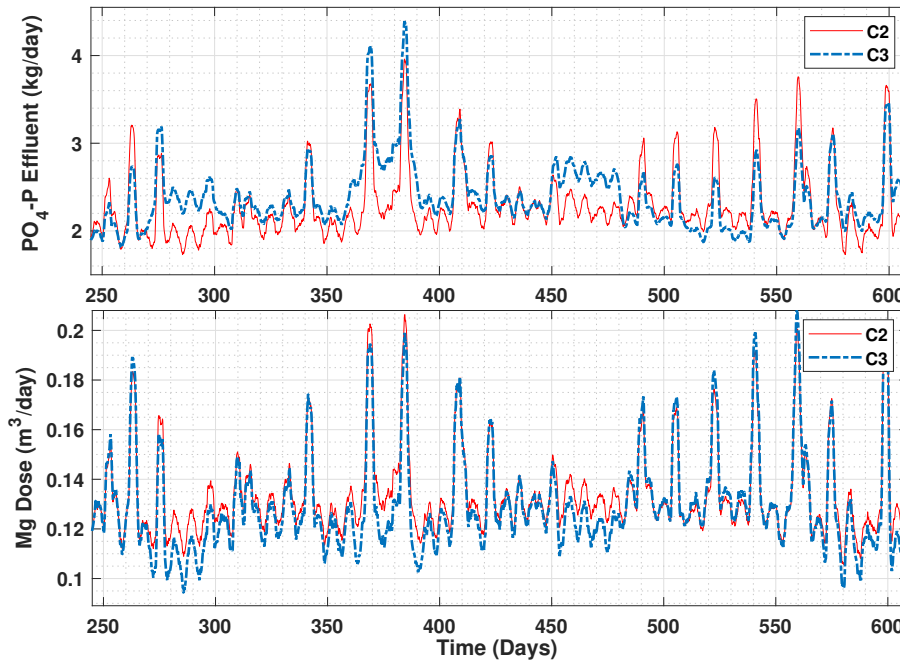


**Figure 5.11.** Comparing C2 and C3 control strategies. (Top) Mass flowrate of phosphates in the effluent. (Bottom) Volumetric flowrate of magnesium.

**Table 5.4.** Economic assessment for time varying struvite costs.

Performance Criteria	Constant Dosing C0	Proportional Dosing C1	EMPC C2	EMPC C3
Struvite Production (kgP/day)	91.1	98.4	102.5	102.1
Mg Consumed (kg/day)	78.9	72.1	72.2	70.9
Profit (€/day)	291.73	388.56	413.13	447.83

# Chapter 6

## Thesis Contributions

The main contributions of research activities carried out as a part of this thesis work are highlighted as follows.

- Development of a simplified dynamic model that can be used in a soft sensor for nutrient removal processes. The mathematical expressions of the simplified model are constructed by combining material balances of nutrient compositions, biological nutrient removal kinetics (simplified Monod's expressions), and statistical correlations between nutrient composition and easy-to-measure physical parameters. (**Paper A** and **Paper B**)
- Demonstrating that the EKF based hybrid soft sensor can be used for real-time estimation of several water-quality parameters in a nutrient removal process with both sequential batch as well as a continuous multi-stage configuration. (**Paper A** and **Paper B**)
- Developing a strategy for improving the robustness of soft sensors by successively updating the model parameters with data from standardized lab tests. (**Paper B**)
- Development of a cost-effective, open-source, non-intrusive IoT infrastructure for remote monitoring of sensor data and soft sensor deployment. (**Paper C**)
- Demonstrating that the soft-sensor scripts written in commonly used scientific programming languages such as MATLAB or Python can be integrated with most of the commercially available SCADA. (**Paper C**).
- Optimizing the nutrient removal process in a WRRF by implementing a model-based optimal control strategy to curtail the number of effluent violations and reduce the aeration costs. (**Paper D**).

- Integrating recursive parameter estimations with a linear MPC strategy to improve its performance when applied to highly complex nonlinear processes such as biological nutrient removal. (**Paper D**).
- Incorporating economic parameters in the MPC strategy (EMPC) for maximizing the profitability of the resource (struvite) recovery process installed in a WRRF. (**Paper E**).

# Chapter 7

## Conclusions and Outlook

The research work presented in this thesis attempts to improve the efficiency of nutrient removal process, increase the recovery of nutrients, and reduce the operating cost in WRRF. The research objectives are addressed by utilizing the concepts of online monitoring, state-estimation, and advanced optimal control. The following conclusions are drawn from the results presented in the preceding chapter.

- The simplified hybrid models developed in this work can adequately explain biological nutrient removal process as well as correlations between nutrient compositions and easy-to-measure parameters such as pH, EC, and DO. These hybrid models when used in conjunction with the EKF and information from pH and DO sensors can provide reliable estimations of  $\text{NH}_4\text{-N}$ ,  $\text{NO}_3\text{-N}$ , and  $\text{PO}_4\text{-P}$  in an SB-MBBR process. The soft sensing method, when implemented in a CM-MBBR process, can estimate sCOD and  $\text{PO}_4\text{-P}$  concentrations in their anaerobic chambers using a series of on-line EC sensors. In addition, the soft sensor can also estimate  $\text{NH}_4\text{-N}$  concentrations in the aerobic chambers of the CM-MBBR process using flow and DO sensors. Frequent update of model parameters using data from standardized lab measurements shows an improvement in the robustness of the hybrid soft sensor. The hybrid soft sensor is therefore a viable alternative for obtaining reliable measurements of water-quality parameters in the nutrient removal process. (**Paper A** and **Paper B**)
- A case-study on strategies to enhance process surveillance in CM-MBBR shows that using soft sensors to monitor  $\text{NH}_4\text{-N}$  cost one-third the price as compared to using physical  $\text{NH}_4\text{-N}$  ISE sensors. The same study also shows that deploying soft sensors using the new open-source IoT system is about 45% cheaper than the default options provided by the commercial SCADA manufacturer. The new IoT infrastructure allows the integration of

scripts written in commonly used scientific programming languages such as MATLAB or Python into most of the commercially available SCADA systems. Soft sensors, when combined with the new open-source IoT infrastructure, resulted in a considerable reduction in the costs associated with online monitoring in WRRF. (**Paper C**)

- Model-based control strategy such as MPC is a relatively efficient method for aeration-control compared to the conventional constant DO set-point or PI-NH cascade control. The MPC control strategy using a simplified nonlinear prediction model (NLMPC) performs better than the ones using a linear prediction (LMPC) model, demonstrating a considerable reduction in both aeration energy as well as the percentage of effluent violations. The AMPC, which recursively updates the linear prediction model parameters, performs almost as good as the NLMPC. The AMPC also works twice as fast as an NLMPC, presenting itself as a potential strategy for aeration control in a nutrient removal process. (**Paper D**)
- The performance of a struvite recovery process has shown considerable improvements when an EMPC is used to decide the optimal dosage of magnesium hydroxide. The EMPC demonstrates a 12.5% increase in struvite production while simultaneously reducing the consumption of magnesium hydroxide by 8.49% compared to the constant dosing strategy. The overall profits showed a significant improvement when compared to the constant (44%) as well as the feed-forward flow proportional (8.37%) dosing strategy. Including economic parameters in the objective function of the EMPC makes the controller less susceptible to changes in the market price of struvite. The EMPC, with a time-varying struvite market price in its objective function showed a further 8.1% increase in overall profits as compared to the strategy using a constant struvite market price. (**Paper E**)

The overall aim of improving nutrient removal and recovery is demonstrated through simulator-based validations on the BSM2 platform. Implementing advanced control strategies have curtailed the number of effluent violations, decreased the aeration energy consumed in nutrient removal process, and increased the overall profitability of the nutrient recovery process in WRRF. A reliable and economical alternative to the expensive online monitoring infrastructure, has been demonstrated through pilot-scale tests and validations of hybrid soft sensors. The results presented in this thesis highlight the potential of online monitoring and advanced optimal control in improving the operations of WRRF. The contributions of this work present a small step towards the final goal of transforming WRRFs into a self-sustainable energy-positive entity capable of producing value-added products.



# Chapter 8

## Recommendations for Future Work

**Soft sensors** - The soft sensors presented in **Paper B** estimates  $\text{PO}_4\text{-P}$  and sCOD in the anaerobic chamber of CM-MBBR. As a next step to this research, the soft sensing method can be further extended to estimate  $\text{PO}_4\text{-P}$  in the aerobic chambers. The thesis has provided a qualitative validation of nitrifier concentrations in the CM-MBBR pilot plant in **Paper C**. The approach used in this paper could be potentially used to construct a soft sensor for estimating active biomass compositions in the biological nutrient removal systems. The soft sensor strategy can also be expanded beyond the SB-MBBR and CM-MBBR to verify their applicability to other WRRF processes such as activated sludge, IFAS, MBR or granulated activated sludge systems.

**Optimal Control for CM-MBBR** - The CM-MBBR process has been one of the first process configurations to have succeeded in achieving biological phosphorus removal in an MBBR system (Saltnes et al., 2017). The multi-stage configuration provides tremendous operational flexibility in removing several nutrients from municipal wastewater. The updated monitoring capabilities of the CM-MBBR, presented in **Paper B** and **Paper C**, enable the possibility of implementing advanced control strategies to improve its performance. Designing a model-based optimal control strategy for CM-MBBR similar to the strategies presented in **Paper D** and **Paper E** can be a potential research direction to explore.

**Full-scale implementation** - The soft sensor validations presented in this work are conducted on a pilot-scale unit. Although the influent raw wastewater to the pilot plant contains sufficient unmeasured disturbances, the variations are comparatively lower when compared to the disturbances occurring in a full-scale process. Implementations in a full-scale operational unit and

a thorough investigation of the practical problems encountered would be the next step for the work presented in this thesis.

**IoT infrastructure** - The new IoT infrastructure presented in the thesis is not limited to remote monitoring of sensor data or deployment of soft sensors. The system can also be used to deploy control algorithms written in Python or MATLAB. Remote deployment of MPC control scripts on a pilot or full-scale WRRF using the open-source IoT infrastructure would be an interesting research activity. Control script deployment would further expand the applicability of the IoT system described in this thesis.

**Improving struvite product quality** - Several experiments have been conducted to study the influence of operating parameters on the crystal dimensions, settling properties, and the separation of struvite crystals in the recovery unit (Shaddel et al., 2019). The EMPC strategy discussed in this thesis limits itself to the simultaneous optimization of phosphorus recovery and magnesium hydroxide consumption. However, the control strategy can be expanded to include new objectives (larger crystal size, faster settling, etc.) that are critical to the struvite recovery process. Updating EMPC's objective function and developing a mathematical model to correlate operating parameters with the components in the economic-oriented objective function could be the next research step to further improve the recovery process.

# References

- Abonyi, J., Farsang, B. and Kulcsar, T., 2014. Data-driven development and maintenance of soft-sensors. *Proceedings of IEEE the 12<sup>th</sup> International Symposium on Applied Machine Intelligence and Informatics*, Herlany, Slovakia. 239–244, doi: 10.1109/SAMI.2014.6822414.
- Aguado, D., Ferrer, A., Seco, A. and Ferrer, J., 2006. Comparison of different predictive models for nutrient estimation in a sequencing batch reactor for wastewater treatment. *Chemometrics and Intelligent Laboratory Systems*, **84**(1–2), 75–81., doi: 10.1016/j.chemolab.2006.03.009.
- Ahmad, I., Ayub, A., Kano, M. and Cheema, I.I., 2020. Gray-box Soft Sensors in Process Industry: Current Practice, and Future Prospects in Era of Big Data. *Processes*, **8**(2), 243, doi: 10.3390/pr8020243.
- Al-Dasoqi, N., Mason, A., Alkhaddar, R. and Al-Shammaa, A., 2011. Use of Sensors in Wastewater Quality Monitoring - a Review of Available Technologies. *In: World Environmental and Water Resources Congress 2011: Bearing Knowledge for Sustainability*, May 22–26, Palm Springs, California, USA, doi: 10.1061/41173(414)354.
- Albalawi, F., Durand, H. and Christofides, P.D., 2017. Distributed economic model predictive control for operational safety of nonlinear processes. *AICHE Journal*, **63**(8), 3404–3418, doi: 10.1002/aic.15710.
- APHA, AWWA, WEF, 2012. Standard methods for the examination of water and wastewater, 22<sup>nd</sup> Ed, *American Public Health Association*, Washington, D.C, ISBN: 9780875532875.
- Aydin, E., Arkun, Y. and Is, G., 2016. Economic Model Predictive Control (EMPC) of an Industrial Diesel Hydroprocessing Plant. *IFAC Papers Online*, **49**(7), 568–573, doi: 10.1016/j.ifacol.2016.07.403.
- Barnard, J.L. and Crowther, R., 1993. Instrumentation in biological nutrient removal plants. *6<sup>th</sup> LAWQ Workshop on ICA of Water and Wastewater Treatment and Transport Systems*. June 17–19, Banff, Canada.
- Basford, P.J., Johnston, S.J., Perkins, C.S., Garnock-Jones, T., Tso, F.P., Pezaros, D., Mullins, R.D., Yoneki, E., Singer, J. and Cox, S.J., 2020. Performance analysis of single board computer clusters, *Future Generation Computer Systems*, **102**, 278–291, doi: 10.1016/j.future.2019.07.040.

- Bohlin T.P., 2006. Practical Grey-box Process Identification: Theory and Applications, *Springer Science and Business Media*, Berlin, Germany, ISBN:978-1-84628-403-8.
- Boyd, S., El Ghaoui, L., Feron, E. and Balakrishnan, V., 1994. Linear matrix inequalities in system and control theory. *Society for industrial and applied mathematics*, Philadelphia, US, ISBN:978-0-89871-485-2.
- Bratby, J. 2006. Coagulation and Flocculation in Water and wastewater Treatment. 2<sup>nd</sup>, *IWA Publishing*, London, U.K, ISBN:139781843391067.
- Brdjanovic, D., Meijer, S.C.F., López Vázquez, C.M., Hooijmans, C.M. and van Loorsdrecht, M.C.M., 2015. Applications of Activated Sludge Models. *IWA Publishing*, London, UK. ISSN:9781780404639.
- Brdys, M.A., Grochowski, M., Gminski, T., Konarczak, K. and Drewa, M., 2008. Hierarchical predictive control of integrated wastewater treatment systems. *Control Engineering Practice*, **16**(6), 751–767, doi: 10.1016/j.conengprac.2007.01.008.
- Budka, M., Eastwood, M., Gabrys, B., Kadlec, P., Martin-Salvador, M., Schwan, S., Tsakonas, A., Zliobaitė, I., 2014. From Sensor Readings to Predictions: On the Process of Developing Practical Soft Sensors. *In Advances in IDA XIII*, **8819**, 49–60.
- Busch, J., Elixmann, D., Kühl, P., Gerkens, C., Schlöder, J.P., Bock, H.G. and Marquardt, W., 2013. State estimation for large-scale wastewater treatment plants. *Water Research*, **47**(13), 4774–4787. doi: 10.1016/j.watres.2013.04.007.
- Cadet, C., 2014. Simplifications of activated sludge model with preservation of its dynamic accuracy. *IFAC Proceedings Volumes*, **47**(3), 7134-7139, doi: 10.3182/20140824-6-ZA-1003.01140.
- Cakici, A. and Bayramoglu, M., 1996. An approach to controlling sludge age in the activated sludge process. *Water Research*, **29**(4), 1093–1097, doi: 10.1016/0043-1354(94)00249-7.
- Chai, Q., Furenes, B. and Lie, B., 2007. Comparison of state estimation techniques, applied to a biological wastewater treatment process. *IFAC Proceedings Volumes*, **40**(4), 357-362, doi: 10.3182/20070604-3-MX-2914.00061.
- Chislock, M.F., Doster, E., Zitomer, R.A. and Wilson, A.E., 2013. Eutrophication: Causes, Consequences, and Controls in Aquatic Ecosystems. *Nature Education Knowledge*. **4**(4), 10.
- Carstensen, J., Harremoës, P. and Strube, R., 1996. Software sensors based on the grey-box modelling approach. *Water Science and Technology*, **33**(1), 117-126, doi: 10.1016/0273-1223(96)00164-3.
- Chen, X., Heidarinejad, M., Liu, J. and Christofides, P.D., 2012. Distributed economic MPC: application to a nonlinear chemical process network, *Journal of Process Control*, **22**(4), 689-699, doi: 10.1016/j.jprocont.2012.01.016.

- Copp, J.B., 2002. The COST Simulation Benchmark. Description and Simulator Manual. *Office for official publications of the European communities*, Luxembourg.
- Cordell, D. and White, S., 2011. Peak phosphorus: Clarifying the key issues of a vigorous debate about long-term phosphorus security. *Sustainability*, **3**(10), 2027-2049, doi: 10.3390/su3102027.
- Devisscher, M., Bogaert, H., Bixio, D., Van de Velde, J. and Thoeye, C., 2002. Feasibility of automatic chemicals dosage control a full-scale evaluation. *Water Science and Technology*, **45**(4-5), 445-452, doi: 10.2166/wst.2002.0647.
- Ellis, M., Durand, H. and Christofides, P.D., 2014. A tutorial review of economic model predictive control methods. *Journal of Process Control*, **24**(8), 1156-1178, doi: 10.1016/j.jprocont.2014.03.010.
- Ellis, M., Liu, J. and Christofides, P.D. 2017. Economic Model Predictive Control, *Springer International Publishing*, Switzerland, ISBN 978-3-319-41107-1.
- El-Bestawy, E., Hussein, H., Baghdadi, H.H. and El-Saka, M.F., 2005. Comparison between biological and chemical treatment of wastewater containing nitrogen and phosphorus. *Journal of Industrial Microbiology and Biotechnology*, **32**, 195-203. doi: 10.1007/s10295-005-0229-y.
- Elser, J. and Bennett, E., 2011. A broken biogeochemical cycle. *Nature*, **478**, 29-31, doi: 10.1038/478029a.
- Erismann, J.W., Sutton, M.A., Galloway, J., Klimont, Z. and Winiwarer, W., 2008. How a century of ammonia synthesis changed the world, *Nature Geoscience*, **1**, 636-639, doi: 10.1038/ngeo325.
- Flores-Alsina, X., Solon, K., Kazadi-Mbamba, C., Tait, S., Gernaey, K.V., Jeppsson, U. and Batstone, D.J., 2016. Modelling phosphorus (P), sulfur (S) and iron (Fe) interactions for dynamic simulations of anaerobic digestion processes. *Water Research*, **95**, 370-382, doi: 10.1016/j.watres.2016.03.012.
- Forbes, M.G., Patwardham, R.S., Hamadah H. and Gopulani, R.B., 2015. Model predictive control in industry: Challenges and opportunities. *IFAC-PapersOnLine*, **48**(8). 531-538, doi: 10.1016/j.ifacol.2015.09.022.
- Gasperi, J., Laborie, B. and Rocher, V., 2012. Treatment of combined sewer overflows by ballasted flocculation: Removal study of a large broad spectrum of pollutants. *Chemical Engineering Journal*, **211-212**, 293-301, doi: 10.1016/j.cej.2012.09.025.
- Gellings, C.W. and Parmenter, K.E., 2004. Energy efficiency in fertilizer production and use, in: Gellings, W., Parmenter, K. (Eds.), *Efficient Use and Conservation of Energy. Encyclopedia of life support systems (EOLSS) Publishers*, Oxford, UK, ISBN:1905839324.
- Gernaey, K.V., Flores-Alsina, X., Rosen, C., Benedetti, L. and Jeppsson, U., 2011. Dynamic influent pollutant disturbance scenario generation using a phenomenological modelling approach. *Environmental Modelling and Software*, **26**(11), 1255-1267, doi: 10.1016/j.envsoft.2011.06.001.

- Gernaey, K.V, Jeppsson, U., Vanrolleghem, P.A. and Copp, J.B., 2014. Benchmarking of Control Strategies for Wastewater Treatment Plants. *Scientific and Technical Report No. 23*, IWA Publishing, London, U.K. ISBN:9781843391463.
- Glassey, J., Montague, G.A., Ward, A.C. and Kara, B.V., 1994. Artificial Neural Network Based Experimental Design Procedures for Enhancing Fermentation Development. *Biotechnology and Bioengineering*, **44**(4), 397-405, doi: 10.1002/bit.260440402.
- Godfray, H.C.J., Beddington, J.R., Crute, I.R., Haddad, L., Lawrence, D., Muir, J.F., Pretty, J., Robinson, S., Thomas, S.M. and Toulmin, C., 2010. Food security: The challenge of feeding 9 billion people. *Science*, **327**(5967), 812-818, doi: 10.1126/science.1185383.
- Gujer, W., Henze, M., Mino, T., Matsuo, T., Wentzel, M.C. and Marais, G.v.R., 1995. The Activated Sludge Model No. 2: Biological phosphorus removal, *Water Science and Technology*, **31**(2), doi: 10.1016/0273-1223(95)00175-M.
- Haimi, H., Mulas, M., Sahlstedt, K. and Vahala, R., 2009. Advanced operation and control methods of municipal wastewater treatment processes in Finland. Helsinki University of Technology, Water and Wastewater Engineering, Helsinki. ISBN:978-951-22-9975-1.
- Haimi, H., Mulas, M., Corona, F. and Vahala, R., 2013. Data-Derived Soft sensors for Biological Wastewater Treatment Plants: An overview., *Environmental Modelling and Software*, **47**, 88-107. doi: 10.1016/j.envsoft.2013.05.009.
- Haimi, H., Corona, F., Mulas, M., Sundell, L., Heinonen, M. and Vahala, R. 2015. Shall we use hardware sensor measurements or soft-sensor estimates? Case study in a full-scale WWTP. *Environmental Modelling Softwares*, **72**, 215-229, doi: 10.1016/j.envsoft.2015.07.013.
- Haugen, F., Bakke, R. and Bernt, L., 2014. State Estimation and Model-based Control of a Pilot Anaerobic Digestion Reactor. *Journal of Control Science and Engineering*, **2014**, doi: 10.1155/2014/572621.
- Henze, M., Grady, C.P.L., Gujer, W., Marais, G.v.R. and Matsuo, T., 1987. Activated Sludge Model No. 1. *IAWPRC Scientific and Technical Report No. 1.*, London: IAWPRC
- Henze, M., Gujer, W., Mino, T., Matsuo, T., Wentzel, M.C., Marais, G.v.R. and van Loosdrecht, M.C.M., 1999., Activated Sludge Model No. 2d., *Water Science and Technology*, **39**(1), 165-182, doi: 10.2166/wst.1999.0036.
- Hou, D., Al-Tabbaa, A., Guthrie, P. and Watanabe, K., 2012. Sustainable waste and materials management: National policy and global perspective. *Environmental Science and Technology*, **46**(5), 2494-2495, doi: 10.1021/es3004552.
- Ingildsen, P., Jeppsson, U. and Olsson, G., 2002. Dissolved oxygen controller based on on-line measurements of ammonium combining feed-forward and feedback, *Water Science and Technology*, **45**(4-5), 453-460, doi: 10.2166/wst.2002.0649.

- Jenkins, D. and Wanner, J. 2014., *Activated Sludge - 100 Years and Counting*, IWA Publishing, London, U.K, ISBN:9781780404936.
- Jeong, Y.K., and Hwang, S.J., 2005. Optimum doses of Mg and P salts for precipitating ammonia into struvite crystals in aerobic composting. *Bioresource Technology*, **96**(1), 1–6, doi: 10.1016/j.biortech.2004.05.028.
- Jeppsson, U., Rosen, C., Alex, J., Copp, J.B., Gernaey, K.V., Pons, M.-N. and Vanrolleghem, P.A., 2006. Towards a benchmark simulation model for plant-wide control strategy performance evaluation of WWTPs. *Water Science and Technology*, **53**(1), 287–295, doi: 10.2166/wst.2006.031.
- Jeppsson, U. and Olsson, G., 1993. Reduced order models for on-line parameters identification of the activated sludge process. *Water Science and Technology*, **28**(11-12), 173-183, doi: 10.2166/wst.1993.0657.
- Jeppsson, U. and Pons, M.N., 2004. The COST 624 benchmark simulation model—current state and future perspective. Editorial. *Control Engineering Practice*, **12**(3), 299–304, doi: 10.1016/j.conengprac.2003.07.001.
- Jeppsson, U., Alex, J., Pons, M.N., Spanjers, H. and Vanrolleghem, P.A., 2002. Status and future trends of ICA in wastewater treatment – A European perspective. *Water Science and Technology*, **45**(4–5), 485–494, doi: 10.2166/wst.2002.0653.
- Jeppsson, U., Pons, M.-N., Nopens, I., Alex, J., Copp, J., Gernaey, K.V., Rosen, C., Steyer, J.P. and Vanrolleghem, P.A., 2007. Benchmark simulation model no 2 – general protocol and exploratory case studies. *Water Science and Technology*, **56** (8), 67–78, doi: 10.2166/wst.2007.604.
- Julien, S., Babary, J.P. and Lessard, J.P., 1998. Theoretical and practical identifiability of a reduced order model in an activated sludge process doing nitrification and denitrification. *Water Science and Technology*, **37**(12), 309-316, doi: 10.1016/S0273-1223(98)00375-8.
- Kabouris, J.C. and Georgakakos A.P., 1990. Optimal control of the activated sludge process. *Water Research*, **24**(10), 1197-1208, doi: 10.1016/0043-1354(90)90042-5.
- Koo, J., Park, D., Ryu, S., Kim, G.H. and Lee, Y.W., 2019. Design of a self-tuning adaptive model predictive controller using recursive model parameter estimation for real-time plasma variable control. *Computers and Chemical Engineering*, **123**, 126–142, doi: 10.1016/j.compchemeng.2019.01.002.
- Leverenz, .HL., Asano, T., 2011. Wastewater reclamation and reuse system. *Treatise on Water Science*, **4**, 63-71, doi: 10.1016/B978-0-444-53199-5.00076-2.
- Li, Z., Lu, P., Zhang, D. and Zhang, T., 2018. Practical identifiability analysis and optimal experimental design for the parameter estimation of the ASM2d-Based EBPR anaerobic submodel. *Mathematical Problems in Engineering*, **18**, 1–9, doi: 10.1155/2018/9201085.



- Lindberg, C.F. and Carlsson, B., 1996. Adaptive control of external carbon flow rate in an activated sludge process. *Water Science and Technology*, **34**(3-4), 173-180, doi: 10.1016/0273-1223(96)84212-0.
- Lindelöf, D., Afshari, H., Alisafae, M., Biswas, J., Caban, M., Mocellin, X. and Viaene, J., 2015. Field tests of an adaptive, model-predictive heating controller for residential buildings. *Energy and Buildings*, **99**, 292-302, doi: 10.1016/j.enbuild.2015.04.029.
- Lizarralde, I., Fernández-Arévalo, T., Brouckaert, C., Vanrolleghem, P., Ikumi, D.S., Ekama, G.A., Ayesa, E. and Grau, P., 2015. A new general methodology for incorporating physico-chemical transformations into multiphase wastewater treatment process models. *Water Research*, **74**, 239-256, doi: 10.1016/j.watres.2015.01.031.
- Ljung, L., 1999. System Identification: Theory for the User. *PTR Prentice Hall*, New Jersey, USA. ISBN:978-0136566953.
- Lukasse, L.J.S., 1999. Control and Identification of Activated Sludge Processes, *PhD Thesis*, Wageningen Agricultural University, Wageningen, The Netherlands.
- Ma, Y., Peng, Y. and Wang X., 2009. Improving nutrient removal of the AAO process by an influent bypass flow by denitrifying phosphorus removal. *Desalination*, **246**(1-3), 534-544, doi: 10.1016/j.desal.2008.04.061.
- Ma, J., Qin, S.J. and Salsbury, T., 2014. Application of economic MPC to the energy and demand minimization of a commercial building. *Journal of Process Control*, **24**(8), 1282-1291, doi: 10.1016/j.jprocont.2014.06.011.
- Machado, V.C., Lafuente, J. and Baeza, J.A., 2014. Activated sludge model 2d calibration with full-scale WWTP data: comparing model parameter identifiability with influent and operational uncertainty. *Bioprocess and Biosystems Engineering*, **37**, 1271-1287, doi: 10.1007/s00449-013-1099-8.
- Manamperuma, L., Wei, L. and Ratnaweera, H., 2017. Multi-parameter based coagulant dosing control. *Water Science and Technology*, **75**(9), 2157-2162, doi: 10.2166/wst.2017.058.
- Marsili-Libelli, S., 1984. Optimal control of the activated sludge process. *Transactions of the Institute of Measurement and Control*, **6**(3), 146-152, doi: 10.1177/014233128400600305.
- Marsili-Libelli, S., Ratini, P., Spagni, A. and Bortone, G., 2001. Implementation, study and calibration of a modified ASM2d for the simulation of SBR processes. *Water Science and Technology*, **43**(3), 69-76., doi: 10.2166/wst.2001.0120.
- Marti, N., Bouzas, A., Seco, A. and Ferrer, J., 2008. Struvite precipitation assessment in anaerobic digestion processes, *Chemical Engineering Journal*, **141**(1-3), 67-74, doi: 10.1016/j.cej.2007.10.023.
- Mayne, Q.D., 2014. Model predictive control: Recent developments and future promise. *Automatica*, **50**(12), 2967-2986, doi: 10.1016/j.automatica.2014.10.128.



- Mbamba, C.K, Flores-Alsina, X., Batstone, J.D. and Tait, S., 2016. Validation of a plant-wide phosphorus modelling approach with minerals precipitation in a full-scale WWTP. *Water Research*, **100**, 169–183, doi: 10.1016/j.watres.2016.05.003.
- Mbamba, C.K., Lindblom, E., Flores-Alsina, X., Tait, S., Anderson, S. and Saagi, R., 2019. Plant-wide model-based analysis of iron dosage strategies for chemical phosphorus removal in wastewater treatment systems. *Water Research*. **155**, 12–25, doi: 10.1016/j.watres.2019.01.048.
- Metcalf, L. and Eddy, H.P., 1914. American Sewerage Practice. *McGraw-Hill*, Volume I: Design of Sewers. pp 28-29, New York, USA.
- Nair, A., Cristea, V.M., Agachi, P. Ş. and Brehar, M., 2017. Model calibration and feed-forward control of the wastewater treatment plant – case study for Cluj-Napoca WWTP. *Water and Environment Journal*, **32**(2), 164–172, doi: 10.1111/wej.12310.
- Neset, T.S.S., Cordell, D., 2012. Global phosphorus scarcity: Identifying synergies for a sustainable future. *Journal of the Science of Food and Agriculture*. **92**(1), 2–6, doi: 10.1002/jsfa.4650.
- Newhart, K.B., Holloway, R.W., Hering, A.S. and Cath, T.Y., 2019. Data-driven performance analyses of wastewater treatment plants: a review *Water Research*, **157**, 498-513, doi: 10.1016/J.WATRES.2019.03.030.
- Nopens, I., Benedetti, L., Jeppsson, U., Pons, M., Alex, J., Copp, J.B., Gernaey, K.V., Rosen, C., Steyer, J. and Vanrolleghem, P.A., 2010. Benchmark Simulation Model No 2 - finalisation of plant layout and default control strategy. *Water Science and Technology*, **62**(9), 1967–1974, doi: 10.2166/wst.2010.044.
- O'Brien, M., Mack, J., Lennox, B., Lovett, D. and Wall, A., 2011. Model predictive control of an activated sludge process: A case study. *Control Engineering Practice*, **19**(1), 54–61, doi: 10.1016/j.conengprac.2010.09.001.
- Olsson, G., Nielsen, M.K., Yuan, Z., Lynggaard-Jensen, A., Styer, J.P., 2005. Instrumentation Control and Automation in Wastewater System. Scientific and technical Report No. 15, IWA Publishing, London, pp 90-91.
- Olsson, G. and Jeppsson, U., 2006. Plant-wide control: dream, necessity or reality? *Water Science and Technology*, **53**(3), 121-129, doi: 10.2166/wst.2006.083.
- Olsson, G., 2006. Instrumentation, control and automation in the water industry – state-of-the-art and new challenges. *Water Science and Technology*, **53**(4-5), 1-16, doi: 10.2166/wst.2006.097.
- Olsson, G., 2012. ICA and me - a subjective review., *Water Research*, **46**(6), 1585-1624, doi: 10.1016/j.watres.2011.12.054.
- Olsson, G., Carlsson, B., Comas, J., Copp, J., Gernaey, K.V., Ingildsen, P., Jeppsson, U., Kim, C., Rieger, L., Rodríguez-Roda, I., Steyer, J.P., Takacs, I., Vanrolleghem P.A., Vargas, A., Yuan, Z. and Åmand, L., 2014. Instrumentation, control and automation

- in wastewater - from London 1973 to Narbonne 2013. *Water Science and Technology*, **69**, 1373-1385. doi: 10.2166/wst.2014.057.
- Orhon, D., 1997. Modeling of activated sludge systems. *CRC Press*, USA.
- Patton, R.J., Frank, P.M. and Clark, R.N., 2000. Issues of Fault Diagnosis for Dynamic Systems. *Springer-Verlag*. ISBN 978-1-4471-3644-6.
- Pisa, I., Santín, I., Vicario, J.L., Morell, A. and Vilanova, R., 2019. ANN-Based Soft Sensor to Predict Effluent Violations in Wastewater Treatment Plants. *Sensors*, **19**(6), 1280, doi: 10.3390/s19061280.
- Puznava, N., Zeghal, S. and Reddet, E., 1998. Simple Control Strategies of Methanol Dosing for Post- Denitrification. *Water Science and Technology*, **38**(3), 291-297, doi: 10.1016/S0273-1223(98)00482-X.
- Qin, S.J. and Badgwell, T.A., 2003. A survey of industrial model predictive control technology. *Control Engineering Practice*, **11**(7), 733-764, doi: 10.1016/S0967-0661(02)00186-7.
- Ratnaweera, H. and Fettig, J. 2015. State of the Art of Online Monitoring and Control of the Coagulation Process, *Water*, **7**, 6574–6597, doi: 10.2166/wst.2018.498.
- Regmi, P., Miller, M., Jimenez, J., Stewart, H., Johnson, B., Amerlinck, Y., Volcke, E.I.P., Arnell, M., García, P.J., Maere, T., Torfs, E., Vanrolleghem, P.A., Miletic, I., Rieger, L., Schraa, O., Samstag, R., Santoro, D., Snowling, S. and Takács, I., 2019. The future of WRRF modelling - Outlook and challenges, *Water Science and Technology*, **79**(1), 3-14, doi: 10.2166/wst.2018.498.
- Rieger, L. and Olsson, G., 2012. Why many control systems fail. *Water Environment and Technology*, **24**(6), 3906-3918, doi: 10.2175/193864711802764779.
- Robertson, D.G., Lee, J.H. and Rawlings, J.B., 1996. A Moving Horizon-Based Approach for Least-Squares Estimation. *AIChE Journal*, **42**(8), 2209-2224, doi: 10.1002/aic.690420811.
- Rosen, C., Jeppsson, U. and Vanrolleghem, P.A., 2004. Towards a common benchmark for long-term process control and monitoring performance evaluation. *Water Science and Technology*, **50**(11), 41–49, doi: 10.2166/wst.2004.0669.
- Rosso, D., Larson, L.E. and Stenstrom, M.K., 2008. Aeration of large-scale municipal wastewater treatment plants: state of the art. *Water Science and Technology*, **57**(7), 973–978, doi: 10.2166/wst.2008.218.
- Sahlmann, C., Libra, J.A., Schuchardt, A., Wiesmann, U. and Gnirss, R., 2004. A control strategy for reducing aeration costs during low loading periods. *Water Science and Technology*, **50**(7), 61–68, doi: 10.2166/wst.2004.0417.
- Saltnes, T., Sørensen, G. and Eikås, S., 2017. Biological nutrient removal in a continuous biofilm process. *Water Practice and Technology*, **12**(4), 797–805, doi: 10.2166/wpt.2017.083.

- Serralta, J., Borrás, L., Blanco, C., Barat, R. and Seco, A., 2004. Monitoring pH and electric conductivity in an EBPR sequencing batch reactor. *Water Science and Technology*, **50**(10), 145–152, doi: 10.2166/wst.2004.0630.
- Shaddel, S., Ucar, S., Andreassen, J.-P. and Østerhus, S.W., 2019. Engineering of struvite crystals by regulating supersaturation - Correlation with phosphorus recovery, crystal morphology and process efficiency. *Journal of Environmental Chemical Engineering*, **7**(1), 102918, doi: 10.1016/j.jece.2019.102918.
- Simon, D., 2006. Optimal State Estimation, *John Wiley and Sons*, Chichester, UK, ISBN:9780470045343.
- Sohlberg, B. and Jacobsen, E.W., 2008. Grey box modelling—branches and experiences. *IFAC Proceedings Volumes*, **41**(2), 11415–11420, doi: 10.3182/20080706-5-KR-1001.01934.
- Solon, K., Flores-Alsina, X., Kazadi Mbamba, C., Volcke, E.I.P., Tait, S., Batstone, D.J., Gernaey, K.V. and Jeppsson, U., 2015. Effects of ionic strength and ion pairing on (plant-wide) modelling of anaerobic digestion processes. *Water Research*, **70**, 235–245, doi: 10.1016/j.watres.2014.11.035.
- Solon, K., Flores-Alsina, X., Mbamba, C.K, Ikumi, D., Volcke, E.I.P., Vaneekhaute, C., Ekama, G., Vanrolleghem, P.A., Batstone, D.J., Gernaey, K.V. and Jeppsson, U., 2017. Plant-wide modelling of phosphorus transformations in wastewater treatment systems: Impacts of control and operational strategies. *Water Research*, **113**, 97–110, doi: 10.1016/j.watres.2017.02.007.
- Solon, K., Jia, M. and Volcke, E.I.P., 2019. Process schemes for future energy-positive water resource recovery facilities. *Water Science and Technology*, **79**(9), 1808–1820, doi: 10.2166/wst.2019.183.
- Solon, K., Volcke, E.I.P., Spérandiob, M. and van Loosdrecht, M.C.M., 2019. Resource recovery and wastewater treatment modelling. *Environmental Science: Water Research and Technology*, **5**, 631–642, doi: 10.1039/c8ew00765a.
- Sriwiriyarat, T. and Randall, C.W., 2005. Evaluation of integrated fixed film activated sludge wastewater treatment processes at high mean cells residence time and low temperatures. *Journal of Environmental Engineering*, **131**(11), 1550–1556, doi: 10.1061/(ASCE)0733-9372(2005)131:11(1550).
- Stare, A., Hvala, N. and Vrečko, D., 2006. Modeling, Identification, and Validation of Models for Predictive Ammonia Control in a Wastewater Treatment Plant - A Case Study. *ISA transactions*, **45**(2), 159–174, doi: 10.1016/S0019-0578(07)60187-6.
- Stare, A., Vrečko, D., Hvala, N. and Strmčnik, S., 2007. Comparison of control strategies for nitrogen removal in an activated sludge process in terms of operating costs: a simulation study. *Water Research*, **41**(9), 2004–2014, doi: 10.1016/j.watres.2007.01.029.

- Steffens, M.A. and Lant, P.A., 1999. Multivariable control of nutrient-removing activated sludge systems. *Water Research*, **33**(12), 2864–2878, doi: 10.1016/S0043-1354(98)00521-1.
- Stentoft, P.A., Munk-Nielsen, T., Vezzaro, L., Madsen, H., Mikkelsen, P.S. and Møller, J.K., 2019. Towards model predictive control: Online predictions of ammonium and nitrate removal by using a stochastic ASM. *Water Science and Technology*, **79**, 51–62, doi: 10.2166/wst.2018.527.
- Sutton, M.A., Bleeker, A., Howard, C.M., Bekunda, M., Grizzetti, B., de Vries, W., van Grinsven, H.J.M, Abrol, Y.P, Adhya, T.K., Billen, G., Davidson, E.A., Datta, A., Diaz, R., Erisman, J.W., Liu, X.J., Oenema, O., Palm, C., Raghuram, N., Reis, S., Scholz, R.W., Sims, T., Westhoek, H. and Zhang, F.S., 2013. Our nutrient world: The challenge to produce more food and energy with less pollution. *Report: Global Overview of Nutrient Management, Centre for Ecology and Hydrology*, Edinburgh, UK.
- Sweeney, M.W. and Kabouris, J.C., 2015. Modeling, Instrumentation, Automation, and Optimization of Water Resource Recovery Facilities, *Water Environment Research*, **87**(10), 1178-1195, doi: 10.2175/106143015x14338845155589.
- Takács, I., Patry, G.G., and Nolasco, D., 1991. A dynamic model of the clarification thickening process. *Water Research*, **25**(10), 1263–1271, doi: 10.1016/0043-1354(91)90066-Y.
- Thomas, O., Baurès, E. and Pouet, M.F., 2005. UV spectrophotometry as a non-parametric measurement of water and wastewater quality variability, *Water Quality Research Journal of Canada*, **40**(1), 51-58, doi: 10.2166/wqrj.2005.004.
- Thomas, O. and Pouet, M.F. Wastewater quality monitoring: on-line/on-site measurement In: Barceló D. (eds) *Water Pollution. The Handbook of Environmental Chemistry*, Springer, Berlin, Germany, ISBN:978-3-540-22229-3.
- Thomson, H.A. and Kisbye, K., 1996. N and P on-line meters: requirements, maintenance and stability. *Water Science and Technology*, **33**(1), 147-157, doi: 10.2166/wst.1996.0014.
- Tsai, C.C., Teng, F.J. and Lin, S.C., 2003. Direct self-tuning model following predictive control of a variable-frequency oil-cooling machine. *American Control Conference*, Denver, CO, USA, doi: 10.1109/ACC.2003.1239085.
- Tscheikner-Gratl, F., Zeisl, P., Kinzel, C., Leimgruber, J., Ertl, T., Rauch, W. and Kleidorfer, M., 2016. Lost in calibration: Why people still do not calibrate their models, and why they still should - A case study from urban drainage modelling. *Water Science and Technology*, **74**(10), 2337–2348, doi: 10.2166/wst.2016.395.
- Udugama, I.A., Petersen, L.A.H., Falco, F.C., Junicke, H., Mitic, A., Alsina, X.F., Mansouri, S.S., Gernaey, K.V., 2020. Resource recovery from waste streams in a water-energy-food nexus perspective: Toward more sustainable food processing. *Food and Bioproducts Processing*, **119**, 133–147. doi: 10.1016/j.fbp.2019.10.014.

- Vanrolleghem, P.A. and Vaneekhaute, C., 2014. Resource Recovery from Wastewater and Sludge: Modelling and Control Challenges., *In Proceedings of the IWA Specialist Conference on Global Challenges: Sustainable Wastewater Treatment and Resource Recovery*, Kathmandu, Nepal, 26–30 October 2014.
- Vanrolleghem, P.A. and Lee, D.S., 2003. On-Line Monitoring Equipment for Wastewater Treatment Processes: State of the Art. *Water Science and Technology*, **47**(2), 1-34, doi: 10.2166/wst.2003.0074.
- Vrečko, D., Hvala, N., Stare, A., Burica, O., Stražar, M., Levstek, M., Cerar, P., Podbevšek, S., 2006. Improvement of ammonia removal in activated sludge process with feedforward-feedback aeration controllers. *Water Science and Technology*, **53**(4-5), 125-132, doi: 10.2166/wst.2006.098.
- Vrečko, D., Hvala, N. and Stražar, M. 2011. The application of model predictive control of ammonia nitrogen in an activated sludge process. *Water Science and Technology*, **64**(5), 1115–1121, doi: 10.2166/wst.2011.477.
- Wacheux, H., Million, J.L., Guillo, C. and Alves, E., 1996.  $\text{NH}_4^+$  automatic analysers for wastewater treatment plant: evaluation test at laboratory and field level. *Water Science and Technology*, **33**(1), 193-201, doi: 10.1016/0273-1223(96)00172-2.
- Wang, X., Teichgraber, H., Palazoglu, A. and El-Farra, N.H., 2014. An economic receding horizon optimization approach for energy management in the chlor-alkali process with hybrid renewable energy generation, *Journal of Process Control*, **24**(8), 1318–1327, doi: 10.1016/j.jprocont.2014.04.017.
- Wei, L. and Ratnaweera, H., 2016. Improvement of multi-parameter based feed-forward coagulant dosing control systems with feed-back functionalities. *Water Science and Technology*. **74**(2), 491–499, doi: 10.2166/wst.2016.180.
- Weijers, S. (2000). Modelling, Identification and Control of Activated Sludge Plants for Nitrogen Removal, *PhD Thesis*, Technische Universiteit Eindhoven, Eindhoven, The Netherlands.
- Xu, J., Li, Y. and Wang, H., 2017. Exploring the feasibility of energy self-sufficient wastewater treatment plants: a case study in eastern China. *Energy Procedia*, **142**, 3055–3061, doi: 10.1016/j.egypro.2017.12.444.
- Yin, S., Ding, S.X., Haghani, A., Hao, A. and Zhang, P., 2012. A comparison study of basic data-driven fault diagnosis and process monitoring methods on the benchmark Tennessee Eastman process, *Journal of Process Control*, **22**(9), 1567-1581, doi: 10.1016/j.jprocont.2012.06.009.
- Yu R., Liaw S., Chang C., Lu H. and Cheng W., 1997. Monitoring and Control Using On-line ORP on the Continuous-Flow Activated Sludge Batch Reactor System. *Water Science and Technology*, **35**(1), 57-66, doi: 10.1016/S0273-1223(96)00879-7.
- Yuan, Z., Bogaert, H., Rosen, C. and Verstraete, W., 2001. Sludge Blanket Height Control in Secondary Clarifiers. *In Proceedings of the 1<sup>st</sup> IWA Conference on Instrumentation, Control and Automation*, Malmö, Sweden, June 3-7, 81-88.

- Yuan, Z., Oehmen, A. and Ingildsen, P., 2002. On the Control of Nitrate Recirculation Flow in Predenitrification Systems. *Water Science and Technology*, **45**(4-5), 29-36, doi: 10.2166/wst.2002.0544.
- Zarrad, W., Harmand, J., Devisscher, M. and Steyer, J.P., 2004. Comparison of advanced control strategies for improving the monitoring of activated sludge processes. *Control Engineering Practice*, **12**(3), 323-333, doi: 10.1016/S0967-0661(03)00169-2.
- Zeng, J., Liu, J., Zou, T. and Yuan, D., 2016. Distributed extended Kalman filtering for wastewater treatment processes. *Industrial and Engineering Chemistry Research*, **55**(28), 7720-7729, doi: 10.1021/acs.iecr.6b00529.
- Zhang, Q., 2000. Some Implementation Aspects of Sliding Window Least Squares Algorithms. *IFAC Proceedings Volumes*, **33**(15), 763-768, doi: 10.1016/S1474-6670(17)39844-0.
- Zhang, T., Zhang, D., Li, Z. and Cai, Q., 2010. Evaluating the structural identifiability of the parameters of the EBPR sub-model in ASM2d by the differential algebra method. *Water Research*, **44**(9), 2815-2822. doi: 10.1016/j.watres.2010.02.027.
- Zhang, A., Yin, X., Liu, S., Zeng, J. and Liu, J., 2019. Distributed economic model predictive control of wastewater treatment plants. *Chemical Engineering Research and Design*, **141**, 144-155., doi: 10.1016/j.cherd.2018.10.039.
- Zhang, A. and Liu, J., 2019. Economic MPC of wastewater treatment plants based on model reduction. *Processes*, **7**, 682, doi: 10.3390/pr7100682.
- Zhao, L., Chai, T. and Cong, Q., 2006. Hybrid dynamic model of anoxic-aeration biological wastewater treatment plant. *6<sup>th</sup> World Congress on Intelligent Control and Automation*, Dalian, China, 1, 4781-4785. doi: 10.1109/WCICA.2006.1713291.
- Åmand, L., Olsson, G. and Carlsson, B., 2013. Aeration control - A review., *Water Science and Technology*, **67**(1), 2374-2398, doi: 10.2166/wst.2013.139.
- Ødegaard, H., Rusten, B. and Westrum, T., 1994. A new moving bed biofilm reactor - applications and results. *Water Science and Technology*, **29**(10-11), 157-165, doi: 10.2166/wst.1994.0757.

# List of Appended Papers

## Paper A

**Nair, A.M.**, Fanta, A., Haugen, F.A. and Ratnaweera, H., 2019. Implementing an Extended Kalman Filter for estimating nutrient composition in a sequential batch MBBR pilot plant, *Water Science and Technology*, **80**(2), 317-328, doi: 10.2166/wst.2019.272.

## Paper B

**Nair, A.M.**, Gonzales, B.M., Haugen, F.A., Ratnaweera, H. and Østershus, S.W., 2020. Real-time monitoring of enhanced biological phosphorus removal in a multistage EBPR-MBBR using a soft-sensor for phosphates, *Journal of Water Process Engineering*, **37**, 101494, doi: 10.1016/j.jwpe.2020.101494.

## Paper C

**Nair, A.M.**, Hykkerud, A. and Ratnaweera, H., 2020. A cost-effective IoT strategy for remote deployment of soft sensors – a case study on implementing a soft sensor in a multistage MBBR plant, *Water Science and Technology*, **81**(8), 1733–1739, doi: 10.2166/wst.2020.067.

## Paper D

**Nair, A.M.**, Haugen, F.A. and Ratnaweera, H. An adaptive Model Predictive Control strategy for ammonia based aeration control in a water resource recovery facility - a simulation study, *Submitted to Control Engineering Practices*.

## Paper E

**Nair, A. M.**, Haugen, F.A. and Ratnaweera, H. Economic Model Predictive Control for optimal struvite recovery. *Submitted to Journal of Environmental Management*.








# Paper A






## Implementing an Extended Kalman Filter for estimating nutrient composition in a sequential batch MBBR pilot plant

Abhilash M. Nair , Abaynesh Fanta, Finn Aakre Haugen  and Harsha Ratnaweera 


### ABSTRACT

Online monitoring of water quality parameters can provide better control over various operations in wastewater treatment plants. However, a lack of physical online sensors, the high price of the available online water-quality analyzers, and the need for regular maintenance and calibration prevent frequent use of online monitoring. Soft-sensors are viable alternatives, with advantages in terms of price and flexibility in operation. As an example, this work presents the development, tuning, implementation, and validation of an Extended Kalman Filter (EKF) on a grey-box model to estimate the concentration of volatile fatty acids (VFA), soluble phosphates ( $\text{PO}_4\text{-P}$ ), ammonia nitrogen ( $\text{NH}_4\text{-N}$ ) and nitrate nitrogen ( $\text{NO}_3\text{-N}$ ) using simple and inexpensive sensors such as pH and dissolved oxygen (DO). The EKF is implemented in a sequential batch moving bed biofilm reactor (MBBR) pilot scale unit used for biological phosphorus removal from municipal wastewater. The grey-box model, used for soft sensing, was constructed by fitting the kinetic data from the pilot plant to a reduced order version of ASM2d model. The EKF is successfully validated against the standard laboratory measurements, which confirms its ability to estimate various states during the continuous operation of the pilot plant.

**Key words** | biological phosphorus removal, Extended Kalman Filter, sequential batch biofilm process, soft-sensor

Abhilash M. Nair  (corresponding author)  
Harsha Ratnaweera   
Faculty of Science and Technology,  
Norwegian University of Life Sciences,  
P.O. Box 5003, 1432 Aas,  
Norway  
E-mail: muralabh@nmbu.no

Abaynesh Fanta  
Department of Hydraulic and Environmental  
Engineering,  
Norwegian University of Science and Technology  
(NTNU),  
S. P. Andersens vei 5, Trondheim 7491,  
Norway

Finn Aakre Haugen   
University of South-Eastern Norway,  
Kjølnes ring 56, Porsgrunn,  
Norway

### INTRODUCTION

There has been a rapid increase in the implementation of advanced control strategies in process industries, including water resource recovery facilities (WRRF). These control strategies are essential for the optimal operation of process plants (O'Brien *et al.* 2011). Advanced control strategies such as model predictive control (MPC) would require continuous, real-time information of various wastewater compositions (Liukkonen *et al.* 2013).

A number of online instruments for measuring nutrient composition are available in the market today. However, their use is often limited to large-scale urban treatment facilities (Häck & Wiese 2006). Despite considerable developments in online instrumentation in the past decade,

physical sensors for real-time measurement of some of the wastewater quality parameters are either extremely expensive or do not exist. Moreover, sensors available in today's market are vulnerable to fouling, drift or other inaccuracies resulting in unreliable measurement (Olsson & Jeppsson 2006). A lot of effort is put into fault detecting systems (either manual or real-time) to remove errors and correct sensors readings. Most online sensors (both ion selective and optical) require a lot of attention in terms of data quality checks, through regular inspection and adjustment (Olsson 2012). On the other hand, composition analyzers provide an accurate measurement of parameters such as ammonia, nitrate, chemical oxygen demand (COD), and phosphates, but are extremely expensive. Due to these problems, most WRRF depend on standardized laboratory measurements rather than online monitoring. However, parameters such as pH, oxidation-reduction potential (ORP), dissolved

This is an Open Access article distributed under the terms of the Creative Commons Attribution Licence (CC BY 4.0), which permits copying, adaptation and redistribution, provided the original work is properly cited (<http://creativecommons.org/licenses/by/4.0/>).

doi: 10.2166/wst.2019.272

oxygen (DO) and conductivity can be measured with relative ease and higher accuracy. Therefore, these sensors, which are often inexpensive, are installed in almost all treatment plants including small to medium WRRF.

Soft sensors are an alternative to expensive composition analyzers and unreliable in-situ sensors (Thürlimann *et al.* 2018). Soft sensors, also denoted as state estimators, virtual sensors, etc., use system knowledge enclosed in the process model together with available measurements. These software sensors can be used not only as alternative to expensive analyzers but also as a support system for the existing composition analyzers by acting as a reliable backup in case of an instrument malfunction (Haimi *et al.* 2013). A detailed compilation of statistical models such as artificial neural networks (ANN), partial least-square regression (PLSR) or auto-regressive models (ARX) used for real-time estimation is provided in Haimi *et al.* (2013). Mechanistic models describing biological processes such as activated sludge model (ASM) can also be used with state estimators such as Extended Kalman Filter (EKF) or Moving Horizon Estimator (MHE) for developing soft sensors (Busch *et al.* 2013). However, most of these state estimators are tested and validated on the BSM 1 simulator. We have not found reports of implementation of state estimators with mechanistic models for soft sensing in a real system.

The aim of this work is to develop a dynamic state-estimator to provide real-time estimations of  $\text{PO}_4\text{-P}$ , volatile fatty acids (VFA),  $\text{NH}_4\text{-N}$ , and  $\text{NO}_3\text{-N}$  in a sequential batch reactor, by using data obtained from online sensors such as pH and DO.

## MATERIALS AND METHODS

### Pilot plant setup

The sequential batch moving bed Bio-P (SB-MBBR Bio-P) pilot plant, located in the wastewater laboratory at Norwegian University of Science and Technology (NTNU) was used to test and validate the soft-sensor algorithm. Figure 1 depicts the pilot plant and the data acquisition system. The sequential batch reactor (SBR) contains polyurethane carriers (with 60% filling) which are exposed to raw wastewater to ensure biofilm growth and attachment to the carriers (see Supplementary Figure 1, available with the online version of this paper). The reactor has a total working volume of 13 L. It operates with a fixed cycle time of 8 h and a temperature of  $16 \pm 0.5$  °C. The carrier media have a cylindrical shape (10 mm in diameter and length) with a cross

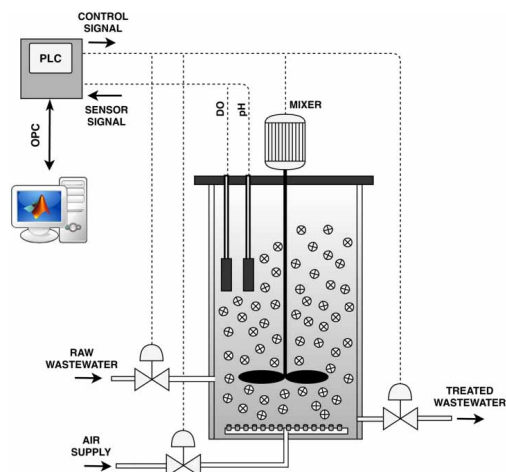


Figure 1 | Pilot plant layout and the data acquisition system.

inside the cylinder and longitudinal fins outside, providing a large surface area for biofilm growth (Ødegaard *et al.* 1994). The SBR is fed with wastewater from a storage tank, which receives steady supply of raw wastewater from a nearby municipal sewer. The storage tank has a total volume of  $3.5 \text{ m}^3$  and a residence time of 24 h, which ensures an uninterrupted supply of wastewater while maintaining sufficient variations in influent wastewater quality.

After ensuring the attachment of active biofilm to the carrier, the reactor operates in an alternating anaerobic-aerobic cyclic process with a hydraulic retention time of 8 h (3 h anaerobic, 5 h aerobic, 3 min filling and 3 min emptying). A sieve at the outlet line retains the carriers in the SBR, allowing just the treated water and detached biomass to exit the reactor. The reactor operates as a biofilm process and all active biomass is attached to the carrier media. Therefore, the SBR can be operated with a 100% volume exchange ratio, resulting in a cycle time equal to the hydraulic retention time. The system is mechanically agitated using a custom-made mixer for the entire cycle period. During the aerobic phase, air is supplied with a constant flow rate of  $4.5 \text{ L min}^{-1}$ . The algorithm to execute the cycle time and the operational sequence is stored in the Supervisory Control and Data Acquisition (SCADA) system of the plant.

During the anaerobic-stage, the active biomass (primarily PAOs) utilizes the acetate from raw wastewater and converts it into polyhydroxy-alkanoates ( $X_{\text{PHA}}$ ). As a result,  $\text{PO}_4\text{-P}$  is released due to Poly-P degradation, thus increasing its concentration in bulk solution. In anaerobic conditions,

the readily biodegradable organic matter (BOD) is also converted to VFA by fermentation, and the PAOs utilize it for further  $\text{PO}_4\text{-P}$  release. When aeration begins, the PAOs utilize the stored  $X_{\text{PHA}}$  as an energy source to grow and take up  $\text{PO}_4\text{-P}$  from the water phase and synthesize new storage products within the biomass ( $X_{\text{PP}}$ ). The biomass also contains significant proportions of nitrifying organisms, which convert  $\text{NH}_4\text{-N}$  to  $\text{NO}_3\text{-N}$ . The biomass also contains heterotrophs, which consume BOD during the aerobic stage.

When the biofilm layer on the carriers reach a steady thickness, the system exhibits more than 80%  $\text{PO}_4\text{-P}$  removal. In this period, a constant amount of  $\text{PO}_4\text{-P}$  is added at the beginning of every cycle to avoid low influent  $\text{PO}_4\text{-P}$  concentration due to dilution of wastewater by storm-water ( $9 \pm 3 \text{ mg P L}^{-1}$ ). However, the soluble COD ( $127 \pm 30 \text{ mg COD L}^{-1}$ ),  $\text{NH}_4\text{-N}$  ( $28 \pm 16 \text{ mg N L}^{-1}$ ) is not adjusted.

After the biomass activity shows steady conditions, kinetic tests are conducted in the reactor. Samples are collected for the entire cycle every 30 min and immediately filtered through  $0.45 \mu\text{m}$  filters to determine the concentration of soluble COD (sCOD), orthophosphate ( $\text{PO}_4\text{-P}$ ), ammonium nitrogen ( $\text{NH}_4\text{-N}$ ) and nitrate nitrogen ( $\text{NO}_3\text{-N}$ ). All these compositions are measured using Dr. Lange cuvette and HACH LANGE GmbH (DR 1900, China) spectrophotometer. All analyses are performed immediately during the cycle test. The DO and pH sensor installed in the pilot plant are connected to the plants SCADA system. The data from the online sensors are logged every minute. The data received from the laboratory analyses and the online sensors are used to calibrate the model.

## Mathematical model

A number of mechanistic models explaining the process of removal of phosphorus, nitrogen, and carbon in sequential batch reactors are available in the literature. However, using a complex model such as ASM2d (Henze *et al.* 1999) for estimation and control would be challenging, especially when the number of measurements available in the reactors are limited (Jeppsson & Olsson 1994). The usual approach is to reduce the number of state variables by either lumping two or more states or assuming some of the states with relatively slower dynamics as constants (Steffens *et al.* 1997). We find similar model-reduction strategies implemented on ASM1 model, for use in state estimation and control (Julien *et al.* 1999; Gómez-Quintero *et al.* 2000; García-Usach *et al.* 2006).

## Model reduction strategy

The original ASM2d model (Henze *et al.* 1999) consists of 19 states and 21 processes. It describes the growth and decay of three types of biomass; the phosphate accumulating organisms ( $X_{\text{PAO}}$ ), autotrophs ( $X_{\text{AUT}}$ ) and heterotrophs ( $X_{\text{H}}$ ), followed by the subsequent uptake and release of various substrates and storage products in the biomass. The following assumptions, similar to the simplification strategies presented in Zhang *et al.* (2010), Cadet (2014) and Li *et al.* (2018) were made to reduce the model.

- The effect of particulate hydrolysis reactions appears to be insignificant in the process and has been ignored.
- The non-reacting states in the model: particulate inert ( $X_{\text{I}}$ ), soluble inert ( $S_{\text{I}}$ ) and alkalinity ( $S_{\text{ALK}}$ ) are eliminated.
- Since there is no anoxic condition in the SBR's operational sequence, all kinetics pertaining to denitrifiers in the biomass are removed. However, the denitrification reactions by  $X_{\text{PAO}}$  has been retained.
- The effect of growth and decay kinetics of all three biomass types can be excluded. Hence, the model only considers the kinetics of substrate degradation processes.

This reduced order model explains the dynamics of storage and consumption of soluble substrates such as readily biodegradable substrate ( $S_{\text{F}}$ ), volatile fatty acids ( $S_{\text{A}}$ ), phosphates ( $S_{\text{PO}}$ ), ammonia ( $S_{\text{NH}}$ ) and nitrates ( $S_{\text{NO}}$ ). The model also includes the kinetics of storage products such as polyhydroxy-alkanoates ( $X_{\text{PHA}}$ ) and polyphosphates ( $X_{\text{PP}}$ ). The description of substrates and storage products used in the model is presented in Table 1. The list of processes included in the reduced order ASM2d model is presented in Table 2.

**Table 1** | State variables describing the model

States	Description	Unit
$S_{\text{F}}$	Readily biodegradable substrate	$\text{mg COD L}^{-1}$
$S_{\text{A}}$	Fermentation products (Volatile fatty acids/acetate)	$\text{mg COD L}^{-1}$
$X_{\text{PP}}$	Stored poly-phosphate of PAO	$\text{mg P L}^{-1}$
$X_{\text{PHA}}$	Organic storage products of PAO	$\text{mg COD L}^{-1}$
$S_{\text{NH}}$	Ammonium	$\text{mg N L}^{-1}$
$S_{\text{NO}}$	Nitrate	$\text{mg N L}^{-1}$
$S_{\text{PO}}$	Phosphate	$\text{mg P L}^{-1}$
$S_{\text{O}}$	Dissolved oxygen	$\text{mg O}_2 \text{ L}^{-1}$

Table 2 | Petersen matrix and rate kinetics for the reduced order model (see Supplementary Figure 2, available with the online version of this paper)

Process	S <sub>F</sub>	S <sub>A</sub>	X <sub>PP</sub>	X <sub>PHA</sub>	S <sub>NH</sub>	S <sub>NO</sub>	S <sub>PO</sub>	S <sub>O</sub>	Rate kinetics
1 COD uptake	-1							-1	$r_1 \frac{S_F}{K_S + S_F} \frac{S_O}{K_O + S_O}$
2 Fermentation	-1	1			0.1		0.01		$r_2 \frac{S_F}{K_{fGH} + S_F} \frac{K_{NO}}{K_O + S_O} \frac{K_{NO}}{K_{NO} + S_{NO}}$
3 Storage of PHA Release of P		-1	-Y <sub>PO4</sub>	1			Y <sub>PO4</sub>		$r_3 \frac{S_A}{K_A + S_A} \frac{X_{PP}}{K'_{PP} + X_{PP}}$
4 Storage of PP Uptake of P			1	-Y <sub>PHA</sub>			-1		$r_4 \frac{S_O}{K_O + S_O} \frac{S_{PO}}{K'_{PS} + S_{PO}} \frac{X_{PHA}}{K'_{PHA} + X_{PHA}} \frac{K'_{MAX} - X_{PP}}{K'_{PP} + (K'_{MAX} - X_{PP})}$
5 Nitrification					-1	1		-4.32	$r_5 \frac{S_O}{K_{O, AOB} + S_O} \frac{S_{NH}}{K_{NH, AOB} + S_{NH}}$
6 Denitrification						-1			$r_6 \frac{K_O}{K_O + S_O} \frac{S_{NO}}{K_{NO} + S_{NO}} \frac{X_{PHA}}{K'_{PHA} + X_{PHA}} \frac{K'_{MAX} - X_{PP}}{K'_{PP} + (K'_{MAX} - X_{PP})}$
7 Aeration (u)									K <sub>L</sub> a (8.5 - S <sub>O</sub> )

The following modifications are implemented to reduce the number of parameters in the process rate kinetics.

- All the biological processes involved in the aerobic uptake of (S<sub>F</sub>) are written as a Monod equation with a rate constant r<sub>1</sub> and saturation coefficients K<sub>S</sub> and K<sub>O</sub>.
- The maximum fermentation rate q<sub>fc</sub> is lumped with X<sub>H</sub> and represented as a single term r<sub>2</sub>.
- The rate constant for X<sub>PHA</sub> storage q<sub>PHA</sub> is lumped with X<sub>PAO</sub> to form a term r<sub>3</sub>.
- The rate constant for X<sub>PP</sub> storage q<sub>PP</sub> is lumped with X<sub>PAO</sub> to represent a single term r<sub>4</sub>.
- The maximum growth rate of autotrophs μ<sub>AUT</sub> and Y<sub>A</sub> is lumped with X<sub>AUT</sub> to represent a single term r<sub>5</sub>. This rate equation assigned for aerobic growth of autotroph is used to explain the kinetics of ammonia nitrification.
- All the reactions pertaining to denitrification by PAO are lumped with X<sub>PAO</sub> to represent a single term r<sub>6</sub>.
- The Monod saturation coefficients associated with X<sub>PHA</sub> (K<sub>PHA</sub>) and X<sub>PP</sub> (K<sub>PP</sub>) and (K<sub>MAX</sub>) was lumped with X<sub>PAO</sub> to obtain the terms K'<sub>PP</sub>, K'<sub>PHA</sub> and K'<sub>MAX</sub>, respectively.

After considering the aforementioned modifications, the rate kinetics can be transformed to the equations mentioned in Table 2. All the kinetic parameters mentioned in this model will be estimated in the model calibration stage.

### State-space equations

The state-space equation denotes the rate of changes in the state variables. Equation (1) presents the model equation in the continuous-time state space form; where x = [S<sub>F</sub> S<sub>A</sub> X<sub>PP</sub> X<sub>PHA</sub> S<sub>NH</sub> S<sub>NO</sub> S<sub>PO</sub> S<sub>O</sub>] are the state variables and u = K<sub>L</sub>a is the manipulated variable. The process rate equations f<sub>c</sub> are presented as a Petersen matrix in Table 2.

$$\dot{x} = f_c(x, u) \tag{1}$$

The reduced order ASM2d model has to be calibrated before use in a specific case (García-Usach et al. 2006). The data obtained from the kinetic studies conducted in the pilot plant are used to estimate the stoichiometric and kinetic parameters of the model. The optimization procedure involving minimization of a quadratic error function (Marsili-Libelli et al. 2009; Nair et al. 2017) is used to fit the experimental data to the model. The optimization problem statement is presented in Equations (2)–(4).

$$\min_p f_{OBJ}(p) \quad (2)$$

$$f_{obj}(p) = \sum_{i=1}^{N_i} (y_i - m_i(p))^2 \quad (3)$$

$$lb \leq p \leq ub \quad (4)$$

' $p$ ' is a vector consisting of the model parameters that are to be estimated; the upper and lower bounds of the parameter vector is represented as  $ub$  and  $lb$ , respectively. The objective function  $f_{OBJ}$  is defined as the least-square error between the experimental values  $y_i = [\text{sCOD NH}_4\text{-N NO}_3\text{-N PO}_4\text{-P}]$  and its corresponding model predicted values  $m_i(p) = [(S_A + S_F) \quad S_{NH} \quad S_{NO} \quad S_{PO}]$ . The half-saturation constants and stoichiometric parameters were constrained within  $-100\%$  and  $+150\%$  of the original ASM2d model parameters, but a wider constraints range is provided to the rate constants. The initial concentrations of  $S_F$  and  $X_{PP}$  are also taken as parameters, which would be estimated by the optimizer. The non-linear optimization solver function in MATLAB (`fmincon`) is used to solve the optimization problem and obtain the parameters.

### Observation equations

The observation equation expresses the online measurements as functions of the state variables (see Supplementary Table 1, available with the online version of this paper). The work presented in Serralta *et al.* (2004) and Aguado *et al.* (2006) demonstrates the possibility of expressing the pH as a function of various ionic species available in the wastewater treatment system ( $S_A$ ,  $S_{PO}$ ,  $S_{NH}$ ,  $S_{NO}$ ). A generic equation, which contains a weighted combination of the linear terms, squared terms, and binary interaction terms, is used as the preliminary model structure. The mathematical form of the equation is presented in Equations (5) and (6). A similar model structure can be found in dosing control predictors, and are found to fit a wide range of data (Ratnaweera & Fettig 2015). The regression learner app in MATLAB is used to establish a correlation between the ionic species ( $\theta = [S_A \quad S_{NH} \quad S_{NO} \quad S_{PO}]$ ) and the data received from pH sensors and obtain the coefficients  $\alpha_i$ ,  $\beta_i$  and  $\gamma_{ij}$ . The second measurement, dissolved oxygen is equivalent to the state  $S_O$  in the model. The measurement function  $h(x)$  can be expressed as Equation (7).

$$pH_{MODEL} = \alpha_0 + \sum_{i=1}^n \alpha_i \theta_i + \sum_{i=1}^n \beta_i \theta_i^2 + \sum_{i=1}^{n-1} \sum_{j=i+1}^n \gamma_{ij} \theta_i \theta_j \quad (5)$$

$$\theta = [S_A \quad S_{NH} \quad S_{NO} \quad S_{PO}] \quad (6)$$

$$h(x) = \begin{bmatrix} pH_{MODEL}(S_A, S_{NH}, S_{NO}, S_{PO}) \\ S_O \end{bmatrix} \quad (7)$$

### State estimator

The Kalman Filter is an optimal state estimator for linear systems with Gaussian noise. However, a number of versions of original Kalman Filter algorithm such as Unscented Kalman Filter (UKF), and particle filters (PF) can be used to estimate the states of a non-linear system. In this case, the Extended Kalman Filter is used as a state estimator for the SBR. The equations of the EKF are given in Equations (8)–(15). The equations were written in the same order in which they were implemented in the PLC.

$$x_k^- = x_{k-1}^+ + T_s f_c(x_{k-1}^+, u_{k-1}) \quad (8)$$

$$y_k = h(x_k^-) \quad (9)$$

$$P_k^- = F_{k-1} P_{k-1}^+ F_{k-1}^T + Q_{k-1} \quad (10)$$

$$K_k = P_k^- H_k^T (H_k P_k^- H_k^T + R_{k-1})^{-1} \quad (11)$$

$$x_k^+ = x_k^- + K_k (z_k - y_k) \quad (12)$$

$$P_k^+ = (I - K_k H_k) P_k^- \quad (13)$$

$$F_k = I + T_s \left. \frac{\partial f_c}{\partial x} \right|_{x_k^+, u_k} \quad (14)$$

$$H_k = \left. \frac{\partial h}{\partial x} \right|_{x_k^+, u_k} \quad (15)$$

The discrete form of state-space equation presented in Equation (8) is derived from the continuous-time system function  $f_c$  (in Equation (1)) by an explicit Euler discretization method with a constant sampling time of  $T_s$ .  $f_c$  and  $h$  are the nonlinear state transition and measurement functions. In the equations above,  $x_k$  is the state variable at time  $k$ ,  $z_k$  is the measurement,  $Q$  and  $R$  are the covariance matrices of the process and measurement noise, respectively.  $F$  is the state transition matrix, and  $H$  is the measurement matrix.  $I$  is the identity matrix,  $x_k^-$  is the *a priori* estimate of the state,  $x_k^+$  the *a posteriori* estimate of the state,  $K_k$  the Kalman gain,  $P_k^-$  the covariance of *a priori* estimation error, and  $P_k^+$  the covariance matrix of the *a posteriori* estimation error.

### Implementing the EKF

Before implementing the estimator to the pilot plant a series of simulations are conducted to identify the appropriate tuning parameters that would result in a reasonably good correction of the states by the EKF. For this purpose, the

mathematical model and the EKF equation described in the previous section were implemented in MATLAB. The model equations are written symbolically and the Jacobian function in MATLAB's symbolic toolbox is used to linearize the process model and obtain the  $F$  and  $H$  matrix at every time step. The implementation schematic is presented in Figure 2. The block mentioned as 'simulator' consists of the mathematical model and 'plant' represents the real pilot plant. The EKF equations are written as a separate section in MATLAB, which can accept the measurement  $z_k$  and the control variable  $u_k$  from either a simulator or from the plant's SCADA system. This shift from simulator based testing to a pilot plant implementation is done with the switch S1 and S2, as indicated in Figure 2. During the tuning of the EKF parameters, the simulated state vector,  $x_k$  generated

by the model is compared to the estimated state  $x_k^+$  predicted by the EKF to test the estimator's ability to provide a reliable estimation.

The SBR pilot plant SCADA provides an Open Platform Communication (OPC) server, which enables communication with other devices through the standard OPC protocol. A communication layer is written in MATLAB using its OPC toolbox to pull real-time data from the OPC server into the MATLAB workspace. This method enables scripts written in MATLAB to be used directly in any industrial PLC without the hassle of re-writing the code in a different programming language. While implementing the EKF in the pilot plant, a few overriding constraints are included in the estimator algorithm to prevent EKF from overshooting during the emptying and filling stages of the

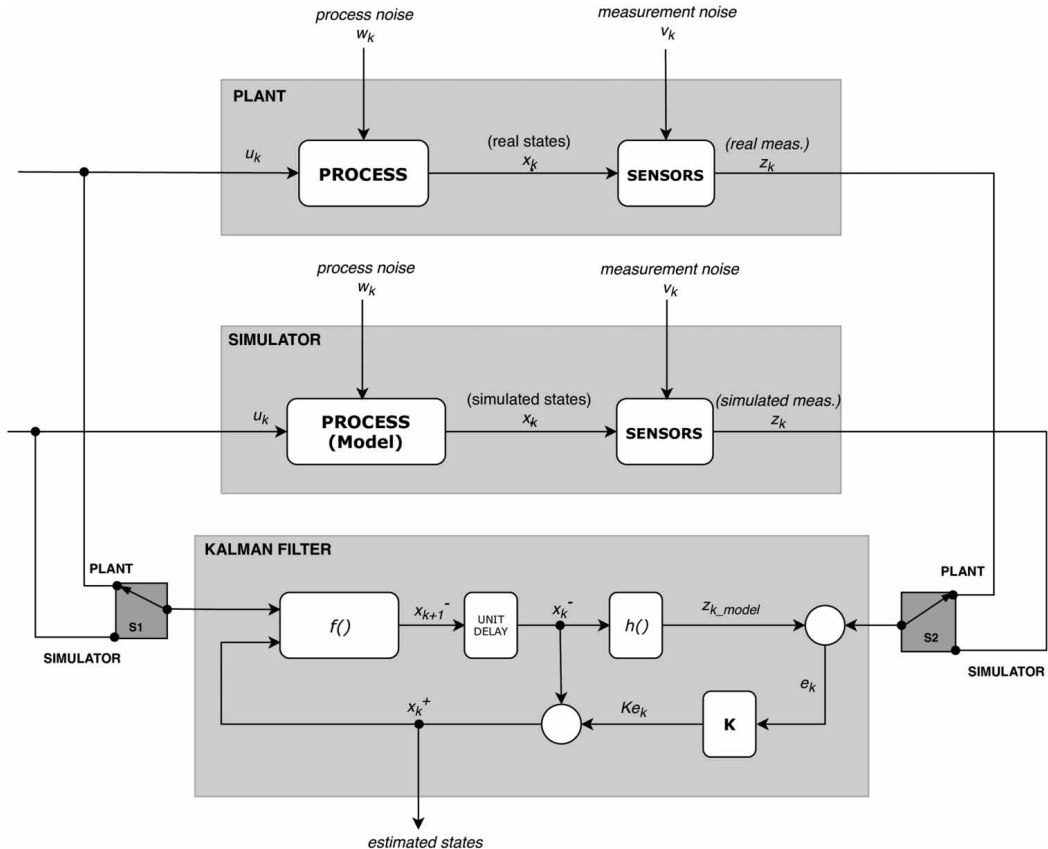


Figure 2 | Implementation schematic of EKF code in simulator and real plant.



SBR. The states and the auto-covariance matrix are reinitialized at the beginning of every cycle and the estimator is kept on hold until the anaerobic conditions begin ( $DO = 0$ ) and the pH sensor value stabilizes. Once the EKF is started, the algorithm continues to run until the end of the aerobic stage. When the emptying stage begins, the estimated states are frozen until the next filling stage begins.

## RESULTS AND DISCUSSION

### Model calibration results

The results of the model calibration step, obtained by the proposed optimization procedure, are presented in Table 3. The graphs presented in Figure 3 show the comparison between the model predicted values and the data obtained from the kinetic studies conducted in the pilot plant. The figure also provides the normalized root-mean-square error (NRSME) and  $R^2$  values obtained during the model calibration. The  $R^2$  values presented in the graph show that the values predicted by the model are close to

the measured data collected from the pilot plant. Hence, the model can be considered to provide a good representation of the SBR process.

The optimization algorithm used for estimating the model parameters (Equations (2)–(4)) is also included in the MATLAB code. The model parameters presented in Table 3 can be updated by running the optimizer code with a new data set obtained from laboratory analysis. This strategy provides an effective platform for model calibration and effortless update of parameters whenever a drift is observed between the laboratory results and estimated values. It also generates a possibility of adapting model parameters such that the soft-sensor algorithm can be implemented in any SBR plant with similar operational sequence.

### Tuning parameters of the EKF

The values of  $x_0^+$ ,  $P_0^+$ ,  $Q$  and  $R$  described in Equations (8)–(15) can be used as the tuning parameters of the Kalman Filter. In practical applications, these parameters are not known precisely, and therefore, trial-and-error

Table 3 | Stoichiometric and Kinetic parameters for the reduced order model

Parameter	Parameter	Model Value	Min	Max	Units
$K_{feH}$	Saturation coefficient of fermentation	3.58	2	6	$g\ COD\ m^{-3}$
$K_A$	Saturation coefficient of acetate	2.20	2	6	$g\ COD\ m^{-3}$
$K'_{pp}$	Saturation coefficient of polyphosphate	10.19	1	50	$g\ P\ m^{-3}$
$K_O$	Saturation coefficient of oxygen	2.96	0.1	4	$g\ O_2\ m^{-3}$
$K'_{PHA}$	Saturation coefficient of polyphosphate	119	1	200	$g\ COD\ m^{-3}$
$K_{PS}$	Saturation coefficient of phosphorus	0.2	0.1	1	$g\ P\ m^{-3}$
$K'_{MAX}$	Maximum values of $X_{pp}$	132	1	200	$g\ P\ m^{-3}$
$K_{NO}$	Saturation coefficient of nitrate	1.02	0.1	1.5	$g\ N\ m^{-3}$
$K_{O_{AOB}}$	Saturation coefficient of oxygen (nitrifiers)	1.57	0.1	4	$g\ O_2\ m^{-3}$
$K_{NH_{AOB}}$	Saturation coefficient of ammonia (nitrifiers)	1	0.1	4	$g\ N\ m^{-3}$
$r_1$	Rate constant for aerobic uptake of BOD	500	50	5000	$g\ COD\ m^{-3}d^{-1}$
$r_2$	Rate constant for fermentation	135	50	5000	$g\ COD\ m^{-3}d^{-1}$
$r_3$	Rate constant for PHA storage	2690	50	5000	$g\ COD\ m^{-3}d^{-1}$
$r_4$	Rate constant for PP storage	4110	50	5000	$g\ P\ m^{-3}d^{-1}$
$r_5$	Rate constant for nitrification	430	50	5000	$g\ N\ m^{-3}d^{-1}$
$r_6$	Rate constant for denitrification	310	50	5000	$g\ N\ m^{-3}d^{-1}$
$Y_{PHA}$	PHA requirement for PP storage	1.496	0.1	4.0	$g\ COD\ g^{-1}\ P$
$Y_{PO}$	PP requirement per PHA storage	0.577	0.1	0.6	$g\ P\ g^{-1}\ COD$
$S_{F0}$	Initial concentration of biodegradables	45	20	120	$mg\ COD\ L^{-1}$
$X_{pp0}$	Initial concentration of PP	65	20	120	$mg\ P\ L^{-1}$
$k_{La}$	Mass transfer coefficient for dissolved oxygen	912	100	1500	$d^{-1}$

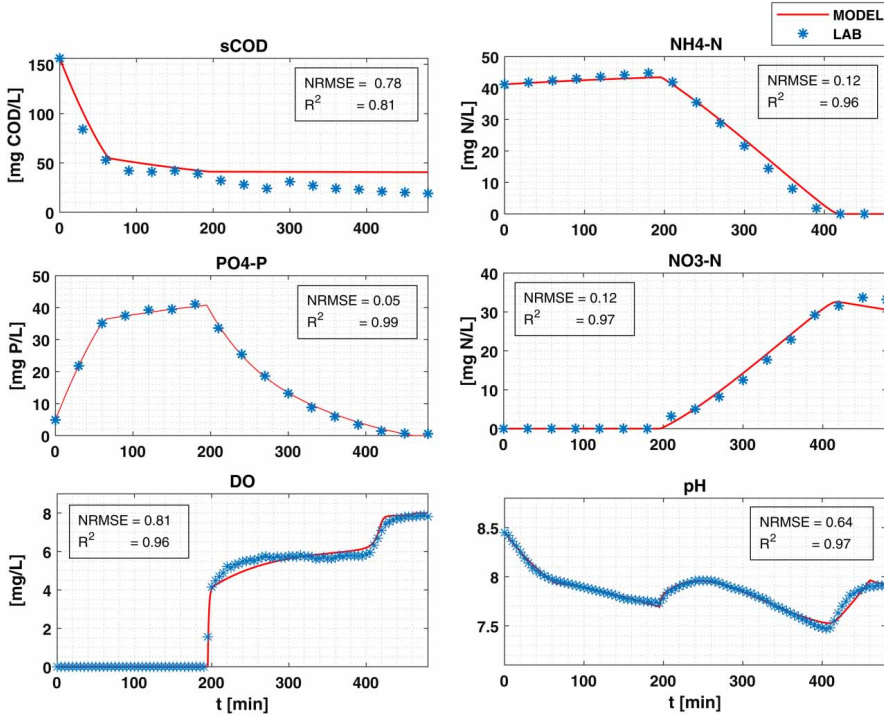


Figure 3 | Model calibration results – reduced order model versus laboratory measured values.

tuning must be expected. We have tuned the EKF as explained below, mainly following the guidelines in Haugen et al. (2014).

*Tuning of  $x_0^+$* : A reasonable value of  $x_0^+$  is a representative steady state, here set equal to the designed operating point of the process. For an SBR operation, we chose the design values of influent water quality as  $x_0^+$ .

$$x_0^+ = [S_{F0} S_{A0} X_{PP0} X_{PHA0} S_{NH0} S_{NO0} S_{PO0} S_{O0}] = [45 \ 20 \ 65 \ 0 \ 45 \ 0 \ 5 \ 0] \tag{16}$$

*Tuning of  $P_0^+$* : It is commonly set as a diagonal matrix. The values are adjusted based on how close our initial estimates are to the real value of states. The knowledge on raw wastewater composition can help provide a good guess for the initial composition of some of the states in the process.

- The raw wastewater does not contain any nitrates, therefore the value of  $S_{NO}$  is  $0 \text{ g-N m}^{-3}$ .

- The stored PHA in the biomass usually depletes before the cycle ends, therefore we can assume that the initial concentration of  $X_{PHA0} = 0 \text{ mg COD L}^{-1}$ .
- $S_{O} = 0 \text{ mg L}^{-1}$  since there is no dissolved oxygen in the anaerobic stage.
- The states  $S_F$  and  $X_{PP}$  do not affect the measurements (pH) in the anaerobic zone. These states exist in the model merely for the purpose of maintaining the model dynamics. A fixed initial value of  $X_{PP} = 65 \text{ mg P L}^{-1}$  and  $S_F = 45 \text{ mg COD L}^{-1}$  is provided to make the model fit to the kinetic data. These values should not be confused with the actual P content in the biomass or the available soluble BOD.

Therefore, the only uncertain initial estimates are  $S_{A0}$ ,  $S_{NH0}$ , and  $S_{PO0}$ . The  $P_0^+$  corresponding to the states  $S_{F0}$ ,  $X_{PP0}$ ,  $X_{PHA0}$ ,  $S_{NO0}$ , and  $S_{O0}$  can be set to a very low value or to zero. Therefore, the  $P$  matrix at the beginning of the cycle can be expressed as the following.

$$P_0^+ = \text{diag} [0 \ P_{S_A} \ 0 \ 0 \ P_{S_{NH}} \ 0 \ P_{S_{PO}} \ 0] \tag{17}$$

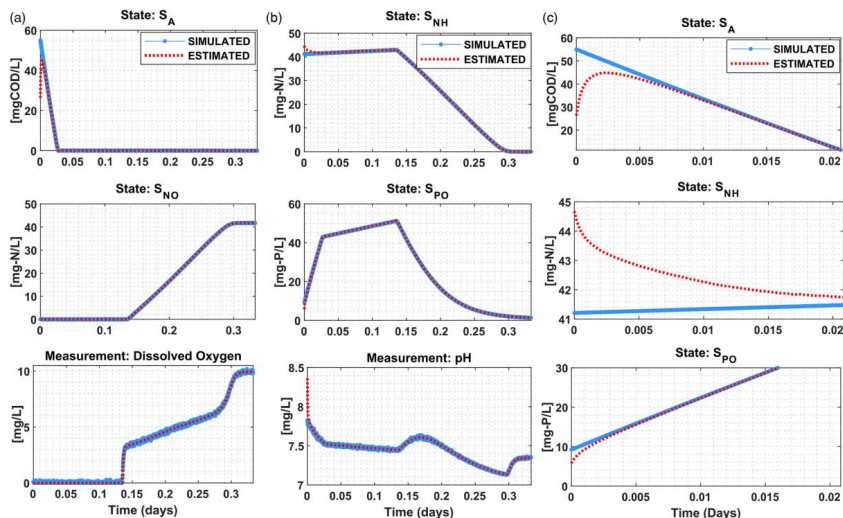


**Figure 4** | (a)–(b) Simulated vs estimated values of states for a complete cycle of 8 h. (c) State-correction by EKF during the first 30 min of the cycle.

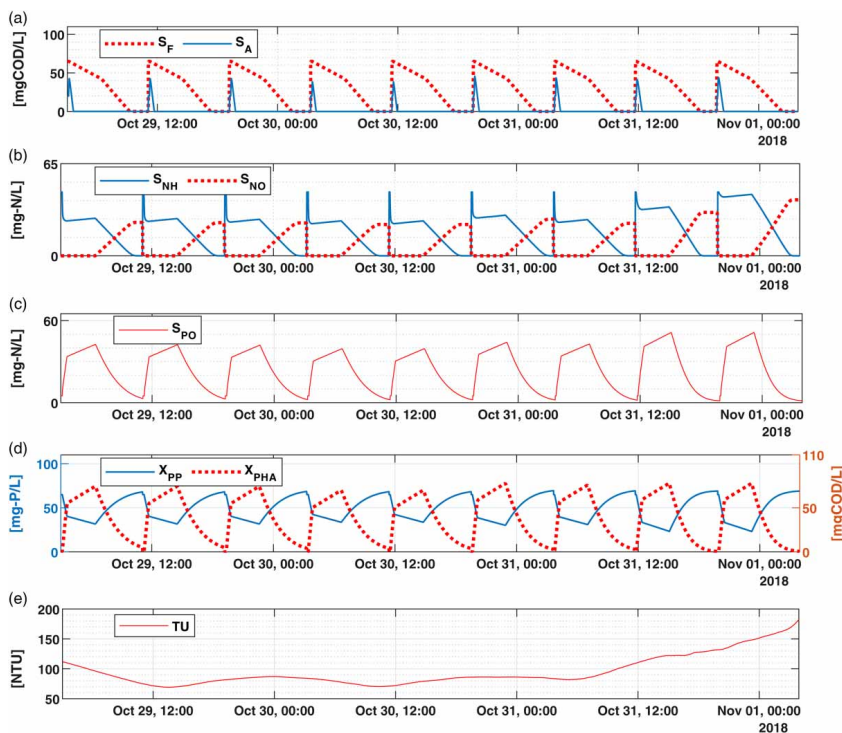


**Figure 5** | (a)–(d) Estimated states in the pilot plant for a 3-day period. (e) Turbidity measurement at influent raw water.

By trial and error, it was found that the following values provide a good estimation.

$$P_{S_A} = 316; \quad P_{S_{NH}} = 0.12; \quad P_{S_{PO}} = 0.10 \quad (18)$$

**Tuning of R:** It is estimated as the variance of the measurement time series collected from the SCADA system.

**Tuning of Q:** Typically, Q is used as the main, or final, tuning parameter. It is assumed a diagonal matrix with diagonal elements related to the initial guess of the pertinent state variable through factors  $l_i$ :

$$Q_c = \text{diag}([l_i x_{o,i}^+]^2) \quad (19)$$

In the simulator based testing, proper values of trial-and-error were found as

$$\{l_i\} = [1 \ 1 \ 1 \ 1 \ 2 \ 1 \ 1 \ 1.5]^+ 10^{-3} \quad (20)$$

### Simulator test results

The EKF is updated with the tuning parameters presented in Equations (16)–(20). The results presented in Figure 4(a) and 4(b) show a comparison between the state variable obtained from the simulator and the states estimated by the tuned EKF during an 8 h cycle. The state correction by EKF is not clearly visible in Figure 4(a) and 4(b) since the estimated states usually approach the simulated states within the first 30 min of the SBR cycle. Therefore, the simulation result for the first 30 min is presented in Figure 4(c), where the state correction by the EKF is noticeable. The convergence of the estimated value to a randomly selected initial composition confirms that the EKF parameters are correctly tuned.

### Pilot plant implementation results

The tuned EKF algorithm is implemented in the pilot plant and the estimator results are recorded for a period of two weeks. Figure 5 presents a subset consisting of estimated states for a duration of 3 days (nine cycles). The variations in nutrient composition during the cycle follow similar trends to those observed in a typical SBR operation, as presented in literature such as Marsili-Libelli *et al.* (2001) and Sin & Vanrolleghem (2006). Due to the high holdup in the buffer tank, the diurnal variations in influent concentration is barely noticeable. However, a significant change in influent concentration can be observed during rain or snowmelt events, causing storm-water infiltration at the raw wastewater source. These variations can be

observed in Figure 5(e), which shows the data from the online turbidity sensor installed in the raw wastewater tank. The estimation results presented in Figure 5(a)–5(d) show the increase in the estimated value of  $S_{NH}$ ,  $S_{PO}$ , and  $S_A$  on 31 October 2018 around 12.00 h. This event corresponds to the influx of wastewater with a rather higher nutrient concentration at 9:00 AM on the same day. This provides a qualitative validation for the soft-sensor's ability to detect variations in influent wastewater quality (see Supplementary Table 2, available with the online version of this paper).

Further validation tests were conducted on 4 November 2018. Samples were collected every 30 min during the complete 8-h cycle and the composition of  $NH_4-N$ ,  $PO_4-P$ , and  $NO_3-N$  are measured using standardized laboratory tests. These values are compared to the states  $S_{NH}$ ,  $S_{PO}$ , and  $S_{NO}$  estimated by the EKF algorithm during the cycle. The comparison plots along with the NRSME and  $R^2$  values are presented in Figure 6. This demonstrates the EKF's potential to estimate the states in the pilot plant.

The estimated value of the effluent water quality is also recorded for each treatment cycle. This is executed by logging the estimated value of  $S_{NH}$ ,  $S_{PO}$  and  $S_{NO}$  at the end of every SBR cycle. The pilot plant achieves complete

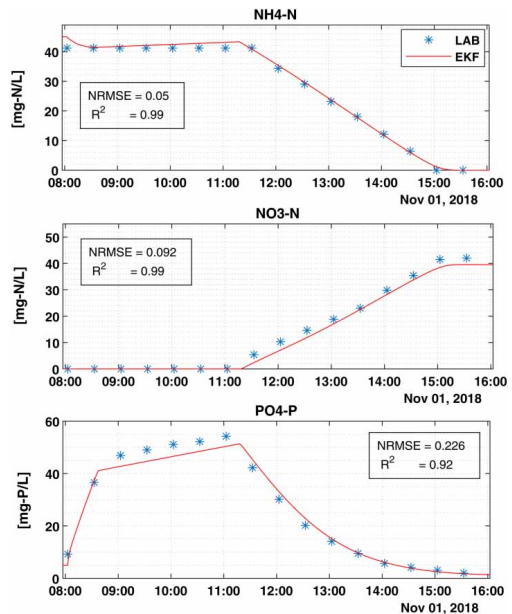


**Figure 6** | Soft-sensor validation. Estimated values (continuous red line) versus laboratory measurements (blue discrete points). Please refer to the online version of this paper to see this figure in colour: <http://dx.doi.org/10.2166/wst.2019.272>.

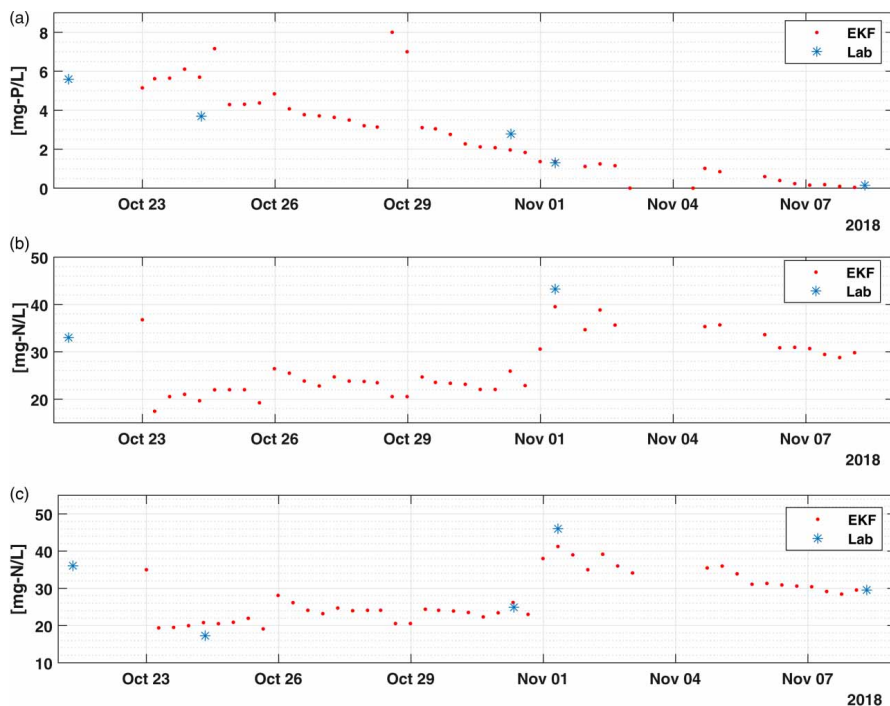


Figure 7 | Comparison of estimated values of (a) effluent  $\text{PO}_4\text{-P}$ , (b) effluent  $\text{NO}_3\text{-N}$  and (c) influent  $\text{NH}_4\text{-N}$  composition with laboratory measurements.

nitrification, resulting in a very low effluent ammonia concentration close to zero. However, the effluent concentrations of  $S_{\text{NO}}$  and  $S_{\text{PO}}$  are rather susceptible to variations in raw wastewater quality. These variations can be observed in Figure 7(a) and 7(b).

The soft-sensor is also used to estimate the ammonia concentration in the raw wastewater. It is observed that the concentration of  $\text{NH}_4\text{-N}$  stays nearly constant during the anaerobic stage. However, it can also be observed from Figure 4(b) that the estimator converges to the real state variables within the first 30 min of the cycle time. Therefore, it would be safe to assume the value of  $S_{\text{NH}}$  at  $t=30$  min to be very close to the concentration of ammonia in raw wastewater. The estimated value of  $S_{\text{NH}}$  at  $t=30$  min for the entire testing period is presented in the third plot in Figure 7(c). These estimated values of the influent and the effluent wastewater composition is compared to the periodic laboratory measurements. Except for the erroneous estimates received on 3–5 November 2018 due to an unexpected power failure, the plots presented in Figure 7(c) demonstrate an acceptable

match between the experimental data and the values estimated by the EKF algorithm.

## CONCLUSIONS

The grey box model discussed in this article explains the SBR with sufficient level of accuracy to constitute the basis of a state estimator for the reactor. The model calibration strategy discussed in this work provides the flexibility in adapting the model to any plant with similar process configuration. The validation tests conducted in the pilot plant demonstrates the possibility to estimate the concentration of VFA,  $\text{NO}_3\text{-N}$ ,  $\text{NH}_4\text{-N}$  and  $\text{PO}_4\text{-P}$  in a SBR operating in alternative anaerobic-aerobic mode for the biological phosphorus removal process, by using physical sensors such as pH and DO. The EKF based soft-sensor can also provide accurate estimations of the ammonia concentration in the influent wastewater. Since the EKF algorithm is written in MATLAB's OPC compatible framework this soft-sensor code can easily be implemented in



any treatment plant which has an OPC enabled PLC, SCADA or a distributed control system (DCS), without additional hardware requirement or modifications to the MATLAB code.

The change in biomass concentration over a longer operational period could lead to minor drift in state estimation. However, periodic model calibration and parameter re-tuning can resolve this problem. The optimization code estimating the model parameters is also included as a part of the overall estimator package. This allows the model to be recalibrated with relative ease. A cost-effective method of state-estimation using soft sensors can be a prelude to implementing advanced model based control strategies in wastewater treatment and recovery processes.

## REFERENCES

- Aguado, D., Ferrer, A., Seco, A. & Ferrer, J. 2006 Comparison of different predictive models for nutrient estimation in a sequencing batch reactor for wastewater treatment. *Chemometrics and Intelligent Laboratory Systems* **84** (1–2), 75–81.
- Busch, J., Elixmann, D., Kühl, P., Gerkens, C., Schlöder, J. P., Bock, H. G. & Marquardt, W. 2013 State estimation for large-scale wastewater treatment plants. *Water Research* **47** (13), 4774–4787.
- Cadet, C. 2014 Simplifications of activated sludge model with preservation of its dynamic accuracy. *IFAC Proceedings Volumes* **19** (3), 7134–7139.
- García-Usach, F., Ferrer, J., Bouzas, A. & Seco, A. 2006 Calibration and simulation of ASM2d at different temperatures in a phosphorus removal pilot plant. *Water Science and Technology* **53** (12), 199–206.
- Gómez-Quintero, C., Queinnec, I. & Babary, J. P. 2000 A reduced nonlinear model of an activated sludge process. *IFAC Proceedings Volumes* **33** (10), 1001–1006.
- Häck, M. & Wiese, J. 2006 Trends in instrumentation, control and automation and the consequences on urban water systems. *Water Science and Technology* **54** (11–12), 265–272.
- Haimi, H., Mulas, M., Corona, F. & Vahala, R. 2013 Data-derived soft-sensors for biological wastewater treatment plants: an overview. *Environmental Modelling and Software* **47**, 88–107.
- Haugen, F., Bakke, R. & Bernt, L. 2014 State estimation and model-based control of a pilot anaerobic digestion reactor. *Journal of Control Science and Engineering* **2014**, 1977.
- Henze, M., Gujer, W., Mino, T., Matsou, T., Wentzel, M. C., Marais, G. V. R. & Van Loosdrecht, M. C. M. 1999 Activated sludge model NO. 2D, ASM2D. *Water Science and Technology* **39** (1), 165–182.
- Jeppsson, U. & Olsson, G. 1994 Reduced order models for on-line parameter identification of the activated sludge. *Water Science and Technology* **28** (11), 173–183.
- Julien, S., Barbary, P. & Lessard, P. 1999 A reduced order model for control of a single reactor activated sludge process. *Mathematical and Computer Modelling of Dynamical Systems* **5** (4), 337–350.
- Li, Z., Lu, P., Zhang, D. & Zhang, T. 2018 Practical identifiability analysis and optimal experimental design for the parameter estimation of the ASM2d-Based EBPR anaerobic submodel. *Mathematical Problems in Engineering* **18**, 1–9.
- Liukkonen, M., Laakso, I. & Hiltunen, Y. 2015 Advanced monitoring platform for industrial wastewater treatment: multivariable approach using the self-organizing map. *Environmental Modelling and Software* **48**, 193–201.
- Marsili-Libelli, S., Ratini, P., Spagni, A. & Bortone, G. 2001 Implementation, study and calibration of a modified ASM2d for the simulation of SBR processes. *Water Science and Technology* **43** (3), 69–76.
- Nair, A., Cristea, V. M., Agachi, P. Ş. & Brehar, M. 2017 Model calibration and feed-forward control of the wastewater treatment plant – case study for Cluj-Napoca WWTP. *Water and Environment Journal* **32** (2), 164–172.
- O'Brien, M., Mack, J., Lennox, B., Lovett, D. & Wall, A. 2011 Model predictive control of an activated sludge process: a case study. *Control Engineering Practice* **19** (1), 54–61.
- Ødegaard, H., Rusten, B. & Westrum, T. 1994 A new moving bed biofilm reactor – applications and results. *Water Science and Technology* **29** (10–11), 157–165.
- Olsson, G. 2012 ICA and me – A subjective review. *Water Research* **46** (6), 1585–1624.
- Olsson, G. & Jeppsson, U. 2006 Plant-wide control: dream, necessity or reality? *Water Science and Technology* **53** (3), 121–129.
- Ratnaweera, H. & Fettig, J. 2015 State of the art of online monitoring and control of the coagulation process. *Water* **7** (11), 6574–6597.
- Serralta, J., Ferrer, J., Borrás, L. & Seco, A. 2004 An extension of ASM2d including pH calculation. *Water Research* **38** (19), 4029–4038.
- Sin, G. & Vanrolleghem, P. A. 2006 Evolution of an ASM2s-like model structure due to operational changes of an SBR process. *Water Science and Technology* **53** (12), 237–245.
- Steffens, M. A., Lant, P. A. & Newell, R. B. 1997 A systematic approach for reducing complex biological wastewater treatment models. *Water Research* **31** (3), 590–606.
- Thürlimann, C. M., Dürrenmatt, D. J. & Villez, K. 2018 Soft-sensing with qualitative trend analysis for wastewater treatment plant control. *Control Engineering Practice* **70**, 121–133.
- Zhang, T., Zhang, D., Zhenliang, L. & Qing, C. 2010 Evaluating the structural identifiability of the parameters of the EBPR sub-model in ASM2d by the differential algebra method. *Water Research* **44** (9), 2815–2822.

First received 1 May 2019; accepted in revised form 1 August 2019. Available online 12 August 2019

# SUPPLEMENTARY MATERIAL

## SUPPLEMENTARY DIAGRAMS

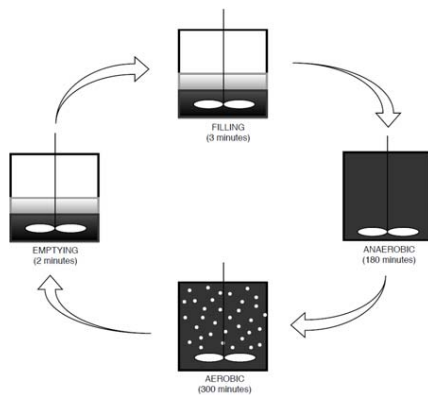


**Figure Supplementary 1.** The sequence of SB-MBBR Bio-P.

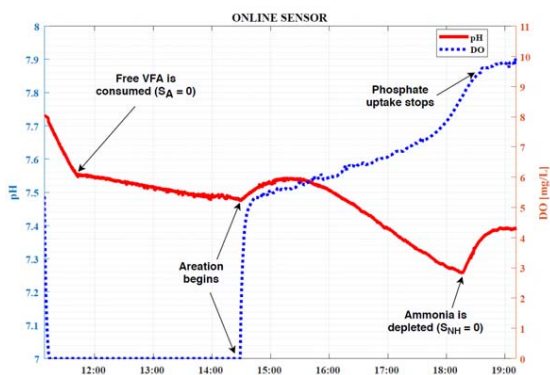


**Figure Supplementary 2.** Variation of pH and DO during a single SBR cycle.

## SUPPLEMENTARY TABLES

Table 1. Kinetics study – Experimental Data for Calibration

Time (h)	PO <sub>4</sub> -P (mg/L)	NH <sub>4</sub> N (mg/L)	COD (mg/L)	NO <sub>3</sub> -N (mg/L)
0	4.89	41.19	156	0
0.5	21.80	41.42	84	-
1	35.10	42.18	53	-
1.5	37.50	42.68	42	-
2	39.25	43.17	41	-
2.5	39.45	44.17	42	-
3	41.10	44.76	39	-
3.5	33.60	41.86	32	3.20
4	25.40	35.46	28	5.00
4.5	18.60	28.84	24	8.20
5	13.20	21.64	31	12.50
5.5	8.80	14.44	27	17.70
6	5.90	8.01	24	22.90
6.5	3.40	1.80	23	29.20
7	1.42	0.00	21	31.60
7.5	0.67	0.00	20	33.70
8	0.56	0.00	19	33.20

Table 2. Kinetics study – Experimental Data for Validation

Time (h)	PO <sub>4</sub> -P (mg/L)	NH <sub>4</sub> N (mg/L)	COD (mg/L)	NO <sub>3</sub> -N (mg/L)
0	9.23	40.60	155	0
0.5	36.60	-	68	-
1	46.90	-	45	-
1.5	49.00	-	42	-
2	51.10	-	45	-
2.5	52.20	-	43	-
3	54.20	-	42	-
3.5	42.20	41.21	40	5.4
4	30.20	34.34	32	10.3
4.5	20.20	29.06	34	14.6
5	14.10	23.16	33	18.8
5.5	9.63	18.10	28	23.6
6	5.70	12.14	25	29.8
6.5	4.16	6.41	26	35.4
7	3.10	0.00	23	41.5
8	1.30	0.00	21	43.3



# Paper B

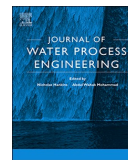






Contents lists available at ScienceDirect

## Journal of Water Process Engineering

journal homepage: [www.elsevier.com/locate/jwpe](http://www.elsevier.com/locate/jwpe)

## Real-time monitoring of enhanced biological phosphorus removal in a multistage EBPR-MBBR using a soft-sensor for phosphates

Abhilash M. Nair<sup>a,\*</sup>, Blanca M. Gonzalez-Silva<sup>b</sup>, Finn Aakre Haugen<sup>c</sup>, Harsha Ratnaweera<sup>a</sup>, Stein W. Østerhus<sup>b</sup><sup>a</sup> Faculty of Science and Technology, Norwegian University of Life Sciences, P.O. Box 5003, 1432 Ås, Norway<sup>b</sup> Department of Hydraulic and Environmental Engineering, Norwegian University of Science and Technology (NTNU), S. P. Andersens vei 5, Trondheim 7491, Norway<sup>c</sup> University of South-Eastern Norway, Kjølnes ring 56, Porsgrunn, Norway

## ARTICLE INFO

## Keywords:

Biological phosphorus removal  
Extended Kalman Filter  
MBBR process  
Soft-sensor  
Hybrid model

## ABSTRACT

Enhanced biological phosphorus removal (EBPR) from municipal wastewater has been achieved in a multistage Moving Bed Biofilm Reactor (MBBR) configuration. The process operations can be further optimized by real-time monitoring of water quality parameters in the individual chambers of the EBPR-MBBR process. This work presents a hybrid, soft-sensor as a cost-effective monitoring option for real-time estimation of phosphates ( $\text{PO}_4^{3-}\text{-P}$ ) and soluble COD (sCOD) concentrations in the anaerobic chambers of a multistage EBPR-MBBR pilot plant. The soft-sensor is developed by implementing an Extended Kalman filter on a reduced-order nutrient removal model. The hybrid model is constructed by combining mechanistic elements of phosphorus release kinetics in anaerobic conditions, and a statistical model correlating  $\text{PO}_4^{3-}\text{-P}$  and sCOD concentration with conductivity measurements. A systematic method for developing, calibrating a reduced-order model and tuning of the Kalman filter parameters have been discussed in this work. The drift in soft-sensor performance was studied and practical solutions were suggested for re-calibrating the model utilizing data from periodic lab measurements. The estimation results are successfully validated against standardized lab measurements to demonstrate the accuracy of the soft-sensing algorithm.

## 1. Introduction

Enhanced biological phosphorus removal (EBPR) process is a treatment configuration designed for phosphorus removal from wastewater. The EBPR process consists of an anaerobic stage before the aeration stage, where a specific species of biomass called polyphosphate-accumulating organisms (PAO) is enriched [1]. A novel configuration was reported by [13] for achieving EBPR in a continuous moving bed biofilm reactor (MBBR) process. The reactor performance is currently monitored using off-line laboratory analysis of  $\text{PO}_4^{3-}\text{-P}$ , soluble Chemical Oxygen Demand (sCOD) volatile fatty acids (VFA) ammonium ( $\text{NH}_4^+\text{-N}$ ), nitrites ( $\text{NO}_2^-\text{-N}$ ) and nitrates ( $\text{NO}_3^-\text{-N}$ ). However, off-line monitoring implies a low sampling frequency, leading to potential non-optimal conditions between the sampling instances, and a subsequent delay between sampling time, hampering adjusting of the process conditions, and data availability. Manual sample collection, sample preparation, and lab analysis involve additional man-hours and costs associated with chemicals and kits required for lab analysis.

Real-time measurement of nutrient concentration can result in faster detection of process abnormalities. Online monitoring of nutrients in the plant can also enable the possibility of implementing various control strategies to ensure stable and optimal performance of the treatment process [2]. However, the unavailability of sensor probes and the high price of online nutrient analyzers often discourage their use in treatment plants [3]. Soft-sensors are a viable alternative for expensive composition analyzers or unreliable sensor probes [4]. A review on the use of data-driven soft-sensors for enhancing online monitoring in wastewater treatment operations is presented in [5]. Several case-studies on simulator-based evaluation as well as full-scale implementation of soft-sensors in wastewater treatment processes are reported in literature [6,7].

Parameters such as pH, oxidation-reduction-potential (ORP), dissolved oxygen (DO), and electrical conductivity (EC) can be measured using inexpensive and low-maintenance sensors. Conductivity measurements, which directly correlate to the ionic strength of the solution, can be used to predict the nutrient concentrations in biological

\* Corresponding author.

E-mail addresses: [muralabh@nmbu.no](mailto:muralabh@nmbu.no) (A.M. Nair), [blanca.g.silva@ntnu.no](mailto:blanca.g.silva@ntnu.no) (B.M. Gonzalez-Silva), [Finn.Haugen@usn.no](mailto:Finn.Haugen@usn.no) (F.A. Haugen), [harsha.ratnaweera@nmbu.no](mailto:harsha.ratnaweera@nmbu.no) (H. Ratnaweera), [stein.w.osterhus@ntnu.no](mailto:stein.w.osterhus@ntnu.no) (S.W. Østerhus).<https://doi.org/10.1016/j.jwpe.2020.101494>

Received 11 May 2020; Received in revised form 22 June 2020; Accepted 3 July 2020

2214-7144/ © 2020 The Author(s). Published by Elsevier Ltd. This is an open access article under the CC BY license (<http://creativecommons.org/licenses/by/4.0/>).

Nomenclature			
<b>Variables</b>		$K_S$	Saturation coefficient of PHA storage ( $g\ COD. m^{-3}$ )
$x_k$	State variable at discrete time instance $k$	$r_1$	Rate constant for hydrolysis ( $g\ P. m^{-3} h^{-1}$ )
$T_k$	Time step ( $h$ )	$r_2$	Rate constant for PHA storage ( $g\ COD. m^{-3} h^{-1}$ )
$z_k$	Measurement vector	$\theta_1$	Temperature coefficient for $r_1$
$\tau$	Residence time in each chamber ( $h$ )	$\theta_2$	Temperature coefficient for $r_2$
$X_{s,in}$	Particulate biodegradable in influent ( $g\ COD. m^{-3}$ )	$Y_{PO}$	Yield coefficient for PO release ( $g\ P/g\ COD$ )
$X_{s,i}$	Particulate biodegradable in chamber $i$ ( $g\ COD. m^{-3}$ )	$\alpha_i$	Regression parameters
$S_{s,in}$	Soluble biodegradable in influent ( $g\ COD. m^{-3}$ )	$J_{OBJ}$	Objective Function
$S_{s,i}$	Soluble biodegradable in chamber $i$ ( $g\ COD. m^{-3}$ )	$\mathcal{N}$	Number of datapoints
$S_{po,in}$	Soluble ortho-phosphates in influent ( $g\ COD. m^{-3}$ )	$\varphi_{exp}$	Experimental Data
$S_{po,i}$	Soluble ortho-phosphates in chamber $i$ ( $g\ P. m^{-3}$ )	$\varphi_{model}$	Model Predicted Values
$C_{in}$	Conductivity measurements in the influent ( $\mu S/cm$ )	$\mathcal{N}$	Number of points in the dataset
$C_i$	Conductivity measurements in the chamber $i$ ( $\mu S/cm$ )	$F$	Linearized state transition matrix
$f$	Nonlinear state transition function	$H$	Linearized measurement vector
$h$	Nonlinear measurement function	$P_0^+$	Initial estimate of Autocovariance matrix
$K_H$	Saturation coefficient of fermentation ( $g\ COD. m^{-3}$ )	$x_0^+$	Initial estimate of EKF
		$R$	Covariance matrix of measurement noise
		$Q$	Covariance matrix of process noise

wastewater treatment processes [8]. Both mechanistic [9,10], as well as data-driven models [11], have been used to demonstrate a positive correlation between conductivity measurements and the concentration of  $PO_4^{3-}P$  as well as acetates (which can be one of the components of sCOD) concentrations in biological nutrient removal process. However, most work has been done either in a lab-scale using synthetic wastewater or in a sequential batch reactor [12]. We have not yet found reports of its implementation in a continuous treatment process with unmeasured variations in the influent wastewater quality.

The multistage MBBR is a novel process, designed for EBPR from municipal wastewater [13]. Several lab-scale studies have established a

correlation between the anaerobic phase-length and the overall  $PO_4^{3-}P$  removal during EBPR process. Control strategies aimed at manipulating the anaerobic phase-length in pilot plant or the dosage of external carbon source requires real-time monitoring of water quality parameters in the multistage MBBR process. The unfeasibility of installing nutrient sensors in each chamber establishes the importance of a cost-effective online monitoring system in the pilot plant. This work attempts to enhance the online monitoring system in a multistage EBPR-MBBR process [13] by implementing a conductivity based soft-sensor for real-time estimation of water quality parameters such as  $PO_4^{3-}P$  and sCOD in their anaerobic stages.

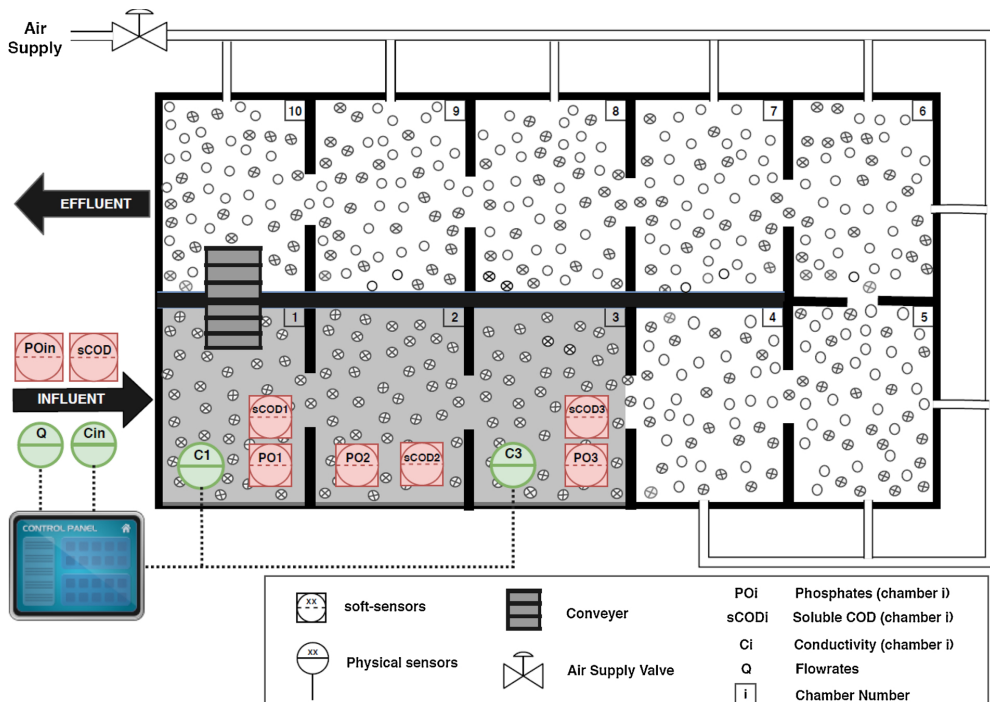


Fig. 1. Process flow diagram (top view) and the sensor network installed in the pilot plant. (Figure modified from [13]).

## 2. Materials and methods

### 2.1. Pilot plant setup and operational data

The pilot plant located in the wastewater lab at the Norwegian University of Science and Technology (NTNU) was used to test and validate the phosphate soft-sensor [13]. The reactor has a total working volume of 1 m<sup>3</sup>, divided into 10 chambers of equal volume, operating with a hydraulic retention time (HRT) of 6.5 h (Fig. 1). The pilot plant contains the standard biofilm carriers (Kaldnes K1) with 60 % filling in each of the chambers. The opening in the separation walls of the chamber allows the flow of wastewater and carriers between different zones. Mechanical agitators ensure sufficient mixing of the carriers in the anaerobic zones. The first three chambers of the pilot plant operate as anaerobic reactors, and the subsequent chambers are aerated. The carriers from the last aerobic zone (Chamber 10) are transported to the first anaerobic zone (Chamber 1) by a conveyor belt. The pilot plant layout, online monitoring, and the data acquisition system are presented in Fig. 1. The pilot plant is fed continuously with wastewater (3.6 m<sup>3</sup>/day) from a storage tank which receives fresh wastewater from a nearby sewer once every hour. The raw wastewater undergoes primary treatment, where it is passed through a fine sieve to remove larger particles, before sending it to the biological stage (MBBR).

The pilot plant is equipped with a state-of-the-art online monitoring system with remote data access capabilities. It has a conductivity sensor in chamber 1, chamber 3, and the influent (Fig. 1). All the online sensors are connected to a Supervisory Control And Data Acquisition System (SCADA) provided by DOSCON AS.

The mean values of sCOD and PO<sub>4</sub><sup>3-</sup>-P in the influent and effluent streams and the average removal (%) in the pilot plant are presented in Table 1. The multistage MBBR can operate with a flexible anaerobic/aerobic phase length by controlling the aeration in Chamber 2 and 3 of the pilot plant. Monitoring PO<sub>4</sub><sup>3-</sup>-P concentrations in chamber 1–3 provides real-time information on the phosphorus released in the anaerobic phase. Real-time control of anaerobic phase length based on feedback from the PO<sub>4</sub><sup>3-</sup>-P soft-sensors can provide an indirect way of controlling the percentage of PO<sub>4</sub><sup>3-</sup>-P removed by the pilot plant.

### 2.2. Mathematical model

Various models explaining biological nutrient removal exist in the literature [14]. These models vary from comprehensive mechanistic models such as ASM 2d [15] to data-driven statistical models [16]. Literature also mentions the use of a reduced-order version of the comprehensive ASM models for state estimation [17,18]. Mathematical models combining the mechanistic understanding of the nutrient removal process with a statistical correlation between nutrient composition and physical parameters such as pH, DO, or conductivity can also be used to develop soft-sensors for biological nutrient removal processes [19].

#### 2.2.1. Reduced-order PO<sub>4</sub><sup>3-</sup>-P release model

In this work, a simplified version of the phosphorus release model was implemented. The kinetic equations explaining PO<sub>4</sub><sup>3-</sup>-P release during the anaerobic phase of the EBPR can be found in literature [15]. These equations were used as a basis to develop the mathematical model for the anaerobic chamber of the multistage MBBR pilot plant. The sub-model includes the following three processes occurring in parallel.

- Hydrolysis of particulate biodegradable COD (X<sub>s</sub>) to soluble biodegradable COD (S<sub>s</sub>).
- Uptake of soluble biodegradable COD (S<sub>s</sub>) to store poly-hydroxy-alkanoates (PHA) in the biomass.
- Consumption of stored polyphosphates (PP) in the biomass and simultaneous release of soluble ortho-phosphates (S<sub>PO</sub>).

The original ASM2d model with 19 states and 21 processes poses a significant challenge in their utility as a model for soft-sensing. The usual strategy is to reduce the number of states in the original ASM2d model by either assuming the states with relatively slower dynamics as constants or by eliminating processes with a relatively insignificant effect on rate-kinetics. Several examples regarding the use of reduced-order sub-models for soft-sensing are reported in literature [20,21]. The model reduction strategies discussed in [22–24] were used to make the following assumptions.

- The growth and decay kinetics of biomass are ignored. Hence, the model only considers the kinetics of substrate degradation processes.
- The release of ammonium (S<sub>NH</sub>) due to ammonification is considered insignificant in the anaerobic chambers, and hence it is ignored.
- The release of soluble ortho-phosphates (S<sub>PO</sub>) during hydrolysis of particulate biodegradable COD (X<sub>s</sub>) is ignored since it is negligible compared to (S<sub>PO</sub>) released due to the consumption of stored polyphosphates (PP).
- The rate of storage of PHA would not be affected by PHA concentration in the biomass.
- The temperature dependency of the rate constant for hydrolysis (r<sub>1</sub>) and rate constant for PHA storage (r<sub>2</sub>) follow the exponential term with coefficients (θ<sub>1</sub>) and (θ<sub>2</sub>).

The schematics of the process equations and the rate-kinetics occurring during the anaerobic stages of the biological phosphorus removal, and the bench-scale setup used to study the reaction kinetics are presented in Fig. 2.

#### 2.2.2. State-space equations

Every chamber in the multistage MBBR system is modelled as a continuous-stirred tank reactor (CSTR). The mass balances and rate kinetics are adapted for all three anaerobic chambers of the CSTR. The influent concentrations of particulate COD (X<sub>s,in</sub>), soluble COD (S<sub>s,in</sub>), and phosphates (S<sub>PO,in</sub>) are modelled as ‘random-walk’ and included in the state-vector [29]. The augmented state variables, to be estimated by the soft-sensor, is presented in Eq. 1. The Monod’s rate-kinetics in the continuous state-space form is presented in Eq. 2. The discrete state-space form of the model (Eq. 5) is obtained by discretizing the continuous-time model using an explicit Euler forward method with time-step T<sub>s</sub>.

$$x = [X_{s,in} \ S_{s,in} \ S_{PO,in} \ X_{s,1} \ S_{s,1} \ S_{PO,1} \ X_{s,2} \ S_{s,2} \ S_{PO,2} \ X_{s,3} \ S_{s,3} \ S_{PO,3}] \quad (1)$$

$$\frac{dx}{dt} = f_i = \begin{cases} 0 & i = 1, 2, 3 \\ \tau^{-1}(x(i-3) - x(i)) - r_1 \frac{x(i)}{K_H + x(i)} \theta_1^{T-20} & i = 4, 7 \\ \tau^{-1}(x(i-3) - x(i)) + r_1 \frac{x(i-1)}{K_H + x(i-1)} \theta_1^{T-20} & i = 5, 8 \\ -r_2 \frac{x_k(i)}{K_S + x(i)} \theta_2^{T-20} & \\ \tau^{-1}(x(i-3) - x(i)) + Y_{PO} r_2 \frac{x(i)}{K_S + x(i)} \theta_2^{T-20} & i = 6, 9 \end{cases} \quad (2)$$

**Table 1**  
Influent and effluent wastewater quality to the pilot plant and average removal percentages.

Parameter	Influent			Effluent			Average Removal (%)
	mean	min	max	mean	min	max	
sCOD	155.4	32	357.1	30.9	17.1	62	80.1
PO <sub>4</sub> <sup>3-</sup> -P	4.3	0.5	7.6	1.01	0.096	2.41	76.1

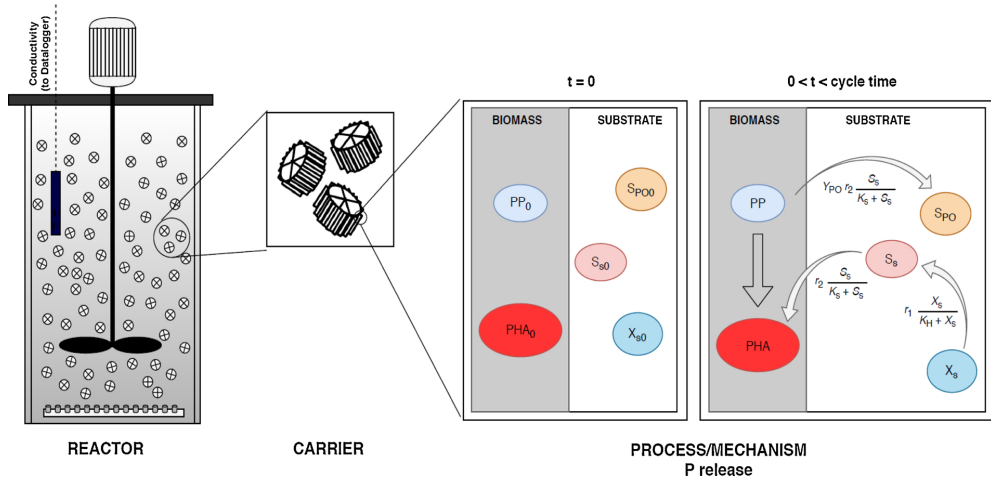


Fig. 2. Setup for batch kinetic experiment and associated mechanism for phosphorus release during the anaerobic phase.

Table 2  
Stoichiometric and Kinetic parameters for the reduced order model.

Parameter	Description	Value	Min	Max	Units
$K_H$	Saturation coefficient of hydrolysis	0.10	0.01	6	g COD m <sup>-3</sup>
$K_S$	Saturation coefficient of PHA storage	5.548	0.1	50	g COD m <sup>-3</sup>
$r_1$	Rate constant for hydrolysis	205	1	2000	g P m <sup>-3</sup> h <sup>-1</sup>
$r_2$	Rate constant for PHA storage	421	1	2000	g COD m <sup>-3</sup> h <sup>-1</sup>
$\theta_1$	Temperature coefficient for $r_1$	1.093	1	5	
$\theta_2$	Temperature coefficient for $r_2$	1.047	1	5	
$Y_{PO}$	Yield coefficient for PO <sub>4</sub> <sup>3-</sup> -P	0.064	0	1	g P/ g COD

$$y_k = h(x(3i - 1), x(3i)) \quad i = 1, 3, 5 \quad (3)$$

$$z_k = [C_{in} \ C_1 \ C_3] \quad (4)$$

$$x_k = x_{k-1} + T_S f(x_{k-1}) \quad (5)$$

In Eqs. (1)–(5),  $k$  is the discrete-time index and  $\tau$  is the residence

time in each chamber.  $x_k$  is the state-vector at time instance  $k$ . The variables  $X_{s,j}$ ,  $S_{s,j}$ , and  $S_{p0,j}$  correspond to the particulate biodegradable, soluble biodegradable and soluble ortho-phosphates in chamber  $j$  ( $j = 1, 2, 3$ ).  $f$  and  $h$  are the nonlinear state transition and measurement function respectively.  $z_k$  is the measurement vector, and  $y_k$  is the model predicted value of the conductivity measurement at time instance  $k$ . The kinetic parameters  $K_H$ ,  $K_S$ ,  $r_1$ ,  $r_2$ ,  $\theta_1$ ,  $\theta_2$ , and the stoichiometric parameters  $Y_{PO}$  (explained in Table 2) are determined by fitting the model to the data obtained from performing kinetic tests in a batch scale reactor.

2.2.3. Measurement equation

The data from the batch kinetic experiments, as well as results presented in literature [9,10], indicate a clear relationship between electrical conductivity and various nutrient compositions present in wastewater. The mathematical equations to quantitatively express conductivity as a function of ionic species in the wastewater had been previously reported [8,25]. However, the simplified model used in this work has just two species, represented as state variables  $S_s$  and  $S_{p0}$  influencing the changes in electrical conductivity. Therefore, we use a

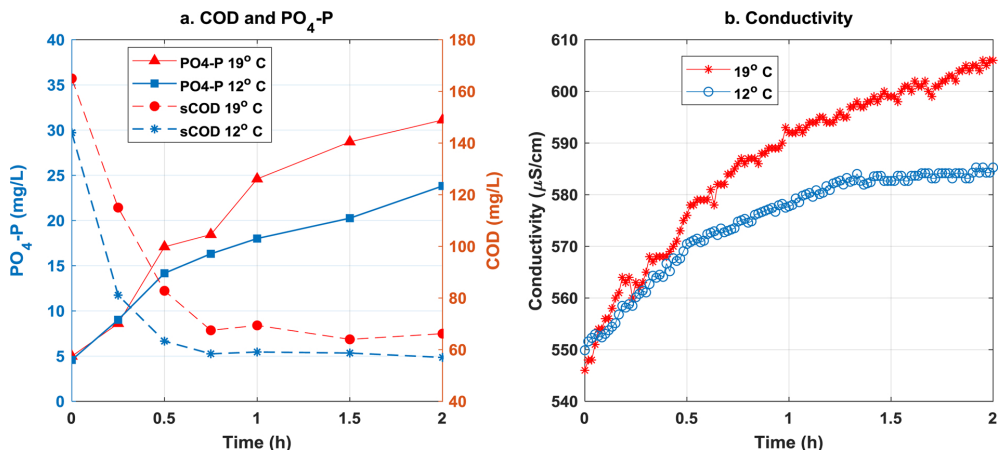


Fig. 3. Variations in (a) PO<sub>4</sub><sup>3-</sup>-P and sCOD (b) Conductivity during the batch tests.

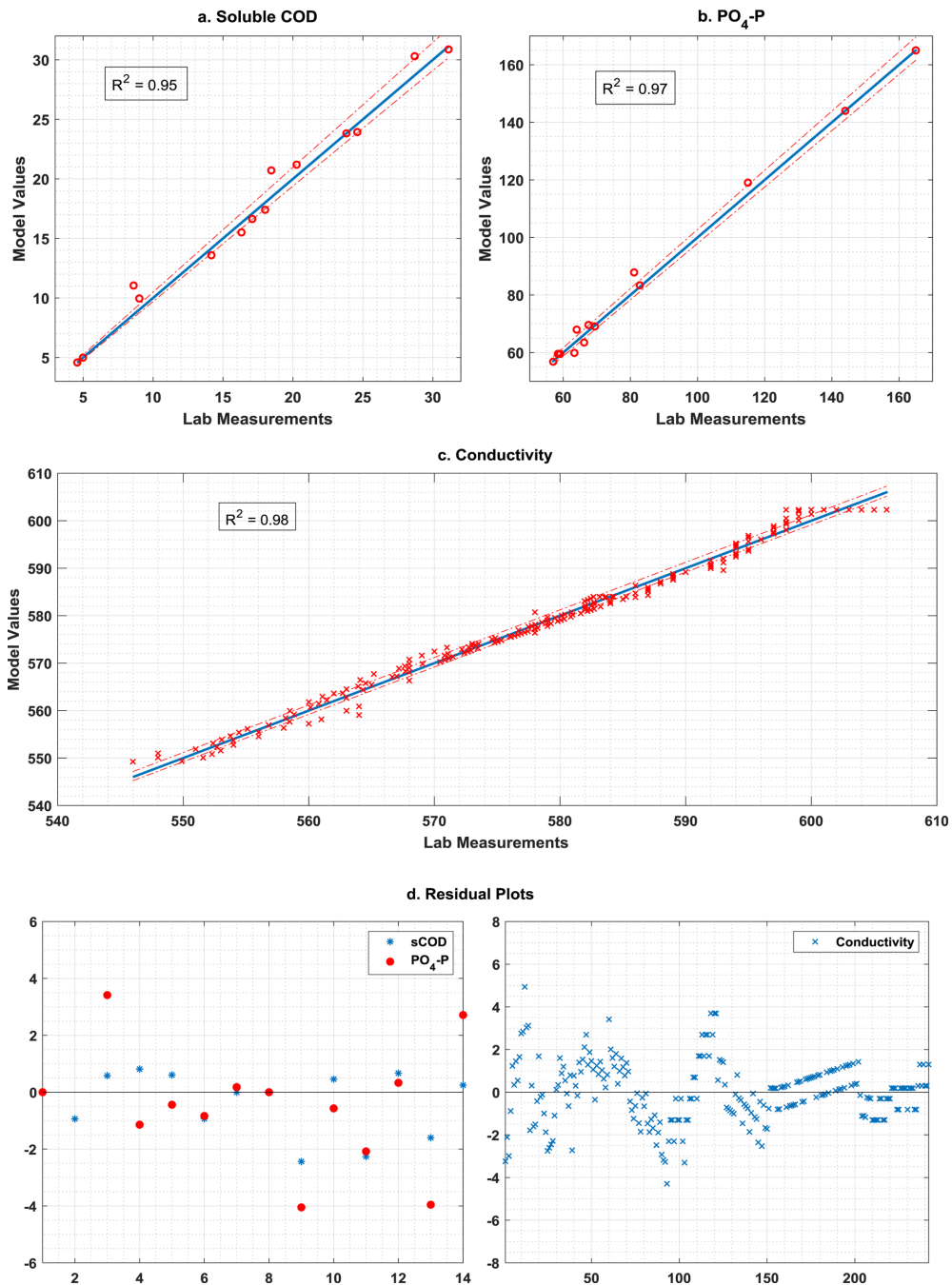


Fig. 4. Regression plot experimental results versus model predicted values (a) soluble COD, (b) soluble PO<sub>4</sub><sup>3-</sup>P, (c) Conductivity, and (d) Residual plots.

statistical method to regress the data obtained from the kinetic tests to a generic equation form which includes higher powers and binary interaction terms of the predictors ( $S_s$  and  $S_{po}$ ). The use of similar model forms to correlate water quality parameters have been previously

reported in literature [33].

$$h(S_s, S_{po}) = C = \alpha_0 + \alpha_1 S_s + \alpha_2 S_{po} + \alpha_3 S_s^2 + \alpha_4 S_{po}^2 + \alpha_5 S_s S_{po} \quad (6)$$

The Regression Learner Toolbox in MATLAB was used to identify a

**Table 3**  
Regression parameters for the measurement model.

Parameter	$\alpha_0$	$\alpha_1$	$\alpha_2$	$\alpha_3$	$\alpha_4$	$\alpha_5$
Values	539	-0.0031	1.91	0.000610	0.00141	-0.0220
Confidence Interval	$\pm 14.8$	$\pm 0.0005$	$\pm 0.12$	$\pm 0.00007$	$\pm 0.0008$	$\pm 0.0014$
p-Value	1.28e-11	3.63e-4	8.43e-8	4.31e-5	2.17e-16	1.81e-7

correlation between the species  $S_{po}$ ,  $S_s$  and the data received from the conductivity sensor installed in the experimental unit used for the kinetic study. The final model form (Eq. 6) was derived by assessing the significance of each regression coefficients using t-statistic and selecting the parameters that significant at 5% significance level.

### 2.3. Batch experiments and model calibration

To evaluate the biomass kinetics and to estimate the kinetic and stoichiometric coefficients of the reduced-order model, a series of batch experiments were conducted. To perform the experiment, the carriers colonized with PAOs were taken from the MBBR pilot and filled in a 1 L beaker at 60 % filling degree and raw wastewater. Nitrogen gas was initially bubbled through the reactor to remove the oxygen from the wastewater and ensure perfect anaerobic conditions. The beaker was continuously mixed using a mechanical stirrer. The batch reactor was equipped with an online conductivity sensor for continuous monitoring of electrical conductivity during the cycle. A data logger was connected to the conductivity sensor and was configured to log the conductivity measurement every 1 min during the entire duration of the batch test. The breaker was sealed to maintain anaerobic conditions during the test. The schematic of the test beaker is presented in Fig. 2. Samples for analysis of sCOD and  $PO_4^{3-}$ -P were taken every 15 min for an entire test period of 2 h. The water quality parameters were measured using Dr. Lange cuvettes (LCK 350 and LCK 348 for  $PO_4^{3-}$ -P and LCI400 and LCK 314 for COD) and HACH LANGE GmbH (DR 1900, China) spectrophotometer.

The data obtained from the batch experiment was fit to the mathematical model explained in Eq. (1) to Eq. (6). The optimization procedure, using the minimization of quadratic-error function [26], was used to fit the model and obtain the kinetic parameters. The optimization problem is expressed in Eqs. 7 and 8.

$$\min_p \left\{ \sum_{i=1}^{\mathcal{N}} [\varphi_{\text{exp}} - \varphi_{\text{model}}(p)]^2 \right\} \quad (7)$$

$$lb \leq p \leq ub \quad (8)$$

'p' is a vector consisting of the model parameters that are to be estimated. The terms *ub* and *lb* are the upper and lower bounds of the parameter vector.  $\mathcal{N}$  is the number of datapoints obtained from the kinetic experiment. The objective function is defined as the least-square error between the experimental values  $\varphi_{\text{exp}} = [s\text{COD}PO_4^{3-}\text{-P}]$ , and their corresponding model predicted values  $\varphi_{\text{model}}(p) = [S_s S_{po}]$ . The *lb* and *ub* of the parameter vector *p*, along with the results of the optimization problem are presented in Table 2. Due to the lack of an appropriate initial guess for the parameters, a high range was provided to *lb* and *ub* to ensure a wider search area for the optimization algorithm. The optimization problem was solved with MATLAB. The *fmincon* function using the interior-point algorithm was combined with the grid search method to solve the optimization problem and obtain the model parameters.

### 2.4. Soft-sensor algorithms

The Kalman Filter is a commonly used algorithm for estimating the state variables in linear systems. Several versions of the original Kalman Filter algorithm can be used to estimate the states of a nonlinear system.

The Extended Kalman Filter (EKF) computes the Kalman gain by using a linearized version of the nonlinear functions describing the state-space as well as measurement equations. Eqs. (9) – (15) describe the EKF algorithm used for estimating the states of the MBBR system. The equations are written in the order they have been programmed in Python.

$$F_{k-1} = I + T_s \left. \frac{\partial f}{\partial x} \right|_{x_{k-1}^+, u_k} \quad (9)$$

$$x_k^- = x_{k-1}^+ + T_s f(x_{k-1}^+, u_{k-1}) \quad (10)$$

$$P_k^- = F_{k-1} P_{k-1}^+ F_{k-1}^T + Q_{k-1} \quad (11)$$

$$H_k = \left. \frac{\partial h}{\partial x} \right|_{x_k^-, u_k} \quad (12)$$

$$K_k = P_k^- H_k^T (H_k P_k^- H_k^T + R_{k-1})^{-1} \quad (13)$$

$$x_k^+ = x_k^- + K (z_k - h(x_k^-)) \quad (14)$$

$$P_k^+ = (I - K_k H_k) P_k^- \quad (15)$$

In the equations above,  $x_k$  is the state variable at time instance *k*,  $z_k$  is the measurement vector, *Q* and *R* are the covariance matrices of the process and measurement noise, respectively. *f* and *h* are the nonlinear state space and measurement functions. *F* is the linearized state transition matrix, and *H* is the linearized measurement matrix. *I* is the identity matrix,  $x_k^-$  is the *a priori* estimate of the state,  $x_k^+$  the *a posteriori* estimate of the state,  $K_k$  the Kalman gain,  $P_k^-$  the covariance of *a priori* estimation error, and  $P_k^+$  the covariance matrix of the *a posteriori* estimation error.

### 2.5. Implementation in pilot plant

The pilot plant SCADA system provides access to real-time data from the online sensors through a remote SQL server. The mathematical model (Eqs. (1)–(6)) and the EKF algorithm (Eqs. (9)–(15)) are written as a Python script and can be executed on a single board computer (Raspberry Pi 3B+). This open-source, non-intrusive, remote deployment strategy [27] is used to implement the soft-sensor algorithm in the pilot plant. The Python script was used for simulator-based testing, tuning of the EKF parameter, and the real-time deployment of the soft-sensing algorithm.

## 3. Results and discussion

### 3.1. Model calibration results

The results obtained from the batch experiments are presented in Fig. 3. The plots indicate an increase in conductivity measurements when the  $PO_4^{3-}$ -P ions are released and sCOD is consumed under anaerobic conditions. These observations are consistent with the results obtained from similar experiments [12,25,8].

The results from the parameter estimation exercise, showing a comparison between model-predicted and experimental values followed by their residual plots are presented in Fig. 4. The  $R^2$  values of 0.96 and 0.97 indicate a good correlation between the experimental data and the model. The stoichiometric and kinetic parameters obtained by implementing the parameter estimation algorithm (Eqs.



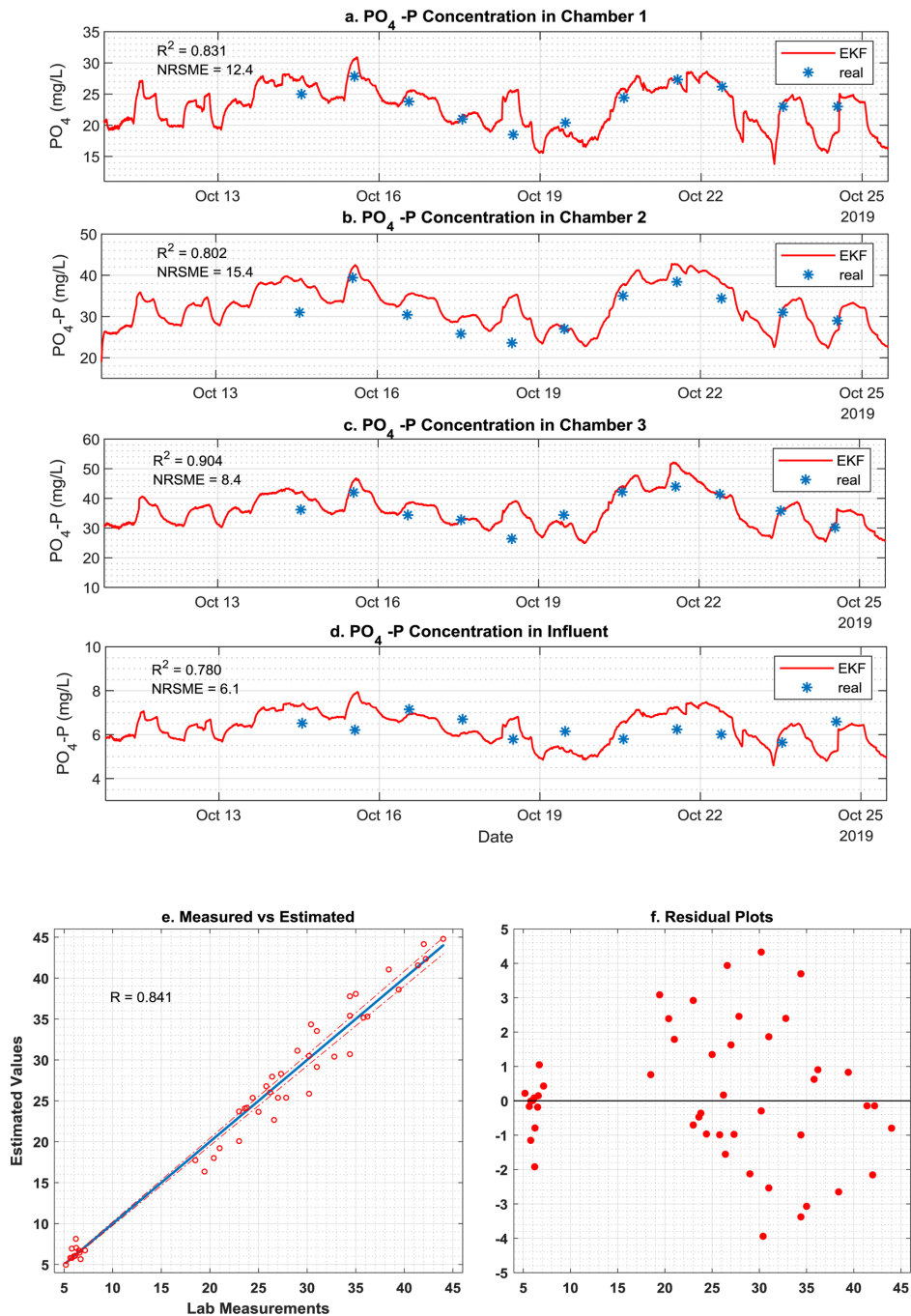


Fig. 5. Soft-sensor validation for phosphates (a) Chamber 1 (b) Chamber 2 (c) Chamber 3 (d) Influent (e) Measured versus estimated values (f) Residual plots.

(7)–(8)) on the data obtained from the batch experiments are presented in Table 2. A good match between experimental versus model predicted values and the corresponding R values close to 1 and a random

distribution of the errors along the zero-error line (presented in the residual plot) validates the accuracy of the model.

The coefficients of the measurement model (Eq. 6) obtained by

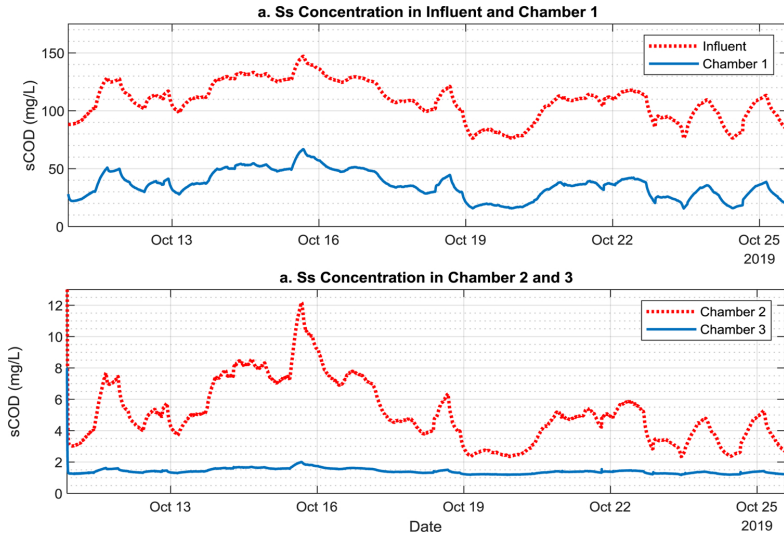


Fig. 6. Soft sensing results for sCOD concentration in the anaerobic chambers.

correlating the ionic concentration to the conductivity measurement, using the Regression Learner toolbox is presented in Table 3. Table 3 also presents the results of significance tests for all the estimated parameters obtained by conducting the t-statistics on the model. The p-value for the t-statistic of the hypothesis test indicates that all the parameters are significant within the 5% significance interval.

### 3.2. Tuning the EKF parameters

The tuning parameters of Kalman filter  $x_0^+$ ,  $P_0^+$ ,  $Q$ , and  $R$  described in Eq. (9) to Eq. (15) have to be obtained before using it to estimate the concentration of phosphates ( $\text{PO}_4^{3-}\text{-P}$ ) and sCOD in the pilot plant. Some guidelines for tuning EKF parameters have been suggested in literature [28]. However, in practical applications, a little trial-and-error combined with some operational knowledge of the process would be used to tune these parameters. The guidelines mentioned in [29] have been used as a base for the simulator-based testing of the EKF and to obtain the tuning parameters.

**Tuning of  $x_0^+$ :** A reasonable initial guess of  $x_0^+$  is its steady-state values. In our case, this value of  $x_0^+$  is set equal to the designed steady-state values of the state variables in each chamber.

$$x_0^+ = [230 \ 150 \ 4.4 \ 169 \ 54.9 \ 14.0 \ 109 \ 9.1 \ 20.6 \ 48.9 \ 3.4 \ 30.1] \quad (16)$$

**Tuning of  $P_0^+$ :** The initial guess for the apriori estimation error is an  $n \times n$  diagonal matrix. The values are decided based on the confidence levels in the initial estimation of state variables.

$$P_0^+ = \text{diag} [k_i \ x_i] \quad (17)$$

By trial and error, it was found that the following values provide a good estimation, where the estimated states approach the simulated state within a reasonable short time-span (30 min in our case).

$$k_i = [15 \ 5.1 \ 6 \ 2 \ 1 \ 0.5 \ 3 \ 2 \ 1.1 \ 2 \ 1 \ 0.5] * 10^{-3} \quad (18)$$

**Tuning of  $R$ :** A gaussian noise with a standard deviation of 0.01 was observed in the measurements provided by conductivity sensors. Therefore, the measurement noise covariance matrix  $R$  was calculated as the square of the standard deviation of the noise observed in conductivity sensors installed in chamber 1, 3, and the influent.

$$R = [0.01^2 \ 0.01^2 \ 0.01^2] = [1 \ 1 \ 1] * 10^{-4} \quad (19)$$

**Tuning of  $Q$ :** The process noise covariance matrix,  $Q$ , is assumed to be a diagonal matrix, with diagonal elements related to the initial guess of the pertinent state variable scaled through the factors  $l_i$ :

$$Q = \text{diag}([l_i \ x_{0,i}^+]^2) \quad (20)$$

In the simulator-based testing, values of  $l_i$  are adjusted so that the estimated values converge faster (within 30 min) to the assumed true value and at the same time do not exhibit too much noise in the estimated values. By trial and error, the values were found to be as follows.

$$\{l_i\} = [1.2 \ 0.21 \ 1.4 \ 2 \ 1 \ 3.7 \ 1 \ 1 \ 1.6 \ 2 \ 2.1 \ 3.3] * 10^{-3} \quad (21)$$

### 3.3. Validation in pilot plant

The soft sensor was implemented in the pilot plant, and the estimation results for phosphate concentration in the anaerobic chamber and the influent are observed for a period of two weeks. During the evaluation period, one grab sample was collected every day and analyzed for  $\text{PO}_4^{3-}\text{-P}$  concentration. Fig. 5 presents a comparison between the phosphate concentration estimated by the soft-sensor and the values measured using standardized lab tests. The comparisons are provided for the influent and all three anaerobic chambers. The normalized root-mean-square error (NRSME) and  $R^2$  values are also presented in Fig. 5. The  $R^2$  value above 0.8 even with a limited data series demonstrates the EKF's potential to estimate the phosphate concentration in the pilot plant.

The soft-sensor can also potentially estimate the sCOD in the system. The estimation results for sCOD in each chamber are presented in Fig. 6. Although no rigorous validation tests (similar to the  $\text{PO}_4^{3-}\text{-P}$  measurement) were conducted to assess the accuracy of sCOD estimations in each anaerobic chamber, a comparison between the influent sCOD estimation and the corresponding sCOD lab measurements presented in Fig. 7b demonstrates their potential in estimating influent sCOD concentrations. However, more rigorous validations have to be conducted to confirm their ability to estimate sCOD concentrations in all the anaerobic chambers.

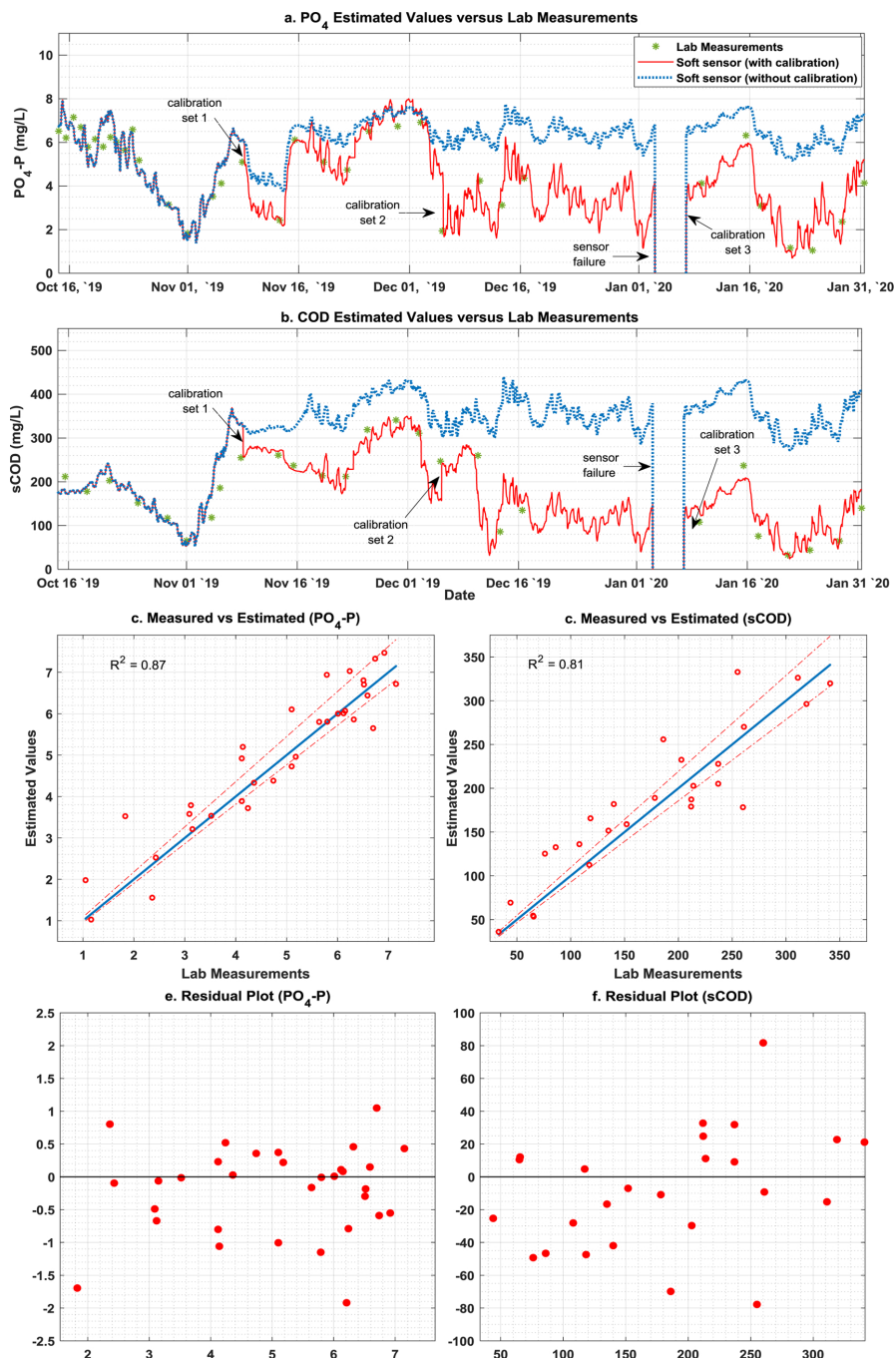


Fig. 7. Long-term evaluation of soft-sensor performance and influence of recalibration strategy on (a) influent PO<sub>4</sub><sup>3-</sup>P (b) influent sCOD. Measured vs estimated values (c) PO<sub>4</sub><sup>3-</sup>P (d) sCOD. Residual Plots (e) PO<sub>4</sub><sup>3-</sup>P (f) sCOD.

**Table 4**  
Regression parameters of the measurement model obtained during recalibration.

Parameter	Calibration Date	R <sup>2</sup>	$\alpha_0$	$\alpha_1$	$\alpha_2$	$\alpha_3$	$\alpha_4$	$\alpha_5$
Set 1	08–11-2019	0.93	527 ( ± 14.8)	−0.0036 ( ± 0.00050)	2.21 ( ± 0.12)	0.000600 ( ± 0.00007)	0.00321 ( ± 0.0008)	−0.0220 ( ± 0.0035)
Set 2	05–12-2019	0.96	519 ( ± 11.8)	−0.0016 ( ± 0.00015)	2.91 ( ± 0.16)	0.000510 ( ± 0.00006)	0.00241 ( ± 0.0004)	−0.0202 ( ± 0.0077)
Set 3	07–01-2020	0.87	511 ( ± 13.8)	−0.0036 ( ± 0.00025)	2.01 ( ± 0.11)	0.000110 ( ± 0.00002)	0.00671 ( ± 0.0001)	−0.0402 ( ± 0.0060)

### 3.4. Influence of recalibration strategy

To assess the robustness of the conductivity based soft-sensor and to study their long-term performance, the estimated values  $S_{s,in}$  and  $S_{po,in}$  were monitored for an additional period of 3 months (14th October 2019 to 06th February 2020). The assessment was performed by comparing the lab results from the biweekly measurements of sCOD and  $PO_4^{3-}$ -P concentrations in raw wastewater to the corresponding values of  $S_{s,in}$  and  $S_{po,in}$ , respectively, estimated by the soft-sensor. Preliminary assessment of soft-sensor showed that, although the estimation results were very close to the lab measurements for the first 3 weeks, from the beginning of week 4 (on 5th November 2019), the first sign of drift from the lab measurements started to appear.

The accuracy of the mathematical model is a vital element in the performance of the soft sensor. A possible reason could be attributed to the drift in the measurement model adopted in this work. It should be noted that the parameters ( $\alpha_i$ ) mentioned in Eq. (6) is obtained by correlating the conductivity measurements to the concentration of sCOD and  $PO_4^{3-}$ -P obtained from the kinetic tests on a batch scale. However, in reality, the wastewater used in the batch tests contains many other ionic species affecting the conductivity measurements [8]. A few prior works, such as [30], report a stable correlation between electrical conductivity and  $PO_4^{3-}$ -P release during anaerobic conditions of an EBPR process. However, a substantial change in the ratio between various ionic species of the influent wastewater over an extended period may affect the accuracy of the initial measurement model obtained from the batch experiments. Including the additional ionic species as extra state variables in the model could offer a possible solution, but it would affect the observability of the model and undermine the idea of using a simple reduced-order model, for estimating the states using an EKF.

An alternative solution for this problem would be to frequently calibrate the measurement model and update the model parameters presented in Table 3. The significance of regular calibration of mathematical models has been emphasized in [31]. The measurement model was updated using the recent values of sCOD,  $PO_4^{3-}$ -P, and the corresponding conductivity measurements. The calibration algorithm used for obtaining initial regression parameters was used to obtain the new set. The model calibration followed by the update of model parameters was carried out once every month or whenever the percentage error between the estimated value and the lab measurement was more than 50 %. For the purpose of comparison, the soft-sensor using the initial measurement model (presented in Table 3) was also executed in parallel with the model that was regularly calibrated. Both these data were logged in the remote SQL server.

The soft sensor was calibrated at three different instances, as indicated in Fig. 7a and b. A comparison between the estimated values of sCOD and  $PO_4^{3-}$ -P along with the experimental data for chamber 1, 2 and 3 are provided in Fig. 7c and d. The updated parameters of the measurement model obtained from each calibration instance along with their 95 % confidence intervals are mentioned in Table 4. The first calibration of the soft-sensor was carried out on 8th November 2019 followed by another two on 05th December 2019, and 07th January 2020 subsequently. The first update of the measurement model (Set 1) demonstrated a minor difference between the calibrated and uncalibrated estimation. However, the difference increased significantly over time, especially after the second (Set 2) and third (Set 3)

calibration instances. The confidence interval presented in Table 4 indicates that the parameters ( $\alpha_i$  where  $i = 1, 2, \dots, 5$ ) estimated during all three calibration instances are well within the 95 % significance intervals.

A comparison plot, along with the corresponding R<sup>2</sup> values, is presented in Fig. 7. The plots presented in Fig. 7a and b demonstrate that the estimations of sCOD and  $PO_4^{3-}$ -P with a regularly calibrated model was closer to the actual values (obtained from standardized lab measurements) when compared to the uncalibrated model. This could infer that periodic calibration of the soft-sensor model by updating the measurement function would solve the estimation error caused by the drift in the measurement model. Additional plots regarding the estimated  $PO_4^{3-}$ -P and sCOD in chamber 1, 2, and 3 are provided in Appendix as Fig. A1 and Fig. A2.

## 4. Conclusions

A reduced-order model explaining the dynamics of phosphorus release during the anaerobic stage of biological wastewater treatment process was developed. The hybrid model combining statistical methods with the mechanistic elements of biological nutrient removal process, adequately explains the reactions while still retaining its ability to be used in conjunction with EKF for estimating the states of the model. The simulator-based testing of the mathematical model provides theoretical validations for the ability of the soft-sensor to provide reliable estimations of states in the anaerobic stages of the EBPR-MBBR pilot plant. The implementation of the EKF based soft sensor in the pilot plant and the corresponding validation studies demonstrate the ability of the soft-sensor to provide reliable estimations of  $PO_4^{3-}$ -P and sCOD concentration in the anaerobic chamber of a multistage EBPR-MBBR pilot plant. The work also emphasizes the importance of regular model calibration. A systematic calibration strategy, discussed in this work, addresses the issue of drift in soft-sensor caused by the measurement model mismatch. The approach involving the regular model calibration provides a practical solution to the drift caused by model error. A comparison of the soft-sensor performance using the uncalibrated model and the frequently calibrated model with the lab measurements demonstrates the importance of calibration in enhancing the performance of the soft-sensor. The cost-effective method for estimation of influent  $PO_4^{3-}$ -P and sCOD concentration as well as the  $PO_4^{3-}$ -P concentrations in the anaerobic chambers of a continuous multistage MBBR pilot plant may be beneficial in the implementation of advanced control strategies for optimal operation of wastewater treatment plants designed for enhanced biological phosphorus removal.

## Declaration of Competing Interest

The authors declare that they have no known competing financial interests or personal relationships that could have appeared to influence the work reported in this paper.

## Acknowledgements

This research was funded by the Norwegian Research Council (NFR) Project RECOVER. The authors acknowledge the technical and financial support from DOSCON AS.

Appendix A

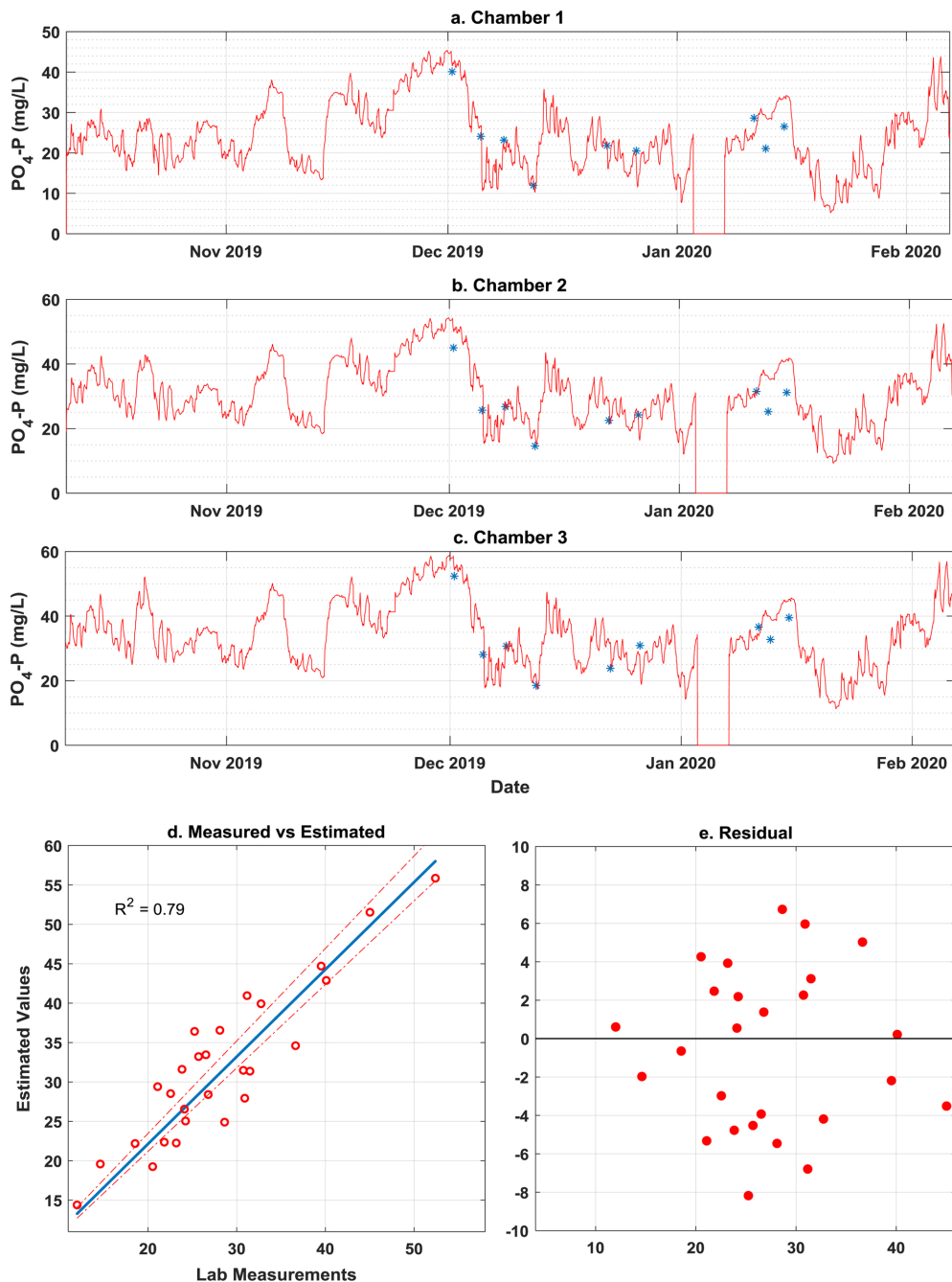


Fig. A1. Long-term measured versus estimated plots for  $PO_4^{3-}\text{-P}$  in (a) Chamber 1, (b) Chamber 2, (c) Chamber 3. (d) Measured versus estimated (e) Residual Plots.

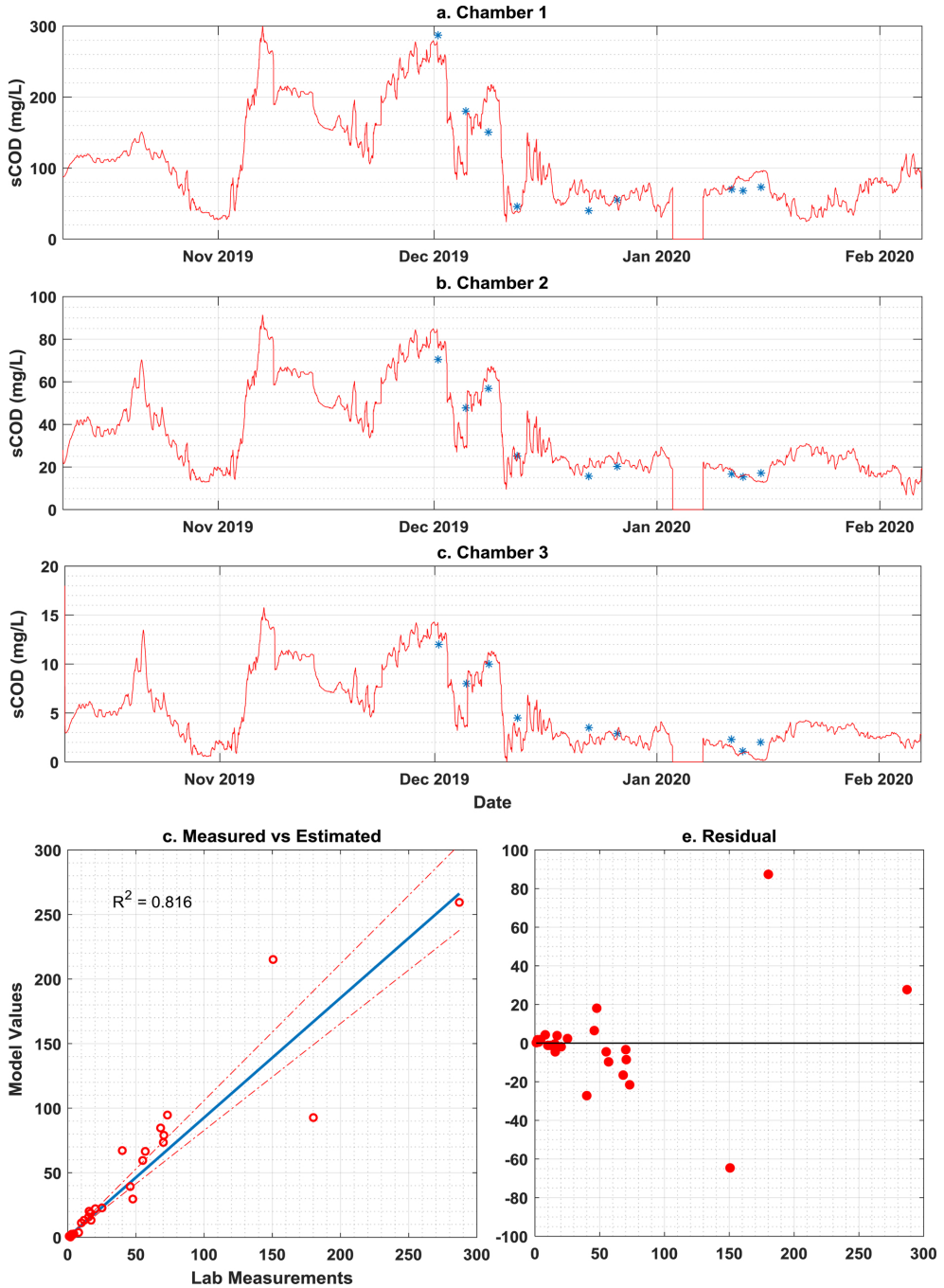


Fig. A2. Long-term measured versus estimated plots for sCOD in (a) Chamber 1, (b) Chamber 2, (c) Chamber 3. (d) Measured versus estimated (e) Residual Plots.



## References

- [1] T. Mino, M.C.M. van Loosdrecht, J.J. Heijnen, Microbiology and biochemistry of the enhanced biological phosphate removal process, *Water Res.* 32 (11) (1998) 3193–3207, [https://doi.org/10.1016/S0043-1354\(98\)00129-8](https://doi.org/10.1016/S0043-1354(98)00129-8).
- [2] P.A. Vanrolleghem, D.S. Lee, On-line monitoring equipment for wastewater treatment processes: state of the art, *Water Sci. Technol.* 47 (2) (2003) 1–34, <https://doi.org/10.2166/wst.2003.0074>.
- [3] G. Olsson, ICA and me - A subjective review, *Water Res.* 46 (6) (2012) 1585–1624, <https://doi.org/10.1016/j.watres.2011.12.054>.
- [4] D. Dochain, P. Vanrolleghem, *Dynamical Modelling and Estimation in Wastewater Treatment Processes*, IWA Publishing, London, U.K, 2001, pp. 250–274, <https://doi.org/10.2166/9781780403045>.
- [5] H. Haimi, F. Corona, M. Mulas, L. Sundell, M. Heinonen, R. Vahala, Shall we use hardware sensor measurements or soft-sensor estimates? Case study in a full-scale WWTP, *Environ. Model. Softw.* 72 (2015) 215–229, <https://doi.org/10.1016/j.envsoft.2015.07.013>.
- [6] J. Busch, D. Elikmann, P. Kühn, C. Gerkens, J.P. Schlöder, H.G. Bock, W. Marquardt, State estimation for large-scale wastewater treatment plants, *Water Res.* 47 (13) (2013) 4774–4787, <https://doi.org/10.1016/j.watres.2013.04.007>.
- [7] N. Patel, J. Ruparelia, J. Barve, Prediction of total suspended solids present in effluent of primary clarifier of industrial common effluent treatment plant: mechanistic and fuzzy approach, *J. Water Process. Eng.* 34 (2020) 101146, <https://doi.org/10.1016/j.jwpe.2020.101146>.
- [8] K.S. Kim, J.S. Yoo, S. Kim, H.J. Lee, K.H. Ahn, I.S. Kim, Relationship between the electric conductivity and phosphorus concentration variations in an enhanced biological nutrient removal process, *Water Sci. Technol.* 55 (1–2) (2007) 203–208, <https://doi.org/10.2166/wst.2007.053>.
- [9] D. Aguado, A. Ferrer, A. Seco, J. Ferrer, Comparison of different predictive models for nutrient estimation in a sequencing batch reactor for wastewater treatment, *Chemom. Intell. Lab. Syst. 84* (1–2) (2006) 75–81, <https://doi.org/10.1016/j.chemolab.2006.03.009>.
- [10] D. Aguado, T. Montoya, J. Ferrer, A. Seco, Relating ions concentration variations to conductivity variations in a sequencing batch reactor operated for enhanced biological phosphorus removal, *Environ. Model. Softw.* 21 (6) (2006) 845–851, <https://doi.org/10.1016/j.envsoft.2005.03.004>.
- [11] D. Aguado, M. Zarzo, A. Seco, A. Ferrer, Process understanding of a wastewater batch reactor with block-wise PLS, *Environmetrics* 18 (2007) 551–560, <https://doi.org/10.1002/env.828>.
- [12] J. Serralta, L. Borrás, C. Blanco, R. Barat, A. Seco, Monitoring pH and electric conductivity in an EBPR sequencing batch reactor, *Water Sci. Technol.* 50 (10) (2004) 145–152, <https://doi.org/10.2166/wst.2004.0630>.
- [13] T. Salmes, G. Sorensen, S. Eikås, Biological nutrient removal in a continuous biofilm process, *Water Pract. Technol.* 12 (4) (2017) 797–805, <https://doi.org/10.2166/wpt.2017.083>.
- [14] M.F.R. Zuthi, W.S. Guo, H.H. Ngo, L.D. Nghiem, F.I. Hai, Enhanced biological phosphorus removal and its modeling for the activated sludge and membrane bioreactor processes, *Bioresour. Technol.* 139 (2013) 363–374, <https://doi.org/10.1016/j.biortech.2013.04.038>.
- [15] M. Henze, W. Gujer, T. Mino, T. Matsuo, M.C. Wentzel, Gv.R. Marais, M.C.M. Van Loosdrecht, Activated sludge model No. 2D, ASM2D, *Water Sci. Technol. Technol.* 39 (1) (1999) 165–182, [https://doi.org/10.1016/S0273-1223\(98\)00829-4](https://doi.org/10.1016/S0273-1223(98)00829-4).
- [16] K.B. Newhart, R.W. Holloway, A.S. Hering, T.Y. Cath, Data-driven performance analyses of wastewater treatment plants: a review, *Water Res.* 157 (2019) 498–513, <https://doi.org/10.1016/j.watres.2019.03.030>.
- [17] U. Jeppsson, G. Olsson, Reduced order models for on-line parameter identification of the activated sludge, *Water Sci. Technol. Technol.* 28 (11) (1994) 173–183, <https://doi.org/10.2166/wst.1993.0657>.
- [18] X. Yin, J. Liu, State estimation of wastewater treatment plants based on model approximation, *Comput. Chem. Eng.* 111 (2018) 79–91, <https://doi.org/10.1016/j.compchemeng.2018.01.003>.
- [19] J. Carstensen, P. Harremoës, R. Strubee, Software sensors based on the grey-box modelling approach, *Water Sci. Technol.* 33 (1) (1996) 117–126, [https://doi.org/10.1016/0273-223\(96\)00164-3](https://doi.org/10.1016/0273-223(96)00164-3).
- [20] C. Gómez-Quintero, I. Queinnee, M. Spérandio, A reduced linear model of an activated sludge process, *Ifac Proc. Vol. 37* (3) (2004) 219–224, [https://doi.org/10.1016/S1474-6670\(17\)32586-7](https://doi.org/10.1016/S1474-6670(17)32586-7).
- [21] V.K. Madyastha, V. Prasad, V. Mahendrakar, Reduced order model monitoring and control of a membrane bioreactor system via delayed measurements, *Water Sci. Technol.* 64 (8) (2011) 1675–1684, <https://doi.org/10.2166/wst.2011.437>.
- [22] M.A. Steffens, P.A. Lant, R.B. Newell, A systematic approach for reducing complex biological wastewater treatment models, *Water Res.* 31 (3) (1997) 590–606, [https://doi.org/10.1016/S0043-1354\(96\)00273-4](https://doi.org/10.1016/S0043-1354(96)00273-4) (1997).
- [23] T. Zhang, D. Zhang, Z. Li, Q. Cai, Evaluating the structural identifiability of the parameters of the EBPR sub-model in ASM2d by the differential algebra method, *Water Res.* 44 (9) (2010) 2815–2822, <https://doi.org/10.1016/j.watres.2010.02.027>.
- [24] Z. Li, P. Lu, D. Zhang, T. Zhang, Practical identifiability analysis and optimal experimental design for the parameter estimation of the ASM2d-Based EBPR anaerobic submodel, *Math. Probl. Eng.* 2018 (2018) 1–9, <https://doi.org/10.1155/2018/9201085>.
- [25] M. Maurer, W. Gujer, Monitoring of microbial phosphorous release in batch experiments using electric conductivity, *Water Res.* 29 (11) (1995) 2613–2617, [https://doi.org/10.1016/0043-1354\(95\)00146-C](https://doi.org/10.1016/0043-1354(95)00146-C).
- [26] A. Nair, V.M. Cristea, P.S. Agachi, M. Brehar, Model calibration and feed-forward control of the wastewater treatment plant – case study for CLUJ-Napoca WWTP, *Water Environ. J.* 32 (2) (2018) 164–172, <https://doi.org/10.1111/wej.12310>.
- [27] A.M. Nair, A. Hykkerud, H. Ratnaweera, A cost-effective IoT strategy for remote deployment of soft sensors – a case study on implementing a soft sensor in a multistage MBBR plant, *Water Sci. Technol.* (2020), <https://doi.org/10.2166/wst.2020.067>.
- [28] D. Simon, *Optimal State Estimation: Kalman, H, and Nonlinear Approaches*, John Wiley & Sons, USA, 2006, <https://doi.org/10.1002/0470045345>.
- [29] F. Haugen, R. Bakke, L. Bernt, State estimation and model-based control of a pilot anaerobic digestion reactor, *J. Control. Sci. Eng.* 2014 (2014) 572–621, <https://doi.org/10.1155/2014/572621>.
- [30] A. Colin Wylie, Investigation of Electrical Conductivity As a Control Parameter for Enhanced Biological Phosphorus Removal in a Pilot Scale Sequencing Batch Reactor. Thesis, University of British, Columbia, 2001, <https://doi.org/10.14288/1.0067103> 2009. Print.
- [31] F. Tscheikner-Gratl, P. Zeisl, C. Kinzel, J. Leimgruber, T. Ertl, W. Rauch, M. Kleidorfer, Lost in calibration: why people still do not calibrate their models, and why they still should – a case study from urban drainage modelling, *Water Sci. Technol.* 74 (10) (2016) 2337–2348, <https://doi.org/10.2166/wst.2016.395>.
- [32] S. Daneshgar, P.A. Vanrolleghem, C. Vaneckhaute, A. Buttafava, A.G. Capodaglio, Optimization of P compounds recovery from aerobic sludge by chemical modeling and response surface methodology combination, *Sci. Total Environ.* 668 (2019) 668–677, <https://doi.org/10.1016/j.scitotenv.2019.03.055>.





# Paper C





## A cost-effective IoT strategy for remote deployment of soft sensors – a case study on implementing a soft sensor in a multistage MBBR plant


A. M. Nair , A. Hykkerud  and H. Ratnaweera 


### ABSTRACT

Model-based soft sensors can enhance online monitoring in wastewater treatment processes. These soft sensor scripts are executed either locally on a programmable logic controller (PLC) or remotely on a system with data-access over the internet. This work presents a cost-effective, flexible, open source IoT solution for remote deployment of a soft sensing algorithm. The system uses low-priced hardware and open-source programming language to set up the communication and remote-access system. Advantages of the new IoT architecture are demonstrated through a case study for remote deployment of an Extended Kalman Filter (EKF) to estimate additional water quality parameters in a multistage moving bed biofilm reactor (MBBR) plant. The soft-sensor results are successfully validated against standardised laboratory measurements to prove their ability to provide real-time estimations.

**Key words** | digital water, IoT, MBBR, soft sensor

A. M. Nair  (corresponding author)

A. Hykkerud 

H. Ratnaweera 

Faculty of Science and Technology,  
Norwegian University of Life Sciences,  
1432 Ås,  
Norway

E-mail: muralabh@nmbu.no

### INTRODUCTION

The rise of digital water, driven by a rapid increase in information technology, has created an impetus to develop smarter and more efficient monitoring tools in wastewater treatment plants. Soft sensors have gained importance as a viable alternative to expensive online sensors (Olsson *et al.* 2014; Wang *et al.* 2019). Soft sensors are computer codes, which use a process model together with available online measurements from treatment plants to estimate additional wastewater quality parameters (Haimi *et al.* 2015). These soft sensor scripts are executed in a programmable logic controller (PLC), which has access to real-time data from the online sensors. Soft-sensors can also be implemented in a remote device if the plant's supervisory control and data acquisition (SCADA) has remote monitoring capabilities.

Most commercial SCADA vendors use proprietary software for programming their PLCs. Therefore, implementing the soft sensor in a PLC requires the code to be written in its proprietary programming suite, which limits the possibility of running soft sensor scripts written in commonly used scientific/academic programming languages such as Matlab or Python in industrial PLCs. The alternative is to develop a communication layer interface between a client (with the soft sensor script) and a server that has

access to data from the online sensors. Open Platform Communication (OPC) has recently emerged as a global standard for communication between various sensors, PLCs and SCADA providers (González *et al.* 2017). Most SCADA vendors provide OPC servers with remote access options. These remote services do, however, come at an additional cost.

This work discusses an alternative, cost-effective IoT strategy, which provides flexible and secure remote access to the PLC. The new IoT architecture is implemented at a multistage moving bed biofilm reactor (MBBR) pilot plant to access the data from the online sensors remotely. Access to real-time data from the pilot enables remote deployment of an Extended Kalman Filter (EKF) to estimate additional water quality parameters in the plant.

### MATERIAL AND METHODS

#### Pilot plant schematic and monitoring station

Figure 1 presents the operational schematic and monitoring station of a multistage MBBR pilot plant for municipal wastewater treatment (Saltnes *et al.* 2017). The reactor has

doi: 10.2166/wst.2020.067

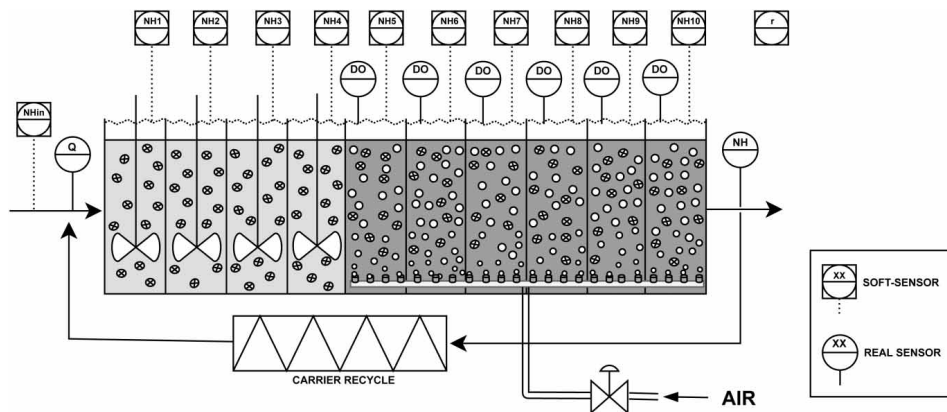


Figure 1 | Process flow diagram and sensor network in the pilot plant.

four anaerobic chambers, followed by six aerobic chambers. The plant is retrofitted with dissolved oxygen sensors from chamber 5 to 10 and an ammonia sensor in the effluent line. All online sensors are connected to a PLC provided by Beijer Electronics (<https://www.beijerelectronics.no/>). The current monitoring system is enhanced by deploying an array of soft sensors for monitoring additional water quality parameters. The aim of the soft-sensor array is to estimate the ammonia concentration in the influent raw wastewater as well as in each stage of the pilot plant. The soft sensor also provides estimates on additional parameters (such as the biomass activity of the nitrifiers) that cannot be measured directly using a physical sensor. Real-time data from soft sensors enable plant operators to adjust carrier recycle and aeration rate (manually or through control valves) to achieve optimal operation. The estimation of ammonia concentration in each aerobic chamber can enable the possibility of implementing ammonia-based aeration control (Rieger *et al.* 2013), which has proven to be a superior control strategy compared to a constant dissolved oxygen (DO) setpoint control (Vrečko *et al.* 2011).

### Mathematical model for the multistage MBBR

Several mathematical models explaining biological nitrification are available in the literature. They vary from comprehensive models (Henze *et al.* 1987) used in design and optimization to simplified reduced-order models (Julien *et al.* 1999; Madyastha *et al.* 2011) used for monitoring and control. In this work, the nitrification kinetics for the biofilm process mentioned in Stare *et al.* (2006) are adapted

for a multistage MBBR system. Equations (1)–(6) describe model equations in a discrete state-space form. Influent  $\text{NH}_4\text{-N}$  concentration ( $S_{\text{NH},\text{in}}$ ) and the nitrification rate ( $r$ ) are estimated by augmenting them as additional state variables in the model.

$$x_{k+1} = x_k + T_s f(x, u) \quad (1)$$

$$x = [S_{\text{NH},1} \ S_{\text{NH},2} \ S_{\text{NH},3} \ S_{\text{NH},4} \ S_{\text{NH},5} \ S_{\text{NH},6} \ S_{\text{NH},7} \ S_{\text{NH},8} \ S_{\text{NH},9} \ S_{\text{NH},10} \ S_{\text{NH},\text{in}} \ r] \quad (2)$$

$$u = [0 \ 0 \ 0 \ 0 \ S_{\text{O},5} \ S_{\text{O},6} \ S_{\text{O},7} \ S_{\text{O},8} \ S_{\text{O},9} \ S_{\text{O},10}] \quad (3)$$

$$y = S_{\text{NH},10} \quad (4)$$

$$f_i = \begin{cases} \tau^{-1}(S_{\text{NH},\text{in}} - S_{\text{NH},1}) - \rho_i, & i = 1 \\ \tau^{-1}(S_{\text{NH},i-1} - S_{\text{NH},i}) - \rho_i, & 1 \leq i \leq 10 \\ 0, & 11 \leq i \leq 12 \end{cases} \quad (5)$$

$$\rho_i = \begin{cases} 0, & i \leq 4 \\ r^* \frac{S_{\text{NH},i}}{K_{\text{NH}} + S_{\text{NH},i}} * \frac{1}{1 + e^{-K_1 S_{\text{O},i} + K_2}}, & i \geq 5 \end{cases} \quad (6)$$

$T_s$  is the sampling rate,  $k$  is the time subscript, and  $\tau$  is the residence time in each chamber. The term  $(S_{\text{NH},i})$  represents the ammonia concentration and  $(S_{\text{O},i})$  represents the dissolved oxygen concentration in the  $i^{\text{th}}$  chamber. The model-predicted value of the ammonia concentration in the effluent is denoted as  $y$ . The values of kinetic parameters  $K_1$ ,  $K_2$  and  $K_{\text{NH}}$  are taken from Stare *et al.* (2006).

### Soft-sensor algorithm

The EKF is a widely used soft sensor algorithm for non-linear systems. Several examples for successful implementation of model-based soft sensors in biological wastewater treatment process using EKF can be found in the literature (Sotomayor *et al.* 2002; Busch *et al.* 2013; Zeng *et al.* 2016). The basic equations in an EKF are presented in Equations (7)–(13).

$$F_k = I + T_s \left. \frac{\partial f}{\partial x} \right|_{x_k, u_k} \quad (7)$$

$$x_{k+1}^- = x_k + T_s f(x_k, u_k) \quad (8)$$

$$P_{k+1}^- = F_{k+1} P_k F_k^T + Q \quad (9)$$

$$H_k = \left. \frac{\partial h}{\partial x} \right|_{x_{k+1}^-, u_k} \quad (10)$$

$$K_k = P_{k+1}^- H_k^T (H_k P_{k+1}^- H_k^T + R)^{-1} \quad (11)$$

$$x_{k+1} = x_{k+1}^- + K_k (z_k - h(x_{k+1}^-)) \quad (12)$$

$$P_{k+1} = (I - K_k H_k) P_{k+1}^- \quad (13)$$

In the equations above,  $x_k$  is the state vector and  $z_k$  is the measurement vector at a time instance  $k$ . The process and measurement noise covariance matrices are represented as  $Q$  and  $R$  respectively.  $I$  is the identity matrix,  $x_{k+1}^-$  is the *a priori* estimate of the state,  $P_{k+1}^-$  the covariance of *a priori* estimation error and  $P_k$  the covariance matrix of the *a posteriori* estimation error. The sequential order of executing the EKF equations is presented as a flowchart in Figure 3(b).

Before implementing the soft-sensor in the pilot plant, the mathematical model (Equations (1)–(6)) and the EKF (Equations (7)–(13)) were implemented on a simulator platform to assess the system observability and identify the minimum number of online sensors required to estimate the ammonia concentration in each chamber. The simulator-based testing strategy implemented in Nair *et al.* (2019) was

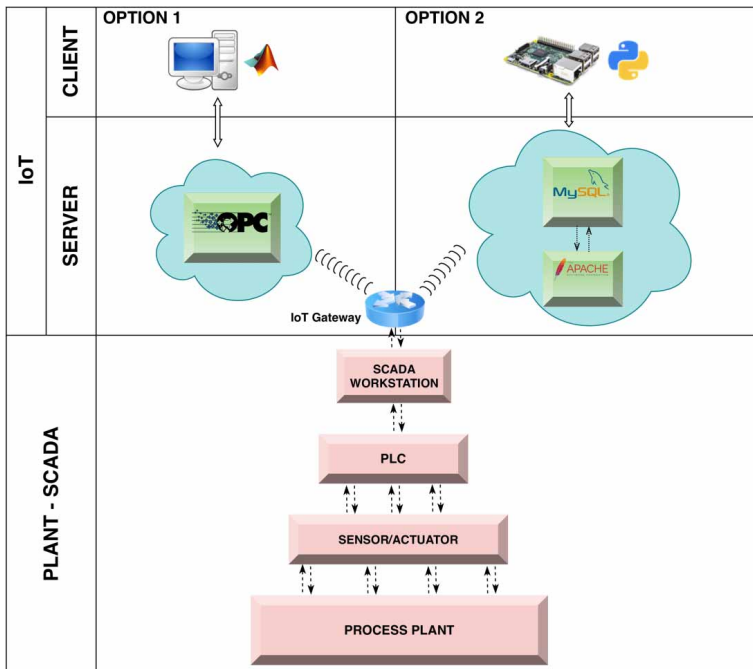


Figure 2 | IoT schematic option 1 (OPC) and option 2 (MySQL).

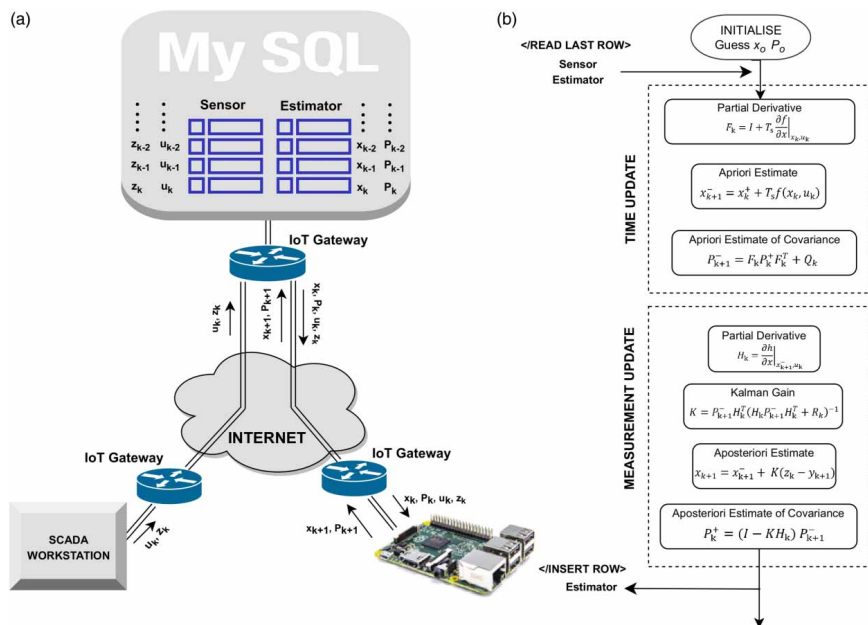


Figure 3 | (a) Data flow during remote deployment of EKF; (b) flowchart for EKF implementation.

used to assess the performance of EKF. The values of the tuning parameters of EKF;  $Q, R, P_0, x_0$  are obtained using the tuning methods described in [Haugen et al. \(2014\)](#).

### IoT schemes and soft sensor deployment

Figure 2 presents two possible schematics for remote deployment of the soft sensor code. Option 1 presents the default system provided by the SCADA vendor, which consists of an OPC server accessible through a secure VPN connection. The EKF is written as a script in Matlab and is executed remotely on a PC. The OPC Client toolbox in Matlab is used to receive real-time sensor data from the OPC servers. The second option includes an IoT gateway, which forms an interface between the PLC and a remote MySQL server, which is made accessible using Dynamic DNS (DDNS). The soft sensor algorithm is written as a Python script, which is then deployed on a single board computer – Raspberry Pi (<https://www.raspberrypi.org/>).

The network architecture for the remote deployment of the soft sensor is presented in Figure 3(a). The IoT gateway at the pilot plant collects data from online sensors and inserts them as a new row in a table created in the remote

MySQL server. The client running the EKF code (in the Raspberry Pi) begins the cycle by reading the last row of the table. This table consists of the estimated states  $x_k$ , the covariance matrix of estimation error  $P_k$ , measurements from online sensor  $z_k$  and  $u_k$ . The EKF algorithm then calculates new values of the estimated state  $x_{k+1}$  and covariance matrix of estimation error  $P_{k+1}$ . The updated values are inserted as a new row in the MySQL table. The Python script for implementing an EKF on a non-linear state-space model, the communication code that enables read and write of data from the remote SQL database, and the associated configuration files are provided in the Supplementary Material. The code has a modular structure and can be easily adapted to a new system by anyone with basic knowledge of programming in Python.

## RESULTS AND DISCUSSION

### Soft-sensor validation

The estimation results for a period of 1 month (28th January 2019–12th March 2019) are presented in the following

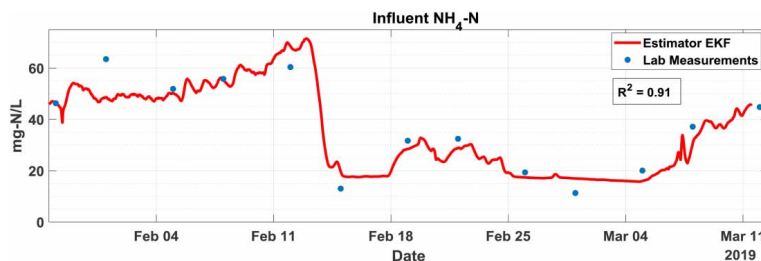


Figure 4 | Soft sensor results for a duration of 1 month. EKF vs. laboratory measurements.

figures. Figure 4 shows the comparison between the influent  $\text{NH}_4\text{-N}$  concentration estimated by soft sensor and the biweekly measurements obtained by standardized laboratory tests (Hach-Lange kits). The  $R^2$  values presented in the graph show that the values predicted by the estimator are close to the ammonia measurements from the laboratory. This demonstrates the effectiveness of soft sensors in providing real-time values of influent  $\text{NH}_4\text{-N}$  concentration.

The estimation results for  $\text{NH}_4\text{-N}$  concentrations at various stages in the pilot plant are presented in Figure 5. The time span for ammonia concentration in the individual chamber is shortened to one week for better visualisation of data.

Figure 6 presents the value of the nitrification rate  $r$  estimated by the soft sensor. A simplified nitrification model, such as the one used in this work, is derived from the comprehensive activated sludge model by considering certain assumptions. One such assumption involves excluding the kinetics of biomass growth and death and considering a

constant biomass concentration (Julien *et al.* 1999). However, a time-varying estimate of the nitrification rate in the pilot could be a result of variations in biomass activity. Therefore, the real-time estimation of the time-varying parameter  $r$  could provide significant insight on variations in the concentration of active nitrifiers in the pilot plant. A qualitative assessment of the trends (presented in Figure 6) indicates a positive correlation between the nitrification rate and the ammonia concentration of influent wastewater. The nitrification rate ( $r$ ) showed a steady decline on February 13th, a few hours after the influent ammonia concentration dropped. The pilot plant showed a lower nitrification rate from February 15th until March 6th, when the influent ammonia concentration was low. The nitrification rate started to increase after March 6th, when the influent ammonia concentration started to rise. This observation corresponds to the usual behavior of nitrifiers present in a biological wastewater treatment plant. However, a detailed analysis of the estimated results and cross-validation against

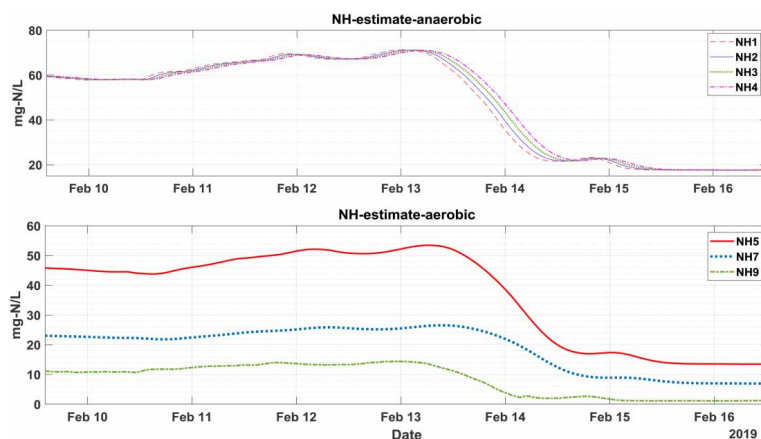


Figure 5 | Soft sensing results for  $\text{NH}_4\text{-N}$  concentration in anaerobic chamber (top) and aerobic chamber (bottom).

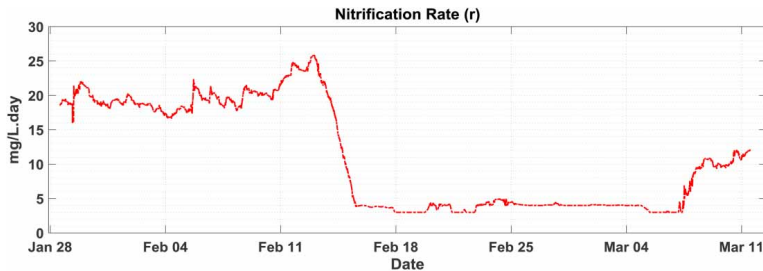


Figure 6 | Soft sensing results for nitrification rate.

laboratory measurements should be performed to substantiate the claim and fine-tune the estimator for soft sensing the concentration of autotrophs in the pilot plant.

### Cost comparison

A cost comparison between the default option provided by the SCADA vendor (Option 1) and two different versions (Option 2 and Option 3) of the new IoT system is presented in Table 1. Table 1 also presents the cost incurred while using a physical ammonia sensor (ion selective electrode) for measuring ammonia concentration in all six aerobic chambers. It can be inferred from the overall cost that using a soft-sensor can result in significant savings.

Among the options for soft-sensors, the default option provided by the SCADA provider has an average cost of about 1,580 € compared to the new system, which costs about 155 € (with SSL certificates). There is the possibility of running the setup without SSL, which would bring the cost down to 35 €, but this is not recommended due to security concerns (Buchanan et al. 2017). Recently there are providers

that supply free SSL certificates (Aertsen et al. 2017), but with a slightly lower security level than the commercial options due to limited support. This could be a valid option for security if the system is not critical and other operational security measures like limited access control levels and network monitoring are taken into consideration. For more critical water infrastructure, additional layers of security can be added to the communication network by providing a VPN or an intermediate API link. The open source VPN software OpenVPN is relatively easy to implement, but API links require significant design considerations and can become inflexible. The new system discussed in this work provides a cost-effective option where the only investment is in the hardware (Raspberry Pi) and the cost associated with the purchase of commercial services for establishing a secure data connection.

### CONCLUSIONS

This work illustrates a functioning example of a cost-effective and flexible alternative for non-intrusive remote

Table 1 | Cost comparison between option 1 (default) and options 2 and 3 (alternative IoT strategy) option 4 (physical sensor)

	Option 1		Option 2		Option 3		Option 4	
	Service	Cost (€)	Service	Cost (€)	Service	Cost (€)	Service	Cost (€)
Server	OPC (Codesys)	160	MySQL	-	MySQL	-	-	-
Remote access	VPN (Insys)	560	DDNS	-	DDNS	-	-	-
Security/encryption	Inbuilt	-	SSL key	120	-	-	-	-
Client hardware	PC	200-1,000	Raspberry Pi	35	Raspberry Pi	35	-	-
Client software	Matlab	220	Python	-	Python	-	-	-
Client software	Matlab	220	Python	-	Python	-	-	-
NH <sub>4</sub> -N sensor (ISE)	1 unit	1,500	1 Unit	1,500	1 Unit	1,500	6 Units	1,500
IoT cost		980-1,940		155		35		0
Overall cost		2,480-3,440		1,655		1,535		9,000



monitoring in a wastewater treatment plant. The soft-sensor array deployed in the pilot plant proves the ability to bolster the monitoring system in a treatment process. The ability to monitor additional wastewater treatment parameters that are otherwise difficult to monitor via conventional online sensors would enable the implementation of multi-parameter based optimal control strategies. The case study presented in this work also illustrates the possibility of integrating scripts written in commonly used scientific programming languages such as Matlab or Python into any commercial SCADA. The cost comparison between the new IoT system and the options available in the market today shows that remote deployment of soft sensors can be achieved at much lower costs. This novel cost-effective option also opens up new possibilities to develop more comprehensive soft-sensing algorithms for estimating water quality parameters, which are otherwise difficult to monitor by a physical sensor.

## ACKNOWLEDGEMENTS

We acknowledge the financial support provided by Norwegian Research Council (RECOVER project) and the technical support from the research team at Norwegian University of Science and Technology (NTNU).

## SUPPLEMENTARY MATERIAL

The Supplementary Material for this paper is available online at <https://dx.doi.org/10.2166/wst.2020.067>.

## REFERENCES

- Aertsen, M., Korczynski, K., Moura, C. M. G., Tajalizadehkhoo, S. & Berg, J. 2017 No domain left behind: is Let's Encrypt democratizing encryption? *ANRW* **17**, 48–54.
- Buchanan, W. J., Helme, S. & Woodward, A. 2017 Analysis of the adoption of security headers in HTTP. *IET Information Security* **12** (2), 118–126.
- Busch, J., Elixmann, D., Kühl, P., Gerkens, C., Schlöder, J. P., Bock, H. G. & Marquardt, W. 2013 State estimation for large-scale wastewater treatment plants. *Water Research* **47** (15), 4774–4787.
- González, I., Calderón, A., Barragán, A. & Andújar, J. 2017 Integration of sensors, controllers and instruments using a novel OPC architecture. *Sensors* **17** (7), 1512.
- Haimi, H., Corona, F., Mulas, M., Sundell, L., Heinonen, M. & Vahala, R. 2015 Shall we use hardware sensor measurements or soft-sensor estimates? Case study in a full-scale WWTP. *Environmental Modelling and Software* **72**, 215–229.
- Haugen, F., Bakke, R. & Bernt, L. 2014 State estimation and model-based control of a pilot anaerobic digestion reactor. *Journal of Control Science and Engineering* **2014** (3), 1977–1996.
- Henze, M., Grady, C. P. L., Gujer, W., Marais, G. v. R. & Matsuo, T. 1987 *Activated Sludge Model No.1*. IAWPRC Scientific and Technical Reports No. 1. IWA Publications, London.
- Julien, S., Lessard, P. & Barbary, J. P. 1999 A reduced order model for control of a single reactor activated sludge process. *Mathematical and Computer Modelling of Dynamical Systems* **5** (4), 337–350.
- Madyastha, V. K., Prasad, V. & Mahendrakar, V. 2011 Reduced order model monitoring and control of a membrane bioreactor system via delayed measurements. *Water Science & Technology* **64** (8), 1675–1684.
- Nair, A. M., Fanta, A., Haugen, F. A. & Ratnaweera, H. 2019 Implementing an Extended Kalman Filter for estimating nutrient composition in a sequential batch MBBR pilot plant. *Water Science and Technology* **80** (2), 317–328.
- Olsson, G., Carlsson, B., Comas, J., Copp, J., Gernaey, K. V., Ingildsen, P., Jeppsson, U., Kim, C., Rieger, L., Rodriguez-Roda, I., Steyer, J. P., Takács, I., Vanrolleghem, P. A., Vargas, A., Yuan, Z. & Åmand, L. 2014 Instrumentation, control and automation in wastewater – from London 1973 to Narbonne 2013. *Water Science and Technology* **69** (7), 1373–1385.
- Rieger, L., Jones, R. M., Dold, P. L. & Bott, C. B. 2013 Ammonia-based feedforward and feedback aeration control in activated sludge processes. *Water Environment Research* **86** (1), 63–73.
- Saltnes, T., Sørensen, G. & Eikås, S. 2017 Biological nutrient removal in a continuous biofilm process. *Water Practice and Technology* **12** (4), 797–805.
- Sotomayor, O. A., Park, S. W. & Garcia, C. 2002 Software sensor for on-line estimation of the microbial activity in activated sludge systems. *ISA Transactions* **41** (2), 127–143.
- Stare, A., Hvala, N. & Vrečko, D. 2006 Modeling, identification, and validation of models for predictive ammonia control in a wastewater treatment plant—a case study. *ISA Transactions* **45** (2), 159–174.
- Vrečko, D., Hvala, N. & Stražar, M. 2011 The application of model predictive control of ammonia nitrogen in an activated sludge process. *Water Science and Technology* **64** (5), 1115–1121.
- Wang, X., Kvaal, K. & Ratnaweera, H. 2019 Explicit and interpretable nonlinear soft sensor models for influent surveillance at a full-scale wastewater treatment plant. *Journal of Process Control* **77**, 1–6.
- Zeng, J., Liu, J., Zou, T. & Yuan, D. 2016 Distributed extended Kalman filtering for wastewater treatment processes. *Industrial & Engineering Chemistry Research* **55** (28), 7720–7729.

First received 31 October 2019; accepted in revised form 6 February 2020. Available online 18 February 2020



# Paper D





# An Adaptive Model Predictive Control Strategy for Ammonia Based Aeration Control in a Water Resource Recovery Facility - A Simulation Study

Abhilash M Nair<sup>1</sup>, Finn Aakre Haugen<sup>2</sup>, Harsha Ratnaweera<sup>1</sup>

<sup>1</sup> Faculty of Science and Technology, Norwegian University of Life Sciences, P.O. Box 5003, 1432 Aas, Norway

<sup>2</sup> University of South-Eastern Norway, Kjølnes ring 56, Porsgrunn, Norway.

## Abstract

Nutrient-based aeration control has gained popularity in recent times because of its ability to reduce operational costs while maintaining the stringent effluent discharge norms. Simulation studies, as well as pilot-scale testing of various aeration control strategies, has demonstrated that model predictive control (MPC) has superior performance compared to the conventional PI control. However, a lack of reliable models restricts its implementation in real plants. Discussions continue whether to use a better predicting nonlinear model (NLMPC) or a computationally simpler linear model (LMPC) for MPC. This paper explores the use of an Adaptive MPC (AMPC), which is constructed by combining a linear MPC with a recursive parameter. A comparison between the different MPC strategies and the classic proportional-integral (PI) algorithm is provided by evaluating their performances on the standardized Benchmark Simulation Model No. 2. The results obtained from the simulator-based testing indicate a significant performance improvement in AMPC compared to an LMPC. The AMPC is less computationally demanding, thus being a faster alternative to NLMPC.

**Keywords:** *Adaptive MPC, Aeration control, Recursive model estimator, WRRF.*

## Introduction

The rephrasing of wastewater treatment plants (WWTP) as Water Resource Recovery Facilities (WRRF) is changing the way treatment plants are being operated. The primary aim of process operations is to move towards a sustainable framework focused on achieving energy-positive operation and resource recovery (Regmi *et al.* 2018). Given the current limitations in technology along with the stringent effluent discharge standards, this transformation appears to be a challenging endeavor. Implementing advanced control strategies to ensure optimal performance of various energy-intensive operations in the process could present a possible solution to achieve this transformation.

One of the most energy-consuming operations in biological wastewater treatment is the aeration of the aerobic chambers (Rosen *et al.* 2002). A high rate of aeration is often avoided since it would decrease efficiency and oxygen transfer rate. On the other hand, lower aeration rates would result in lower treatment efficiency and poor effluent quality. The availability of online nutrient sensors (NH<sub>4</sub>-N, NO<sub>3</sub>-N, and COD) has enabled the possibility of implementing aeration control strategies based on real-time information from these sensors. Various control schemes can be found in the literature for optimal aeration in WRRFs. They span from conventional feedback and feedforward PI control to advanced multivariate control (Steffens

& Lant 1999). Designing a nutrient-based aeration control strategy for a WRRF is a challenging task due to system nonlinearities, multiple time scales of processes, and a strong interaction between operational parameters. The conventional ammonia-based aeration control (ABAC) using a well-tuned proportional-integral (PI) algorithm has demonstrated considerable improvement when compared to constant dissolved oxygen (DO) setpoint strategy (Várhelyi *et al.* 2019). However, the PI algorithm attempts to maintain a constant ammonia setpoint without considering the aeration costs. Control strategies based on real-time optimization can further improve the aeration control by considering multiple operational parameters in their objective function. Model-based controllers such as model predictive control (MPC) which utilizes a mathematical model of the process can serve as a potential strategy for improving aeration control.

Although the concept of MPC does not restrict itself to a specific model form, the prediction model used in the MPC can strongly affect the controller performance and computation requirements (Qin & Badgwell, 2003). The superior performance of model-based predictive control of ammonia, nitrate, or oxygen using nonlinear models is demonstrated in (Vrečko *et al.* 2011). The use of linear predictive models in MPC for the control of aeration in WRRF is reported in (Steffens & Lant 1999; Sotomayor & Garcia 2002; Holenda *et al.* 2008). Linear MPC (LMPC) is less computationally intensive since the linear formulation of the optimization problems provides an explicit solution to obtain the optimal control moves. However, the lack of predictive power of the linear models often hampers the controller performances, especially when they are implemented in a highly nonlinear system such as ammonia nitrification in the activated sludge process. Nonlinear MPC (NLMPC) provides better performance compared to the linear MPC at the cost of higher computational requirements. The adaptive MPC is a version of LMPC where the controller employs a systematic procedure to update the parameters of the linear prediction model using a recursive model estimator algorithm. The real-time parameter update enables the MPC's prediction model to adjust the model parameters in case of changes in operational conditions in WRRF. Improving the performance of MPC by adopting a self-adaptive strategy has been previously demonstrated in several systems (Koo *et al.* 2019; Kothare *et al.* 1997).

This paper presents the idea of using an adaptive linear MPC (AMPC) for optimal aeration control strategy based on the ammonia concentration. The control strategies are implemented on the standard Benchmark Simulation Model 2d (Nopens *et al.* 2010; Solon *et al.* 2017). A comparison between adaptive MPC, linear MPC (LMPC), nonlinear MPC (using a reduced order nitrification model), and a conventional PI cascade control is performed based on standardized evaluation criteria simulator manual (Jeppsson *et al.*, 2007).

## **Materials and Methods**

### **Benchmark Simulation Model No 2**

The Benchmark Simulation Model No. 2 (BSM2) is a standard simulator platform used to test and evaluate various operational sequences and control strategies in a WRRF. The plant layout, process model, influent data, test procedures, and evaluation criteria for simulator-based testing are mentioned in literature (Jeppsson *et al.*, 2007; Nopens *et al.* 2010; Jeppsson *et al.*, 2013).

### Plant layout and process model

The treatment line in BSM2 simulator consists of a primary clarifier, biological treatment stage (AAO configuration with two anaerobic, two anoxic, and three aerated compartments), and a secondary clarifier to separate sludge from mixed liquor. The biological process is described using IWA Activated Sludge Model No. 2d (Henze *et al.* 2006). The secondary settler is modeled as a 10-layer process using a hindered settling velocity model proposed by (Takács *et al.* 1991). The simulator also consists of a sludge treatment line, where the primary and secondary sludge are mixed and thickened in a sludge thickener. The thickened sludge is fed to an anaerobic digester for biogas production. After anaerobic digestion, the sludge is dewatered and the digestate is stored temporarily in a tank before recycling it back to the treatment train. The plant layout and the control structure are presented in Figure 3. The internal recycle  $Q_{IR}$ , return activated sludge rate  $Q_R$ , and sludge wastage rate  $Q_W$  are maintained at a constant value as indicated in Figure 1. The default values of the operational parameters return activated sludge rate and waste activated sludge rate were the same as in the default steady-state value provided in (Solon *et al.* 2017).

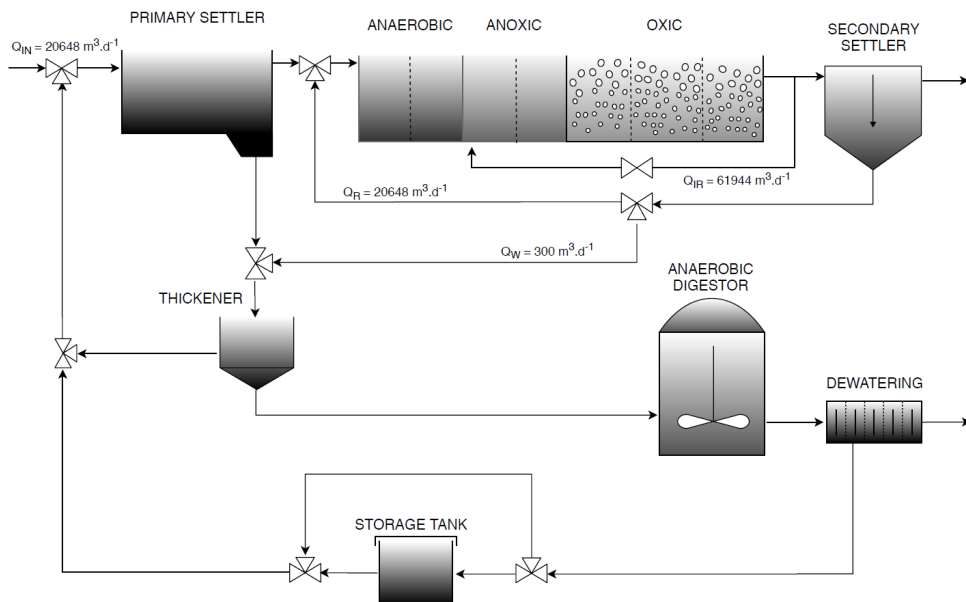


**Figure 1.** Plant Layout of the BSM2d Simulator

### Influent Data

The standards and the phenomenological principles for generating steady-state as well as dynamic influent files are provided in literature (Gernaey *et al.* 2011). The steady-state conditions for the influent concentrations are described based on an average influent pollution load of 8386 kg COD.d<sup>-1</sup> for carbon, 1014 kg N.d<sup>-1</sup> for total nitrogen, and 197 kg P.d<sup>-1</sup> for total phosphorus respectively (Solon *et al.* 2017). The dynamic influent file, generated based on the methods and reasons described in (Martin and Vanrolleghem 2014; Snip *et al.* 2016), presents variations in influent flowrate and compositions for a period of 609 days with changes at an interval of 15 minutes.

### Evaluation Criteria

Several evaluation criteria are defined in the benchmark to assess the performance of a control strategy. In this work, the aeration costs (AE), Average effluent ammonia concentration ( $Avg S_{NH,e}$ ), percentage time of effluent violation for ammonia ( $\%TS_{NH}$ ), Integral Absolute Error (IAE) between the ammonia concentration in the aerobic chamber and the ammonia setpoint were calculated. The other performance evaluation criteria mentioned in the manual are ignored since the primary goal of this work is limited to examine the impact of various MPC strategies on ammonia nitrification.

Average aeration energy (AE) is calculated from day 245 to day 609 for the dynamic effluent file using Eq. 1.

$$AE = \frac{S_o^{sat}}{T * 1.8 * 1000} \int_{T=245 d}^{T=609 d} \sum_{i=5}^{i=7} V_i * K_{La,i}(t) dt \quad (1)$$

The average effluent ammonia ( $Avg S_{NH,e}$ ) is the average per day amount of ammonia discharged during the evaluation period. It is calculated by Eq. 2.

$$Avg S_{NH,e} = \frac{1}{T * 1000} \int_{245 d}^{609 d} S_{NH,e}(t) dt \quad (2)$$

The Effluent Quality Index (EQI) is a measure of the total pollution discharge into receiving waters. The EQI was calculated using the cost function equations mentioned in (Vanrolleghem *et al.* 1996; Gernaey *et al.* 2004).

$$EQI = \frac{1}{T * 1000} \int_{245 d}^{609 d} \beta_{SS} TSS_e(t) + \beta_{COD} COD_e(t) + \beta_{TKN} TKN_e(t) + \beta_{NO} NO_e(t) \quad (3)$$

The parameters  $\beta_{TSS} = 2$ ,  $\beta_{COD} = 1$ ,  $\beta_{TKN} = 30$  and  $\beta_{NO} = 10$  are as in (Nopens *et al.* 2010) and the calculation for effluent concentrations of TSS, COD, and TKN are explained in Eqs. (4) – (6).

$$TSS = 0.75 (X_S + X_I + X_{B,H} + X_{B,A} + X_P) \quad (4)$$

$$COD = S_S + S_I + X_S + X_I + X_{B,H} + X_{B,A} + X_P \quad (5)$$

$$TKN = S_{NH,e} + S_{ND} + X_{ND} + i_{XP}(X_I + X_P) + i_{XB}(X_{B,H} + X_{B,A}) \quad (6)$$

The percentage time for effluent violations ( $\%TS_{NH}$ ) is defined as the percentage of total evaluation period where the effluent ammonia was above the limit  $C_{NH,e,lim} = 4 \text{ mgN/L}$ .

The computation time is obtained by recording the time consumed (in hours) during a simulation run for the dynamic influent file.

### Aeration Control in Biological WRRF

The BSM2 simulator, which is a representative of a full-scale WRRF, consists of three aerobic chambers (5, 6, and 7) in series. The performance evaluation of several aeration control strategies on the standard BSM 2d simulator is available in literature (Vrecko *et al.* 2006; Jeppsson *et al.* 2007; Revollar *et al.* 2020). In this work, the strategies presented in (Nopens *et*



al. 2010) are chosen as the base control strategy against which the MPC controllers explained in the subsequent sections shall be compared. The baseline control strategies which include constant DO setpoint control, classical PI ammonia-based aeration control followed by the advanced MPC control are presented in Figure 2.

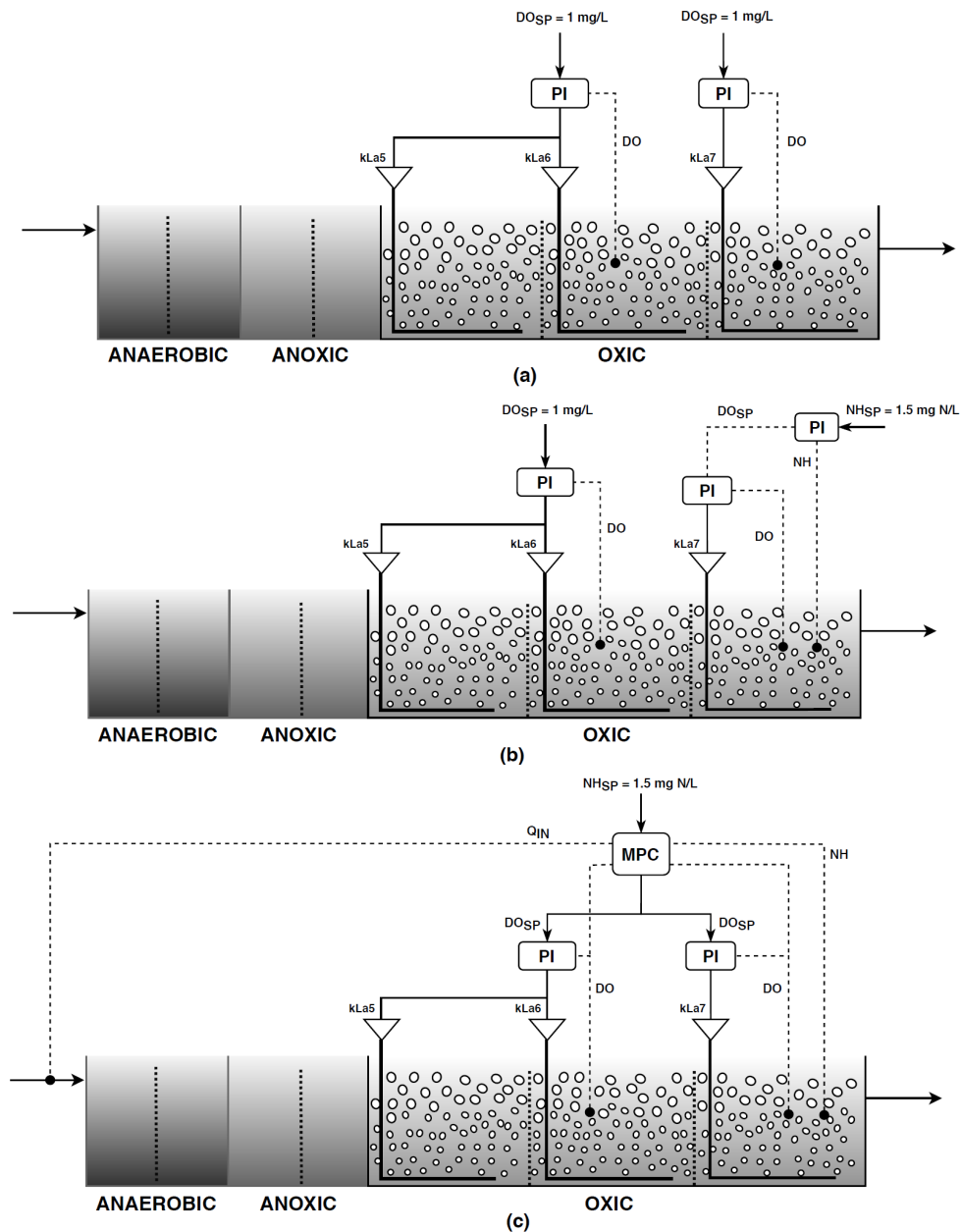


**Figure 2.** (a) Aeration control with a constant DO setpoint. (b) Ammonia-based aeration control with cascade PI control setpoint. (c) Aeration Control using MPC.

The base open-loop scenario (A0) implements constant aeration ( $kLa5 = kLa6 = 120$  and  $kLa7 = 60$ ) in all three aerobic chambers of the biological treatment unit. The control strategy A1 (Figure 2a) consists of two PI DO controllers maintaining DO setpoint of 1 mg/L in chamber 4 (by manipulating  $kLa5$  and  $kLa6$ ) and chamber 7 (by manipulating  $kLa7$ ). The control strategy A2 (Figure 2b) is a combination of a DO and an ammonia (NH) controller. The DO controller in chamber 6 is identical to the controller explained in A2. In addition to the DO controller, a PI NH controller is provided to maintain a constant ammonia concentration of 1.5 mg N/L in chamber 7. The NH controller works in the outer loop as a master control providing the setpoint values to a PI DO controller working in the inner loop to maintain the DO setpoint in chamber 7 by manipulating  $kLa7$ . The final scenario A3 (Figure 2c) consists of a cascade ammonia MPC in the outer loop which provides DO setpoints to two slave PI DO controllers in the inner loop. The PI DO controller in the inner loop maintains the DO setpoint by manipulating the  $kLa5$  and  $kLa6$  for chamber 6 and  $kLa7$  for chamber 7. The MPC decides on the optimal values of DO setpoints by utilizing the real-time data from DO sensors in chambers 6 and 7, ammonia sensor in the chamber 7, and the flowmeter in the influent of the biological units.

### Model Predictive Control

The Model Predictive Control (MPC) is a commonly used optimal control strategy that decides the control actions based on the real-time optimization of a user-defined cost function. In an MPC, the outputs  $y_{k+i}$  are predicted for the finite prediction-interval  $N_p$  using a mathematical model. The controller then calculates the present and future control moves ( $u_k, u_{k+1}, \dots, u_{k+N_c-1}$ ) for a control horizon  $N_c$  to minimize a quadratic objective function  $J$ . The standard form of the objective function used in an MPC is presented in Eq. 7. The terms  $k$  and  $i$  are the time indices along the prediction horizon,  $r_{k+i}$  is the reference value (setpoint).  $w_{SP}$ ,  $w_u$ , and  $w_{\Delta u}$  are the weights for the control error, manipulated variables, and change in manipulated variables respectively.

$$J = \sum_{i=0}^{N_p-1} \|r_{k+i} - y_{k+i}\|_{w_{SP}}^2 + \sum_{i=0}^{N_c} \|u_{k+i-1}\|_{w_u}^2 + \sum_{i=0}^{N_c} \|\Delta u_{k+i-1}\|_{w_{\Delta u}}^2 \quad (7)$$

The standard objective function is modified by including a penalty function which exponentially increases when the ammonia concentration in chamber 7 approaches the upper limit ( $ul$ ) of ammonia in the effluent. The modified objective function is provided in Eq. 8. The upper limit in this case is chosen as the effluent discharge limit  $C_{NH_e,lim} = 4 \text{ mg/L}$ .

$$J = \sum_{i=0}^{N_p-1} \|r_{k+i} - y_{k+i}\|_{w_{SP}}^2 + \sum_{i=0}^{N_p-1} \left\| \frac{1}{\|ul - y_{k+i}\|} \right\|_{w_L}^2 + \sum_{i=0}^{N_c} \|u_{k+i-1}\|_{w_u}^2 + \sum_{i=0}^{N_c} \|\Delta u_{k+i-1}\|_{w_{\Delta u}}^2 \quad (8)$$

Eqs. (9) - (10) present the mathematical model used by the MPC to predict the behavior of the process over the prediction horizon. The prediction model explains the influence of measured disturbance  $d_k$  and manipulates variable  $u_k$  on the system output  $y_k$  using the nonlinear state-space function  $f$  and the measurement function  $h$ . In ammonia-based aeration control, the DO setpoints in chambers 6 and 7 are the manipulated variables ( $u_k$ ), the influent flow-rate to the WWRF is the measured disturbance ( $d_k$ ) and the ammonia concentration in chamber 7 is the control variable ( $y_k$ ).

$$x_{k+i} = f(x_k, u_k, d_k) \quad (9)$$

$$y_k = h(x_k, u_k) \quad (10)$$

Various model types can be used to predict the future values of ammonia concentration based on the concentration of dissolved oxygen in chambers 6 and 7. A list of potential ammonia models used in MPC are evaluated in (Stare *et al.* 2006). The ammonia nitrification models can either be a data-driven input-output model or a conceptual model obtained by extracting the nitrification kinetics from the activated sludge model. The prediction models evaluated in this work are described in the subsequent sections.

### Linear Prediction Model

The state-space representation of a linear prediction model is presented in Eqs. (11) – (12).

$$x_{k+1} = Ax_k + B \begin{bmatrix} u_k \\ d_k \end{bmatrix} \quad (11)$$

$$y_k = Cx_k + D \begin{bmatrix} u_k \\ d_k \end{bmatrix} \quad (12)$$

The linear model described in this section is an input-output (black box) model, where the  $x_{k+1}$  are canonical state variables. The values of A, B, C, and D matrices are obtained by performing offline system identification on the data obtained from the real process plant. In our study, the data required for system identification are obtained from BSM2 simulator operated with the dynamic influent file. The n4sid function, provided as a part of MATLABs System Identification Toolbox was used to regress the data and obtain the linear model parameters A, B, C, and D.

### Nonlinear Prediction Model

The nonlinear model used in an ammonia MPC is derived by extracting the rate equations of the ammonia nitrification process from the ASM 2d (Henze *et al.* 2006). Eqs. (13) – (14) describe the nonlinear model in a discrete state-space form, derived from the mass balance of ammonia in the aerobic chambers.

$$S_{NH6,k+1} = S_{NH6,k} + T_s \left( \frac{Q}{V} (S_{NH5,k} - S_{NH6,k}) - \mu \frac{S_{O6,k}}{S_{O6,k} + K_O} \frac{S_{NH6,k}}{S_{NH6,k} + K_{NH}} \right) \quad (13)$$

$$S_{NH7,k+1} = S_{NH7,k} + T_s \left( \frac{Q}{V} (S_{NH6,k} - S_{NH7,k}) - \mu \frac{S_{O7,k}}{S_{O7,k} + K_O} \frac{S_{NH7,k}}{S_{NH7,k} + K_{NH}} \right) \quad (14)$$

The  $S_{NH_i,k}$  ( $i \in 5, 6, 7$ ) is the ammonia concentration in the aerobic chamber  $i$  at time instance  $k$ ,  $Q$  ( $Q = Q_{IN} + Q_R + Q_{IR}$ ) is the volumetric flow-rate entering the aerobic unit,  $V$  is the volume of the aerobic reactor,  $\mu$  is the nitrification rate constant,  $K_O$  and  $K_{NH}$  are the Monod's half-saturation coefficients, and  $T_s$  is the time-step. The design parameter  $V$ , the operational parameters  $Q_R$ ,  $Q_{IR}$ , and the steady-state value of influent raw water flowrate  $Q_{IN0}$  obtained from the simulator description (Solon *et al.* 2017) are presented in Table 1.

**Table 1.** Parameters of nonlinear nitrification model.

Parameter	$Q_R$	$Q_{IR}$	$Q_{IN0}$	$T_s$	$V$
Value	20648	61,944	20645	15	3000
Unit	m <sup>3</sup> /day	m <sup>3</sup> /day	m <sup>3</sup> /day	min	m <sup>3</sup>

The values of the parameters  $K_O$ , and  $K_{NH}$  are obtained by executing a steady-state batch calibration method (Nair *et al.* 2018) on the data obtained from the default open-loop simulation with the dynamic influent data. The reaction rate parameter  $\mu$  has been reported to vary with time (Vrečko *et al.* 2006), and there is no sensor for online measurement of  $\mu$ . Therefore, the nitrification rate parameter  $\mu$  is modeled as a random walk and included as a state variable. The state variables, including the augmented states ( $x = [S_{NH,5} \ S_{NH,6} \ S_{NH,7} \ \mu]$ ) are estimated using an Extended Kalman Filter.

### Adaptive MPC

Adaptive linear MPC uses a linear plant model form (Eqs. (11) – (12)) as a prediction model. However, unlike the linear MPC, the adaptive MPC uses time-varying values of A, B, C, and D matrices. Figure 3 shows the control structure of an adaptive MPC. These time-varying parameters of the linear model are obtained by running a system identification in parallel to the controller, which updates the model at every time step. The online system identifier estimates the model parameters based on the process inputs  $u_k$ ,  $d_k$  and outputs  $y_k$ , and applies them to the controller in real-time. For every change in operating condition, an approximate linear model is updated with new parameters. The real-time model update helps the MPC adjust their prediction model at run-time to compensate for nonlinear or time-varying characteristics of the system. This method works best for processes where no reliable model exists or to a system with time-varying model parameters.

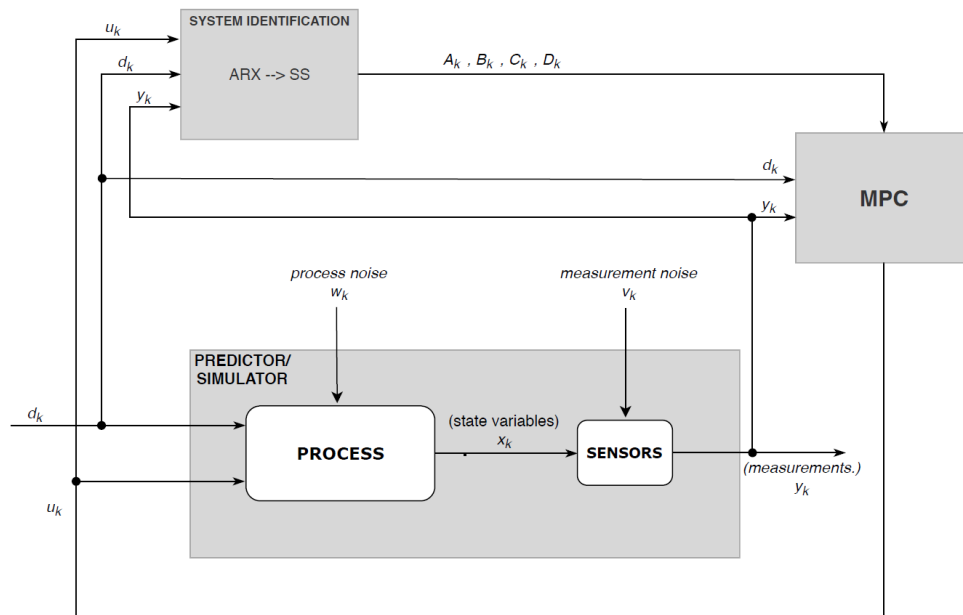


**Figure 3.** Adaptive MPC

The structure of the auto-regressive (ARX) model that was used to fit the input and output measurements is presented in Eq. 15, where  $q$  is the time-shift operator,  $n_k$  is the input delay,  $na$  and  $nb$  represent the order of the polynomial vector  $\xi(q)$  and  $\phi(q)$  respectively.

$$\xi(q)y(t) = \phi(q)u(t - n_k) + e(t) \quad (15)$$

where,

$$\xi(q) = 1 + a_1q^{-1} + a_2q^{-2} + \dots + a_{na}q^{-na} \quad (16)$$

$$\phi(q) = b_1 + b_2q^{-1} + b_3q^{-2} + \dots + b_{nb}q^{-(nb-1)} \quad (17)$$

The recursive estimation algorithm using a Kalman filter interpretation (Zhang 2000) is used to estimate the model parameters. This is accomplished by expressing the ARX model as Eqs. (18) - (21), where  $w_k$  and  $v_k$  are white noise with co-variances  $R_1$  and  $R_2$ .

$$\theta_k = \theta_{k-1} + w_k \quad (18)$$

$$y_k = \Psi_k^T \theta_{k-1} + v_k \quad (19)$$

where

$$\theta = [a_1 \ a_2 \ \dots \ a_{na} \ b_1 \ b_2 \ \dots \ b_{nb}] \quad (20)$$

$$\Psi_k^T = [-y_{k-1} \ -y_{k-2} \ \dots \ -y_{k-na} \ u_{k-n_k} \ u_{k-n_k-1} \ \dots \ u_{k-n_k-nb+1}] \quad (21)$$

The Kalman filter adaptation method is described in Eqs. (22) - (24), where  $\hat{\theta}_k$  is the estimated parameter and  $P_k$  is the auto-covariance matrix.

$$\hat{\theta}_k = \hat{\theta}_{k-1} + K_k(y_k - \Psi_k^T \hat{\theta}_{k-1}) \quad (22)$$

$$K_k = P_k \Psi_k = \frac{P_{k-1} \Psi_k}{R_2 + \Psi_k^T P_{k-1} \Psi_k} \quad (23)$$

$$P_k = P_{k-1} + R_1 - \frac{P_{k-1} \Psi_k \Psi_k^T P_{k-1}}{R_2 + \Psi_k^T P_{k-1} \Psi_k} \quad (24)$$

The parameter estimated by the recursive estimator is converted to a standard state-space form using the procedure mentioned in (Ljung 1987). The linear state-space model, thus identified, is used as the prediction model for a linear MPC. The `n4sid` function, used to identify the linear state-space model parameters (Eqs. (11) – (12)) also provides the possibility of deciding the optimal model order by comparing the Hankel singular values for each state in the linear model (Boyd *et al.* 1994). The Hankel singular values obtained by fitting the data obtained from BSM2 simulator to a linear state-space model shows a significant drop when model order is increased beyond 2, which suggests that using a linear model with two canonical state-variables is sufficient to preserve most of the system characteristics and obtain an accurate prediction model. Therefore, the values of  $na = 2$ ,  $nb = 2$ , and  $nk = 0$  are chosen for the ARX model to obtain the same model order as mentioned in Eqs. (11) - (12).

### *Implementation in a Simulink Platform*

The plant layout (BSM2) and the aeration control strategy are implemented in MATLAB/Simulink version R2019b. The implementation of BSM2 in Simulink (Solon *et al.* 2017) was used as the basis to develop, test, and evaluate the control strategies. The Model Predictive Control Toolbox in Simulink provides all three versions of the MPC (LMPC, NLMPC, and AMPC) controllers. The MPC blocks were used to design and configure the control strategies explained in the previous section. Three files, with three different MPC controllers, were created and simulated separately. The system identification toolbox in Simulink provides various algorithms for recursive parameter estimation. For this study, the

recursive polynomial model estimator block is used in combination with the ARX to SS model converter block to provide real-time estimates of the linear state-space model parameter for the adaptive MPC. The Extended Kalman filter block provided as a part of MATLABs System Identification Toolbox is used to provide the estimation of states for the nonlinear MPC.

The standard procedure executing the simulator is provided in the BSM2d simulator manual (Jeppsson *et al.* 2007). The following steps were applied for simulation and subsequent evaluation of the control strategies.

1. Initialize the BSM2d simulator with the default values provided in the simulator.
2. Simulate 300 days forward using the constant influent data.
3. Initialize the Simulink model with the final values of the steady-state simulation. This allows the next simulation (with dynamic influent data) to begin at the exact position as where the steady-state files had ended.
4. Simulate the model with the dynamic influent file for a period of 609 days.
5. The data from the dynamic simulation is stored in the MATLAB workspace.
6. Utilize the data recorded from T=245 to T=609 to assess the performance parameters mentioned in Eqs. (1) - (6).

## Results and Discussion

### MPC settings

The choice of prediction and control horizon, limits of manipulated variables, and weights in the MPC cost function determine the performance of an MPC. Systematic procedures are explained to determine the optimal values of these tuning parameters (Lee & Yu 1994). In our case, the parameters were tuned based on experience gained from running the BSM2 simulator with the dynamic influent data. These parameters were tuned manually to obtain an acceptable performance of the MPC. The MPC parameters used in the simulations are presented in Table 2.

**Table 2.** MPC Settings

Parameter	Description	Value	Unit
$T_S$	Time step	15	min
$N_P$	Prediction Horizon	5	
$N_C$	Control Horizon	3	
$u_{\min}$	Minimum value of Manipulated Variable DO	0.1	mg L <sup>-1</sup>
$u_{\max}$	Maximum value of Manipulated Variable DO	8	mg L <sup>-1</sup>
$w_{SP}$	Weights for control error	1	
$w_u$	Weights for manipulated variable	0.65	
$w_{\Delta u}$	Weights for change in manipulated variables	0.01	
$w_L$	Weights for upper limit	0.41	

The values of prediction and control horizon were gradually increased from a lower value  $N_P = 3$  and  $N_C = 2$ , and the controller performance was evaluated at every step. The controller performance showed no significant improvement above  $N_P = 5$  and  $N_C = 3$ . The weight on the setpoint error and the weight on the manipulated variable change can be used to choose between reducing the aeration costs or obtaining a better effluent quality. The MPC tuning parameters are maintained at the same value for all three types of MPC controllers.

## Results from System Identification

The data received from executing the BSM2 simulator with the dynamic influent data is used to develop the linear and the nonlinear ammonia nitrification models. The data is split to training data 80% ( $T = 0$  to  $T = 488$ ) and 20% validation data ( $T = 489$  to  $T = 609$ ). The training data is used to calibrate the model and obtain the  $A$ ,  $B$ ,  $C$ , and  $D$  matrices in Eqs. (11) – (12) as well as the parameters  $K_O$  and  $K_{NH}$  in Eqs. (13) – (14). The linear state-space matrices obtained from the subspace identification method presented in Eqs. (25) – (26) and the nonlinear kinetic parameters obtained from the model calibration is presented in Eq. 27.

$$A = \begin{bmatrix} 0.96 & 0.04 \\ 0.04 & 0.97 \end{bmatrix}; B = \begin{bmatrix} -0.0118 & 0.0078 & 0.0014 \\ -0.0036 & 0.0041 & 0.054 \end{bmatrix} \quad (25)$$

$$C = [8.5 \quad -1.9]; D = [0 \quad 0] \quad (26)$$

$$K_{NH} = 1.51 \text{ mgN L}^{-1}; K_O = 0.84 \text{ mgCOD L}^{-1} \quad (27)$$

The validation plot, showing a comparison between the validation dataset and the value of ammonia in chamber 7 predicted by both the linear and nonlinear ammonia nitrification models is presented in Figure 4.

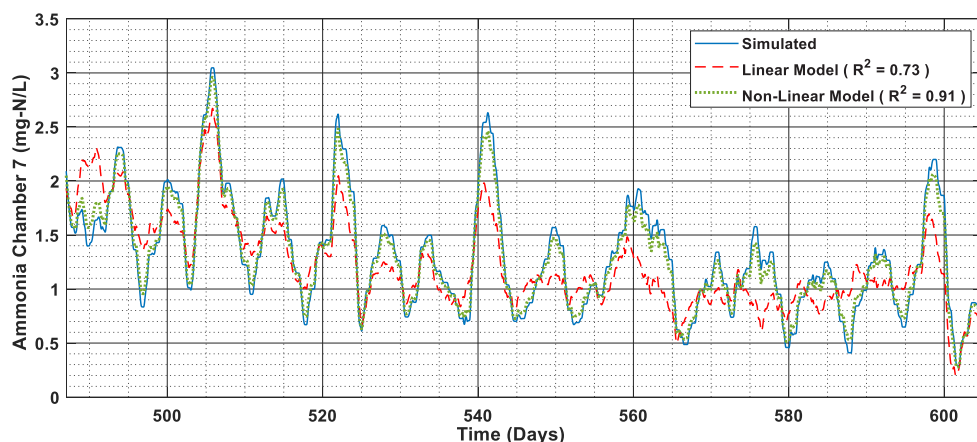


**Figure 4.** Simulated data versus values predicted by linear and nonlinear ammonia nitrification model.

A good match between the measured data and the data predicted by the mathematical model is observed in the plot presented in Figure 4. The  $R^2$  values (0.79 for linear and 0.91 for nonlinear model), justifies their ability to be used as a prediction model for the MPC controllers. However, based on the  $R^2$  values it can also be inferred that nonlinear model can explain better the biological nitrification of ammonia in the aerobic chamber compared to the linear model.

## Controller Performance with dynamic influent

The data obtained from implementing the control strategies A0, A1, A2, and A3 on the BSM2 simulator are used to generate comparison plots (Figure 5, Figure 6, and Figure 7) and to calculate the performance indices (Table 4) explained previously in Eqs. (1) – (6). A detailed analysis of the controller performance is provided in the subsequent sections.

### Advantages of ABAC

The advantages of using an ammonia-based aeration control are well established in literature (Rieger *et al.* 2013; Schraa *et al.* 2019). Similar inferences can be derived from Figure 5 which presents the effluent NH concentration for control strategies A0, A1, and A2. The performance indices presented in Table 4 also demonstrate the advantages of ABAC over constant DO setpoint aeration control strategy.

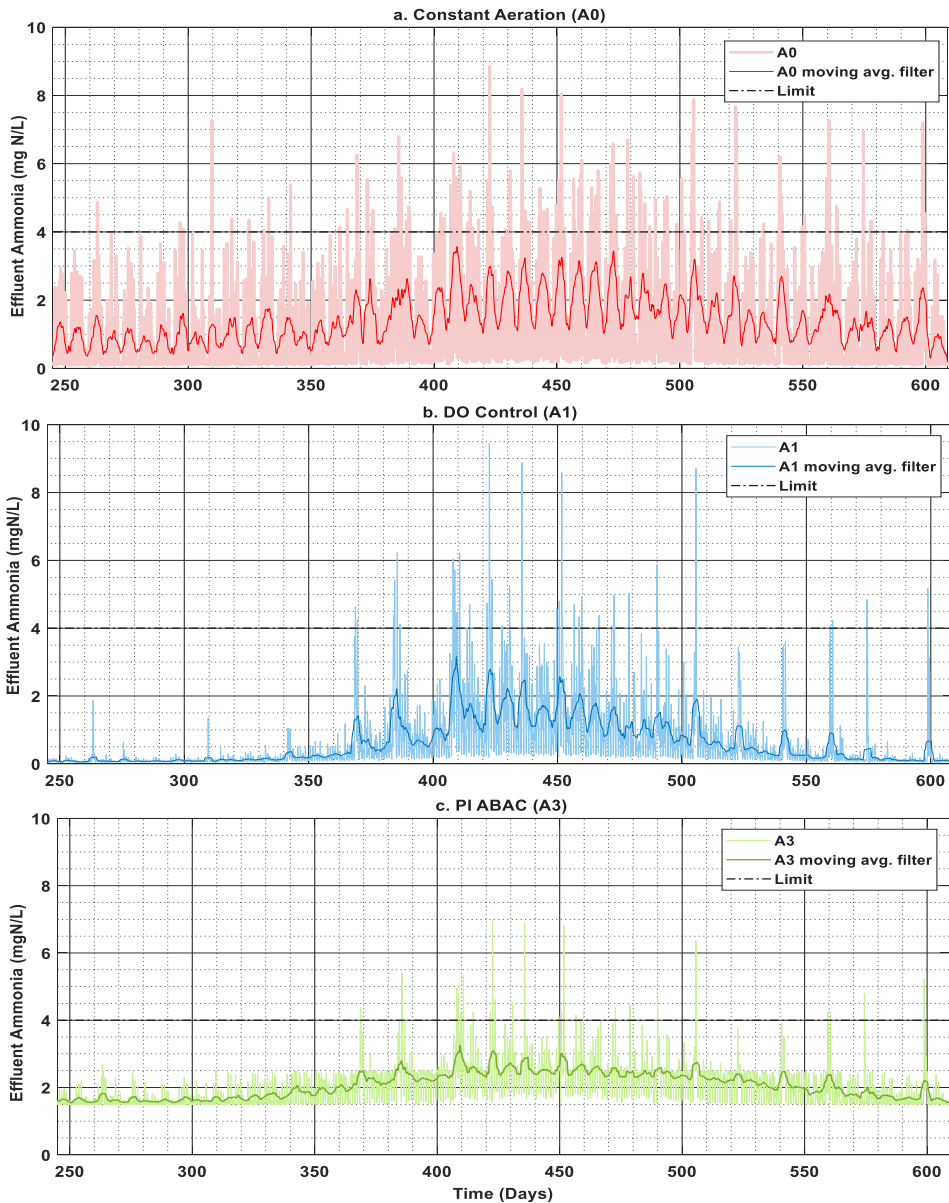


**Figure 5.** Effluent ammonia concentration for ABAC (A2) compared to open loop (A0) and DO-SP control (A1). A 3-day moving average filter is provided for better visualization.



The PI-ABAC control strategy (A2) provides a 32.2% reduction in %T $S_{NH,e}$  and a 5.51% reduction in aeration energy, compared to constant DO setpoint control (A2). However, Figure 5c also shows that the classical PI control strategy fails to maintain the NH setpoint during high ammonia peak loads. As a result, several effluent violations can be observed especially between T=350 to T=550 where,  $S_{NH,e}$  crossed the limit of 4 mg/L. The limitations of using a feedback PI control strategy in reducing the ammonia peaks are already mentioned in literature (Rieger *et al.* 2012). Replacing the conventional error-minimization approach with a predictive multivariate control strategy (such as MPC) that combines feedback as well as feedforward elements has the potential to further improve the performance of ABAC.

### PI versus MPC

The performance of the adaptive MPC control strategy is compared with the classical PI algorithm for ABAC. The plots presented in Figure 6 as well as the values of IAE (184 for PI and 229 for AMPC) presented in Table 4 suggest that the PI controller has better setpoint tracking compared to the MPC controller. However, a higher number of effluent ammonia violations is also observed in PI ABAC controller (0.314%) compared to the AMPC (0.144%).

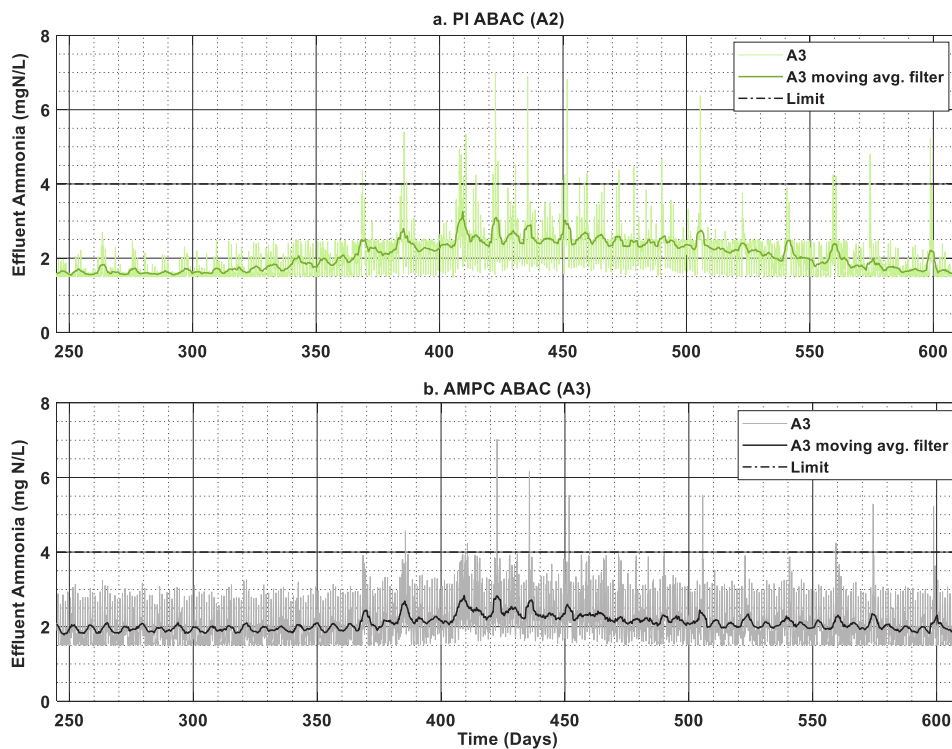


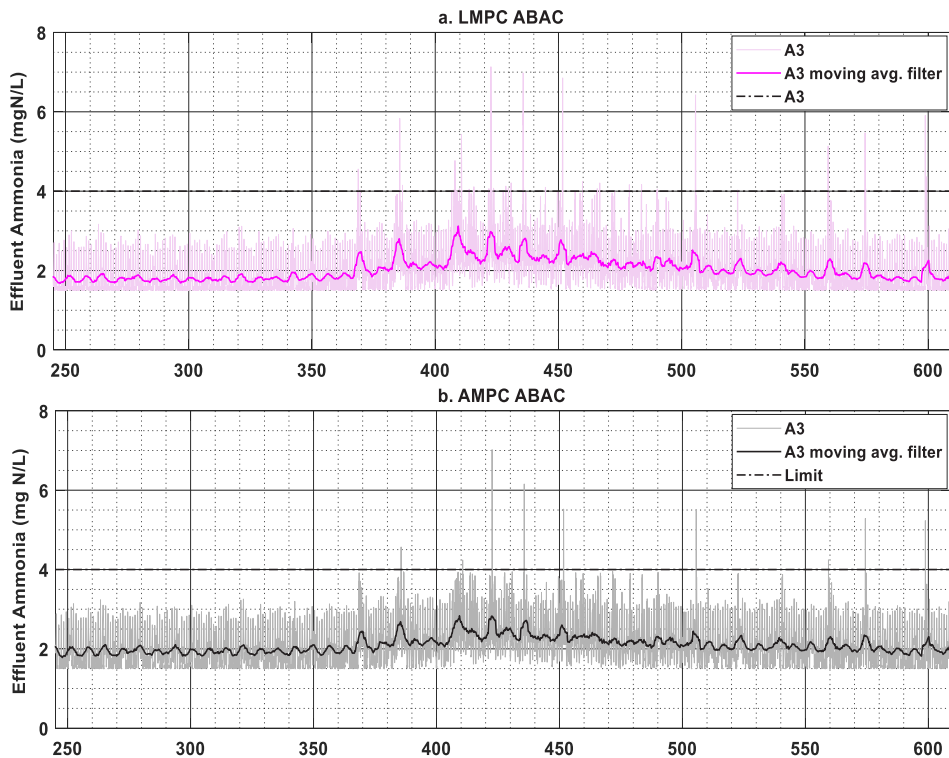
**Figure 6.** Effluent ammonia concentration for various MPC control strategies. A 3-day moving average filter is provided for better visualization.

A tradeoff between maintaining a constant setpoint or maintaining low aeration can be decided by adjusting the weights  $w_{SP}$  and  $w_u$  in the objective function. Therefore, the AMPC control strategy allows deviations from the NH setpoint in favor of maintaining a low aeration cost. However, the AMPC control strategy shows lower effluent violations compared to the PI

algorithm. This is primarily due to the weight  $w_L$  provided to effluent violation penalty term in Eq. 8 which results in an exponential increase of objective function as the ammonia concentration in the chamber 7 reaches closer to the effluent ammonia limit of 4 mg/L. The effect of introducing a limit penalty function can be clearly observed in Figure 6b where although a strict value of  $S_{NH,e}$  (close to NH setpoint) is not maintained, a comparatively lower number of effluent violations occur. A comparison between the classical PI and MPC strategy presented in Table 4 demonstrated a 10.31% reduction in aeration costs with a 17.91% increase in the average effluent ammonia concentration. Although there has been an increase in effluent ammonia concentration, a 30.1% reduction in the percentage time of effluent violation can be observed in AMPC ABAC when compared to the PI ABAC.

#### Prediction models (LMPC, NLMPC, and AMPC)

The quantitative assessment of MPC control strategies with different prediction models has been conducted. A comparison between the MPC control strategy using the linear, nonlinear, and the adaptive strategies based on  $S_{NH,e}$ , presented in Figure 7, shows a better performance of NLMPC compared to the LMPC. Similar inferences can be derived by comparing the performance indices presented in Table 4. The poor performance of LMPC could result from the inability of a linear model in capturing the high process nonlinearity of the biological nitrification process. The results are consistent with the conclusions presented in (Stare *et al.* 2007).



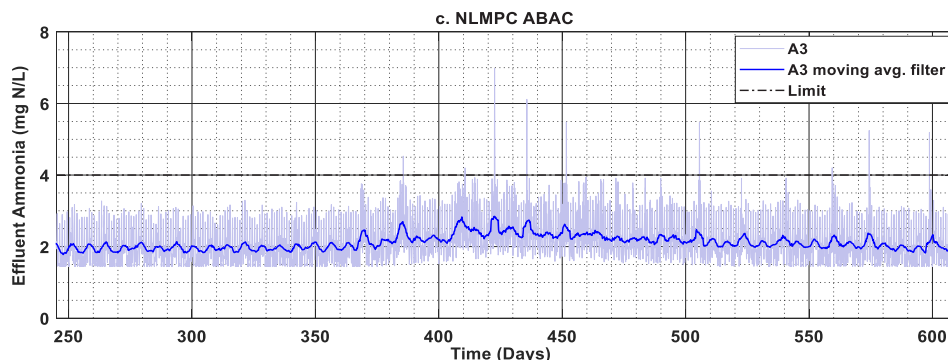


**Figure 7.** Effluent ammonia concentration for various MPC control strategies (a) Linear MPC (b) Adaptive MPC (C) Nonlinear MPC. A 3-day moving average filter is provided for better visualization.

Although there has been a noticeable drop in aeration costs the LMPC has also resulted in a slightly higher number of effluent violations when compared even with the PI controller. It is also observed that the performance of AMPC is very similar to the NLMPC, which suggests that a frequent update of the linear model will result in a linear MPC performing as good as an NLMPC. The NLMPC and AMPC demonstrated a clear performance improvement in terms of reducing the number of effluent violations (31.4% for AMPC and 30.0% for NLMPC) as well as decreasing the aeration energy. The average effluent ammonia concentration is also higher for AMPC (17.9%) and NLMPC (20.6%) compared to the LMPC (10.6%).

**Table 3.** Performance Indices for different control strategies.

Performance Criteria	A0	A1	A2	A3		
	Open loop	DO Control	NH Control	LMPC	AMPC	NLMPC
IAE	703	516	184	210	229	240
AE	4000	4350	4110 (-5.51%)	3990 (-2.91%)	3686 (-10.31%)	3616 (-12.09%)
EQI	10750	9387	11378	12835	13061	13503
%T $S_{NH,e}$	6.241	0.314	0.210 (-33.1%)	0.221 (5.23%)	0.144 (-31.4%)	0.147 (-30.0%)
Avg $S_{NH,e}$	1.49	0.65	1.89 (190.7%)	2.09 (10.6%)	2.23 (17.9%)	2.28 (20.6%)
Simulation time (h)	7.14	7.38	8.04	8.15	8.46	16.31
Simulation speed factor	2.28	2.21	2.02	2.00	1.91	1

Although the performance indices of AMPC is similar to the NLMPC, a significant reduction in computational time has been observed in AMPC. The simulation time and the simulation speed factor, showing the ratio of the simulation time with respect to A3-NLMPC (presented in Table 3) suggests that the AMPC is almost twice as fast as NLMPC. This confirms that AMPC can be used as a suitable replacement for NLMPC. Since the AMPC contains a system identifier, it is an efficient strategy to avoid prediction errors caused by model–plant mismatch.

This considerably reduces the dependency of the MPC on the accuracy of the prediction model used.

## **Conclusion**

The work presents a simulator-based comparison between the classical PI algorithm and various predictive models used in MPC for ammonia-based aeration control in a biological nutrient removal system. A new adaptive MPC was developed by combining the recursive model parameter estimator with the tuned linear MPC controller and tested with the Benchmark Simulation Model No. 2. The results presented in this work show that the applied model predictive control is a relatively efficient method for ammonia-based aeration control compared to control strategies involving constant DO setpoint or the classical PI algorithm. Among various MPC control strategies, it was observed that the MPC with a nonlinear model (NLMPC) demonstrates better performance compared to a linear model (LMPC) with a disadvantage of increased computational requirement. However, bolstering the linear model with an online system identification algorithm, providing real-time parameter updates, resulted in significant performance improvement for the Linear MPC. A quantitative comparison of MPC based on standard evaluation criteria indicates that the performance of the proposed AMPC is similar to an MPC using a nonlinear model. The performance indices also indicate 2 times increase in controller speed for AMPC compared to the NLMPC. These results demonstrate that the AMPC controller can be successfully implemented in an ammonia-based aeration control, providing a better alternative to computationally intensive NLMPC or a less robust LMPC.

## **Acknowledgement**

This research was funded by the Norwegian Research Council (NFR) Project RECOVER. The authors acknowledge the technical and financial support from DOSCON AS. The authors would also like to acknowledge Dr. Kimberley Solon for providing the Simulink files on which the control systems were evaluated.

## List of Variables

ABAC	= Ammonia based aeration control
AE	= Aeration Energy
AMPC	= Adaptive Model Predictive Control
ARX	= Auto-Regressive Model
ASM	= Activated Sludge Model
BSM2	= Benchmark Simulation Model No. 2
COD	= Chemical Oxygen Demand
EQI	= Effluent Quality Index
IAE	= Integral Absolute Error
LMPC	= Linear Model Predictive Control
MPC	= Model Predictive Control
NLMPC	= Nonlinear Model Predictive Control
OCI	= Operational Cost Index
PI	= Proportional Integral
TKN	= Total Kjeldahl nitrogen
TSS	= Total Suspended Solids
WRRF	= Water Resource Recovery Facility
$Avg S_{NH,e}$	= Average Effluent Ammonia Concentration (mgN/L)
$\%T S_{NH}$	= Presentation of time where ammonia concentration has violated (%)
$C_{NH,e,lim}$	= Upper limit for effluent ammonia concentration (mgN/L)
$N_p$	= Prediction Horizon (min)
$N_c$	= Control Horizon (min)
$J$	= Objective Function
$u_{min}$	= Minimum values of manipulated variable ( $m^3/L$ )
$u_{max}$	= Maximum values of manipulated variable ( $m^3/L$ )
$w_{SP}$	= Weights on setpoint error
$w_u$	= Weights on manipulated variable
$w_{\Delta u}$	= Weights on change in manipulated variable
$w_l$	= Weights on approaching the effluent violation limit
$f$	= State-space equation
$h$	= Measurement equation
$x_k$	= State variables at time instance k
$u_k$	= Manipulated variables at time instance k
$y_k$	= Measured variables at time instance k
$d_k$	= Disturbance variables at time instance k
$T_s$	= Time step (min)
$A$	= State matrix
$B$	= Input matrix

$C$	= Output matrix
$D$	= Feedforward matrix.
$Q_{IN}$	= Influent flowrate (kg /day)
$Q_R$	= Recycle flowrate (kg /day)
$Q_{IR}$	= Recycle of mixed recycle (kg /day)
$V$	= Volume of aerobic chambers ( $m^3$ )
$k$	= Time instance
$kLai$	= Aeration intensity (oxygen transfer coefficient)
$r$	= Reference setpoint
$S_{NH,e}$	= Concentration of ammonia nitrogen in the effluent. (mgN/L)
$S_{NH,i}$	= Concentration of ammonia nitrogen in the chamber i. (mgN/L)
$S_{O,i}$	= Concentration of dissolved oxygen in the chamber i. (mg/L)
$K_O$	= Saturation coefficient for oxygen (mg/L)
$K_{NH}$	= Saturation coefficient for ammonia (mgN/L)
$\mu$	= rate of nitrification
$\psi_k^T$	= Regression vector at time k
$P_k$	= Auto-covariance matrix at time k
$\hat{\theta}$	= Estimated parameters at time k
$\hat{w}$	= Estimated parameters at time k
$w_k$	= Process noise at time k
$v_k$	= Measurement noise at time k
$R_1$	= Process noise covariance
$R_2$	= Measurement noise covariance
$q$	= Time-shift operator.
$\xi(q)$	= Time-shift operator polynomial for output vector.
$\phi(q)$	= Time-shift operator polynomial for input vector.

## REFERENCES

- Boyd S, El Ghaoui L, Feron E, Balakrishnan V. Linear matrix inequalities in system and control theory. Society for industrial and applied mathematics, 1994.
- Gernaey K. V. & Jørgensen S. B. 2004 Benchmarking combined biological phosphorus and nitrogen removal wastewater treatment processes. *Control Engineering Practice*, **12**(3), 357–373.
- Gernaey K.V., Flores-Alsina X., Rosen C., Benedetti L. and Jeppsson U. 2011. Dynamic influent pollutant disturbance scenario generation using a phenomenological modelling approach. *Environmental Modelling Software*. **26**(11), 1255-1267.
- Henze M., Gujer W., Mino T. & Loosedrecht M. V. 2006 *Activated Sludge Models ASM1, ASM2, ASM2d and ASM3*. IWA Publishing, London.
- Holenda B., Domokos E., Rédey Á. & Fazakas J. 2008 Dissolved oxygen control of the activated sludge wastewater treatment process using model predictive control. *Computers and Chemical Engineering*, **32**(6), 1270–1278.
- Jeppsson, U., Pons, M.-N., Nopens, I., Alex, J., Copp, J., Gernaey, K. V., Rosen, C., Steyer, J.-P. and Vanrolleghem, P. A. 2007 Benchmark simulation model no 2 - general protocol and exploratory case studies. *Water Science & Technology*. **56**(8), 67–78.
- Jeppsson U., Alex J., Batstone D., Benedetti L., Comas J., Copp J. B., Corominas L., Flores-Alsina X., Gernaey K. V., Nopens I., Pons M.-N., Rodriguez-Roda I., Rosen C., Steyer J.-P., Vanrolleghem P.A., Volcke E. I. P. and Vrecko D. 2013. Benchmark simulation models, quo vadis?, *Water Science and Technoloy*. **68**(1), 1-15.
- Koo J., Park D., Ryu S., Kim G., & Lee Y. 2019 Design of a self-tuning adaptive model predictive controller using recursive model parameter estimation for real-time plasma variable control. *Computers and Chemical Engineering*, **123**, 126–142.
- Kothare M. V., Mettler B., Morari M., Bendotti P., & Falinower C. M. 1997 Linear parameter varying model predictive contr for steam generator level control. *Computers and Chemical Engineering*, **21**, 861-866.
- Lee J. H. & Yu Z. H. 1994 Tuning of model predictive controllers for robust performance. *Computers and Chemical Engineering*, **18** (1), 15-37.
- Ljung L. 1999 *System Identification: Theory for the User*. PTR Prentice Hall, New Jersey.
- Mulas M., Tronci S., Corona F., Haimi H., Lindell P., Heinonen M., Vahala R., & Baratti R. 2015 Predictive control of an activated sludge process: An application to the Viikinmäki wastewater treatment plant. *Journal of Process Control*, **35**, 89–100.
- Nopens I., Benedetti L., Jeppsson U., Pons M. N., Alex J., Copp J. B., Gernaey K. V., Rosen C., Steyer J.-P. and Vanrolleghem P. A. 2010 Benchmark Simulation Model No 2: finalisation of plant layout and default control strategy. *Water Science & Technology*, **62**(9), 1967-1974.
- van Overschee P., and B. De Moor. Subspace Identification of Linear Systems: Theory, Implementation, Applications. Springer Publishing: 1996.
- Qin S. J. & Badgwell T. A. 2003 A survey of industrial model predictive control technology. *Control Engineering Practice*, **11**(7), 733–764.
- Regmi P., Stewart H., Amerlinck Y., Arnell M., Garcia P. J., Johnson B., Maere T., Miletic I.,

- Miller M., Rieger L., Samstag R., Santoro D., Schraa O., Snowling S., Takacs I., Torfs E., van Loosdrecht M. C. M., Vanrolleghem P. A., Villez K., Volcke E. I. P., Weijers S., Grau P., Jimenez J. & Rosso D. 2018 The future of WRRF modelling – outlook and challenges. *Water Science and Technology*, **79**(1), 3–14.
- Martin C. and Vanrolleghem, P.A. 2014. Analysing, completing, and generating influent data for WWTP modelling: a critical review. *Environmental Modelling Software*, **60**, 188-201.
- Nair A., Cristea V. M., Agachi P. Ş. and Brehar M. 2017 Model calibration and feed-forward control of the wastewater treatment plant – case study for Cluj-Napoca WWTP. *Water and Environment Journal*. **32** (2), 164–172.
- Rosen C., Larsson M., Jeppson U., & Yuan, Z. 2002 A framework for extreme-event control in wastewater treatment. *Water Science and Technology*, **45**(4-5), 299-308.
- Rieger L., Jones R. M., Dold P. L., and Bott C. B. (2012) Myths about ammonia feedforward aeration control. *WEFTEC 2012 - 85th Annual Technical Exhibition and Conference*, New Orleans, Louisiana, USA.
- Rieger L., Jones R. M., Dold P. L. and Bott C. B. (2013) Ammonia-Based Feedforward and Feedback Aeration Control in Activated Sludge Processes. *Water Environment Research*, **86**(1), 63–73.
- Schraa O., Rieger L., Miletić I. and Alex J. (2019) Ammonia-based aeration control with optimal SRT control: Improved performance and lower energy consumption. *Water Science and Technology*, **79**(1), 63–72.
- Snip L., Flores-Alsina X., Plosz B.G., Jeppsson U. and Gernaey K.V. 2014. Modelling the occurrence, transport and fate of pharmaceuticals in wastewater systems. *Environmental Modelling Software*, **62**, 112-127.
- Sotomayor O. A. Z. & Garcia C. 2002 Model-Based Predictive Control of a pre-denitrification plant: a linear state-space model approach. *IFAC Proceedings Volumes*, **35**(1), 429-434.
- Stare A., Hvala N., & Vrečko D. 2006 Modeling, Identification, and Validation of Models for Predictive Ammonia Control in a Wastewater Treatment Plant - A Case Study. *ISA transactions*, **45**(2), 159–174.
- Stare A., Vrečko D., Hvala N., & Strmčnik S. 2007 Comparison of control strategies for nitrogen removal in an activated sludge process in terms of operating costs: A simulation study. *Water Research*, **41**(9), 2004–2014.
- Steffens M. A. & Lant, P. A. 1999 Multivariable Control of Nutrient-Removing Activated Sludge Systems. *Water Research*, **33**(12), 2864–2878.
- Takács I., Patry G. G., & Nolasco D. 1991 A dynamic model of the clarification-thickening process. *Water Research*. **25**(10), 1263-1271.
- Vanrolleghem P. A., Jeppsson U., Carstensen J., Carlsson B., & Olsson G. 1996. Integration of wastewater treatment plant design and operation - A systematic approach using cost functions. *Water Science and Technology*, **34**(3-4), 159-171.
- Várhelyi M., Vasile-Mircea C. and Brehar M. 2019 Improving Waste Water Treatment Plant Operation by Ammonia Based Aeration and Return Activated Sludge Control. *Computer Aided Chemical Engineering*. **46**, 1165-1170.



Vrečko D., Hvala N., Stare A., Burica O., Stražar M., Levstek M., Cerar P., Podbevšek S. 2006. Improvement of ammonia removal in activated sludge process with feedforward-feedback aeration controllers. *Water Science and Technology*., **53** (4–5) (2006), 125-132.

Vrečko D., Hvala N. & Stražar M. 2011 The application of model predictive control of ammonia nitrogen in an activated sludge process. *Water Science and Technology*, **64**(5), 1115–1121.

Zhang Q. 2000 Some Implementation Aspects of Sliding Window Least Squares Algorithms. *IFAC Proceedings Volumes*, **33**(15), 763–768.



# Paper E





# Economic Model Predictive Control for Optimal Struvite Recovery

Abhilash M Nair<sup>1</sup>, Finn Aakre Haugen<sup>2</sup>, Harsha Ratnaweera<sup>1</sup>

<sup>1</sup> Faculty of Science and Technology, Norwegian University of Life Sciences, P.O. Box 5003, 1432 Aas, Norway

<sup>2</sup> University of South-Eastern Norway, Kjolnes ring 56, Porsgrunn, Norway.

## Abstract

Resource recovery from municipal wastewater has been a prime focus for a decade. Although several recovery processes already exist in the market today, the high cost of material, inherent disturbance in the influent quality, lack of real time monitoring of critical parameters, and lack of a robust automation system may result in suboptimal performance. This work attempts to construct a model based predictive control for optimal operation of a struvite recovery unit in a full scale WRRF. A multi-parameter based predictive control has been developed by implementing an Economic Model Predictive Controller (EMPC) for optimal dosing of magnesium hydroxide in a struvite recovery unit. The EMPC used customized objective function for real-time optimization of performance and economical parameters of the crystallization unit. The effectiveness of the proposed EMPC controller is verified through tests conducted on the Benchmark Simulation Model No. 2 (BSM2d.). The results obtained from the simulator-based evaluation of EMPC demonstrate a significant improvement in resource recovery at reduced operational costs. The economic advantages of implementing an EMPC compared to proportional and constant magnesium dosage has also been enumerated.

**Keywords:** *Economic MPC, Dosing control, Water Resource Recovery Facility, Struvite Production.*

## Introduction

The Wastewater Treatment Plants (WWTPs) are consistently upgrading their processes to include more recovery operations and conform to its new terminology as Water Resource Recovery Facilities (WRRFs) (Regmi *et al.* 2019). Innovative treatment technologies are being implemented to enable better processing and disposal of the wastewater sludge. Struvite precipitation is one such process that gained popularity over the past decade (Jensen *et al.* 2015). Struvite (magnesium ammonium phosphate hexahydrate) has been of special interest due to its potential applicability as a slow-release fertilizer. The use of slow-release fertilizers (such as struvite) can offset the environmental deterioration caused by the excessive use of mineral-based fertilizers and eventually play a vital role in the modern eco-friendly sustainable agricultural sector (Rahman *et al.* 2014). Moreover, depleting reserves of mineral phosphorus also encouraged to explore alternative renewable sources (Cordell and Bennett, 2011). Struvite can be precipitated by adding Magnesium Hydroxide ( $Mg(OH)_2$ ) to a stream rich in ammonium ( $NH_4^+$ ) and phosphate ( $PO_4^-$ ) ions. In a typical WRRF, these nutrient-rich streams can be found in the supernatants of the anaerobic-digested sludge (Rahaman *et al.* 2008). Therefore, a struvite recovery unit is often installed after the dewatering unit to recover the Nitrogen (N) and Phosphorus (P) before recycling the supernatant back to the biological reactors.

Although the struvite precipitation process was designed with an aim of generating a commercially marketable slow-release fertilizer, in most WRRFs they are often used as a strategy to prevent the scale formation along the sludge train and eventually reduce the maintenance cost (Shaddel *et al.* 2019). Several social, economic, and technological reasons can be attributed to their inability to produce a commercially marketable product. The prices of  $\text{Mg}(\text{OH})_2$  and the energy required to operate fluidized bed reactors result in higher production costs. The fluctuations in the nutrient concentrations of the influent supernatant and the resulting inability to maintain a stable product quality add to the problem. These disturbances can often result in suboptimal performance of the crystallizers designed for struvite production. Instrument Control and Automation (ICA) offers several control strategies for ensuring optimal operation of various treatment processes. Although several works have already presented the advantages of introducing a struvite crystallization unit in a WRRF (Mbamba *et al.* 2016), we could not find control strategies for optimal operation of struvite production process. Several experimental studies have been conducted for the purpose of identifying the optimal operating conditions for struvite precipitation (Forrest *et al.* 2008; Jia *et al.* 2017). However, a continuous full-scale struvite production facility with ubiquitous disturbance in the influent stream benefits from real-time optimization of operational parameters. A well-designed control strategy using feedback from online nutrient sensors can reduce operating costs, improve struvite production, and enhance the performance of struvite crystallization unit.

The conventional single-input-single-output (SISO) control strategies used in the operations of WWTP have to be significantly upgraded to ensure profitable operations in a WRRF (Vanrolleghem and Vaneekhaute, 2014). Model Predictive Control (MPC) is an advanced control strategy used for optimal control of various operations in process industries (García *et al.*, 1989). Several implementations of MPC in wastewater treatment processes are also reported in literature (Ostace *et al.* 2011; O'Brien *et al.* 2011; Hasanlou *et al.*, 2019). MPC decides the control moves based on a cost minimizing control strategy over a finite time-horizon using a mathematical model (mechanistic or data-driven) of the process. A variant of MPC, that uses the economic cost parameters as their objective function, called as Economic Model Predictive Control (EMPC), has also been reported in literature (Durand *et al.* 2016). Multi-parameter based optimal control strategies such as EMPC are especially suitable for processes that do not have a constant optimal operating setpoint (Ellis *et al.* 2017). Processes such as struvite recovery which is subjected to a considerably high influent disturbance in terms of flowrate, nutrient concentration as well as the final price of products, if operated under constant  $\text{Mg}(\text{OH})_2$  or buffer dosing could result in suboptimal performance (Crutchik *et al.* 2017). Strategies such as EMPC which decide the control moves based on a real-time optimization of an economic cost function can be a potential strategy for optimal control of the struvite crystallization unit.

This work aims to develop a multi-parameter-based EMPC for determining the optimal dosage of magnesium hydroxide ( $Q_{\text{Mg}}$ ) in a struvite crystallization unit. Simulations were carried out on the standard Benchmark Simulation Model 2d. (BSM2d.) to study the effect of the novel EMPC control strategy on operational cost and recovery of phosphorus of a struvite production unit installed at a full-scale WRRF.

## Materials and Methods

### Process

#### *BSM2d Simulator*

The Benchmark Simulation Model No. 2 (BSM2d) is a comprehensive plant-wide model describing several processes in a typical WRRF. BSM2d presents a realistic simulation environment for various operations in a full-scale WRRF. This simulation standard is commonly used for evaluating operational sequences and control strategies in a WRRF. The implementation of BSM2d is available in most of the popularly used simulator platforms such as BioWin, GPS-X, Matlab/Simulink, Simba, STOAT, WEST, etc. (Gernaey *et al.* 2015). The plant layout, process model, influent data, test procedures, and evaluation criteria for simulator-based testing of control strategies are mentioned in the benchmarking standard manual (Nopens *et al.* 2010).

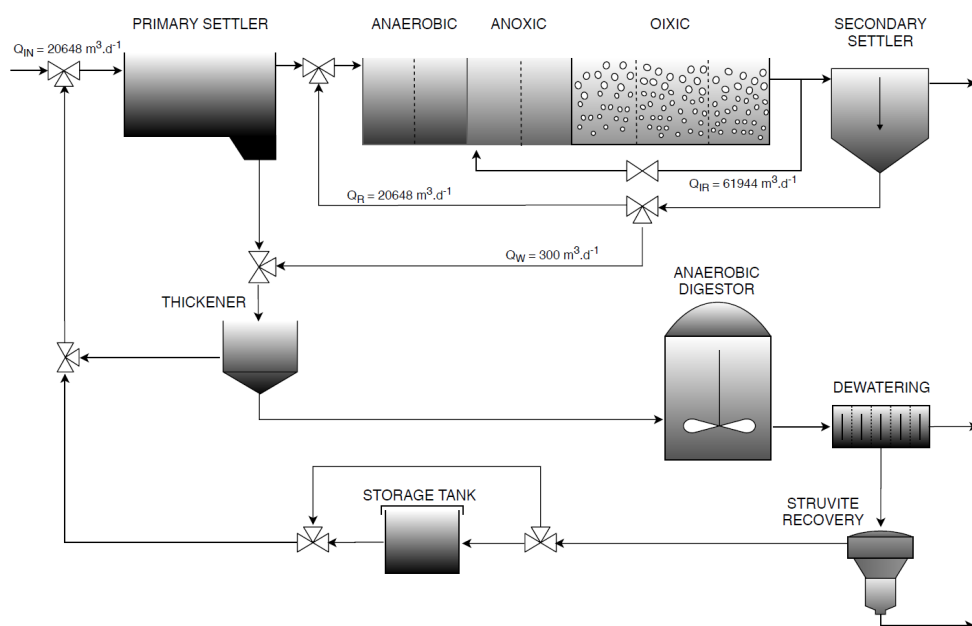


**Figure 1.** BSM2d Simulator with struvite recovery unit, redrawn from (Solon *et al.* 2017).

#### *Struvite Crystallizer in BSM2d*

The original BSM2d model has been upgraded to include phosphorus transformation kinetics and unit operation for phosphorus recovery (Solon *et al.* 2017). The process flow diagram and the location of the struvite crystallization unit in the updated BSM2d is presented in Figure 1. In this new configuration, the supernatant obtained from dewatering the anaerobic digested sludge is supplied to a crystallization unit and the crystallizer overflow is recycled back to the anaerobic chambers of the biological process. In the struvite recovery unit, the nutrient rich supernatant is dosed with Magnesium Hydroxide ( $\text{Mg}(\text{OH})_2$ ) to recover ammonium ( $\text{NH}_4^+$ )

and phosphates ( $\text{PO}_4^{3-}$ ) in the form of struvite. The underlying reaction involved in struvite precipitation is presented in Equation 1.



Experiments have reported that the optimal pH range for struvite crystallization process is between 8.0 and 10.0 (Daneshgar *et al.* 2018). Therefore, the crystallizer is dosed with sodium hydroxide ( $\text{Na}(\text{OH})$ ) to maintain the pH values above 8.1. The steady state operating conditions of the struvite unit and the mass balances for N and P occurring in the struvite crystallization unit in the BSM2d are presented in the Figure 2.

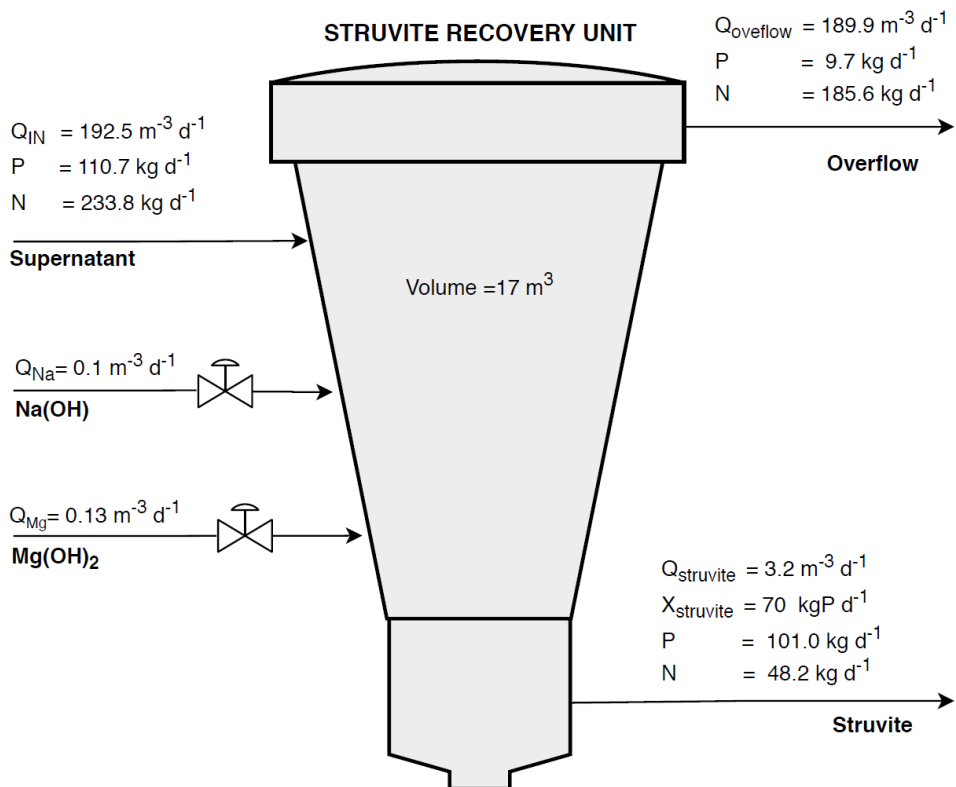


**Figure 2.** Design parameters and steady-state operating conditions in the struvite recovery unit.

### Economic Model Predictive Control

The Model Predictive Control (MPC) is a commonly used strategy for optimal control. In a conventional MPC, the outputs  $y_{k+i}$  are predicted for the finite prediction-interval  $N_p$  using a mathematical model and the control moves  $(u_k, u_{k+1}, \dots, u_{k+N_c-1})$  are calculated for a control horizon  $N_c$  to minimize an objective function  $J$ . The objective function for an error minimization control is calculated by a weighted square average of the control error and change in manipulated variable. In Equation 2 the term  $k$  and  $i$  are the time indices along the prediction horizon,  $r_{k+i}$  is the reference value (set-point),  $w_{SP}$  and  $w_{\Delta u}$  are weights for the control error and change in manipulated variables respectively. Penalizing the control error by increasing



the values of  $w_{SP}$  in the objective function keeps the output variable close to the reference value. Increasing the value of  $w_{\Delta u}$  suppresses rapid changes in the manipulated variables and makes the controller more sluggish.

$$J(u_k) = \sum_{i=0}^{N_P-1} \|r_{k+i} - y_{k+i}\|_{w_{SP}}^2 + \sum_{i=0}^{N_C} \|\Delta u_{k+i-1}\|_{w_{\Delta u}}^2 \quad (2)$$

The Economic model predictive control (EMPC) is a variant of the MPC where the cost function includes process performances, energy savings or overall economic profit rather than the quadratic error between the reference and measured variable. The successful implementation of EMPC for optimal operation of various wastewater treatment processes can be found in literature (Zeng and Liu, 2015; Zhang and Liu, 2019). The cost function used for EMPC control in the struvite recovery process is defined in Equations 3-5.

$$J = \sum_{i=0}^{N_P-1} -P_{\text{Recovery}} \cdot \phi_{\text{STR}} + M_{\text{Mg}} \cdot \phi_{\text{Mg}} \quad (3)$$

$$\text{where } P_{\text{Recovery}} = (PO_{4,\text{IN}} - PO_{4,\text{OUT}}) \cdot Q_{\text{IN}} \quad (4)$$

$$M_{\text{Mg}} = Q_{\text{Mg}} \cdot MW_{\text{Mg}} \cdot \rho_{\text{Mg}} \quad (5)$$

$$MW_{\text{Mg}} = 24.3 \text{ kg/kmol}; \rho_{\text{Mg}} = 25 \text{ kmol/m}^3$$

Where  $PO_{4,\text{OUT}}$  is the phosphate concentration in the overflow from the crystallizer,  $PO_{4,\text{IN}}$  is the phosphate concentration in the influent,  $Q_{\text{IN}}$  is the flowrate of supernatant to the crystallizer and  $P_{\text{Recovery}}$  is the real-time estimate for the mass of phosphate recovered as struvite.  $Q_{\text{Mg}}$  is the volumetric flowrate of magnesium hydroxide,  $MW_{\text{Mg}}$  is the molecular weight of Mg and  $\rho_{\text{Mg}}$  is the molar density of the magnesium hydroxide solution.  $\phi_{\text{STR}}$  is the market price of recovered phosphorus in the form of Struvite and  $\phi_{\text{Mg}}$  the market price of Magnesium hydroxide used in struvite production.

## Prediction Model

The control action of the MPC is taken based on the prediction made by the model. Therefore, adequate model describing the relation between input and output variables are imperative (Revollar *et al.* 2018). Struvite production in the crystallizer depends on several variables which introduce non-linear interdependencies in process chemistry. Physio-chemical models such as PHREEQC can adequately explain the process of struvite precipitation (Daneshgar *et al.* 2019). However, the lack of suitable sensors for measuring the concentration of every ionic species during the precipitation process pose a significant challenge in the use of mechanistic models for the purpose of automation and control. With the advent of data-driven models, various system identification techniques exist that can be used to establish a statistically significant correlation between the input and output variables of the process.

### State-space representation

The discrete form of the linear state-space model is presented in Equations 6-7.

$$x_{k+1} = Ax_k + B \begin{bmatrix} u_k \\ d_k \end{bmatrix} \quad (6)$$

$$y_k = Cx_k + D \begin{bmatrix} u_k \\ d_k \end{bmatrix} \quad (7)$$

In Equations 6-7,  $x_k$  is the state variable at time instance  $k$ ,  $u_k$  is the manipulated variable,  $d_k$  is the measured disturbance and  $y_k$  is the measured output. The list of input ( $u_k = Q_{Mg}$  and  $d_k = [Q_{IN} \ PO_{4,IN}]$ ) and output variables  $y_k = PO_{4,OUT}$  are provided in Table 1.

### Generation of Subspace Identification Model

Several algorithms are mentioned in literature for the purpose of identifying a linear, time-invariant, state-space model from input-output data (Verhaegen, 1994; Van Overschee and De Moor, 2012). In our work, the canonical variate analysis (CVA) approach for system identification algorithm, mentioned in (Larimore, 1990; Ljung, 1999) was used for estimating the state-space matrices of the multiple input-single output (MISO) model. The data for system identification is obtained from simulations performed in the BSM2d simulator using the dynamic influent. The `n4sid` function, provided as a part of the System Identification Toolbox in MATLAB is used to train the model and obtain the A, B, C and D matrices.

### Control Strategy

Four different scenarios, each with a different Magnesium dosing control strategy were evaluated. Details of the control schematics are enumerated in Table 1.

**Table 1.** Control structures for Struvite Crystallization.

Parameter	C0	C1	C2	C3
Measured Variable	-	$Q_{IN}$ $pH$	$PO_{4,IN}$ $PO_{4,OUT}$ $Q_{IN}$ $pH$	$PO_{4,IN}$ $PO_{4,OUT}$ $Q_{IN}$ $pH$
Manipulated Variables	$Q_{Na} = 0.10$ $Q_{Mg} = 0.13$	$Q_{Na} = \begin{cases} 0, & pH > 8.1 \\ 0.1, & pH < 8.1 \end{cases}$ $Q_{Mg} = 0.000675 \cdot Q_{IN}$	$Q_{Na} = \begin{cases} 0, & pH > 8.1 \\ 0.1, & pH < 8.1 \end{cases}$ $Q_{Mg} = f(PO_{4,IN}, PO_{4,OUT}, Q_{IN})$	$Q_{Na} = \begin{cases} 0, & pH > 8.1 \\ 0.1, & pH < 8.1 \end{cases}$ $Q_{Mg} = f(PO_{4,IN}, PO_{4,OUT}, Q_{IN})$
Control Algorithm	-	ON-OFF Proportional	ON-OFF EMPC	ON-OFF EMPC
Costs	-		$\phi_{STR} = 8.65 \text{ €/kg}$ $\phi_{Mg} = 6.00 \text{ €/kg}$	

The base control strategy (C0) is an open loop system using constant dosage of Magnesium ( $Q_{Mg} = 0.13 \text{ m}^3/\text{day}$ ) and Sodium ( $Q_{Na} = 0.10 \text{ m}^3/\text{day}$ ). The second control strategy (C1) is a feed-forward controller, where the  $Q_{Mg}$  is proportional to the flow of supernatant entering the crystallizer  $Q_{IN}$  (Figure 3a). A feed-forward proportionality constant  $K_P = 0.000675$  was provided for the controller C1. The controllers C2 and C3 are EMPC controllers described in Equations 3-5. In C2 the market price of struvite ( $\phi_{STR}$ ) and magnesium hydroxide ( $\phi_{Mg}$ ) are held constant during the evaluation period. In C3 the cost ( $\phi_{STR}$ ) and ( $\phi_{Mg}$ ) are chosen as time

varying inputs to the EMPC controller. The control strategies for C1, C2 and C3 are presented in Figure 3. In addition to control strategies for magnesium dose prediction, an on-off pH controller was provided in C1, C2 and C3 to ensure the pH values stay above 8.1.

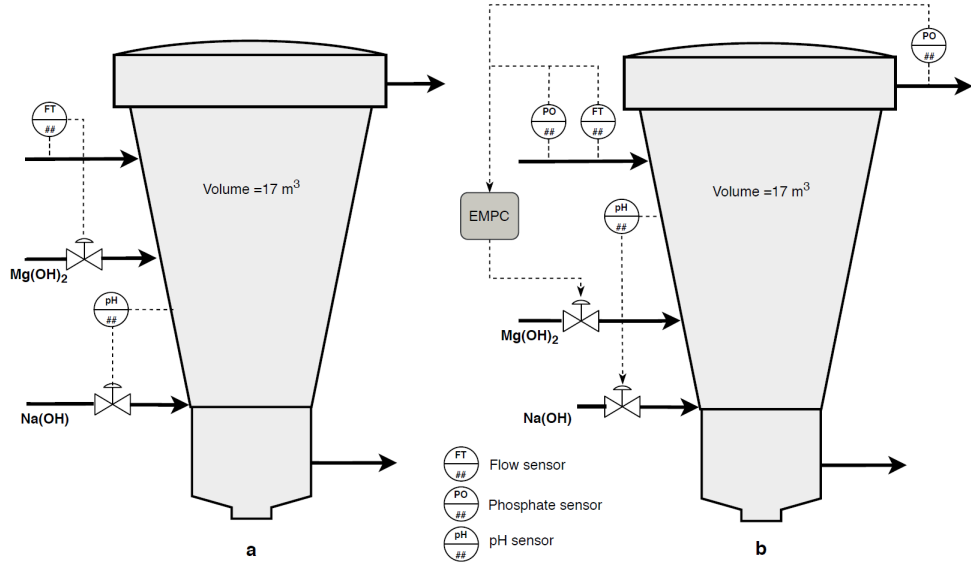


**Figure 3.** Control Schematic of Struvite Crystallization Unit **(a.)** feed forward flow proportional control (C1) and **(b.)** EMPC (C2 and C3).

To study the difference between C2 and C3 control strategy (Figure 3b.), a hypothetical scenario is considered where the cost of struvite ( $\phi_{STR}$ ) is changed once every 30 days. The new values of  $\phi_{STR}$  are randomly selected between the range  $\phi_{STR,MIN} = 7.5$  and  $\phi_{STR,MAX} = 9.5$  in the first day of every month. It should be noted that these prices are mere representative values taken from literature (Solon *et al.* 2017) and do not reflect the exact price of struvite or magnesium hydroxide in the market.

### Performance Evaluation

Several standardized criteria for evaluating the performance of control strategies are reported in literature (Vanrolleghem *et al.* 1996). However, in this work we limit our evaluation to the parameters that are directly influenced by the struvite crystallization unit. The performance criteria used in our evaluations are explained in Equations 8-11.

$M_{STR}$  (kg/day) is the average per day value for the mass of struvite produced by the crystallizer unit during the evaluation period. Equation 8 describes the calculation of  $M_{STR}$ .

$$M_{STR} (kg/day) = \frac{1}{T} \int_{245 d}^{609 d} Q_{STR}(t) \cdot X_{STR}(t) \cdot MW_{STR} \quad (8)$$

$M_{Mg}$  is the average (kg/day) mass for Magnesium hydroxide consumed by the struvite crystallization unit.

$$M_{Mg} (kg/day) = \frac{1}{T} \int_{245 d}^{609 d} Q_{Mg} (t) \cdot MW_{Mg} \cdot \rho_M \quad (9)$$

*Operational Cost Index* (OCI) is a standard economic measure used to calculate the total cost (material and energy) incurred during the daily operation of a WRRF. Since this work focuses on optimizing struvite crystallization, a simpler version of the operational parameters  $Profit_{CRYST}$  was also calculated using factors that has a direct influence on the cost of the struvite crystallization unit.

$$Profit_{CRYST} = M_{STR} \cdot \phi_{STR} - M_{Mg} \cdot \phi_{Mg} \quad (10)$$

For the scenario with time-varying market price of struvite ( $\phi_{STR}(t)$ ), the method for calculating  $Profit_{CRYST}$  is presented in Equation 11.

$$Profit_{CRYST} = \frac{1}{T} \int_{245}^{609} Q_{STR}(t) \cdot X_{STR}(t) \cdot MW_{STR} \cdot \phi_{STR}(t) - Q_{Mg}(t) \cdot MW_{Mg} \cdot \rho_M \cdot \phi_{Mg}(t) \quad (11)$$

$EV_{TP}$  is the number of times effluent total phosphorus limits ( $TP = 2 \text{ gP m}^{-3}$ ) are violated during the evaluation period.

### Implementation in Simulink Platform

The simulink implementation files for the modified BSM2d simulator is available in literature (Solon *et al.* 2017). The basic (C1) as well as advanced (C2, C3) control strategies are constructed in the base open-loop BSM2d SIMULINK file (C0) with constant dose of magnesium. The nonlinear MPC block provided in simulink was used to construct the EMPC and configure the controller parameters for C2 and C3. Four separate files were created each with a different control strategy described in Table1. Each SIMULINK file is simulated separately, and the results are stored in the MATLAB workspace. The results are then used to evaluate the performance parameters described in Equations 8-11. The SIMULINK files for implementation of the EMPC control strategy in a BSM2d can be provided on request. The standard procedure executing the simulator are provided in the BSM2d simulator manual (Jeppsson *et al.* 2007). The following steps were applied for simulation and subsequent evaluation of the control strategies.

1. Initialize the BSM2d simulator with the default values provided in the simulator.
2. Simulate 300 days forward using the constant influent data.
3. Initialize the simulink model with the final values of the steady state simulation. This allows the next simulation (with dynamic influent data) to begin at the exact position as where the steady state files had ended.
4. Simulate the model with the dynamic influent file for a period of 609 days.
5. The data from the dynamic simulation is stored in the MATLAB workspace.
6. Utilize the data recorded from T=245 to T=609 to assess the performance parameters mentioned in equations (8)-(11).

## Results and Discussion

### System identification results

The data received from the dynamic simulation is used as the data to develop the state-space model. The data is split to training data 75% ( $T = 0$  to  $T = 455$ ) and 25% validation data ( $T = 455$  to  $T = 609$ ). The training data is used to calibrate the model and obtain the A, B, C and D matrices (Equation 6-7) defined in the state-space matrix.

$$A = \begin{bmatrix} 0.9914 & -0.0086 & -0.0003 \\ -0.0114 & 0.9753 & 0.1115 \\ 0.0076 & -0.0200 & 0.7998 \end{bmatrix}; B = \begin{bmatrix} -8.6 & 6.8 & 12.8 \\ 1.9 & 156.7 & -2.9 \\ 1.1 & -232.8 & -1.7 \end{bmatrix}$$

$$C = [10.141 \quad -0.044 \quad -0.002]; D = [0 \quad 0 \quad 0]$$

The model is then used to predict the output for the validation data. The validation plot, showing a comparison between the validation dataset and the value predicted by the state-space model is presented in Figure 4.

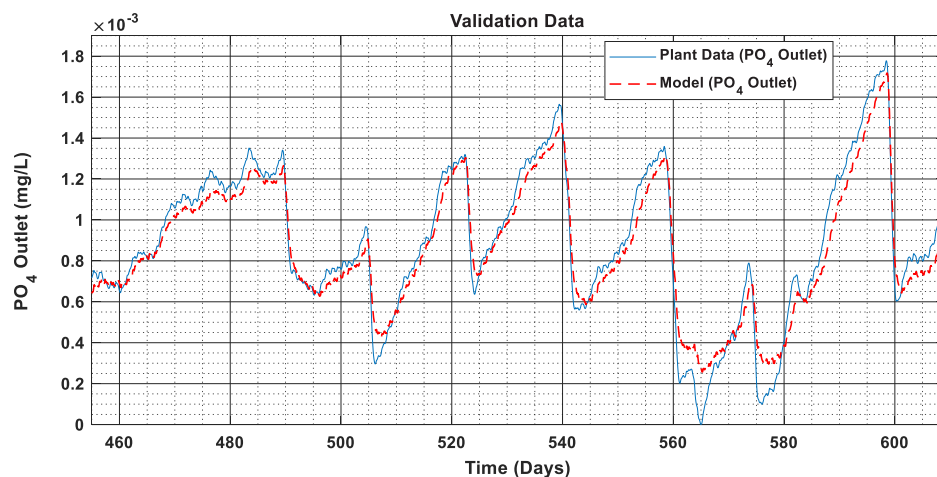


**Figure 4.** System Identification, validation plots model versus simulated values.

A close match is observed between the measured data and the data predicted by the model. The adequate match between the model predicted and plant data as well as the  $R^2$  value of 0.91 demonstrate the ability of the state-space model to predict the output  $PO_4$ -P concentrations in the overhead streams from the crystallizer.

### MPC settings

The choice of prediction and control horizon, limits of manipulated variables determine the performance of an MPC. Systematic procedures are explained to determine the optimal values of these tuning parameters (Lee & Yu 1994). In our case, the parameters were tuned based on experience gained from running the BSM2d simulator with steady-state as well as the dynamic weather data. The MPC parameters used in the simulations are presented in Table 2.

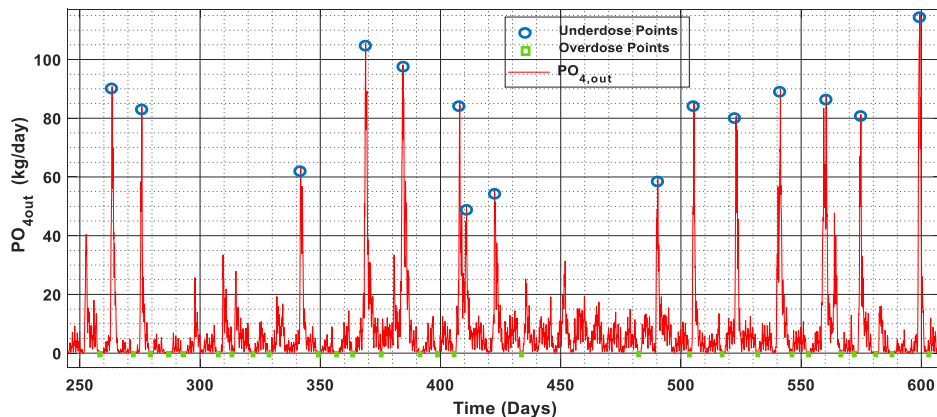
**Table 2.** MPC Settings.

Parameter	Description	Value	Unit
$T_S$	Time step	15	minutes
$N_P$	Prediction Horizon	3	
$N_C$	Control Horizon	2	
$u_{\min}$	Minimum value of $Q_{Mg}$	0.05	$m^3/day$
$u_{\max}$	Maximum value of $Q_{Mg}$	0.30	$m^3/day$

The parameters  $u_{\min}$  and  $u_{\max}$  (Table 2) were determined by adding +0.05 to the maximum  $Q_{Mg}$  and -0.05 to the minimum  $Q_{Mg}$  obtained from the feed-forward proportional control strategy (C1). The values of prediction and control horizon were gradually increased from a lower value  $N_P = 2$  and  $N_C = 1$ , and the controller performance was evaluated at every step. The controller performance showed no significant change when the values were increased above,  $N_P = 3$  and  $N_P = 2$ . Therefore, the values of prediction and control horizon were maintained at 3 and 2 respectively.

### Controller Performance Evaluation

A quantitative assessment is necessary to compare the of the performance of various control strategies presented in Figure 3. The waste-quality parameters of the influent and effluent streams of the struvite crystallization unit for all four strategies are utilized to generate comparison plots and calculate the performance evaluation indicators mentioned in Eqs. (8) - (11). The dynamic values of the soluble  $PO_4\text{-P}$  in the overhead flow of the struvite crystallization unit for the constant dosing scenario (C0) is presented in Figure 5.

**Figure 5.** Effluent  $PO_4\text{-P}$  from the crystallizer for constant dosing condition.

The benefits of introducing a struvite recovery unit in terms of improving effluent water-quality and reducing maintenance costs in WRRF is already reported in literature (Mbamba *et al.* 2016). However, Figure 5 indicates that maintaining a constant magnesium hydroxide flowrate (C0) in the crystallizer would not be the most optimal dosing strategy. Several underdosing points (marked in circles) are indicated where increasing the dosage could have resulted in higher phosphorus recovery in the form of struvite. Figure 5 also indicates overdosing points (marked in squares) where Magnesium was dosed beyond what was required.

The suboptimal performance can be attributed to two factors a. fluctuations in flowrate ( $Q_{IN}$ ) b. fluctuations in influent phosphate concentrations ( $PO_{4,IN}$ ). The flow proportional dosing control strategy (C1) partially offsets the problem of suboptimal dosing because of its ability to detect fluctuations in the flowrate of supernatant to the crystallizer. The improvement in dosing strategy can be reaffirmed in Table 3., which indicates an increase (8.01%) in average phosphorus recovery while reducing (8.62%) the Magnesium consumption. However, the dose prediction is entirely based on the flowrate, and flow-proportional control strategy (C1) does not consider the fluctuations in the  $PO_4$ -P concentrations in the influent. Therefore, suboptimal dosing is observed in situations with higher influent  $PO_4$ -P fluctuations.

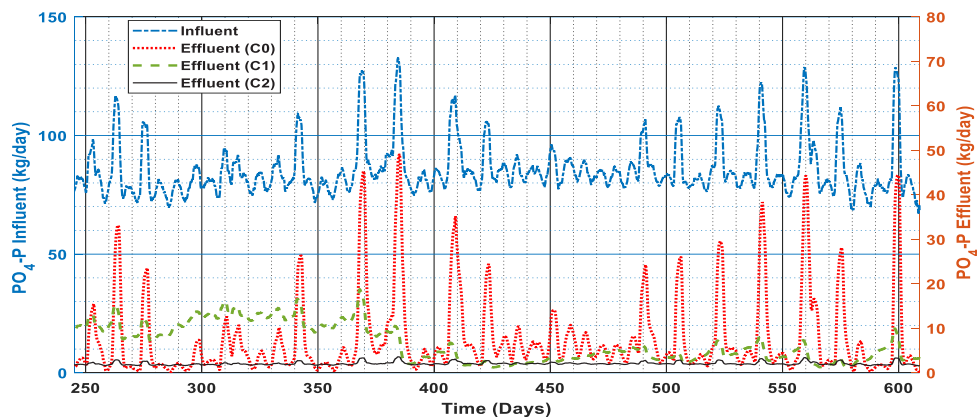


**Figure 6.** A comparison between Mass flowrate of Phosphorus at the inlet and outlet of struvite crystallization unit with dynamic influent data for various control strategies. A 3-day moving-average-filter is used to improve visualization.

The EMPC predicts the dose based on the optimal value of cost function (Equation 3). Since the dose prediction considers both flowrate as well as influent  $PO_4$ -P concentrations, a better control over the recovery of phosphorus can be expected. Figure 6 shows a more stable effluent  $PO_4$ -P in C2 compared to C0 and C1. The dynamic plots for Magnesium consumed, recovery percentage and mass of struvite production are presented in Supplementary Material. A comparison between the performance indices presented in Table 3 indicates a 12.5% increase in the average daily struvite production and an 8.5% drop in total magnesium consumption compared to the base dosing control strategy (C0).

**Table 3.** Performance criteria for the three evaluated control strategies.

Performance Criteria	C0	C1	C2
	Constant	Flow Proportional	EMPC
Struvite Production (kgP/day)	91.1	98.4 (8.01 %)	102.49 (12.50 %)
Mg Consumed (kg/day)	78.9	72.1 (-8.62 %)	72.2 (-8.49 %)
OCI	9105.1	9073.4 (-0.348 %)	9002.1 (-1.131 %)
Profit (€/day)	314.73	418.56 (33.0 %)	453.33 (44.0 %)
EV <sub>TP</sub>	21	18 (14.2 %)	9 (57.1 %)

A comparison between the control strategies in terms of overall profits for struvite production indicate a 33.01% increase for C1 and 44.03% increase for C2 when compared to the base control strategy C0. The increase in overall profits are primarily due to improvements in phosphorus recovery and a reduction in magnesium used in the crystallizer by avoiding overdosing. Apart from the increase in profits for struvite production, implementing EMPC also demonstrates fewer effluent violations in the treated effluent from WRRF (Table 3). Fewer effluent violation would imply fewer effluent penalties, which could further add to the savings.

### Economic Assessment of time varying cost function

The influence of introducing a time varying cost function on the effluent  $PO_4\text{-P}$  and the magnesium dose prediction is presented in Figure 7.

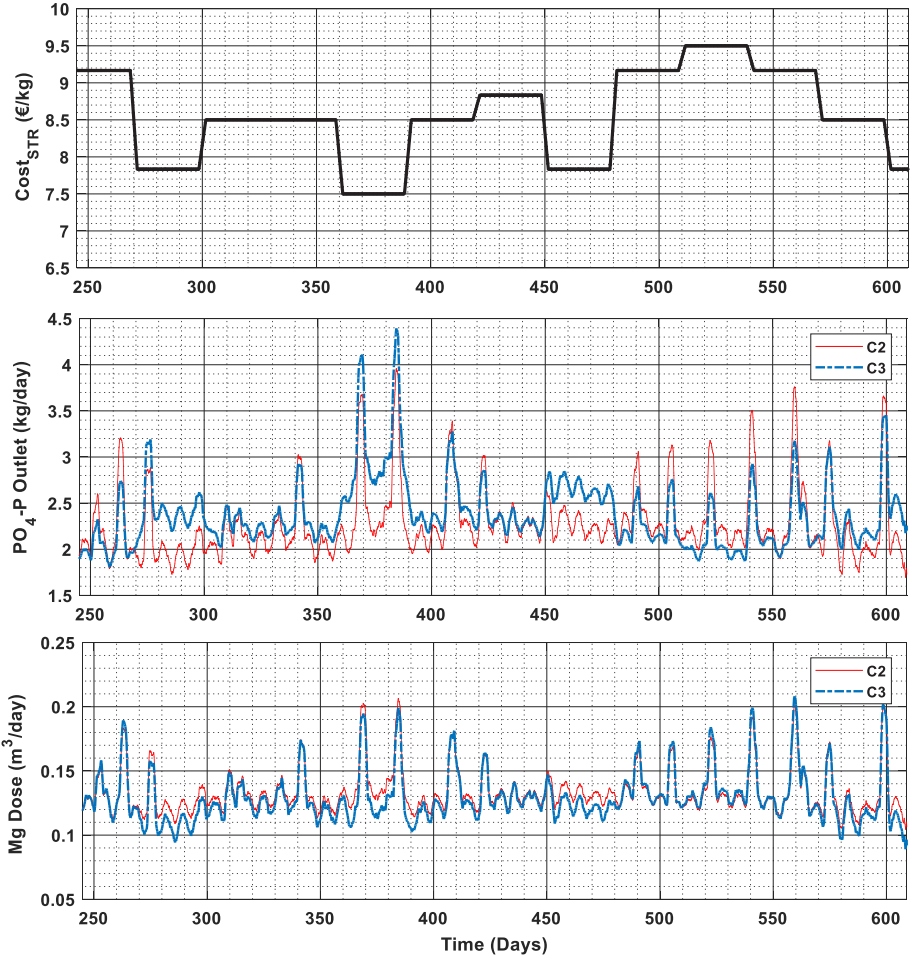


**Figure 7.** A comparison between C2 and C3 control strategy **a.** Market price for struvite during the evaluation period. **b.** Mass flowrate of phosphorus in the crystallizer outlet **c.** Volumetric flowrate of magnesium. A 3-day moving-average-filter is implemented in **b.** and **c.** to improve visualization.



It is observed that in situations with lower  $\phi_{STR}$ , the C3 strategy predicts a lower magnesium dosage and a subsequent reduction in phosphorus recovery. The reduction in struvite prices (reflected in  $\phi_{STR}$ ) moved the optimal dosing point to a lower value (resulting in lower phosphorus recovery percentage) in order to generate savings on the magnesium cost. When the costs are increased, higher recovery of phosphorus (in the form of struvite) is restored. A comparison between the average (kg/day) values of struvite produced, magnesium consumed and the profits for all three control strategies in the presence of a monthly variations in struvite costs are presented in Table 3. It is observed that using costs as inputs to the EMPC controller as opposed to a constant cost function results in an additional 8.1% increment in the overall profits incurred in struvite production.

**Table 4.** Economic Assessment for time varying struvite costs.

Economic Parameters	C0	C1	C2	C3
Struvite Production (kgP/day)	91.1	98.4	102.5	102.1
Mg Consumed (kg/day)	78.9	72.1	72.2	70.9
Profit (€/day)	291.73	388.56	413.13	447.83

A complete list of evaluation parameters for all the three control strategies are presented in the supplementary material. The EMPC strategy also provides a convenient alternative to adjust the controller parameters based on the price factors without the need for retuning the controller parameters. Although the work primarily defines the optimization problem based on two parameters a.) Cost of Struvite b.) Cost of Magnesium, EMPC also provides the possibility of including more optimization parameters (Shaddel *et al.* 2019) as long as a reliable correlation between the manipulated variables and the measured parameters exist.

## Conclusion

The work demonstrates the advantages of a multi-parameter-based control strategy for optimal dosing of magnesium in a struvite crystallization unit. A systematic procedure for developing a data-driven model for establishing a correlation between the input and output parameters of the struvite crystallization process has also been presented. Performance evaluation of the EMPC indicates a significant improvement in the overall profits when compared to both constant as well as flow proportional dosing strategy. The operational flexibility of the EMPC controller was demonstrated by its ability to conveniently switch between multiple operating conditions by using the market price of struvite and magnesium as their input variables. Although the work demonstrated the optimization strategy based merely on two economic parameters (magnesium dose flowrate and phosphorus recovery); the flexible nature of the EMPC allows the possibility of introducing multiple evaluation criteria in the objective function. The multi-parameter based optimal control approach using a data-driven model presents an opportunity to further improve the process operation and achieve better product quality by deploying the optimal dose strategy based on criteria such as struvite crystal dimensions, settling properties etc.

## Acknowledgement

This research was funded by the Norwegian Research Council (NFR) Project RECOVER. The authors acknowledge the technical and financial support from DOSCON AS. The authors would also like to acknowledge Dr. Kimberley Solon for providing the simulink implementation of BSM2d on which the control systems were evaluated.

## List of Variables

OCI	= Operational Cost Index
$EV_{TP}$	= Total Effluent Violations
N	= Nitrogen
P	= Phosphorus
Mg	= Magnesium Hydroxide
$N_P$	= Prediction Horizon (time – step)
$N_C$	= Control Horizon (time – step)
$J$	= Objective Function
$x_k$	= State variable at discrete time instance k
$u_k$	= Manipulated variables at time instance k
$y_k$	= Measured variables at time instance k
$T_s$	= Time step ( Days )
$k$	= Time instance
$r$	= Reference set-point
$PO_{4,IN}$	= Concentration of soluble phosphates in the influent supernatant. ( $\text{kg m}^{-3}$ )
$PO_{4,OUT}$	= Concentration of soluble phosphates in the overhead flow from crystallizer. ( $\text{kg m}^{-3}$ )
$M_{STR}$	= Mass of struvite produced (kg /day)
$M_{Mg}$	= Mass of Magnesium consumed in Crystallizer (kg /day)
$Profit_{CRYST}$	= Profit generated by operating the crystallizer (€/day)
$\phi_{STR}$	= Market price of struvite (€/kg)
$\phi_{Mg}$	= Market price of Magnesium hydroxide (€/kg)
$X_{STR}$	= Concentration of struvite in the Struvite flow ( $\text{kmol/m}^3$ )
$Q_{Mg}$	= Flowrate of Magnesium Hydroxide ( $\text{m}^3/\text{day}$ )
$Q_{Na}$	= Flowrate of Sodium hydroxide ( $\text{m}^3/\text{day}$ )
$Q_{IN}$	= Flowrate of supernatant to the crystallizer ( $\text{m}^3/\text{day}$ )
$P_{Recovery}$	= Mass of phosphorus recovered from crystallizer (kg/ day)
$MW_{Mg}$	= Molecular Weight of Magnesium (23 kg/mole)
$\rho_{Mg}$	= Molar density of Weight of Magnesium ( $25 \text{ kmol/m}^3$ )

## REFERENCES

- Cordell D. and Bennett E. (2011) A broken biogeochemical cycle. *Nature*, **478**, 29–31.
- Crutchik D., Morales N., Vázquez-Padín J. R. and Garrido J. M. (2017) Enhancement of struvite pellets crystallization in a full-scale plant using an industrial grade magnesium product. *Water Science and Technology*, **75**(3), 609–618.
- Daneshgar S., Buttafava A., Capsoni D., Callegari A. and Capodaglio A. G. (2018) Impact of pH and ionic molar ratios on phosphorous forms precipitation and recovery from different wastewater sludges. *Resources*, **7**(4), 1–22.
- Daneshgar S., Vanrolleghem P. A., Vaneekhaute C., Buttafava A. and Capodaglio A. G. (2019) Optimization of P compounds recovery from aerobic sludge by chemical modeling and response surface methodology combination. *Science of the Total Environment*, **668**, 668–677.
- Durand H., Ellis M. and Christofides P. D. (2016) Economic model predictive control designs for input rate-of-change constraint handling and guaranteed economic performance. *Computers and Chemical Engineering*, **92**, 18–36.
- Ellis M., Liu J. and Christofides P. D. (2017) *Brief Overview of EMPC Methods and Some Preliminary Results in Economic Model Predictive Control: Theory, Formulations and Chemical Process Applications*. Springer International Publishing, Switzerland.
- Forrest A. L., Fattah K. P., Mavinic D. S. and Koch F. A. (2008) Optimizing struvite production for phosphate recovery in WWTP. *Journal of Environmental Engineering*, **134**(5), 395–402.
- García C. E., Prett D. M. and Morari, M. (1989) Model predictive control: Theory and practice—A survey. *Automatica*, **25**(3), 335–348.
- Gernaey K. V., Jeppsson U., Vanrolleghem P. A. and Copp, J. B. (2014) *Benchmarking of Control Strategies for Wastewater Treatment Plants*. Scientific and Technical Report No. 23, IWA Publishing, London, U.K.
- Hasanlou H., Torabian A., Mehrdadi N., Kosari A. R. and Aminzadeh, B. (2019) Performance comparison of predictive controllers in optimal and stable operation of wastewater treatment plants. *Pollution*, **5**(4), 821–838.
- Jensen P. D., Yap S. D., Boyle-Gotla A., Janoschka J., Carney C., Pidou M. and Batstone, D. J. (2015) Anaerobic membrane bioreactors enable high rate treatment of slaughterhouse wastewater. *Biochemical Engineering Journal*, **97**, 132–141.
- Jeppsson U., Pons M. N., Nopens I., Alex J., Copp J. B., Gernaey K. V., Rosen C., Steyer J. P. and Vanrolleghem, P. A. (2007) Benchmark simulation model no 2: General protocol and exploratory case studies. *Water Science and Technology*, **56**(8), 67–78.
- Jia G., Zhang H., Krampe J., Muster T., Gao B., Zhu N. and Jin B. (2017) Applying a chemical equilibrium model for optimizing struvite precipitation for ammonium recovery from anaerobic digester effluent. *Journal of Cleaner Production*, **147**, 297–305.
- Kazadi-Mbamba C., Flores-Alsina X., Batstone J. D. and Tait S. (2016) Validation of a plant-wide phosphorus modelling approach with minerals precipitation in a full-scale WWTP. *Water Research*, **100**, 169–183.
- Larimore W. E. (1990) *Canonical variate analysis in identification, filtering, and adaptive control*. 29<sup>th</sup> IEEE Conference on Decision and Control vol.2., 596–604.

- Lee J. H. and Yu Z. H. 1994 Tuning of model predictive controllers for robust performance. *Computers and Chemical Engineering*, **18** (1), 15-37.
- Ljung, L., 1999. System Identification: Theory for the User. PTR Prentice Hall, New Jersey, USA. ISBN:978-0136566953
- Nopens I., Benedetti L., Jeppsson U., Pons M., Alex J., Copp J. B., Gernaey K. V., Rosen C., Steyer J. and Vanrolleghem P. A. (2010) Benchmark Simulation Model No 2 : finalisation of plant layout and default control strategy. *Water Science and Technology*, **62**(9), 1967–1974.
- O'Brien M., Mack J., Lennox B., Lovett D. and Wall A. (2011) Model predictive control of an activated sludge process: A case study. *Control Engineering Practice*, **19**(1), 54–61.
- Ostace G. S., Cristea V. M. and Agachi P. Ş. (2012) Cost reduction of the wastewater treatment plant operation by MPC based on modified ASM1 with two-step nitrification/denitrification model. *Computers & Chemical Engineering*, **11**, 2469-2479.
- Van Overschee P. and De Moor B. L. (2012) *Subspace identification for linear systems: Theory—Implementation—Applications*, Springer Science & Business Media.
- Rahaman M. S., Ellis N. and Mavinic, D. S. (2008) Effects of various process parameters on struvite precipitation kinetics and subsequent determination of rate constants. *Water Science & Technology*, **57**(5), 647–654.
- Rahman M. M., Salleh M. A. M., Rashid U., Ahsan A., Hossain M. M., and Ra C. S. (2014) Production of slow release crystal fertilizer from wastewaters through struvite crystallization - A review. *Arabian Journal of Chemistry*, **7**(1), 139–155.
- Regmi P., Miller M., Jimenez J., Stewart H., Johnson B., Amerlinck Y., Volcke E. I. P., Arnell M., García P. J., Maere T., Torfs E., Vanrolleghem P. A., Miletić I., Rieger L., Schraa O., Samstag R., Santoro D., Snowling S. and Takács I. (2019) The future of WRRF modelling - Outlook and challenges. *Water Science and Technology*, **79**(1), 3–14.
- Revollar S., Álvarez H., Lamanna R., Vega P. and Goldar A. (2018) Economic Model Predictive Control of a Wastewater Treatment Plant using Neural and Fuzzy models, *Computer Aided Chemical Engineering*, **43**, 1237–1242.
- Shaddel S., Ucarb S., Andreassen J. P and Østerhus S. W. 2019. Engineering of struvite crystals by regulating supersaturation – Correlation with phosphorus recovery, crystal morphology and process efficiency. *Journal of Environmental Chemical Engineering*, **7**(1). 102918.
- Shaddel S., Bakhtiary-Davijany H., Kabbe C., Dadgar F. and Østerhus S. W. (2019) Sustainable sewage sludge management: From current practices to emerging nutrient recovery technologies. *Sustainability* (Switzerland), **11**(12).
- Solon K., Flores-Alsina X., Kazadi Mbamba C., Ikumi D., Volcke E. I. P., Vaneckhaute C., Ekama G., Vanrolleghem P. A., Batstone D. J., Gernaey K. V. and Jeppsson U. (2017) Plant-wide modelling of phosphorus transformations in wastewater treatment systems: Impacts of control and operational strategies. *Water Research*, **113**, 97–110.
- Thomas D. N., Judd S. J., and Fawcett N. (1999) Flocculation modelling: A review. *Water Research*, **33**(7), 1579–1592.
- Vanrolleghem P. A. and Vaneckhaute C. (2014) Resource recovery from wastewater and sludge, modelling and control challenges. IWA Specialist Conference on Global Challenges for Sustainable Wastewater Treatment and Resource Recovery.

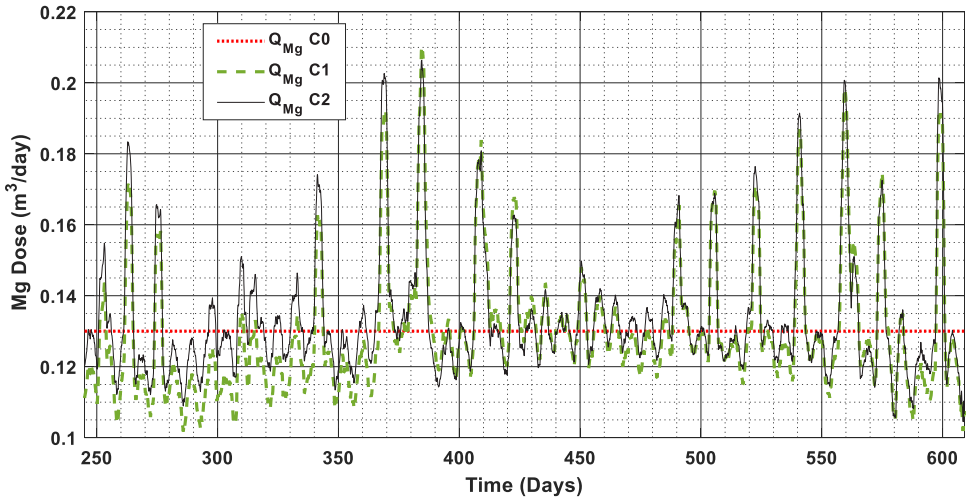
Vanrolleghem P. A., Jeppsson U., Carstensen J., Carlsson B. and Olsson G. (1996) Integration of wastewater treatment plant design and operation - A systematic approach using cost functions. *Water Science and Technology*, **34**(3-4), 159-171.

Verhaegen M. (1994) Identification of the deterministic part of MIMO state space models given in innovations form from input-output data. *Automatica*, **30**(1), 61-74.

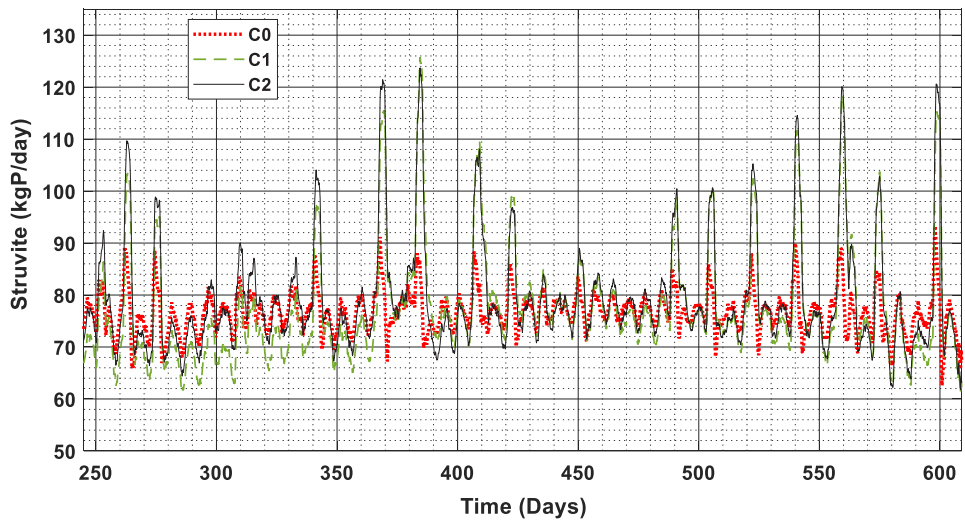
Zeng J. and Liu J. (2015) Economic Model Predictive Control of Wastewater Treatment Processes. *Industrial & Engineering Chemistry Research*, **54**(21), 5710-5721.

Zhang A. and Liu J. (2019) Economic MPC of Wastewater Treatment Plants Based on Model Reduction. *Water*, **7**(10), 1-21.

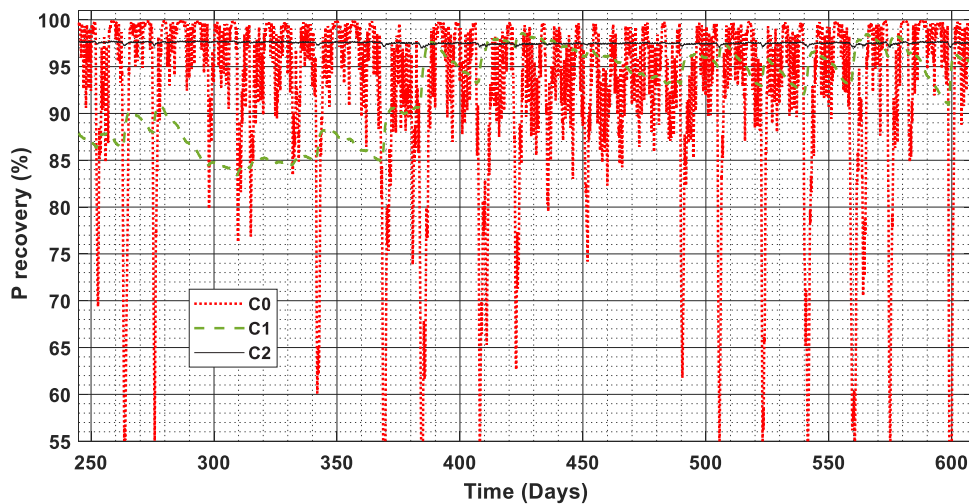
## Supplementary Figures



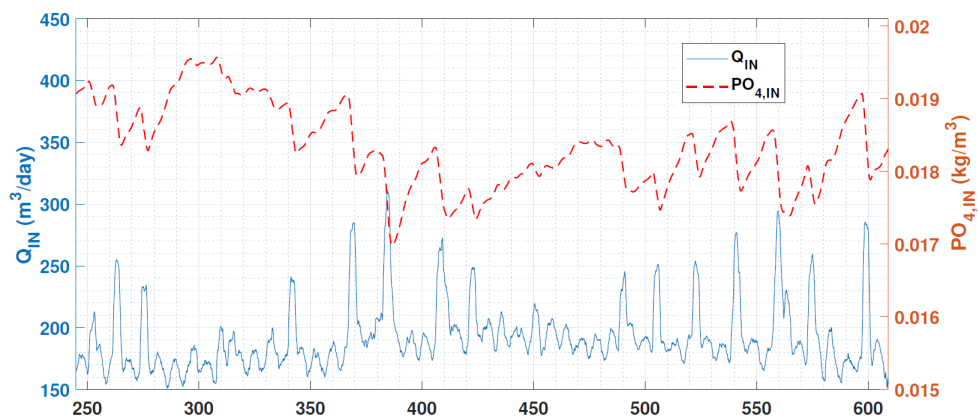
Supplementary Figure 1. Magnesium dose flowrate for control strategies.



Supplementary Figure 2. Struvite production rate for control strategies.



**Supplementary Figure 3.** Phosphorus recovery percentage for control strategies.



**Supplementary Figure 4.** Volumetric flowrate and phosphate concentration of influent to the struvite recovery unit

ISBN: 978-82-575-1735-9

ISSN: 1894-6402



Norwegian University  
of Life Sciences

Postboks 5003  
NO-1432 Ås, Norway  
+47 67 23 00 00  
[www.nmbu.no](http://www.nmbu.no)